Determination of Effective Impervious Area in Urban Watersheds

A Dissertation
SUBMITTED TO THE FACULTY OF
UNIVERSITY OF MINNESOTA
BY

Ali Ebrahimian

IN PARTIAL FULFILLMENT OF THE REQUIREMENTS
FOR THE DEGREE OF
DOCTOR OF PHILOSOPHY

Dr. John S. Gulliver, Dr. Bruce N. Wilson

August 2015

Acknowledgements

I would like to express my sincerest gratitude to my co-advisors Professor John S. Gulliver and Professor Bruce N. Wilson for their strong support, great help, and generous guidance throughout my PhD studies. Dr. Gulliver, I appreciate your availability, dedication and commitment to education as well as your valuable insight. I will always be grateful to you for all the lessons of life I learned from you. Dr. Wilson, thank you for your encouragement and valuable ideas. Your kindness, inspiration, and enthusiasm make working with you full of joy. I wish to extend my gratitude to the other members of my committee Professor Efi Foufoula-Georgio and Professor Omid Mohseni for their helpful advices and comments on my research.

Also, I acknowledge the Minnesota Local Road Research Board for providing the funding for this research. I would like to thank Britta Suppes of the Capitol Region Watershed District, and Brian Vlach of the Three Rivers Park District for providing rainfall- runoff and GIS data in their districts. I gratefully acknowledge Roger Glick of the Austin Watershed Protection Department for providing rainfall-runoff and GIS data in Austin, Texas. I also thank Bill Selbig of the USGS-Wisconsin Water Science Center for providing rainfall-runoff and GIS data in Madison, Wisconsin; Liz Stout of Minnetonka for providing rainfall-runoff monitoring data; Scott Anderson of

Bloomington for providing GIS data in Bloomington, and Ben Janke of the University of Minnesota for his help in this work.

Many thanks go to the former and current research group members in the St. Anthony Falls Laboratory, for their kindness and helps. Group lunches will always be missed.

Finally, I would like to thank my parents, siblings, and in-laws, for their endless love, support, and encouragement. I particularly want to thank my wife, Niloofar, for her constant love, patience and understanding.

Dedication

To my parents, Mansour and Rezvan, for their unconditional love and support.

To my in-laws, Sadegh and Fariba, for their endless encouragement.

And to my lovely wife, my best friend, and my life, Niloofar, for everything.

Abstract

Impervious surfaces have been identified as an indicator of the impacts of urbanization on water resources. The design of stormwater control measures is often performed using the total impervious area (TIA) in a watershed. Recent studies have shown that a better parameter for these designs is the "effective" impervious area (EIA), or the portion of total impervious area that is hydraulically connected to the storm sewer system. Impervious area is hydraulically connected if water travels over an entirely impervious pathway to a stormwater drainage system inlet. EIA is often considerably less than TIA. EIA can be considered the most important parameter in determining urban runoff, and knowledge of EIA is therefore critical in rainfall-runoff modeling. The incorrect use of TIA instead of EIA in urban hydrologic modeling leads to an overestimation of runoff volumes and rates. This overestimation results in the overdesign of associated hydraulic structures. In addition, EIA is the primary contributing area for smaller storms, and therefore the main concern for water quality. Stormwater control measures to improve water quality should therefore use EIA in design. Many of the current and developing management techniques, such as rain gardens, infiltration basins, or pervious pavements, are based on reducing EIA, or disconnecting impervious areas from the drainage system. However, there are no standard methods to assess the impact of these disconnection practices, partly because the connectedness of the existing watershed is not well known.

Methods to improve estimates of EIA are not highly researched, and need further investigation.

The overall goal of this research is to develop a method to accurately estimate EIA in ungauged urban watersheds with data that is readily available. Improving the EIA estimates based on rainfall-runoff data and developing recommendations on estimating EIA with regard to watershed and storm characteristics are among the other objectives of this research.

The most accurate methods for quantifying EIA in urban watersheds use the analysis of observed rainfall-runoff datasets. Estimates of EIA from these datasets are necessary to evaluate the accuracy of other techniques (e.g. GIS techniques). In the first part of the study, issues (e.g. spatial variation of rainfall and runoff measurement error) related to the determination of EIA using the statistical analysis of observed rainfall-runoff data are identified and discussed. A new method, based on Successive Weighted Least Square regression analysis (SWLS method), is developed to decrease the uncertainty of EIA estimates. The proposed method is applied to 40 urban watersheds with different sizes from less than 1 ha to 2,035 ha and various hydrologic conditions, of which 18 watersheds are located in the Twin Cities metro area of Minnesota, 2 in the City of Madison, Wisconsin and 20 in the City of Austin, Texas. The average, median, and standard deviation of EIA fraction (f_{EIA}) for all the forty watersheds of study are 0.213, 0.186, and 0.122, respectively, in our proposed SWLS method. Approximately 20 percent of the total area of our watersheds is hydraulically connected to the drainage

system, on average. The SWLS method is also able to determine initial abstraction (I_a) of impervious surfaces (i.e. the depth of water stored on the surface prior to the onset of runoff). The estimated values obtained with our method are between 0 to 5.6 mm, which is in good agreement with other studies. The average, median and standard deviation of I_a values for all forty watersheds of study are 0.7, 0.3, and 1.1 mm, respectively. The standard deviation of EIA fraction estimates (as a measure of uncertainty) for the SWLS method is, on average, 48% smaller than that obtained using the existing method. The results of the proposed SWLS method provide a better understanding of the urban runoff mechanisms in the watersheds of study and can be used as accurate estimations of EIA for verification of other EIA estimation methods.

To accurately estimate the portion of impervious surfaces in a watershed that is hydraulically connected to the drainage system (i.e. ratio of EIA/TIA), we also needed to calculate TIA in the watersheds of study. TIA is calculated using the land cover layers. High tree canopy coverage in an urban area causes some impervious feature shapes (e.g. roads and buildings) to be hidden from satellite view. This creates challenges in identifying impervious surfaces from aerial photographs and/or satellite imagery and consequently may result in underestimation of TIA. For that reason, tree canopy has been identified as a major factor of inaccuracies in observed TIA. To address this issue, a procedure in ArcGIS was developed to modify the spatial land cover data by un-shading the impervious surfaces obscured by tree canopy. This procedure was applied to the watersheds with high resolution tree canopy/land cover data (study sites in the Capitol

Region Watershed District, MN). The average, median and standard deviation of the EIA/TIA ratio for all the watersheds with residential land use were obtained as 0.45, 0.39, and 0.18, respectively. This simply means that about half of the impervious surfaces in our residential watersheds are hydraulically connected to the drainage system.

Finally, in order to estimate EIA in ungauged watersheds, a new method based on the integration of GIS and Curve Number (CN) is developed. CN, which is the predominant method of working with ungauged watersheds, is evaluated at the basin scale from rainfall-runoff events. While providing the EIA fraction, the method investigates different CN behaviors in urban watersheds and determines the response of each watershed. The latter is particularly attractive for practitioners involved in computing and modeling runoff from urban watersheds and design of associated hydraulic structures and stormwater control measures (SCMs). Using the results of the SWLS method, the proposed GIS-CN method is able to estimate EIA fraction as a function of TIA and saturated hydraulic conductivity of the soil (K_{sat}) in an ungauged watershed. The existing GIS method for EIA determination requires several GIS layers and also has to be completed with field surveys to determine the percentage of rooftops that are connected to the drainage system. This method is time consuming and limited by data availability. However, the required GIS information for our proposed GIS-CN method includes land cover and hydrologic soil group layers that are both readily available from national spatial datasets. Land cover data, if not available in higher resolution, can be extracted from the National Land Cover Database (NLCD) by the Multi-Resolution Land

Characteristics Consortium. Soil data are also available in digital formats from the NRCS Soil Survey Geographic database (SSURGO). The results are used to evaluate the potential and the limitations of the GIS-CN method.

The outcome and applications of this study will eventually lead to the design of a more sustainable urban stormwater infrastructure. Proper EIA values will result in more effective planning, siting and design of SCMs and improved identification of stormwater runoff pollution sources. These outcomes result in cost savings, and in more public consent due to the decreasing size of projects. A wide range of organizations involved in the design of stormwater management, pollution prevention, and transportation structures can benefit from this study. The end users of this research will be cities, counties, watershed districts, watershed management organizations, state departments of transportation, and the consultants who work for these entities in computing and modeling runoff from urban watersheds.

Table of Contents

List of Tables

List of Figures

CHAPTER 1: INTRODUCTION

1.1 Background

Impervious surfaces have been identified as an indicator of the impacts of urbanization on water resources. Some of the affected characteristics of a watershed include hydrological impacts (the amount of runoff, peak discharge rates, and base-flow are altered), physical impacts (stream morphology and temperature are changed), water quality impacts (nutrient and pollutant loads increase), and biological impacts (stream biodiversity decreases) (Chabaeva et al. 2009). Although total impervious area (TIA) has been traditionally used as an indicator of urban disturbance, recent studies suggest that a better indicator of urban runoff is the "effective" impervious area (EIA), or the portion of total impervious area that is hydraulically connected to the storm sewer system. Impervious area is hydraulically connected if water travels over an entirely impervious pathway to a stormwater drainage system inlet. EIA is often considerably less than TIA. Figures 1.1 and 1.2 show examples of EIA and TIA.

Figure 1.1 The Street is an example of EIA.

Figure 1.2 The sidewalk and roofs are incorporated into TIA, but may not contribute to EIA.

Another parameter related to impervious area is the fraction of directly connected impervious area (DCIA) which is the portion of TIA that is directly connected to the drainage system. Since not all the directly connected impervious surfaces are hydraulically connected, the EIA fraction is usually less than DCIA fraction. This can be explained by watershed characteristics (e.g. surface depression storage and vegetative interception) and maintenance issues (cracks on pavements, blockages in gutters, and clogging in inlet points). EIA fraction is typically 80% to 90% of the DCIA fraction (Boyd et al. 1993; Chiew and McMahon 1999).

Current and developing management techniques, such as rain gardens, infiltration basins, or pervious pavements, show awareness of the need to reduce EIA, or 'disconnect' impervious areas from the drainage system (Asleson et al., 2009; Paus et al., 2014; Olson et al., 2013; Ahmed et al., 2015). However, there are no standard methods to assess the impact of these disconnection practices, partly because the connectedness of the existing watershed is not well known. Methods to improve estimates of EIA are not highly

researched, and need further investigation. Development of reliable tools for quantifying EIA rather than TIA is currently one of the most important knowledge gaps (Fletcher et al., 2013).

1.2 Importance of EIA

EIA is an important parameter in determining urban runoff. It is typically fit to measured runoff in calibration of hydrologic models. However, it is subject to large errors because the response is correlated with infiltration parameters that are also determined by calibration. Knowledge of EIA is therefore critical in rainfall-runoff modeling. The use of TIA instead of EIA in urban hydrologic modeling can lead to an overestimation of runoff volumes and rates (Alley & Veenhuis, 1983), or will result in inappropriate curve fitting of other parameters, such as infiltration rates. This overestimation results in the overdesign of associated hydraulic structures. In addition, effective impervious areas are the primary contributing area for smaller storms and thus the main concern for water quality (Lee and Heaney, 2003). Stormwater control measures (SCMs or stormwater BMPs), to improve water quality should therefore use EIA in design.

The outcome and applications of this study will eventually lead to the design of a more sustainable urban stormwater infrastructure. Proper identification of EIA will result in more effective planning, location and design of SCMs, in identifying stormwater runoff pollution sources and environmental pollution control, in cost savings, and in more public consent due to decreasing project size. This study would benefit a wide range of organizations involved in the design of stormwater management, pollution prevention, and transportation structures by improving the accuracy of hydrologic simulations used in

the design process and providing a means to assess the impact of disconnection on discharge from a watershed of interest. These outcomes should result in more effective and properly designed SCMs, with potential improvements in water quality and cost savings for practitioners. The end users of this research will be cities, counties, watershed districts, watershed management organizations, state departments of transportation, and the consultants who work for these entities in computing and modeling runoff from urban watersheds.

1.3 Methods for Determining EIA

Currently, EIA can be estimated by analyzing rainfall-runoff data (Boyd et al., 1993;1994), by using aircraft or satellite-derived spatial data such as land cover and elevation with GIS techniques (Han and Burian, 2009), by empirical equations developed from regression analysis conducted on field calculations (Alley and Veenhuis, 1983), or by conducting field surveys of study sites such as inspection of downspout connectivity, watershed delineation during rainfall events, and identification of street connectivity to drainage system as with or without curb and gutter (Lee and Heaney, 2003). Remote sensing (RS) techniques have also been applied to analyze urban imperviousness in many studies, but the spatial resolution and tree canopy of the imagery limit its accuracy. EIA cannot be distinguished from the total impervious area (TIA) correctly by using only RS techniques. Most available data about urban imperviousness are based on land use or zoning, using image processing techniques with satellite or airborne imagery. However, this spatial resolution and accuracy may be inappropriate for microscale storm water

analyses (Lee and Heaney, 2003). Without a good comparison to EIA determined from rainfall and runoff data, the other techniques to measure EIA cannot be verified.

While the analysis of rainfall-runoff data in a watershed will typically produce the best results, these data can be expensive to collect and may not always be available or be of sufficient quality or resolution for analysis. Field investigations similarly may be time-consuming and costly, and provide limited results. Thus the use of GIS-based tools to estimate EIA becomes particularly attractive due to its applicability to ungauged watersheds, and to the increasing quality and availability of spatial data. Some studies have been performed to assess and compare different techniques for estimating total impervious surfaces (Roso et al., 2006; Chabaeva et al., 2009), but little work has been done for effective impervious area (Janke et al., 2011). The GIS method of Han and Burian (2009) has the advantage of being applicable to ungauged watersheds; however there are some limitation and difficulties that hinder wide use of this method. In order to use the mentioned GIS based method, and in addition to the need for familiarity with specialized software tools (e.g. ArcGIS) and GIS programming, one needs to have three layers of spatial information including the urban land cover, digital elevation model (DEM), and a layer containing the locations of inlets to the stormwater collection system. So the method can be expensive and time consuming. Besides, the method is not able to estimate EIA related to rooftops and requires the user to input the value of connected rooftops manually to determine the actual EIA value, a process that can add significant time and expense to the EIA estimate.

1.4 Objectives

This study has two overall objectives:

1) To improve the existing rainfall-runoff data analysis method for determining EIA in urban watersheds, and apply the developed and improved methods to a number of urban watersheds with different sizes and characteristics in order to quantify the fraction of EIA and ratio of EIA/TIA, and
2) To develop a new method based on integrating the Curve Number (CN) method and GIS. This method is based on evaluating CN at the basin scale from rainfall-runoff events. While providing the EIA fraction, the method investigates different CN behaviors in urban watersheds and determines the response of each watershed. The latter is particularly attractive for practitioners involved in computing and modeling runoff from urban watersheds and design of associated hydraulic structures and stormwater control measures. Also included are recommendations on estimating EIA with regard to watershed characteristics.

1.5 Literature Review

There are several research centers in the US working on different aspects of impervious surfaces, including NEMO (Nonpoint Education for Municipal Officials) program of the Center for Land Use Education and Research (CLEAR) in the University of Connecticut, Center for Watershed Protection, and Ecosystems Research Division of the U.S. Environmental Protection Agency. NEMO has summarized different techniques for impervious surfaces estimation in three main categories as follows: 1-Land Cover

Coefficients, 2- Modeling, and 3- Mapping from Images (NEMO, 2013). While several studies have been performed to assess and compare different techniques for estimating total impervious surfaces (e.g. Roso et al., 2006; Chabaeva et al., 2009), little work has been done for assessment and comparison of different techniques of determining effective impervious area in urban watersheds (Janke et al., 2011). Presented herein is the review of studies that deal with estimation of EIA rather than TIA.

According to the US Environmental Protection Agency (EPA, 2014), directly connected impervious area (DCIA) is the portion of TIA with a direct hydraulic connection to a water body via continuous paved surfaces, gutters, drain pipes, or other conventional conveyance and detention structures that do not reduce runoff volume. EPA uses change in DCIA for the purpose of MS4 (Municipal Separate Storm Sewer Systems) permits. They also recommend Sutherland (1995) empirical formulas for determining DCIA based on TIA in different watershed types. EPA (2014) evaluates the annual change in DCIA based on effectiveness of SCMs employed to reduce associated runoff. Long-term performance of SCMs in terms of runoff reduction is represented as performance curves (Tetra Tech, 2010). EPA (2014) has used these runoff capture performance curves to estimate change in EIA. In fact, EPA (2014) has assumed that runoff volume reduction is equivalent to EIA reduction.

According to Alley and Veenhuis (1983) EIA comprises those impervious surfaces that are hydraulically connected to the channel drainage system. With this definition, streets with curb and gutter and paved parking lots that drain onto streets are examples of effective impervious surfaces. While, non-effective impervious area (NEIA) includes

those impervious surfaces that drain to pervious ground. A roof that drains onto a lawn is an example of NEIA. The authors described two methods for estimating EIA including 1) determining EIA by relating it to the minimum ratio of runoff/rainfall measured for small storms and 2) using aerial photos and field surveys. They also discussed limitations of each method. Three impervious area parameters (i.e. TIA, EIA and EIA/TIA) have been estimated for 19 urban basins in Denver, and the following relation was developed from a log-linear regression:

$$EIA = 0.15\ TIA^{1.41} \tag{1.1}$$

where EIA and TIA are both in percent of watershed area. While the results showed the appropriateness of TIA to be used in black-box models, they also reinforced the importance of distinguishing between effective and total impervious area for deterministic models. The collected data from 19 urban watersheds suggested a large potential for developing relationships between EIA and TIA in urban areas, either through a regression between the two variables or estimates of the ratio EIA/TIA as a function of land use.

Laenen (1983) developed another equation for EIA as a function of TIA as:

$$EIA=3.6 + 0.43\ TIA \tag{1.2}$$

where EIA and TIA are in percent of basin area. This equation was based on rainfall and runoff data from 41 basins in Salem and Portland metro area, OR. EIA values were determined by calibrating the USGS rainfall-runoff model and field surveys in 4 basins.

Laenen (1983) noted that while this equation is not applicable in all basins, it may yield reasonable results for most urban areas in the Willamette Valley, OR.

According to Boyd et al. (1993), several studies had used plots of runoff depth against rainfall depth to determine the initial losses and sizes of the various types of surface (Miller 1978, Miller et al. 1978, Jacobson and Harremoes 1981, Pratt et al. 1984, Bufill and Boyd 1992). Boyd et al. (1993) used a successive regression method to determine effective impervious area and analyze impervious and pervious runoff events in 26 urban basins in Australia and other countries with watershed sizes from 2 to 2690 ha. They found that, in most basins, the effective impervious fraction was less than or equal to the directly connected impervious fraction measured from basin maps. In other words, impervious runoff is generally generated on a portion of the directly connected impervious surfaces.

Boyd et al. (1994) also conducted research on three urban drainage basins of 445 to 2690 ha in Canberra, Australia. Analyzing 47 rainfall-runoff storms with rainfall depths from 2.5 to 139 mm by the regression method, different runoff mechanisms were identified and discussed. Boyd, et al. considered antecedent wetness factors like one-day prior rainfall, five-day antecedent precipitation index, and number of preceding dry days as well as storm characteristics including storm duration and rainfall intensity as possibly affecting pervious area runoff.

Sutherland (1995) found that USGS equation for EIA (Laenen, 1983) works well for TIAs only between 10% and 50% and provides unrealistic EIA values for more urbanized areas. He re-analyzed the USGS data (Laenen, 1983) to develop series of equations for

describing the relationship between EIA and TIA in different urban areas (known as the Sutherland equations). The general form of equations is $EIA=A\ (TIA)^B$ where A and B are specific to each sub-basin conditions as: 1) Average basins: A=0.1, B=1.5, 2) Highly connected basins: A=0.4, B=1.2, 3) Totally connected basins: A=1, B=1, 4) Somewhat disconnected basins: A=0.04, B=1.7, and 5) Extremely disconnected basins: A=0.01, B=2.0.

Lee and Heaney (2003) performed a spatial analysis of urban imperviousness for a 5.81 ha (14.36 acre) residential neighborhood in Boulder, Colorado using geographic information systems and field investigations. The analysis has been performed at "five levels of effort" to show the improvement of accuracy and its impact on the estimated downstream runoff hydrograph for a one-year storm. However the significance of this impact has not been analyzed for larger storms. Flow rates were not monitored and the runoff has been estimated using the Storm Water Management Model (SWMM) 4.4H. The five levels of effort were classified in terms of applying GIS and field investigations as follows.

Level 1- Applying Literature reference data (no GIS application).

Level 2- Classifying all impervious elements (e.g. paved streets, sidewalks and building roofs) as impervious surfaces by applying GIS. The result would be TIA.

Level 3- Subtracting directly connected impervious area (DCIA) from the result of the level 2 analysis by applying GIS. The result of this level would be initial DCIA.

Level 4- GIS application and field investigation for the right-of-way to classify paved streets with curb and gutter as DCIA.

Level 5- GIS application and field investigation for the entire area to determine roof connectivity to drainage system by investigating the roof gutter downspouts.

The obtained percentage of the DCIA was changed from 35.9% in the Level 2 analysis to 13.0% in the Level 5 analysis. The results confirmed Schueler's (1994) finding that transportation-related imperviousness often exerts a greater hydrological impact than the rooftop-related imperviousness, as the rooftop-related DCIA was only 2.8% of the entire DCIA. It was also found that that the condition of the street boundary, (i.e. with or without curb) was the most critical factor to minimize urban DCIA in that study area. While the presented framework by Lee and Heaney (2003) is able to provide important details for hydrologic modeling, it is either too time consuming (Levels 4 and 5), too inaccurate (Levels 1 and 2) or not spatially explicit for application to large watersheds (Levels 3, 4 and 5) (Han and Burian, 2009).

Hatt et al. (2004) proposed the effective imperviousness as a better variable rather than total imperviousness for prediction of loads and concentrations in models of the effects of urban land use. They sampled 15 small streams draining urban and forest sub-basins in Melbourne, Australia for several water quality variables. They showed that the drainage connection (the proportion of impervious area directly connected to streams by pipes or lined drains) has a strong correlation with concentrations of several variables, independent of the correlation with imperviousness. They then suggested that drainage connection may be an important cause of observed variation in water quality among

streams with similar levels of imperviousness. In their study, effective impervious areas have been estimated from proximity to stormwater drains, allowing for local topography, and have been checked by ground truthing. However, based on their findings on the importance of drainage connection, they determined that direct determination of effective imperviousness will greatly increase the predictive power of models of urban impacts on water quality.

Shuster et al. (2005) has listed several studies in which the relationship between TIA and DCIA has been investigated and shown to be variable and elusive. Shuster et al. (2005) cited studies by Wibben (1976) which calculated the average ratio of DCIA to TIA to be 0.22, Miller (1979) which reported a ratio of 0.14, and Dinicola (1989) which reported a ratio of approximately 0.60 for high density residential housing. Lee and Heaney (2003) found the ratio of DCIA to TIA was approximately 0.36 in a residential area, and that the ratio of roadways to TIA was approximately 0.33. However, as stated before, Alley and Veenhuis (1983) found the relationship between EIA and TIA obeyed a power law (Equation (1.1)), and that the ratio between curb-and-guttered urban area to total area was 0.56 for residential areas.

Bochis and Pitt (2005) surveyed 125 neighborhoods in the Little Shades Creek Watershed, near Birmingham, AL and described the details of impervious surfaces in these areas. They estimated EIA through field investigations in both the Little Shade Creek Watershed, AL and 6 monitored drainage areas in Jefferson County, AL. They also performed a preliminary analysis for developing a relationship between EIA and Rv (volumetric runoff coefficient) for sandy and clayey soils through the calibration of the

Source Loading and Management Model for Windows (WinSLAMM) model in the 125 surveyed areas.

Bochis et al. (2008) determined EIA in five highly urbanized drainage areas in Jefferson County, AL by surveying 40 neighborhoods. They used these five basins to re-validate the older regional calibrations of the WinSLAMM model and to investigate the relationships between watershed and runoff characteristics for each of the individual 125 neighborhoods investigated by Bochis and Pitt (2005).

Guo (2008) has investigated DCIA by considering flow path in the determination of runoff coefficient. The area-weighted method is widely employed to determine the watershed runoff coefficient for small catchments. This conventional approach is to weight the imperviousness by the subareas in the watershed. However, this method is not able to consider the flow path, and thus cannot handle infiltration SCM designs. To address this issue, Guo (2008) has adapted the effective imperviousness concept by taking additional infiltration loses due to cascade designs (i.e. different configuration of impervious and pervious surfaces). He has suggested that effective imperviousness for a given area layout be weighted using the runoff volumes separately generated from the impervious and pervious areas.

Wenger et al. (2008) found the relationship between DCIA and TIA, in which the data had been obtained through hand-delineation of both TIA and DCIA for 15 sites of 25–70 ha in Georgia, as:

$$DCIA = (1.046\ TIA) - 6.23 \quad (1.3)$$

where DCIA and TIA are in percent of watershed area and DCIA=0 for TIA values less than 6.23%.

Roy and Shuster (2009) also developed another relationship:

$$DCIA = (0.627\ TIA) - 1.86 \quad (1.4)$$

where DCIA and TIA are in percent of watershed area and DCIA=0 for TIA values less than 1.86%. However, Roy and Shuster (2009) showed that predicted % DCIA based on this model and the other published empirical relations were all similarly ineffective at predicting observed % DCIA.

To address the need for an efficient method to accurately estimate EIA, Han and Burian (2009) presented a two-step process to estimate EIA for a range of applications including urban hydrologic modeling and assessment of runoff control practices. In the first step, data are classified using the supervised maximum likelihood technique into four urban land covers (i.e. building rooftop, asphalt/concrete, water and vegetation). In the second step, the urban land cover dataset is integrated with a DEM and a vector data layer containing the locations of inlets to the stormwater collection system. The three datasets are preprocessed, preparing them for two geospatial analysis tasks: 1) surface flow path tracing and 2) EIA designation. The urban land cover data layer (TIA data layer- the product of step one) is imported into the ArcGIS 9 software package and combined in a project with a DEM and a vector layer of stormwater collection system entrance locations (e.g. curb-opening inlets) and conveyance elements (e.g. open channels, ponds, gutters). An automated macro is written in Visual Basic for Applications (VBA) to geospatially

intersect the impervious surface coverage with a DEM and a vector dataset identifying the locations of stormwater collection infrastructure. After intersection, the geospatial analysis step traces the water flow path from classified impervious pixels until it either enters the drainage system (classified as EIA) or passes over a pervious area (classified as NEIA). They applied their method to a 2.2 km^2 watershed in Fayetteville, Arkansas. The authors found tree canopy to be the major cause of inaccuracies in TIA. The presented automated method is not able to estimate EIA related to rooftops and requires the user to designate a single value to represent the fraction of rooftops connected to impervious areas for an entire watershed and multiply it by the rooftop area to reach the EIA from rooftops. This issue prevents a complete spatial map of EIA to be developed by the method.

Roy and Shuster (2009) assessed the importance of field based delineation of impervious surfaces by delineation of TIA and DCIA in a 1.85-km^2 suburban watershed in Cincinnati, Ohio using a combination of GIS data compilation, aerial photo interpretation, and field assessments. They have evaluated the primary sources of imperviousness and differences between TIA and DCIA data based on land ownership (public vs. private) and impervious surface type.

Ravagnani et al. (2009) investigated how the error committed in estimating the fraction impervious area can affect the peak discharge entering the sewer system by studying five basins with an area of 2.1 to 9.8 ha in the town of Codigoro, Italy. They also examined the effect of classifying the impervious areas as directly and indirectly connected and pervious areas as connected and non-contributing on the peak discharge. The estimation

of impervious and pervious fractions was performed using high resolution satellite images and the result was compared to reference values obtained from field surveys. Identifying the connected and contributing areas was also performed using field surveys. Their results showed that disregarding the connectedness of different surfaces to the sewer system may lead to a marked overestimation of discharges.

Guo et al. (2010) recommended the effective imperviousness based on a pavement-area-reduction factor (PARF) as an incentive index for comparison and selection among various infiltration SCM designs. Four land use components including 1) directly connected impervious area (DCIA), 2) unconnected impervious area (UIA), 3) receiving pervious area, and 4) separate pervious area have been considered in this study and two sets of PARF are derived: conveyance-based and storage-based LID designs.

Pitt (2011) gathered detailed land use characteristics from several site surveys in Jefferson County, AL, Bellevue, WA, Kansas City, MO, Downtown Central Business Districts (Atlanta, GA; Chicago, IL; Los Angeles, CA; New York, NY; and San Francisco, CA), Millburn, NJ, San Jose, CA, Toronto, Ontario, Tuscaloosa, AL, Milwaukee, Madison, and Green Bay, WI, and Lincoln, NE. He grouped the individual data into six major land use categories: commercial, industrial, institutional, open space, residential, and freeway/highway and presented percent DCIA for each of these land uses as 79.5, 54.3, 50.0, 10.2, 24.0, and 31.9, respectively.

Janke et al. (2011) modified the GIS-based tool of Han and Burian (2009) to improve the analysis of tree canopy and applied the tool to two watersheds in the Capitol Region Watershed District, Minnesota, to test the viability of the modified tool. It was found

that, while promising, the tool needs to be applied to more watersheds and catchment areas that have a sufficient quality of precipitation and runoff data to develop an algorithm relating rooftop connections to land-use.

To conclude, the majority of watershed-based EIA estimation techniques are heavily dependent on field investigations which are often costly, time-consuming and even impractical in large watersheds. Also, the rainfall-runoff method cannot be applied to many of watersheds because there are few watersheds with qualified and sufficient monitoring data. So developing GIS based methods to determine effective impervious areas in urban watersheds would be useful.

CHAPTER 2: MONITORING RECORDS

2.1 Introduction

One of the essential requirements of this study is high-quality runoff and precipitation data in watersheds of various sizes and different hydrological conditions. The goal in this chapter is to find the best available data to be used in developing the effective impervious algorithms. The criteria are adequate precipitation and runoff monitoring records that will function well in effective impervious algorithm development.

We first attempted to identify available qualified rainfall-runoff data in Minnesota urban watersheds. There are two kinds of data to be collected: flow (runoff) and precipitation data. Precipitation data are expected to be available from different rain gauges throughout Minnesota watersheds. What is needed in the current study is storm sewer flow data at the outlet point of urban watersheds. Such data are rarely identifiable nor accessible online from websites.

A preliminary study on the EIA determination in two urban catchments in the Capitol Region Watershed District (CRWD) has been performed by Janke et al. (2011). Investigating the monitoring programs and relevant sites, a number of monitored catchments with proper sizes (including small ones) were identified in the Capitol Region Watershed. Based on the findings of the previous study (Janke et al., 2011), the strategy would be starting with smaller (and likely more homogenous) catchments in CRWD, analyzing the results and branching out to larger ones in the Twin Cities metro area and elsewhere.

2.2 Review of Monitoring Records

There are two types of data to be collected: runoff (flow rate, volume, or depth) and precipitation data. Precipitation data are usually available from different rain gauges throughout the watersheds. The Twin Cities Metropolitan Council has recently surveyed watershed districts in the Metro area to assess the level of monitoring in each district. This survey's results show that monitoring of some individual storm sewers are being conducted by a number of watershed districts. All of these watersheds were contacted to make an initial list of monitoring sites with data. After preparing the initial list, we investigated on the quality and adequacy of each site's data by contacting, meeting or talking with the respective staff in each watershed. There were several issues and ambiguities in terms of type, length and reliability of monitoring data which could significantly affect the results of the analyses in the next steps of the study. We thus excluded a number of monitoring sites to result in the data used. In addition, in order to investigate different hydrological conditions, the search for qualified monitoring data was expanded to different parts of the country, including San Diego, Los Angeles, and Ventura County CA, Portland OR, Seattle WA, Salt Lake City UT, Tucson AZ, Denver Area CO, Lawrence KS, Gainesville FL, Blacksburg VA, Washington DC, Baltimore County MD, Raleigh and Durham NC, and Durham NH. This section will elaborate upon the sites used in the study.

The first group of monitoring sites is located in the Capitol Region Watershed District (CRWD), Minnesota. Capitol Region is a 41-square-mile, highly urbanized watershed comprised by a majority of St. Paul and parts of Roseville, Maplewood, Lauderdale, and Falcon Heights (CRWD, 2012). The main land use in the monitoring sites is residential

except for the Sarita wetland, which encompasses farm and institutional land uses. The storm sewer system of the CRWD outlets at several points to the Mississippi River. All the monitoring reports of this district were reviewed and the initial list of monitoring sites was extracted. Based upon the CRWD reports and meeting and conversations with CRWD staff, ambiguities in the monitoring data for the purpose of this study in terms of type, length and reliability of monitoring data were identified and the data from the respective watersheds were either filtered or the watershed was eliminated from consideration.

The second group of monitoring sites is located in the Three Rivers Park District (TRPD). Six small residential sub-watersheds were monitored in the Cities of Maple Grove (MG1 to MG3) and Plymouth (P1 to P3), MN. These sub-watersheds were selected by TRPD to include one newly developed area less than 5-years old (P1 and MG1), one development between 5 and 15-years old (P2 and MG2), and one neighborhood older than 15-years (P3 and MG3) within each of the municipalities (i.e. Maple Grove and Plymouth). The sub-watershed areas were located within 10 kilometers of each other to minimize differences in precipitation and soil types (Barten et al., 2006). The site MG3 was not selected for this study because of the base flow contribution to the flow monitoring data.

Two monitoring sites (Smith Pond and Mall of America) in the City of Bloomington, MN were identified appropriate to be used in this study. The Smith Pond catchment received runoff from land uses that include highway and freeway development. The land use in Mall of America site is dominated by parking and roads associated with the Mall-of-America shopping center (i.e. commercial land use) (Wilson et al., 2007). Also, the

rainfall and runoff data of two monitoring sites were acquired from the City of Minnetonka, MN. The land uses in these two sites (Hedburg Drive and Mayflower Ave) are commercial and residential, respectively.

The monitoring data from two other monitoring basins in the City of Madison, Wisconsin were supplied by the USGS-Wisconsin Water Science Center. The first site (Harper Basin) discharges to Lake Mendota and the other one (Monroe Basin) ends to Lakes Wingra. The main land use in both sites is residential (Waschbusch et al., 1999).

Finally, the monitoring data for twenty small catchments in the City of Austin were provided by the Watershed Protection Department of the City of Austin. The main land use of the sites are residential except for OFA and WBA (commercial), LUA (downtown: mixed commercial and residential), and ERA (airport: transportation) (Glick et al., 2009).

Table 2.1 shows the finalized list of the monitoring sites with adequate rainfall-runoff data in each watershed district/city/dataset. The total number of the monitoring sites to be included in this study is 40.

Table 2.1 Monitoring sites with qualified runoff and precipitation data

Row	Monitoring Site Name	Location	Drainage Area (ha)	Monitoring Years
Capitol Region Watershed District, MN				
1	Arlington-Hamline Underground Facility (AHUG)	Saint Paul	15.9	2007-2012
2	Como Park Regional Pond- inlet (GCP)	Saint Paul	51.8	2008-2012
3	Como 3	Saint Paul	185.8	2009-2012
4	Sarita (inlet)	Saint Paul	376	2006,2008-2009
5	Trout Brouk- East Branch (TBEB)	Saint Paul	377.2	2006-2012
6	East Kittsondale (EK)	Saint Paul	451.6	2005-2012
7	Phalen Creek (PC)	Saint Paul	579.9	2005-2012
8	St. Anthony Park (SAP)	Saint Paul	1007.3	2005-2012
9	Trout Brouk Outlet (TBO)	Saint Paul	2034.8	2007-2012

Row	Monitoring Site Name	Location	Drainage Area (ha)	Monitoring Years
Three Rivers Park District, MN				
10	MG1	Maple Grove	5.5	2001-2003, 2005-2006
11	MG2	Maple Grove	3.5	2001-2003, 2005-2006
12	P1	Plymouth	5.1	2001-2003, 2005-2006
13	P2	Plymouth	6.8	2001-2003, 2005-2006
14	P3	Plymouth	5.6	2001-2003, 2005-2006
City of Bloomington, MN				
15	Smith Pond (SP)	Bloomington	55	2004-2005
16	Mall of America (MOA)	Bloomington	202	2004-2005
City of Minnetonka, MN				
17	Hedburg Drive (HD)	Minnetonka	2.8	2010
18	Mayflower Ave	Minnetonka	11.1	2010
City of Madison, WI				
19	Harper Basin	Madison	16.4	1995
20	Monroe Basin	Madison	92.9	1994
City of Austin, TX				
21	BW1	Austin	146.3	2012-2014
22	EBA	Austin	14.3	2000-2003
23	EHA	Austin	20.8	1994-2002
24	ERA	Austin	40.4	1994-1999
25	HI	Austin	1.2	1985-1987
26	HPA	Austin	17.4	2000-2003
27	LCA	Austin	84.9	1992-1999
28	LOA	Austin	5.4	2008-2011
29	LUA	Austin	5.5	1989-1996
30	MBA	Austin	82.1	1993-1995
31	OFA	Austin	0.6	1993-1997
32	PP1	Austin	2	2009-2012
33	PP2	Austin	1.8	2009-2012
34	PP3	Austin	0.9	2009-2012
35	RRI	Austin	6.4	2003-2007
36	SCA	Austin	2.3	2006-2010
37	TBA	Austin	20	1996-2000
38	TCA	Austin	16.5	1993-1997
39	TPA	Austin	16.8	1993-1997
40	WBA	Austin	0.4	1999-2003

CHAPTER 3: STATISTICAL ANALYSIS

3.1 Introduction

One of the key steps of this study is performing statistical analyses on rainfall-runoff records for watersheds in which there are adequate monitoring data. Results from this step will be used in EIA algorithm development. In this chapter, different issues about the existing rainfall-runoff data analysis method of EIA determination (Boyd et al., 1993) that reduce the accuracy of the method are recognized and discussed. To address these issues, improvements in both the statistical analysis technique and criterion for categorizing rainfall events are proposed. The improved methods are then applied to urban watersheds that were introduced in chapter 2. In order to have a better comparison with the existing method, the Boyd, et al. method and the improved method have been applied to the watersheds identified in Chapter 2. The results associated with each improved method are presented and compared to the original results in order to assess the advantages and limitations of the improved methods.

3.2 Existing Method

The existing method for determining EIA using rainfall-runoff data is that of Boyd et al. (1993). In this method, the runoff depth (i.e. runoff volume divided by total drainage area) is plotted versus rainfall depth for each storm in the record. A regression line is then fitted to this data, where the slope of the line is the fraction of total watershed area contributing to runoff. If all events are assumed to involve only impervious runoff (i.e. runoff that is generated from impervious surfaces), then the events are called EIA events and the slope is the EIA fraction (f_{EIA}). EIA fraction is defined as

$$f_{EIA} = \frac{EIA}{A_T} \quad (3.1)$$

where A_T= total area of watershed.

Depending on the characteristics of rainfall and the watershed of study, one may fit a multiple segment line to the data (Figure 3.1). In this case, the slope of each segment is the fraction of total watershed area contributing to runoff. In figure 3.1, IL represents initial losses or initial abstraction (I_a) (i.e. the depth of water stored on the surface prior to the onset of runoff). Subscripts ic, i, and p correspond to connected impervious, impervious, and pervious area, respectively.

In most cases, pervious area (PA) and non-effective impervious area (NEIA) also contribute to runoff generation from larger storms. The storm events that generate runoff from both pervious and impervious surfaces are called combined events. The data points associated with combined events would lie above the regression line. When points lie well above the regression line, pervious runoff (i.e. runoff that is generated from pervious surfaces) appears to be present. In order to find the EIA fraction, Boyd et al. (1993,1994) recommend omitting the points that are more than 1 mm above the line, fitting the remaining data with a new line and re-examining the data to see if any other points might still appear to be a pervious event (1 mm above the line). They also consider smaller events on each watershed, where it is likely to have only EIA events, and analyze them separately in order to find the EIA fraction.

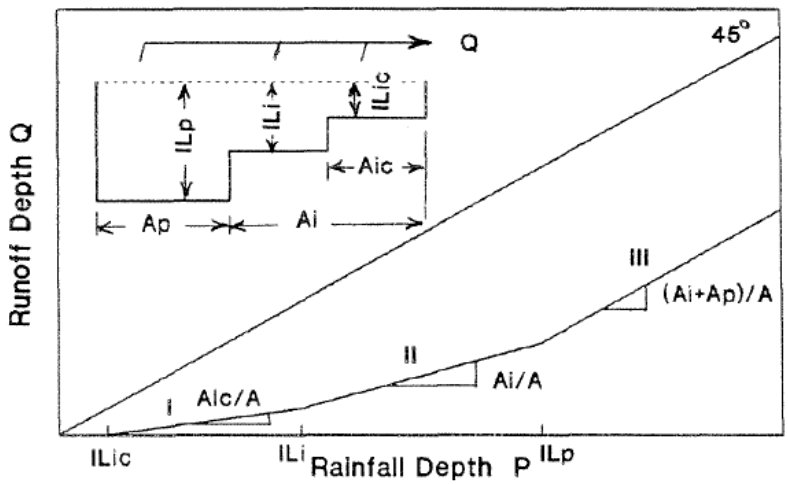

Figure 3.1 Schematic rainfall-runoff relationship (Boyd et al., 1993).

After making several sequential regressions for each watershed during which suspected pervious events are omitted and smaller events are examined, the slope and x-intercept of the regression line are assumed to reflect the f_{EIA} and I_a of the impervious area, respectively. The slope of a regression line fit to the excluded points approximates the contributing area of the combined impervious and pervious runoff events; therefore the difference in slope between this line and the regression line for EIA gives the percent of the watershed that is unconnected impervious plus the percent of contributing pervious surfaces. Significant scatter in these excluded points is generally an indication that the contributing area outside of the effective impervious area (source area) is not consistent, and the initial losses are not fixed. Variable source area and initial losses can be explained by factors like antecedent wetness of the watershed, rainfall intensity, and rainfall duration (Boyd et al., 1993). Since this method is based on successive regressions and an ordinary least square method with a "1 mm" criterion for identifying combined

events among the data points is being utilized, the method is called "Successive Ordinary Least Square (with 1 mm EIA criterion)" or "SOLS (1 mm)" in this study. Figure 3.2 shows the application of the SOLS (1mm) method to a small watershed (MG2) in the City of Maple Grove, MN. As the primary and presumably best method of determining EIA, the method of Boyd, et al. deserves inspection because there are some unaddressed issues that need to be considered.

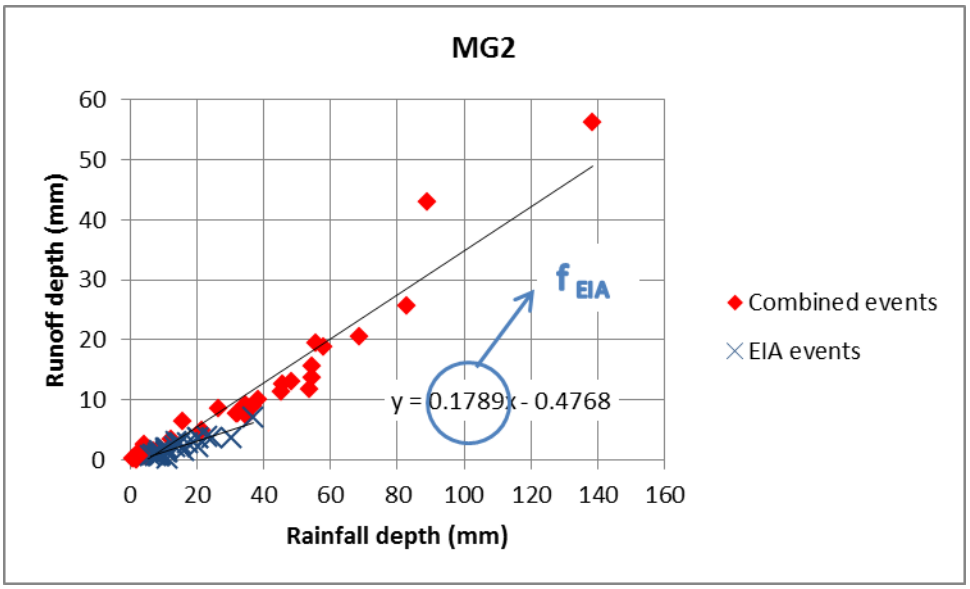

Figure 3.2 Application of the method of Boyd et al. (1993) to the MG2 watershed in Maple Grove, MN. 17.9% of the entire MG2 watershed is hydraulically connected to the drainage system based on this method.

3.3 Issues

By applying the SOLS (1 mm) method to the watersheds of study, different issues associated with the method were identified as follows:

3.3.1 Selection of events

3.3.1.1 Outliers

Failure in monitoring equipment and human errors are common problems especially in the monitoring of storm water runoff volume. Prior to analysis of the rainfall-runoff data, the outliers should be identified and removed from the dataset.

3.3.1.2 Spatial variation of rainfall

Spatial variation of rainfall is a concern, especially in large watersheds. While the SOLS method is highly dependent on an accurate measurement of rainfall within the watershed of study, significant spatial variation of rainfall depth might be present for a given storm (Janke et al., 2011). The depth of each rainfall storm is extracted from continuous rainfall data of a rain gauge in accordance with the corresponding runoff event. In the study of Boyd et al. (1993) there is no discussion on this issue and no procedure for taking the spatial variation of rainfall into account is presented.

3.3.2 Parameter estimation

3.3.2.1 Initial abstraction of impervious surfaces

Utilizing the SOLS method, in some cases, leads to a negative initial abstraction value for the watershed of study (i.e. the x-intercept of the final regression line is negative). We investigated the cases (watersheds) that had a negative x-intercept at the final step of SOLS (1mm) method and found that the negative intercepts are generally small (i.e. close to zero). This is likely because of measurement errors in the precipitation-runoff dataset.

3.3.2.2 EIA criterion

The criterion for identifying combined events among the data points in each step of SOLS method (i.e., EIA criterion) was defined by Boyd et al. (1993) as deviation exceeding 1 mm above the regression line. However, no scientific support has presented for taking the 1 mm value. In addition, the scatter in the data due to the allowable runoff measurement errors has not been considered.

3.3.2.3 Heteroscedasticity

The SOLS method is based on ordinary least square method for estimating f_{EIA} (slope parameter) and I_a (intercept parameter). The relationship for the entire population of rainfall and runoff depth is

$$y_j = \eta_j + \varepsilon_j \tag{3.2}$$

where y_j = dependent variable for the jth observation (runoff depth), ε_j = residual or the random deviation between the linear model and the observation, and η_j = the linear model defined for the population as:

$$\eta_j = \beta_0 + \beta_1(x_j + \varepsilon_{mj}) \tag{3.3}$$

where, ε_{mj} is a random measurement error in x (rainfall depth) for jth event, β_0 and β_1 are the population parameters for f_{EIA} and I_a, and $x_j's$ are the independent variables (rainfall depth).

Equations (3.2) and (3.3) are combined into Eq. (3.4). This equation is a linear model with additive form of errors used by the SOLS method for estimating the regression parameters.

$$y_j = \beta_0 + \beta_1(x_j + \varepsilon_{mj}) + \varepsilon_j \tag{3.4}$$

For n observations, the corresponding linear model in matrix format using a sample of x and y values is defined as Eq. (3.5)(Matrices and vectors are denoted with bold letters).

$$\mathbf{y} = \mathbf{xb} \tag{3.5}$$

where, $\mathbf{y}$ is a n×1 vector of $y_j's$, and $\mathbf{x}$ and $\mathbf{b}$ are defined as:

$$\mathbf{x} = \begin{bmatrix} 1 & x_1 \\ \vdots & \vdots \\ 1 & x_n \end{bmatrix} \tag{3.6}$$

$$\mathbf{b} = \begin{bmatrix} b_0 \\ b_1 \end{bmatrix} \tag{3.7}$$

where b_0 and b_1 are sample estimates of β_0 and β_1 , respectively. For the OLS method, these parameters are estimated by minimizing the sum of the squared residuals (errors).

According to the Gauss-Markov theorem, if a number of statistical assumptions regarding the measurement errors given below are met, the OLS values for b_0 and b_1 are unbiased estimates of β_0 and β_1 and have the minimum variance among all unbiased estimators (Beck and Arnold 1977):

1) Zero random measurement error of x ($\varepsilon_m = 0$);

2) Zero mean errors ($E(\varepsilon_j) = 0$);

3) Normally distributed errors (i.e. $\varepsilon_j's$ have a normal probability distribution);

4) Homoscedasticity or constant variance errors ($VAR\ (\varepsilon_j) = Constant$);

5) Uncorrelated residuals ($COV(\varepsilon_i, \varepsilon_j) = 0$).

where $VAR\ (\varepsilon_j)$ and $COV(\varepsilon_i, \varepsilon_j)$ are variance of ε_j and covariance of ε_i and ε_j , respectively.

The consequence of violating the assumptions 1 to 3 is not generally severe. However, violations of the assumptions 4 and 5 (i.e. heteroscedasticity and correlated residuals, respectively) are important because they increase the uncertainty of estimated parameters (Beck and Arnold, 1977). Our investigation on the Gauss-Markov assumptions through residual plots showed no correlation between residuals in different watersheds. However, several cases of violating the homoscedasticity condition (i.e. presence of heteroscedastic data, or assumption 4) were found. Figure 3.3 shows an example of heteroscedasticity in the MG2 watershed in Maple Grove, MN.

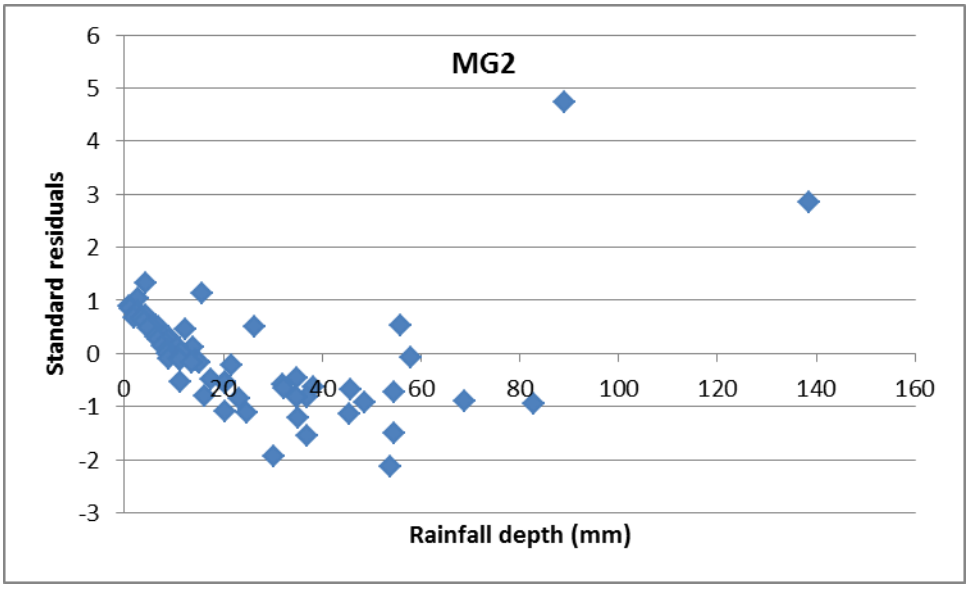

Figure 3.3 Standardized residual plot for the MG1 watershed in Maple Grove, MN. No clear correlation is seen between residuals but residuals do not have a constant variance with rainfall depth, and the condition of homoscedasticity is violated.

3.4 Improvements to the Successive Ordinary Least Squares Method

In order to address the aforementioned issues, improvements have been made to the SOLS method as follows.

3.4.1 Selection of events

3.4.1.1 Removing outliers

Failure in monitoring equipment and human errors are common problems especially in the monitoring of storm water runoff volume. Prior to analysis of the rainfall-runoff data, we utilize a method based on the standardized residual plot for identifying the outliers and removing them from the dataset. First, we draw the standardized residual plot

(standardized residual versus rainfall depth) where the standardized residual for the j-th event (e_j^*) is calculated as

$$e_j^* = \frac{e_j}{\sqrt{MSE}} \quad (j = 1, \dots, n) \tag{3.8}$$

where e_j = residual (error) for the j-th event in dataset (sample estimate of ε_j), which is the difference between the observed value of runoff depth and that predicted by the regression equation, and MSE = residual (error) mean square that is defined as the average squared deviations around the regression line.

$$MSE = \frac{SSE}{n-m} \tag{3.9}$$

where SSE= residual (error) sum of squares, m = number of estimated parameters (here m=2) and n-m is degrees of freedom. Thus, we have

$$MSE = \frac{\sum_{j=1}^{n} e_j^2}{n-2} \tag{3.10}$$

For small rainfall events (e.g. less than 40 mm), all the data points with e_j^* outside the interval [-2, 2] are considered as outliers and removed. However, for the case of large rainfall events (e.g. greater than 40 mm), only the data points with e_j^* less than -2 are removed. The latter is explained by the probability of the existence of combined runoff due to large rainfall events. An example of this method is illustrated in Figure 3.4.

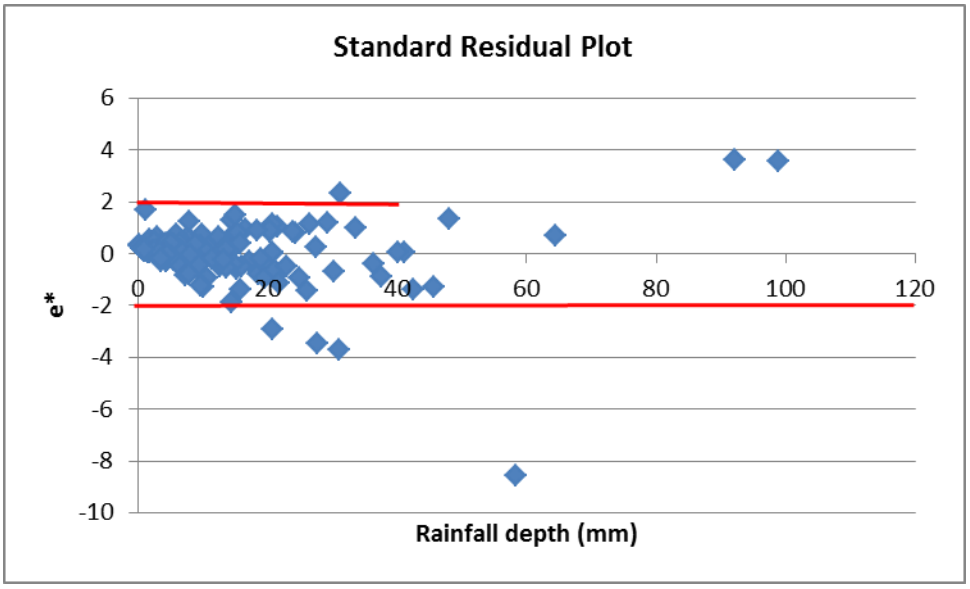

Figure 3.4 The utilized method for removing outliers. The points above the upper red line and below the lower red line in the presented standard residual plot are considered as outliers.

3.4.1.2 Relative root mean square deviation

In order to take into account the spatial variation of rainfall in the watersheds with more than one rain gauge, we propose using relative root mean square deviation (RRMSD) as a measure of spatial variability of rainfall. Assuming N is the number of rain gauges situated inside or closely around the watershed of study (N>1) and subscript i denotes the i-th rain gauge (i=1,2,…,N), we first use the Thiessen polygon technique (Thiessen, 1911) to calculate the weighting factor of each rain gauge. The weighted mean rainfall depth for the j-th event ($j = 1, \dots, n$) in the watershed of study ($\overline{P}_{wj}$) is then determined as

$$\overline{P}_{wj} = \frac{\sum_{i=1}^{N} w_i P_{ij}}{\sum_{i=1}^{N} w_i} \tag{3.11}$$

where w_i = weighting factor of rain gauge i, and P_{ij} = rainfall depth in rain gauge i for the j-th event.

Relative root mean square deviation for the j-th storm in the dataset (i.e. $RRMSD_j$) is computed as

$$\mathrm{RRMSD_j} = \sqrt{\frac{\sum_{i=1}^{N} w_i (P_{ij} - \overline{P}_{wj})^2}{N-1}} \qquad (j = 1, \dots, n) \tag{3.12}$$

RRMSD has a unit of length (e.g. mm). In order to have a measure of spatial variability of rainfall between different rain gauges in a watershed, we define coefficient of spatial variation for the j-th event (CSV_j) as:

$$\mathrm{CSV_j} = \frac{\mathrm{RRMSD_j}}{\overline{P}_{wj}} \qquad (j = 1, \dots, n) \tag{3.13}$$

As an attempt to include more uniform rainfall data in the analysis, we will look for a threshold value for CSV so that we exclude the storm data with high spatial variability (i.e. CSV greater than the threshold value) due to the high uncertainty of the rainfall on the watershed. Each data point is a pair of $(\overline{P}_{wj}, Q_j)$ where Q_j is the runoff depth associated with the j-th event in the dataset for a given watershed. The rainfall-runoff datasets, especially in small urban watersheds, include several small rain events. Since small rainfall depths will have a lower $\overline{P}_{wj}$ and increase CSV_j, a big portion of data might be thrown away. To address this issue, a modified coefficient of spatial variation (MCSV) for each event is introduced as

$$MCSV_j = \frac{RRMSD_j}{\overline{P}_{wj}+k} \qquad (j = 1, \ldots, n) \tag{3.14}$$

where k is a constant with the same unit as $\overline{P}_{wj}$ (e.g. mm). Adding "k" to the denominator of Eq. (3.14) allows for the removal of high spatially variable rainfall events and prevents losing large portions of low rainfall data.

To estimate "k" and a proper threshold value for MCSV, We considered k= 0,1,2,3, and 4 mm and different values between 0.1 and 1.0 as the MCSV threshold and discarded data with an MCSV value greater than the threshold value in each case. We concluded that 2 mm and 0.5 are proper values for "k" and MCSV threshold, respectively, in this study. So, the rainfall data with high spatial variability (i.e. MCSV > 0.5) will be excluded.

3.4.2 Parameter estimation

3.4.2.1 Zero intercept

Cases with a small negative intercept would have a negative initial abstraction. This is not realistic, and the regression lines in the final step of SOLS are forced to go through the origin (i.e. initial abstraction=0). The successive regression process will be continued using the known (zero) intercept until all the data lie within 1 mm (or other distances corresponding to other EIA criteria) above the regression line.

3.4.2.2 Improved EIA criterion

The criterion for identifying combined events (i.e. pervious and non-effective impervious runoff events) among the data points (i.e. EIA criterion) was defined by Boyd et al.

(1993) as a deviation exceeding 1 mm above the regression line. In order to investigate the effect of the EIA criterion value on the results, the method of Boyd et al. was applied to the watersheds of study using different values between 0.5 mm and 2.5 mm as an EIA criterion. While the results of our analysis show that the choice of 1mm is reasonable, it seems that the scatter in the data due to the runoff measurement errors has not been considered in the Boyd et al. method. While a notable part of the scatter of data around the regression line is due to the contribution of non-effective impervious area and pervious area in the runoff generation process (i.e. combined runoff events), another portion is due to runoff measurement errors. In order to address this issue, a new EIA criterion equal to "max (2 SE, 1 mm)" is chosen, where SE stands for the standard error (root mean square error) that is an unbiased sample standard deviation of the residuals in the ordinary least square regression and is defined as

$$\mathrm{SE} = \sqrt{\mathrm{MSE}} \tag{3.15}$$

where MSE is the average squared deviations around the regression line or residual (error) mean square.

The selected EIA criterion which has a minimum value of 1 mm (i.e. Boyd criterion) is equal to the maximum value of 2 SE (in mm) and 1 mm. The outcome of using this new EIA criterion will be presented and discussed in the results section.

3.4.2.3 Weighted least square regression

When the variance of residuals (errors) varies for different events (i.e. heteroscedasticity problem) the OLS estimation technique does not yield minimum variance estimators

(Beck and Arnold, 1977). To account for heteroscedasticity in the dataset, using the weighted least square (WLS) estimation technique instead of OLS is proposed. WLS is used for the case in which the observations (here runoff measurement errors) are uncorrelated but have different variances. Since the values with large variance (i.e. high uncertainty) are less reliable, WLS assigns smaller weights to them and they will have less importance in estimating the regression parameters (i.e. f_{EIA} and I_a). Hence, WLS decreases the uncertainty (variance) of the estimated parameters (Judge et al., 1988). The WLS method, similar to OLS, minimizes the sum of squared errors (SSE). However for the WLS method, the squared residual for each observation is multiplied by an appropriate weight. The SSE for the WLS method is defined as:

$$SSE = \sum_{j=1}^{n} w_j \, {e_j}^2 \tag{3.16}$$

where, w_j is the dimensionless weight for the j-th observation and e_j is the sample estimate of ε_j. It is seen that OLS is a special case of WLS where all the weights are equal. Eq. (3.16) shows that applying the WLS technique to heteroscedastic data results in the regression parameters being defined by weighing the residuals corresponding to their weights, which are inversely proportional to their variances. In the WLS technique, the dimensionless weight for each observation (w_j) is defined as

$$w_j = \frac{\sigma^2}{VAR(\varepsilon_j)} \quad (j = 1, \dots, n) \tag{3.17}$$

where $\mathrm{VAR}(\varepsilon_j) = \sigma_j{}^2 \quad (j = 1, \dots, n)$, σ^2 = constant variance of residuals (ε_j's), and $\sigma_j{}^2$= variance of the j-th observation. In order to estimate the w_j's, we need to find $\mathrm{VAR}(\varepsilon_j)$ values through the variance-covariance matrix of residuals ($E[\varepsilon\varepsilon^T]$) as follows:

$$E[\boldsymbol{\varepsilon\varepsilon^T}] = \begin{bmatrix} VAR(\varepsilon_1) & \cdots & COV(\varepsilon_1, \varepsilon_n) \\ \vdots & \ddots & \vdots \\ COV(\varepsilon_n, \varepsilon_1) & \cdots & VAR(\varepsilon_n) \end{bmatrix} \tag{3.18}$$

where E[ ] denotes the expected value of the argument. For uncorrelated and constant variances, the variance-covariance matrix of residuals is simplified as $E[\boldsymbol{\varepsilon\varepsilon^T}] = \sigma^2\mathbf{I}$ where **I** is the identity matrix. However, having uncorrelated observations with different variances (heteroscedastic dataset) corresponds to the following variance-covariance matrix.

$$E[\boldsymbol{\varepsilon\varepsilon^T}] = \begin{bmatrix} VAR(\varepsilon_1) & \cdots & 0 \\ \vdots & \ddots & \vdots \\ 0 & \cdots & VAR(\varepsilon_n) \end{bmatrix} \tag{3.19}$$

Since the variance-covariance matrix of residuals is not known in this study, the assumption of multiplicative heteroscedasticity in which the variance varies as an exponential function of the independent variable, is made and the unknown weights are estimated accordingly (Judge et al., 1988). Assuming $E[\boldsymbol{\varepsilon\varepsilon^T}] = \sigma^2\boldsymbol{\Psi}$ and using Eq. (3.17), the matrix $\boldsymbol{\Psi}$ is written as a diagonal matrix with diagonal elements as $1/w_j$, $(j = 1, \dots, n)$ and the inverse of this diagonal matrix ($\boldsymbol{\Psi^{-1}}$) will be a diagonal matrix with diagonal elements as w_j , $(j = 1, \dots, n)$. Thus, $\mathbf{b_{wls}}$ can be shown to be as follows:

$$\mathbf{b_{wls}} = (\mathbf{x^T\Psi^{-1}x})^{-1}\mathbf{x^T\Psi^{-1}y} \tag{3.20}$$

where superscripts T and -1 denotes the transpose and inverse of a matrix, respectively.

3.4.2.4 Successive weighted least square (SWLS) method

In order to decrease the uncertainty of f_{EIA} and account for heteroscedasticity in the rainfall-runoff dataset, the weighted least square (WLS) technique will be used in the successive regression process (i.e. successive weighted least square (SWLS) method). SWLS method is recommended when the runoff measurement errors in the dataset are uncorrelated but have different variances. Substituting OLS by WLS and "1 mm" EIA criterion by "max (2 SE, 1 mm)" (as discussed earlier), the general framework of the SWLS method would be similar to the SOLS method. It should be noted that the standard error in WLS (i.e. SE_{WLS}) is based on the transformed variables in the weighted least square method and is different than the SE in OLS. Following Willett and Singer (1988), a "$\mathrm{pseudo}\ SE_{WLS}$" as Eq. (3.21) is proposed to be used in the SWLS method.

$$\mathrm{pseudo}\ SE_{WLS} = \sqrt{\frac{(\mathbf{y}-\mathbf{x}\,\mathbf{b_{wls}})^{T}(\mathbf{y}-\mathbf{x}\,\mathbf{b_{wls}})}{n-m}} \tag{3.21}$$

where m = number of estimated parameters (here m=2). To summarize, the steps of the SWLS method are as follows:

1- Plot runoff depth versus rainfall depth for measurements from each watershed.

2- Fit a regression line using WLS technique to the measured data.

3- Discard the points that are more than "max (2 $\mathrm{pseudo}\ SE_{WLS}$, 1)" mm above the line and recalculate the regression line using WLS.

4- Repeat step 3 until all points above the line are within "SE+1" mm of the line. The slope of the line is equal to f_{EIA}.

3.5 Results

The improvements discussed above have been applied to rainfall-runoff data of all the studied watersheds. As an example, Figures 3.5 and 3.6 show the application of the two discussed methods (i.e. SOLS (1 mm), and SWLS (max (2 pseudo SE_{WLS}, 1mm)) in a small urban catchment (MG1) in Maple Grove, MN. As seen, the EIA fraction has decreased from 0.178 in SOLS (1mm) to 0.117 in SWLS (max (2 pseudo SE_{WLS}, 1mm)) in this case. Also by using the WLS method instead of OLS, the standard deviation of the estimated EIA fraction (as a measure of EIA uncertainty) decreased from 0.027 to 0.013. Similar plots for all the watersheds of study are presented in appendix "A". Table 3.1 presents f_{EIA} and I_a for all the watersheds of study in both discussed methods. In addition, Table 3.2 includes the standard deviation (square root of variance) of the estimated EIA fractions for all the watersheds of study with both OLS and WLS methods.

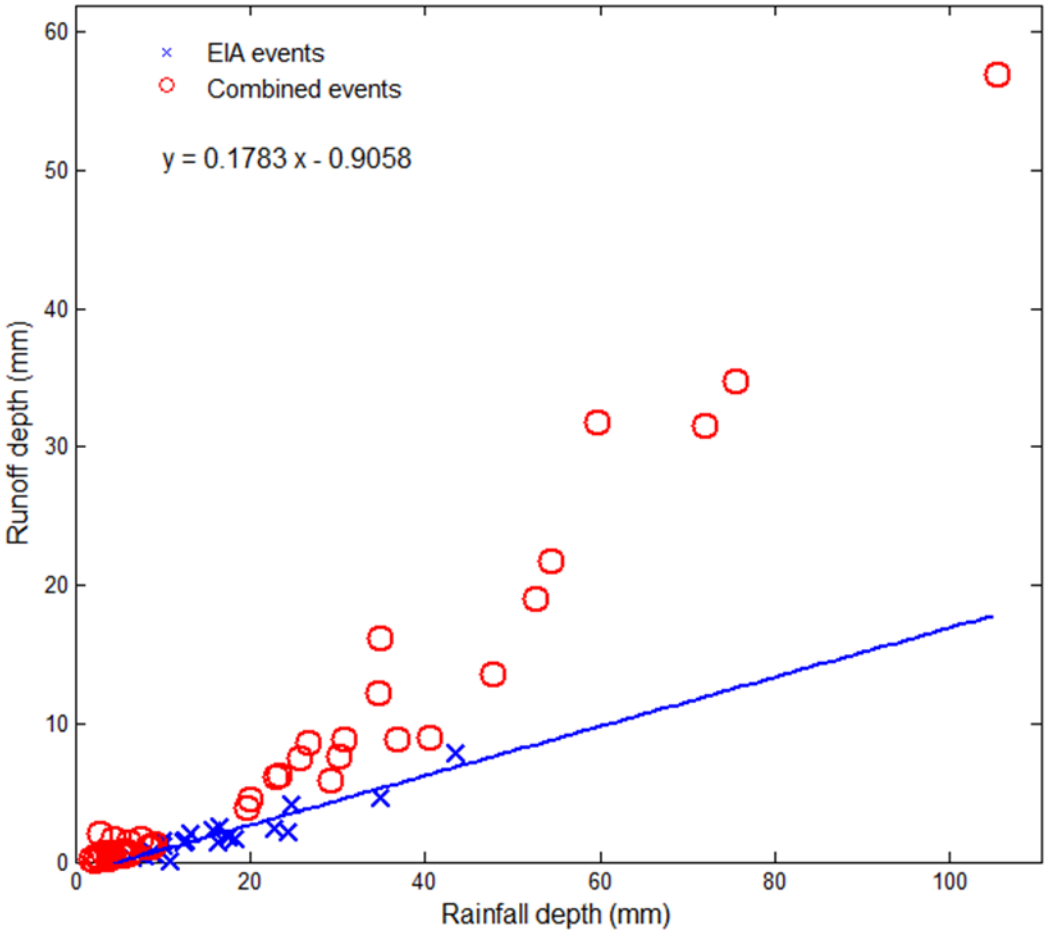

Figure 3.5 Application of the SOLS (1 mm) method to the MG1 catchment in Maple Grove, MN. The graph shows that 17.8% of the entire MG1 area is hydraulically connected to the drainage system based on the SOLS (1 mm) method.

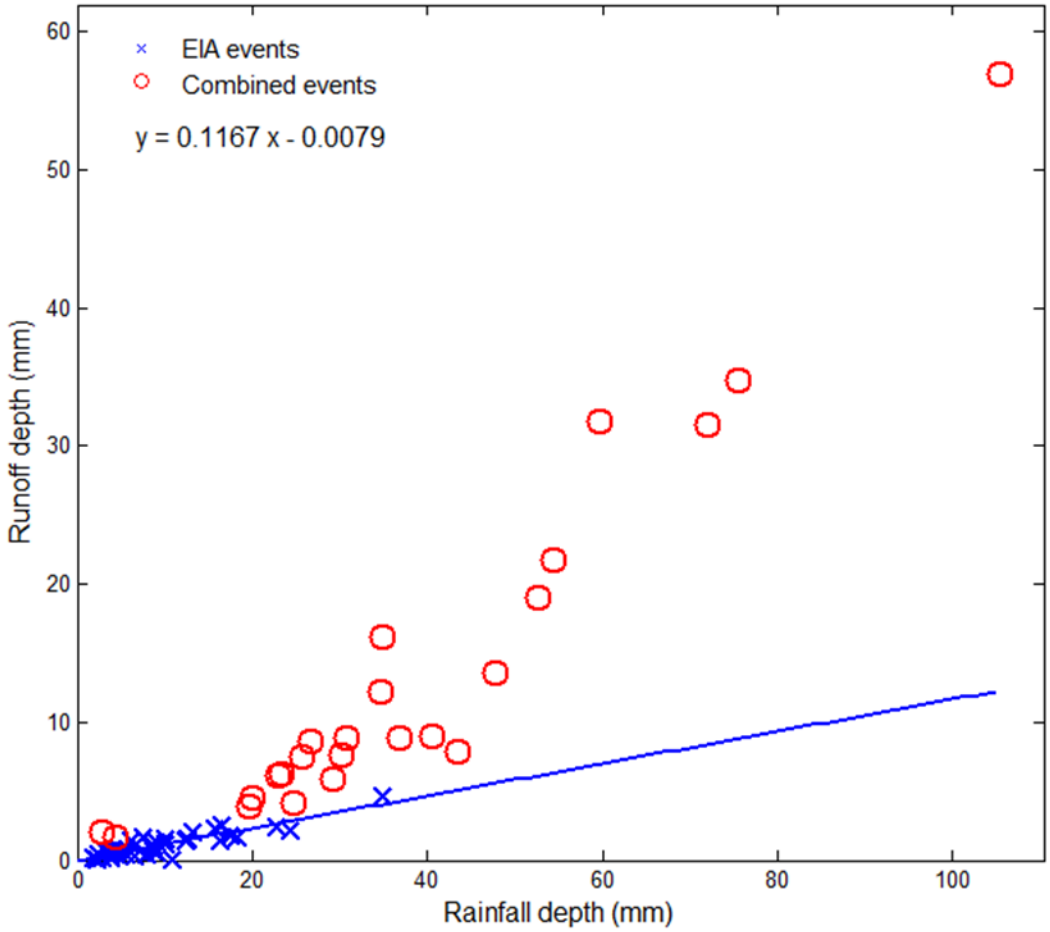

Figure 3.6 Application of the SWLS (max (2 $pseudo\ SE_{WLS}$, 1mm)) method to the MG1 catchment in Maple Grove, MN. The estimated EIA fraction has decreased to 0.117 and less small rainfalls have been categorized as combined events in the SWLS (max (2 $pseudo\ SE_{WLS}$, 1mm)) method. The SWLS method leads to the minimum variance (uncertainty) in the estimated EIA fraction.

Table 3.1 EIA fraction (f_{EIA}) and initial abstraction (I_a) of impervious surfaces for all the watersheds of study in SOLS (1 mm) and SWLS (max (2 $pseudo\ SE_{WLS}$, 1mm)) methods

Row	Monitoring Site Name	SOLS (1 mm)		SWLS (max (2 pseudo SE_{WLS}, 1mm))	
		f_{EIA}	I_a (mm)	f_{EIA}	I_a (mm)
Capitol Region Watershed District, MN					
1	Arlington-Hamline Facility (AHUG)	0.142	0.5	0.137	0.3
2	Como Park Regional Pond inlet	0.224	0.7	0.250	0.6
3	Como 3	0.116	0.8	0.102	0
4	Sarita (inlet)	0.071	4.9	0.030	0.9
5	Trout Brook- East Branch (TBEB)	0.177	0	0.193	0
6	East Kittsondale	0.375	0	0.376	0
7	Phalen Creek	0.273	0	0.310	0
8	St. Anthony Park	0.197	0	0.224	0
9	Trout Brook Outlet	0.191	0	0.284	0
Three Rivers Park District, MN					
10	MG1	0.178	5.1	0.117	0.1
11	MG2	0.179	2.7	0.151	0
12	P1	0.168	2.8	0.204	3.7
13	P2	0.092	0.4	0.089	0
14	P3	0.110	2.6	0.096	0
City of Bloomington, MN					
15	Smith Pond	0.158	12.8	0.076	0
16	Mall of America	0.094	5.7	0.094	5.6
City of Minnetonka, MN					
17	Hedburg Drive	0.532	1.2	0.542	1.1
18	Mayflower Ave (Tapestry)	0.175	2.5	0.169	2.1
City of Madison, WI					
19	Harper Basin	0.293	1.4	0.305	1.6
20	Monroe Basin	0.232	0.6	0.250	1.1
City of Austin, TX					
21	BW1	0.176	2.2	0.152	2.0
22	EBA	0.093	0.2	0.093	0.2
23	EHA	0.346	0.5	0.336	0
24	ERA	0.218	1.8	0.179	0.5
25	HI	0.300	4.9	0.281	0.6
26	HPA	0.292	0.0	0.300	0

Row	Monitoring Site Name	SOLS (1 mm)		SWLS (max (2 pseudo SE_{WLS}, 1mm))	
		f_{EIA}	I_a (mm)	f_{EIA}	I_a (mm)
27	LCA	0.066	0.8	0.064	0.3
28	LOA	0.251	1.4	0.196	0
29	LUA	0.448	0.7	0.484	0.5
30	MBA	0.307	8.0	0.322	1.7
31	OFA	0.588	8.8	0.452	0.8
32	PP1	0.322	3.0	0.229	0.6
33	PP2	0.277	0.7	0.270	0.3
34	PP3	0.147	0.0	0.172	0
35	RRI	0.106	0.2	0.107	0
36	SCA	0.176	1.1	0.157	0.6
37	TBA	0.140	1.6	0.106	0.4
38	TCA	0.107	3.3	0.097	1.9
39	TPA	0.202	3.9	0.142	1.1
40	WBA	0.391	0.7	0.387	0

Table 3.2 Standard deviation of the estimated EIA fractions ($s(f_{EIA})$) for all the watersheds of study in both OLS and WLS methods

Row	Monitoring Site Name	s (f_{EIA})	
		SOLS	SWLS
Capitol Region Watershed District, MN			
1	Arlington-Hamline Facility (AHUG)	0.012	0.006
2	Como Park Regional Pond inlet (GCP)	0.020	0.012
3	Como 3	0.014	0.003
4	Sarita (inlet)	0.047	0.005
5	Trout Brook- East Branch (TBEB)	0.014	0.006
6	East Kittsondale	0.018	0.011
7	Phalen Creek	0.018	0.008
8	St. Anthony Park	0.014	0.007
9	Trout Brook Outlet	0.034	0.012
Three Rivers Park District, MN			
10	MG1	0.027	0.013
11	MG2	0.044	0.009
12	P1	0.007	0.007
13	P2	0.016	0.005

Row	Monitoring Site Name	s (f_{EIA})	
		SOLS	SWLS
14	P3	0.010	0.006
City of Bloomington, MN			
15	Smith Pond	0.025	0.009
16	Mall of America	0.005	0.005
City of Minnetonka, MN			
17	Hedburg Drive	0.018	0.015
18	Mayflower Ave (Tapestry)	0.020	0.013
City of Madison, WI			
19	Harper Basin	0.028	0.016
20	Monroe Basin	0.015	0.011
City of Austin, TX			
21	BW1	0.014	0.010
22	EBA	0.010	0.003
23	EHA	0.007	0.004
24	ERA	0.023	0.008
25	HI	0.050	0.025
26	HPA	0.017	0.009
27	LCA	0.016	0.004
28	LOA	0.012	0.007
29	LUA	0.023	0.015
30	MBA	0.056	0.025
31	OFA	0.037	0.033
32	PP1	0.023	0.014
33	PP2	0.024	0.010
34	PP3	0.012	0.006
35	RRI	0.008	0.005
36	SCA	0.015	0.007
37	TBA	0.052	0.006
38	TCA	0.033	0.010
39	TPA	0.014	0.008
40	WBA	0.010	0.007

3.6 Discussion

Forty monitored watersheds with different sizes and hydrological conditions were analyzed in this study. Eighteen are located in Twin Cities metro area, the first nine in Capitol Region Watershed District (CRWD), the next five in Three Rivers Park District (TRPD), and the last four in the City of Minnetonka and the City of Bloomington. Two watersheds are located in the City of Madison, WI and the remaining twenty watersheds in the City of Austin, TX. In order to provide a better understanding of the urban runoff mechanisms, the analysis has been performed on a wide range of watershed areas from less than 1 ha to 2,035 ha.

The analysis was started by applying the SOLS (1mm) method to our dataset. Using this method, f_{EIA} values ranged from 0.07 to 0.59. At one extreme are LCA in Austin, TX and Sarita in Ramsey County, MN with a f_{EIA} of only 0.07, and at the other extreme are OFA in Austin, TX and Hedburg in Minnetonka, MN with a f_{EIA} of 0.59 and 0.53, respectively. The main land use of the LCA watershed in single family residential and the TIA fraction is 0.225 in this watershed. Also, the main land use within the Sarita watershed is institutional. The fraction of TIA in the watershed is about 0.37 and it encompasses the Minnesota State Fair grounds and open spaces in the University of Minnesota St. Paul Campus. In contrast, both OFA and Hedburg are watersheds with commercial land use and high density of roadways, sidewalks, and parking lots. Total impervious areas form about 86% and 88% of these watersheds, respectively. The average, median, and standard deviation of f_{EIA} for all the forty watersheds of study are 0.223, 0.185, and 0.121, respectively in the SOLS (1 mm) method.

At the next step, the method proposed herein, SWLS (max (2 SE, 1 mm)), was applied to our monitored watersheds. The minimum and maximum f_{EIA} in this method are 0.03 and 0.54, respectively. The minimum EIA fraction value is the Sarita watershed. This value for the LCA is 0.064 which is close to that in the previous method (i.e. 0.07). With regard to the maximum f_{EIA} in this method, the Hedburg watershed in the city of Minnetonka, MN still has a maximum f_{EIA} of about 0.54 in the SWLS (max (2 SE, 1 mm)) method but the EIA fraction of the OFA watershed has decreased to 0.45 in this method. Also, the f_{EIA} value in the LUA watershed in Downtown Austin, TX with a mixed commercial and residential land use is 0.48. The EIA fraction for LUA in the SOLS (1 mm) method was found to be 0.45. The average, median, and standard deviation of f_{EIA} for all the forty watersheds of study are 0.213, 0.186, and 0.122, respectively in our proposed SWLS (max (2 SE, 1 mm)) method.

Table 3.2 presents the uncertainty of f_{EIA} estimates in both the original Boyd et al. (1993, 1994) method (based on OLS) and our proposed method (based on WLS). Standard deviation (square root of the variance) of the f_{EIA} estimates (i.e. $s(f_{EIA})$) has been used as a measure of uncertainty of f_{EIA} estimates. The results reveal that the proposed SWLS method has reduced $s(f_{EIA})$ by 48% on average which should lead to more accurate f_{EIA} estimates. To compare the results of the WLS and OLS methods, f_{EIA} in the SWLS method is plotted against f_{EIA} in the SOLS method in Figure 3.7. It is seen that SWLS results can be both higher and lower than SOLS. The average, median, and standard deviation of f_{EIA} for all the forty watersheds of study are fairly similar in the SWLS and SOLS methods and the average absolute value of difference between the corresponding

f_{EIA} values in the two methods is 0.03. Figure 3.7 shows the agreement between the results of the two methods. Also, the plots of runoff depth against rainfall depth in the appendix "A" show that in many cases SWLS reduces the number of combined events in lower rainfall depths. It is concluded that while the SWLS produces results that can be both higher and lower than SOLS, it reduces the uncertainty in individual EIA fraction estimates. Finally, Smith pond watershed in Bloomington, MN gave an unexpected high initial abstraction (I_a) value of 12.8 mm in the SOLS (1 mm) method. However, it decreased to zero in the proposed SWLS (max (2 SE, 1 mm)) method. This change in initial abstraction value can be explained by the runoff depth versus rainfall depth plots for this watershed in appendix "A". In the SOLS plot, some combined events are seen in rainfall depths less than the initial abstraction value that cannot be correct. This issue is resolved in the SWLS plot where no combined event is seen in smaller rainfall depths. The average, median and standard deviation of I_a values for all forty watersheds of study in our proposed SWLS method are 0.7, 0.3, and 1.1 mm, respectively. The I_a values range up to 5.6 mm in the proposed SWLS method which is in a good agreement with Boyd et al.'s (1993) results (i.e. range up to 6 mm).

Runoff events are divided into two categories, EIA and combined, as the outcome of the applied methods. Figures in appendix "A" show this categorization in each of the forty watersheds of study. Comparing the plots of the proposed SWLS method with the original SOLS method, fewer small events were seen to be categorized as combined events with the SWLS method, which indicates a more reliable result. Combined runoff events are present for all the watersheds except MOA, Hedburg, Harper, and Monroe,

which is explained by the limited number of events and small rainfall depths in these watersheds. The exception is Mall of America (MOA) watershed, which had a large storm with depth of 123 mm categorized as EIA event in both methods. The dominant land use in MOA is commercial with lots of parking and roads associated with the Mall of America shopping center. The temporal distribution of rainfall depths during this large storm may explain the relatively small fraction of runoff (Wilson et al. 2007). This issue as well as the limited number of monitored events in MOA may explain the absence of combined events in this catchment.

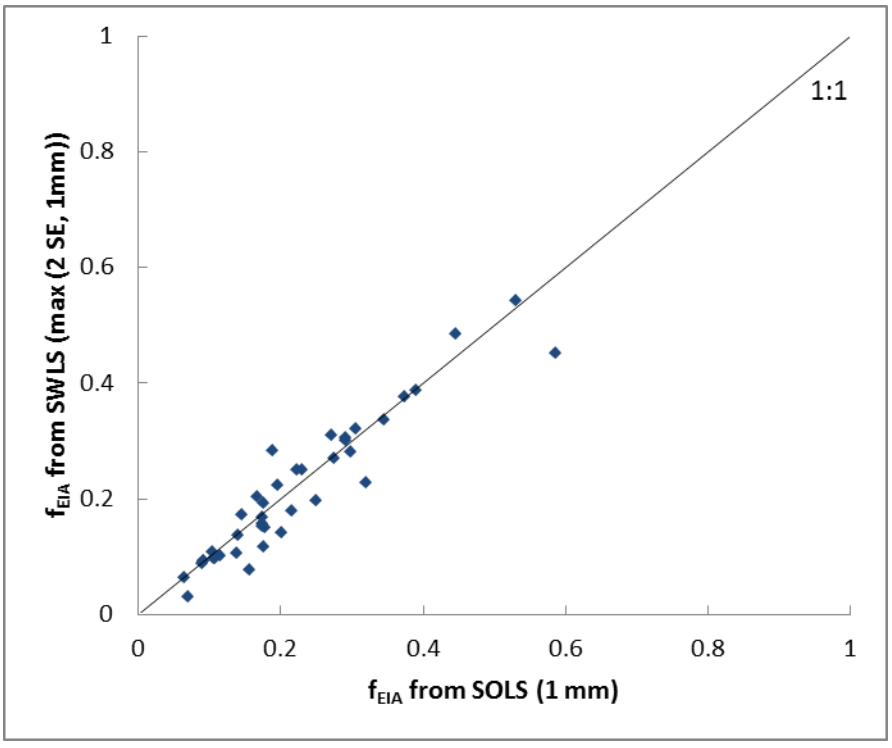

Figure 3.7 EIA fraction in the SWLS (max(2 SE, 1mm)) method versus EIA fraction in the SOLS (1 mm) method. A good agreement is seen between the results of the two methods.

CHAPTER 4: GIS INFORMATION

4.1 Need

One of the key steps in this study is to collect and refine the required GIS information for watersheds of study. As discussed before, we will use the Curve Number (CN) as an index to capture the runoff characteristics of watersheds in our method for determining EIA in ungauged watersheds. Determining this index is therefore a necessary component of the study. Another important activity is determining the extent that the impervious surfaces in the watersheds are hydraulically connected to the drainage system. To address this question, the ratio of EIA/TIA in a watershed will be calculated. The key components of this chapter are to (1) collect and organize the GIS layers for our watersheds, (2) develop and evaluate routines to remove tree cover, (3) analyze the GIS layers for application to our study, and (4) calculate the ratio of EIA/TIA for the watersheds of study. Our activities for these components are summarized into separate sections. In the next step of the study (chapter 5), the refined GIS information along with the results of the rainfall-runoff data analysis will be used to develop a new method for determining effective impervious area in ungauged watersheds.

4.2 Organization of GIS Layers

4.2.1 GIS information sources

The required GIS information for this study includes land cover and hydrologic soil group layers. The following sections discuss the sources for the GIS layers.

4.2.1.1 Land cover

The Department of Forest Resources, University of Minnesota has developed the required land cover data for the cities of Minneapolis and Saint Paul, MN. This dataset has been prepared as part of a project to classify tree canopy coverage in Minneapolis (Bauer et al., 2011) and Saint Paul (Kilberg et al., 2011). It has been derived from a combination of high resolution multi-spectral satellite imagery and LiDAR-based elevation data. The resulting land cover layer consists of 0.6 m-square pixels, classified into seven cover types: (1) tree canopy, (2) grass/shrubs, (3) bare soil, (4) water, (5) buildings (rooftop), (6) Streets, and (6) other impervious area (parking lots, drive ways, etc.). This dataset contains the Capitol Region Watershed District (CRWD), so this land cover layer was used for the watersheds in CRWD, MN. Land cover/ land use layers for the watersheds in Austin, TX were provided by the City of Austin Watershed Protection Department. For the other watersheds, we extracted the required land cover data from the National Land Cover Database (NLCD). The NLCD land cover layer was produced through a cooperative project conducted by the Multi-Resolution Land Characteristics (MRLC) Consortium (http://www.mrlc.gov/). The MRLC consortium is a group of federal agencies including USGS, EPA, and other entities that coordinate and generate consistent and relevant land cover information from Landsat satellite imagery and other supplementary datasets at the national scale for a wide variety of environmental, land management, and modeling applications. The NLCD is distributed as 30-m-resolution raster images and classified into five cover types based on percent total impervious cover, land use and vegetation in urban (developed) areas: (1) open water, (2) open space, (3)

low intensity areas, (4) medium intensity areas, and (5) high intensity areas. Other cover types are also available in NLCD land cover layers for undeveloped areas.

4.2.1.2 Hydrologic soil group

The United States Department of Agriculture (USDA) - Natural Resource Conservation Service (NRCS) classifies soils in the US into four Hydrologic Soil Groups (HSG): A, B, C and D. Hydrologic soil groups are based on estimates of runoff potential, where the soils in group A have the smallest runoff potential and group D the greatest. TR-55 (USDA, 1986) contains the details of this classification.

In the USA, soil survey data are available in digital formats from NRCS Soil Survey Geographic (SSURGO) database. The SSURGO database contains information about soils as collected by the National Cooperative Soil Survey over the course of a century. SSURGO data can be downloaded in ESRI Shape file format from the NRCS Web Soil Survey (http://websoilsurvey.sc.egov.usda.gov/App/HomePage.htm). The SSURGO database for HSG in the watersheds of study was used in this study.

The SSURGO database is a general view of the soils in a region, and urban soils are known for being disturbed and redistributed. Even so, transportation costs will typically dictate that disturbed and redistributed soils do not come from areas that are remote to the watershed, and SSURGO is the best source available to all watersheds.

4.3 Tree Canopies

Tree canopy in an urban land use comprises leaves, branches and stems of trees that cover the ground when viewed from above (Bauer et al., 2011). High canopy coverage in an urban area causes some impervious feature shapes (e.g. roads and buildings) to be hidden from satellite view. This creates challenges in identifying those impervious surfaces from aerial photographs and/or satellite imagery. The trees and associated canopy make the impervious area, particularly streets, to be obscured, ranging from partially shadowed to completely undetectable (Cablk and Minor, 2003). Consequently, it may result in underestimation of total impervious area (TIA) because those impervious features may not be detected below the canopy (Janke et al., 2011). It is for this reason that tree canopy has been identified as a major factor of inaccuracies in observed TIA (Han and Burian, 2009). Since tree canopy can obscure significant portions of impervious surfaces (especially roads), it may disconnect roads into some 'pockets' rather than having a continuous linear shape. To address this issue, the land cover layer should be modified by un-shading the impervious surfaces that have been obscured by tree canopy. Un-shading the impervious surfaces removes the tree cover that obscured those surfaces and changes the classification of the surface in land cover layer from 'tree canopy' to the original impervious surface (e.g. street, rooftop, etc.).

As previously discussed, the land cover layer including tree canopy classification is available for the catchments in CRWD, MN. Also another GIS layer containing all the impervious surfaces (i.e. streets, alleys, rooftops, parking lots, etc.) is available for the CRWD catchments. We developed a method in ArcGIS for un-shading the impervious

surfaces. This method is introduced in the next section and the results of its application to the CRWD catchments are shown in the following section.

4.3.1 Un-shading procedure

Assuming an impervious layer (in vector format) is available as well as a land cover layer (in raster format) for the watersheds of study and both layers have the same coordinate system, the impervious layer can be used to un-shade the land cover layer. The developed procedure for un-shading the land cover layer in ArcGIS environment contains the following steps.

1) Separate different impervious surfaces in the impervious layer.

   Each impervious surface (e.g. roads, alleys, parking lots, structures, etc.) is saved as a new shape file in vector (polygon) format.

2) Convert impervious layers from vector to raster format.

   All the impervious layers (output of step 1) are converted to raster format using the 'conversion tools' supplied with ArcGIS.

3) Assign new values to impervious pixels in raster impervious layers.

   The original values of different land cover types in the land cover layer are as following:

   Tree canopy=1, Grass/Shrub=2, Bare soil=3, Water=4, Buildings=5, Streets=6, Other impervious surfaces=7. New values will be assigned to each impervious pixel in raster impervious layers (output of step 2) as following:

   Structures=50, Roads=60, Alleys=60, Other impervious area=70. This assignment is performed using 'Reclassify' command in the 'Spatial Analyst Tools'.

4) Overlay raster layers.

   The reclassified impervious layers (output of step 3) and the original land cover layer are overlaid using an additive overlay analysis in the 'Spatial Analyst Tools' to obtain a new land cover layer.

5) Assign new values to the new land cover layer.

   In the new land cover layer (output of step 4), all the pixels with values 1 to 7 will be kept the same. Other values greater than 7 will be changed to a proper impervious surface value (5, 6, or 7) according to the type of impervious surfaces using 'Reclassify' command in the 'Spatial Analyst Tools'.

4.3.2 Un-shading results

The proposed un-shading procedure were applied to all the watersheds of study in CRWD, MN and the percent TIA were measured in both original and modified (un-shaded) land cover layers. The TIA values (in percent) for both original and un-shaded land cover are shown in Table 4.1 for all the CRWD watersheds. Table 4.1 shows that un-shading the impervious surfaces has resulted in an average increase of 21% in TIA in CRWD watersheds. The maximum and minimum TIA increase (29% and 6%) has happened in Golf Course Pond (GCP) and Sarita, respectively. It is explained by the amount of tree canopy overhanging the streets and other impervious area in these watersheds. The un-shading results were not ground truthed though. As an example, Figure 4.1 shows the original and modified land cover in Golf Course Pond (GCP) watershed. Due to lack of tree cover layer, the un-shading technique was not applied to the watersheds in the Three Rivers Park District, MN and TIA fractions were extracted

from their technical reports (Barten et al. 2006). This may not make an issue because all the study sites in this watershed have small drainage areas. For the watersheds in Austin, TX, TIA fractions have been determined using planimetric maps developed from aerial photographs by Glick et al. (2009). The impervious surfaces that can be identified in those planimetric maps are buildings, roads, parking lots, driveways longer than 100 feet, and impervious sports courts. To consider the effect of sidewalks and driveways shorter than 100 feet, individual parcels of different land uses were sampled by the City of Austin staff, the results were compared with the aerial photographs, and TIA fractions were modified accordingly (Glick et al. 2009). f_{TIA}values for the study sites in Minnetonka, MN and Madison, WI were determined based on the land cover data which did not need un-shading. TIA fractions were not determined for the sites in Bloomington, MN due to lack of access to the delineation of drainage areas.

Table 4.1 Percent TIA in the CRWD watersheds in both original and modified (un-shaded) land cover

Watershed name	Land cover (original)	Land cover (un-shaded)
AHUG	41	51
GCP	34	44
Como 3	33	40
Sarita	35	37
TBEB	37	45
EK	46	56

Watershed name	Land cover (original)	Land cover (un-shaded)
PC	48	59
SAP	48	61
TBO	40	47

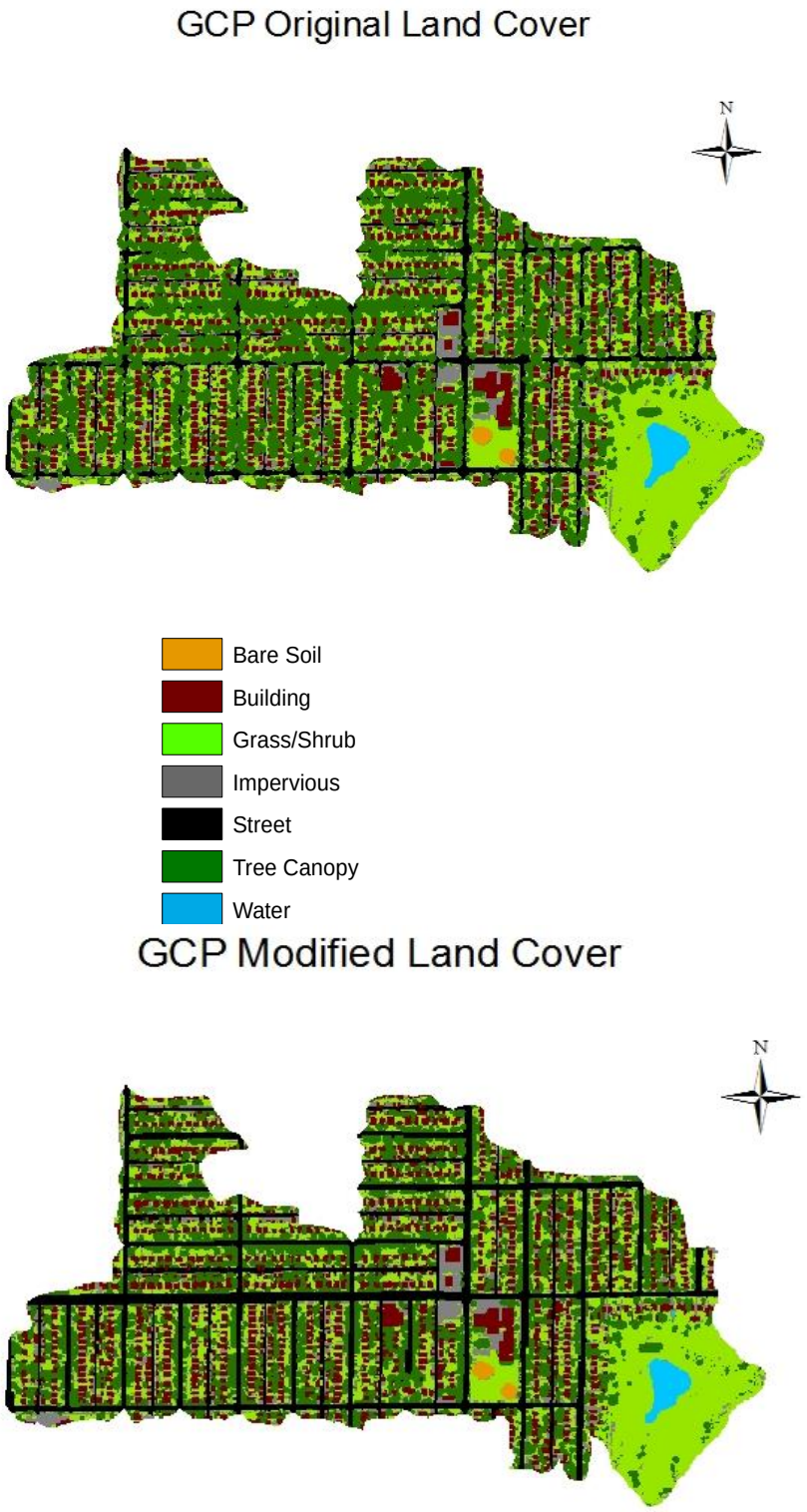

Figure 4.1 Original and modified land cover in GCP watershed. TIA increased from 34% to 44% in this watershed due to the un-shading process.

4.4 Analysis of GIS Information

After collecting land cover and soil layers from the introduced sources, we focused on each watershed separately. In order to obtain the GIS information for each watershed of study, the land cover and soil data were 'clipped' using the watershed-boundary layers in ArcGIS. The detailed analysis of land cover (un-shaded) and soil data was then performed for all the watersheds of study. An example of this analysis for Phalen Creek (PC) watershed is presented in the following sections. The PC watershed has an area of 580 ha and is located in CRWD, MN.

4.4.1 Example of land use analysis

Figure 4.2 shows the un-shaded land cover of PC. The distribution of different surfaces in this watershed is extracted from the PC land cover layer and presented in Table 4.2.

Table 4.2 Distribution of different surface covers in Phalen Creek (PC) watershed

Cover Name	**Area (ha)**	**Percent**
Tree Canopy	137.6	23.74
Grass/Shrub	98.9	17.06
Bare Soil	3.0	0.53
Water	0.2	0.03
Building (Rooftop)	128.8	22.22
Street and Alleys	98.4	16.97
Other Impervious	112.8	19.46
Total	580	100

As seen in Table 4.2, impervious surfaces in this watershed comprise rooftops, streets and alleys, and other impervious area (e.g. parking lots and drive ways) with about 22%, 17% and 19% of the watershed area, respectively. The sum of these three impervious components is the total impervious area in this watershed which is about 340 ha or 59% of the total watershed area.

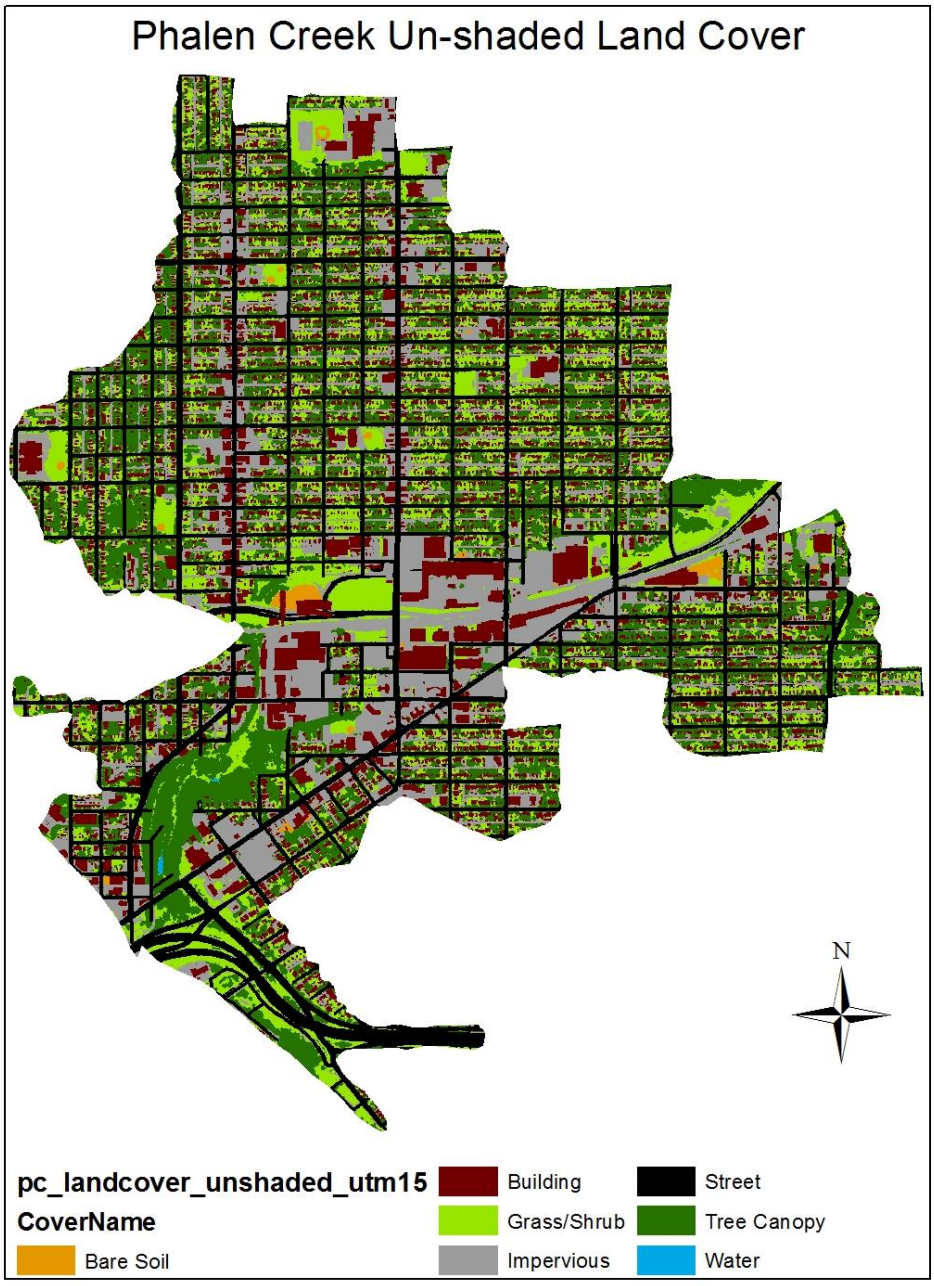

Figure 4.2 Modified (Un-shaded) land cover in PC watershed.

4.4.2 Example of soil analysis

Hydrologic soil groups in the PC watershed from the SSURGO database are shown in Figure 4.3. The percent of different soil groups in this watershed is extracted from the PC land cover layer and presented in Table 4.3.

Table 4.3 Percent of different hydrologic soil groups in Phalen Creek (PC) watershed

Hydrologic Soil Group	**Area (ha)**	**Percent**
A	252.3	43.53
B	327.3	56.46
B,B/D	0.1	0.01
Total	580	100

Table 4.3 reveals that more than half of the soil in PC watershed is in group B and the remaining part of the soil is classified as group A. This generally means that there is a good infiltration capacity through the soil in pervious areas of this watershed, which makes the runoff potential low in those areas. A very small percent of the PC soils (i.e. 0.01%) contains a mix of group B and dual hydrologic soil group of B/D which has been considered as group B in CN calculations.

4.5 Determination of Curve Number (CN)

One objective of the GIS analysis in this study is to obtain the composite curve number (CN_{comp}) for each watershed of study. CN_{comp} is the area weighted average CN for a watershed that has traditionally been used in rainfall-runoff studies of watersheds. GIS is used for determining CN in order to keep the details of the spatial variation of watersheds

characteristics (i.e. land cover and hydrologic soil groups). After obtaining land cover and soil layer for each watershed, we use the standard geo-processing technique of 'intersection' to intersect land cover and soil layers and generate a new layer, called 'landsoil'. The obtained 'landsoil' layer has smaller polygons associated with land cover types and hydrologic soil groups that keep the details of the spatial variation of land cover and soil information (Zhan and Huang, 2004). The curve number for each polygon in the 'landsoil' is then determined from the land cover and soil information and using the tabular values for CN in Table 2-2a of the USDA_NRCS TR-55 (USDA, 1986) that is recommended for CNs in urban areas. The CN determination is based on matching the land cover types in the watershed of study with those of the TR-55 CN table and then assigning a CN value to each polygon accordingly. This step was performed using a GIS tool called SARA v1.0 (Hernandez-Guzman and Ruiz-Luna, 2013). The CN database in SARA v1.0 includes the CN table of TR-55. However, we modified this database by adding interpolated rows to the TR-55 CN table. For example, TIA in Phalen Creek (PC) watershed is 59% which is not available in the Table 2-2a of TR-55. Therefore, based on the assumptions behind this CN table and using the CN values of pervious area (i.e. open spaces in good condition) and impervious area (i.e. residential districts with 65% and 38% impervious area) CN values for residential areas in PC were generated as 74,83,88, and 91 for hydrologic soils groups A, B,C, and D, respectively. In order to reduce processing time in ArcGIS, especially for larger watersheds with a wide variety of land cover types, we can use the 'dissolve' technique in ArcGIS to combine the land cover and soil layers before intersection based on their land cover and soil group attributes (Zhan and Huang, 2004). Once proper CN values assigned to each polygon in the 'landsoil'

layer, the CN_{comp} is calculated as area weighted average CN for the watershed of study as Equation 4.1:

$$CN_{comp} = \frac{\sum_{i=1}^{N} CN_i \times A_i}{A_{total}} \quad (4.1)$$

Where, CN_i is the tabular CN of polygon i, A_i is the area of polygon i, A_{total} is the total area of the watershed, and N is the number of polygons in the 'landsoil' layer.

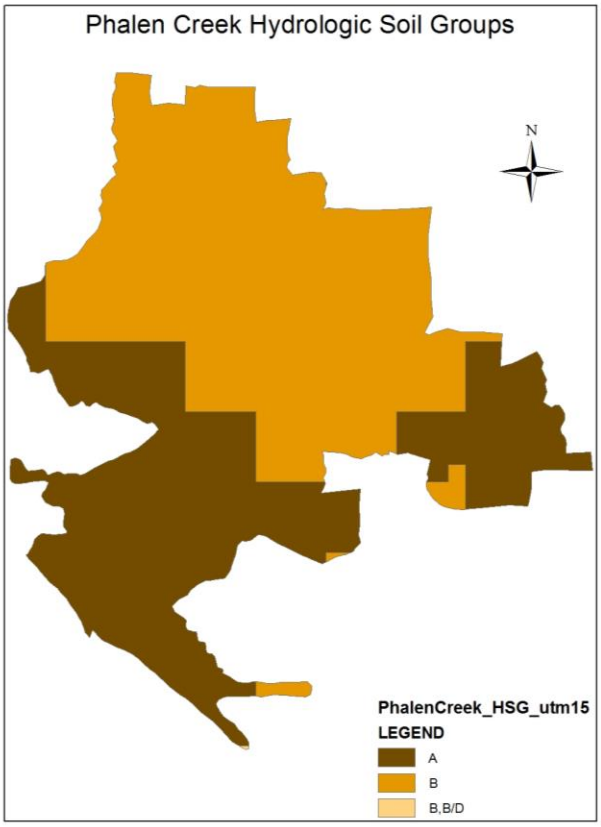

Figure 4.3 Hydrologic soil groups in the Phalen Creek (PC) watershed.

4.5.1 Example of Curve Number determination

The results of the application of the aforementioned method for finding CN_{comp} in the PC watershed are presented in this section. Both of the land cover and soil layers of PC were loaded into ArcGIS and then intersected to generate the PC 'landsoil' layer. Assigning the CNs to each polygon in the 'landsoil' layer was performed using SARA v1.0. Figure 4.4 shows the main screen of this tool that is used for PC watershed. As seen in Figure 4.4, 'Tree canopy' cover type in PC has been matched with residential districts with 59% impervious area in TR-55 CN table. 'Grass/Shrub' cover in PC is considered as open space with a fair condition. 'Bare soils' in PC is paired with 'Newly graded urban areas' in TR-55. A curve number of zero is considered for all 'waters' in PC. Finally, a curve number of 98 is assigned to all the impervious surfaces in PC (i.e. 'Buildings', 'Streets' and 'Other impervious area') according to the TR-55 CN database. The resulted CN values for each pair of land cover type and hydrologic soil group in the PC watershed are presented in Table 4.4. Using Equation 4.1 and the information in Table 4.4, CN_{comp} for PC watershed is calculated as 87.

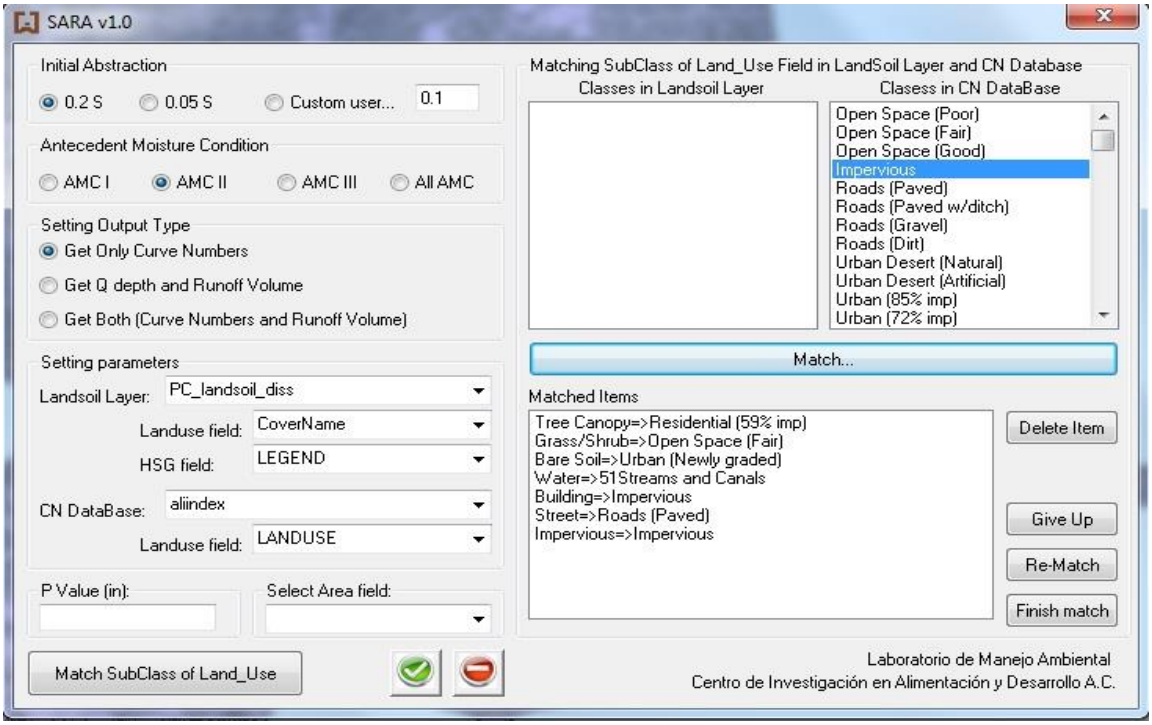

Figure 4.4 Main screen of SARA v1.0 with PC information.

Table 4.4 Curve Number values corresponding to different group of polygons in the 'landsoil' layer of the Phalen Creek (PC) watershed

Cover Name	Hydrologic Soil Group	Area (ha)	CN
Tree Canopy	A	63.8	74
Tree Canopy	B	73.8	83
Grass/Shrub	A	43.1	49
Grass/Shrub	B	55.7	69
Bare Soil	A	1.0	77
Bare Soil	B	2.1	86
Water	A	0.2	0

Cover Name	Hydrologic Soil Group	Area (ha)	CN
Building	A	50.7	98
Building	B	78.1	98
Street	A	46.3	98
Street	B	52.0	98
Other Impervious	A	47.3	98
Other Impervious	B	65.5	98

4.6 Determination of the EIA/TIA Ratio

Another objective of the GIS analysis in this chapter is to calculate the EIA/TIA ratio fraction for the study sites. Table 4.5 presents the TIA fractions for all the forty watersheds of study. In order to calculate the ratio of EIA/TIA in the study sites, the EIA fraction values from our proposed SWLS method (discussed in chapter 3) are also included in Table 4.5. The last column of Table 4.5 contains the values of EIA/TIA ratio for all the study sites.

Table 4.5 The ratio of EIA/TIA for all the study sites. f_{EIA} values are based on the proposed SWLS method.

Row	Monitoring Site Name	f_{TIA}	f_{EIA}	EIA/TIA
Capitol Region Watershed District, MN				
1	Arlington-Hamline Facility (AHUG)	0.507	0.137	0.27
2	Como Park Regional Pond inlet (GCP)	0.438	0.250	0.57

Row	Monitoring Site Name	f_{TIA}	f_{EIA}	EIA/TIA
3	Como 3	0.405	0.102	0.25
4	Sarita (inlet)	0.367	0.030	0.08
5	Trout Brook- East Branch (TBEB)	0.447	0.193	0.43
6	East Kittsondale	0.562	0.376	0.67
7	Phalen Creek	0.587	0.310	0.53
8	St. Anthony Park	0.613	0.224	0.36
9	Trout Brook Outlet	0.473	0.284	0.60
Three Rivers Park District, MN				
10	MG1	0.405	0.117	0.29
11	MG2	0.388	0.151	0.39
12	P1	0.380	0.204	0.54
13	P2	0.351	0.089	0.25
14	P3	0.273	0.096	0.35
City of Bloomington, MN				
15	Smith Pond	#N/A	0.076	#N/A
16	Mall of America	#N/A	0.094	#N/A
City of Minnetonka, MN				
17	Hedburg Drive	0.877	0.542	0.62
18	Mayflower Ave (Tapestry)	0.237	0.169	0.71
City of Madison, WI				
19	Harper Basin	0.338	0.305	0.90
20	Monroe Basin	0.381	0.250	0.66
City of Austin, TX				
21	BW1	0.460	0.152	0.33
22	EBA	0.404	0.093	0.23
23	EHA	0.434	0.336	0.77
24	ERA	0.460	0.179	0.39
25	HI	0.500	0.281	0.56
26	HPA	0.450	0.300	0.67
27	LCA	0.225	0.064	0.28
28	LOA	0.422	0.196	0.46
29	LUA	0.974	0.484	0.50
30	MBA	0.609	0.322	0.53
31	OFA	0.862	0.452	0.52
32	PP1	0.497	0.229	0.46
33	PP2	0.511	0.270	0.53
34	PP3	0.494	0.172	0.35
35	RRI	0.305	0.107	0.35

Row	Monitoring Site Name	f_{TIA}	f_{EIA}	EIA/TIA
36	SCA	0.409	0.157	0.38
37	TBA	0.452	0.106	0.23
38	TCA	0.374	0.097	0.26
39	TPA	0.415	0.142	0.34
40	WBA	0.306	0.387	1.27

Since we did not access to the delineation of drainage areas for the two monitoring sites in the City of Bloomington (Smith Pond and Mall of America), it was not possible to calculate f_{TIA} values for those sites. The minimum ratio of EIA/TIA for the remaining 38 sites in Table 4.5 is 0.08 in Sarita catchment. The amount of open spaces of the Minnesota State Fair grounds and the University of Minnesota St. Paul Campus which both are located in the Sarita watershed explains this low ratio of EIA/TIA. The WBA catchment in Austin, TX had a ratio of EIA/TIA equal to 1.27. This ratio is obviously incorrect. WBA is a small catchment with 0.4 ha drainage area which is located at the Wells Branch Community Center and has a primary land use of office space and parking lots. A small bias in the runoff data could explain the ration greater than 1. The remaining 37 sites, however, indicate a reasonable EIA/TIA ratio, with the maximum being 0.90 at Harper basin. Figure 4.5 shows EIA and combined events in the WBA catchment. As seen in this Figure, many events with small rainfall depth (e.g. less than 40 mm) are categorized as combined events (red points) in this catchment. Table 4.5 shows the average, median and standard deviation of the EIA/TIA ratio for all the 38 study sites as 0.47, 0.45, and 0.22, respectively. The ratio of EIA/TIA for residential watersheds is shown in Figure 4.6. The average, median and standard deviation of the EIA/TIA ratio

for all the watersheds with residential land use are 0.45, 0.39, and 0.18, respectively. This simply means that only about half of the impervious surfaces in our watersheds are hydraulically connected to the drainage system.

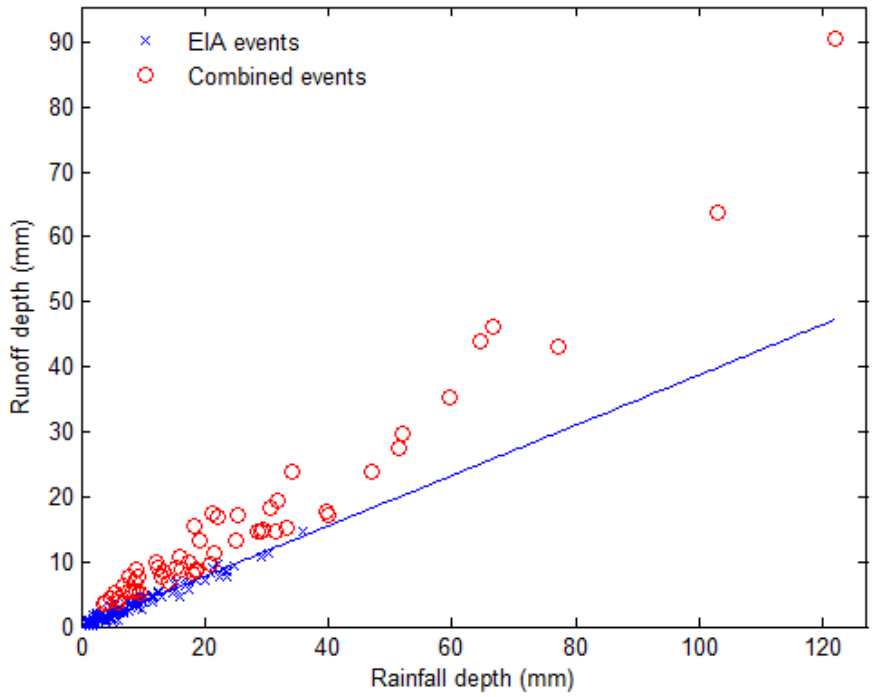

Figure 4.5 Plot of runoff depth against rainfall depth for the WBA catchment at the final step of the proposed SWLS method.

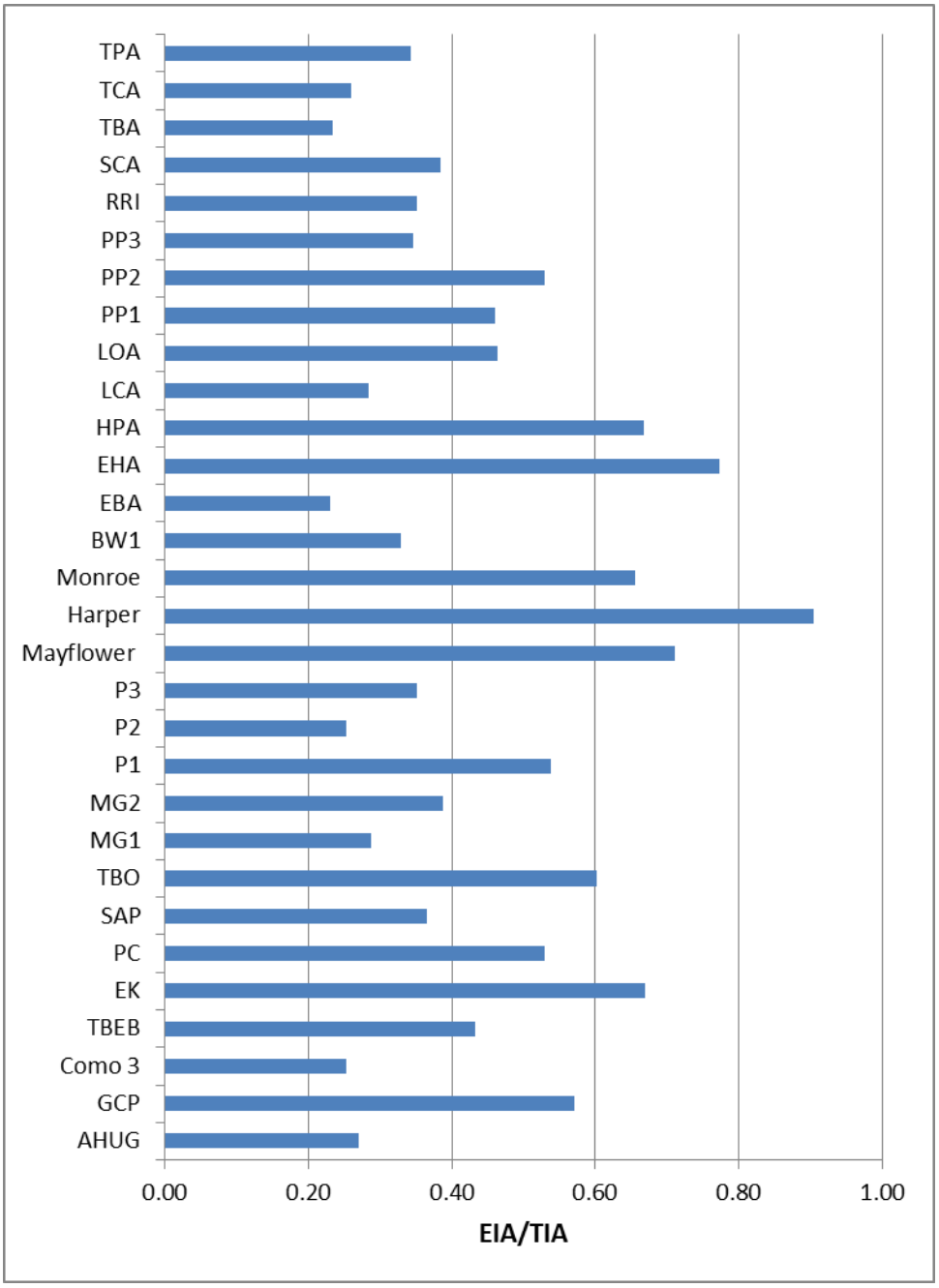

Figure 4.6 The ratio of EIA/TIA for all the study sites with residential land uses (30 sites). The chart shows that only about half of the impervious surfaces are hydraulically connected to the drainage system.

CHAPTER 5: CURVE NUMBER CORRELATIONS

5.1 Need

This chapter describes the development of correlations between watershed characteristics and EIA in order to estimate EIA in ungauged urban watersheds. While using the GIS method of Han and Burian (2009) to estimate EIA is particularly attractive due to its applicability to ungauged watersheds, there are some limitation and difficulties that hinder the wide use of this method. In order to use the mentioned GIS based method, one needs to have three layers of spatial information including the urban land cover, digital elevation model (DEM), and a layer containing the locations of inlets to the stormwater collection system. The method is also not able to estimate EIA related to rooftops and requires the user to input the value of connected rooftops manually to determine the actual EIA value, a process that can add significant time and expense to the EIA estimate. So the method can be expensive and time consuming.

To address the aforementioned issues, the curve number will be utilized as an index to capture the runoff characteristics of watersheds in previous chapters. Determining curve number using the GIS analysis of land cover and soil data in urban watersheds was one of the goals of the chapter 4. In chapter 5, the refined GIS information along with the rainfall-runoff data from 40 urban watersheds in the Twin Cities metro area of Minnesota, Madison, Wisconsin, and Austin, Texas will be used to develop a new method for determining effective impervious area in ungauged urban watersheds. This method which is based on a relatively simple GIS analysis, the Natural Resources Conservation Service (NRCS) Curve Number (CN) method, and Hawkins modification

to the NRCS-CN method (Hawkins 1993) evaluates CN at the basin scale from rainfall-runoff events. While providing the EIA fraction, the method also investigates different CN behaviors in urban watersheds and determines the response of each watershed. The latter is particularly attractive for practitioners involved in computing and modeling runoff from urban watersheds and design of associated hydraulic structures and stormwater control measures (SCMs).

Two main groups of watersheds were analyzed and used in this study. The first group includes 20 urban watersheds, 18 in the Twin Cities metro area of Minnesota and 2 in the City of Madison, Wisconsin. The monitoring data in this group have been provided by the Capitol Region Watershed District (CRWD), Three Rivers Park District (TRPD), City of Minnetonka, City of Bloomington, and USGS-Wisconsin Water Science Center. The second group contains 20 urban watersheds in the city of Austin, Texas. All the data in this group have been provided by the City of Austin Watershed Protection Department.

The key components of chapter 5 are to (1) develop the general framework of the new method for determining fraction of EIA in urban watersheds (2) determine the actual curve number in the study watershed based on rainfall-runoff data (3) develop relation between actual curve number and EIA fraction, (4) develop correlations between watershed characteristics and actual curve number, and (5) examine the sensitivity of runoff depth to EIA fraction in urban watersheds. Our activities for these components are summarized into the following sections.

5.2 General Framework for Determining the Fraction of EIA in Ungauged Watersheds

To address the aforementioned issues regarding estimating EIA in ungauged watersheds, we have developed a new method based on GIS and the Curve Number method. As described in the chapter 4, composite CN (CN_{comp}) is calculated using GIS and spatial information of land cover/land use and hydrologic soil group in watersheds (Zhan and Huang, 2004; Nagarajan and Poongothai, 2012; Hernández-Guzmán and Ruiz-Luna, 2013) based on the available CN table in TR-55 (USDA NRCS, 1986). Since the CN values for urban districts in the CN table are based on assumptions for both impervious and pervious area that are not always valid, we also evaluate the actual CN (CN_{act}) at the basin scale from rainfall-runoff events using the asymptotic fitting method (Hawkins, 1993; Hawkins et al., 2009). Using the area weighted average curve number in the watershed, we then develop a relation between the EIA fraction (f_{EIA}) and CN_{act} in a watershed. For the final step we estimate the CN_{act} as a function of watershed characteristics so that we are able to determine f_{EIA} in ungauged watersheds.

5.3 Determination of Actual Curve Number in the Watersheds Based On Rainfall-Runoff Data

The U.S. Department of Agriculture (USDA), Soil Conservation Service (SCS), currently referred to as Natural Resources Conservation Service (NRCS) (SCS 1964, 1972, 1985; NRCS 2004) introduced a simplified runoff equation as:

$$Q = \frac{(P - I_a)^2}{P - I_a + S} \quad for\ P \geq I_a \tag{5.1}$$

$$Q = 0 \qquad for\ P < I_a \tag{5.2}$$

$$\mathrm{I_a} = \lambda S \tag{5.3}$$

where Q = direct runoff depth (in or mm), P = rainfall depth (in or mm), S = potential maximum retention (in or mm), $\mathrm{I_a}$ is the initial abstraction of rainfall, and λ is the initial abstraction ratio ($\mathrm{I_a}/S$).

The original value of the initial abstraction ratio ($\mathrm{I_a}/S$) or λ has been established by SCS (now NRCS) as 0.2. Therefore, the Equations (5.1) and (5.2) are rewritten as:

$$Q = \frac{(P-0.2S)^2}{P+0.8S} \qquad for\ P \geq 0.2S \tag{5.4}$$

$$Q = 0 \qquad for\ P < 0.2S \tag{5.5}$$

The original value of λ (i.e. 0.2) has been investigated by many researchers and determined to be higher than the actual λ value in most of the watersheds (Hawkins et al. 2009,2010). So, investigating the role of λ in the CN studies is recently emphasized (Hawkins et al. 2009, D'Asaro and Grillone 2012, D'Asaro et al. 2014). Based on the results of several studies, Hawkins et al. (2009) states λ=0.05 as a more appropriate assumption for general application. Also, Woodward et al. (2010) recommends λ=0.05 to NRCS for agency use. To investigate the effect of λ value on the results of the proposed GIS-CN method, all calculations in this chapter were performed using both values of 0.2 and 0.05 for λ. The results did not show a notable difference and hence, only the results corresponding to the original value of λ (i.e. 0.2) are presented in this chapter. However, all calculations and results for the case of λ=0.05 can be found in appendix "C". From

now on all calculation and results on the Curve Number method in this chapter is based on the original assumption of λ=0.2.

The potential maximum retention *S* in Eq. (5.4) is transformed to a dimensionless index, *CN*, as:

$$CN = \frac{1000}{S+10} \tag{5.5}$$

where *S* is in inches, and when *S* is in millimeters.

$$CN = \frac{25400}{S+254} \tag{5.6}$$

The above equations show that *CN* is not a constant value for all the storm events in a watershed and, in fact, there is a unique *CN* value for each storm event or each pair of rainfall and runoff depth (*P*,*Q*) in the dataset.

The actual *CN* of our watersheds of study were determined using the asymptotic fitting method (Hawkins, 1993; Hawkins et al., 2009). In this method, at first the rainfall and runoff depth data (*P*'s and *Q*'s) are sorted separately and then realigned on a rank-order basis. This is called frequency matching and is done in order to equate return period of rainfall and runoff events (Hjelmfelt 1980; Hawkins 1993). The new rainfall-runoff record is called ordered data (versus original data). Using the basic *CN* equation (Eq. 5.4), the storage index, *S*, for each pair of (*P*,*Q*) is determined as:

$$S = 5[P + 2Q - (4Q^2 + 5PQ)^{1/2}] \tag{5.7}$$

A unique *CN* is then determined for each storm event in the ordered dataset using equations (5.5) or (5.6). In the next step, the obtained *CN* values are plotted against their corresponding rainfall depth (*P*). Three different patterns have been observed by researchers working on different watersheds in the world. The most common pattern in small watersheds is the standard behavior, where *CN* declines with increasing *P*, but asymptotically approaches a constant value for larger storms. This stable value is called CN_∞ and assumed to be the watershed *CN*. Figure 5.1 shows an example of the standard behavior in the AHUG subwatershed of the Capitol Region Watershed District, MN.

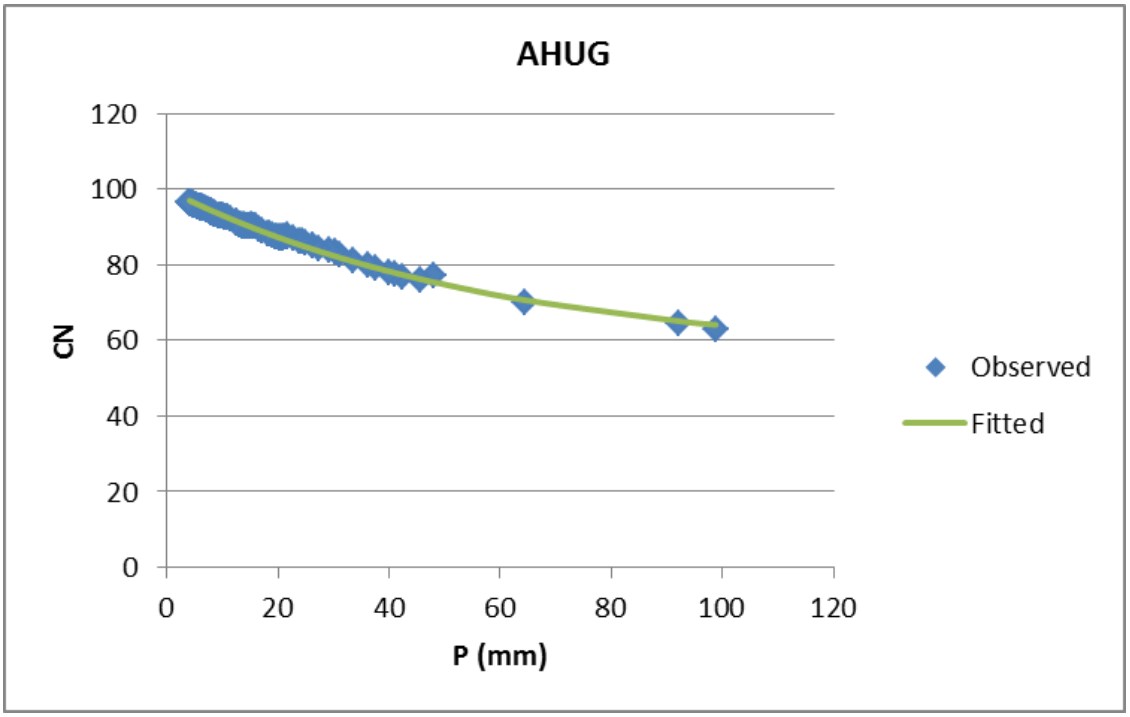

Figure 5.1 Curve Number (CN) against rainfall depth (P) in the AHUG subwatershed of the Capitol Region Watershed, MN. The plot shows a standard CN behavior and CN_∞ is about 56 in this small urban catchment.

The other possible pattern is complacent behavior in which *CN* declines as *P* increases but does not approach a stable value at larger storms. This often happens when there is insufficient data at high precipitation. The watershed CN cannot be determined in this case. The plots of *CN* vs. *P* for the Monroe (in Madison, WI) and Hedburg (in Minnetonka, MN) catchments are presented in Figures 5.2 and 5.3. Both of these catchments show a complacent *CN* behavior.

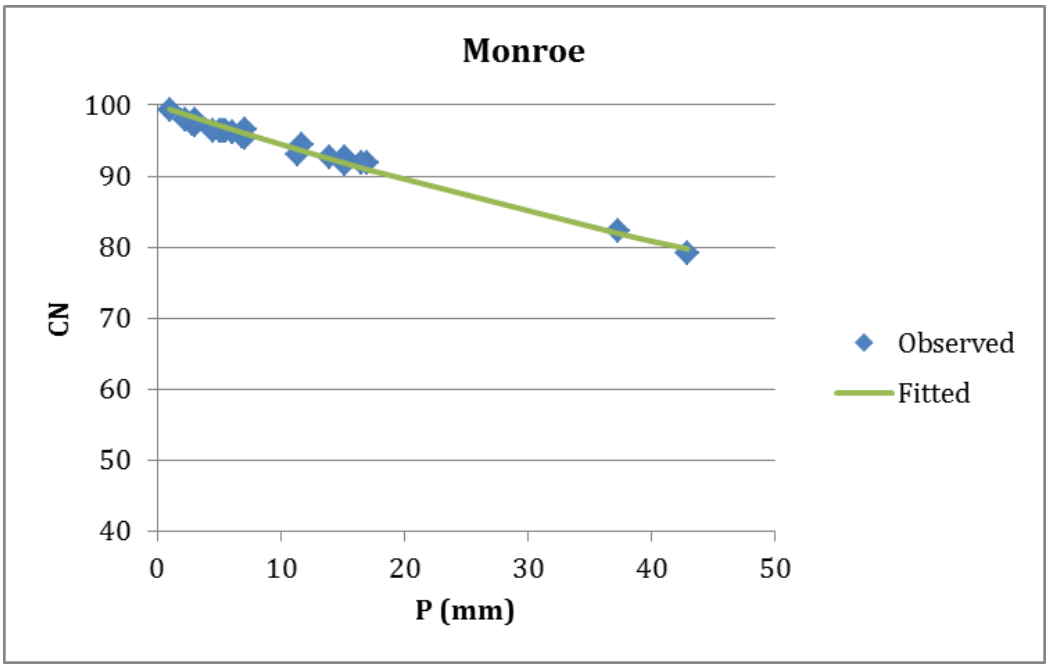

Figure 5.2 Curve Number versus rainfall depth (P) in the Monroe drainage basin in the City of Madison, Wisconsin. The plot shows a complacent response; however, the maximum rainfall depth is about 40 mm and by collecting more data on larger rainfall events it is possible to have other CN patterns.

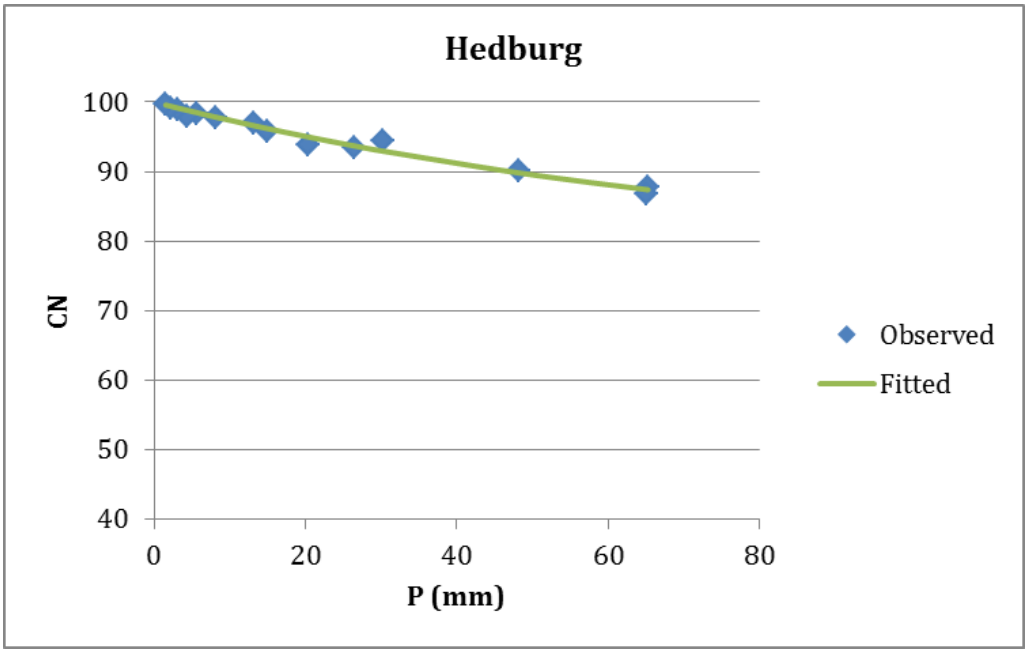

Figure 5.3 Curve Number versus rainfall depth (P) in the Hedburg drainage basin in the City of Minnetonka, Minnesota. The response looks like a complacent behavior; however, the monitoring data is only for 1 year and the number of monitored events is not adequate to make a judgment on the type of CN pattern in this basin.

The third observed pattern is called violent behavior in which *CN* declines at lower rainfalls but suddenly rises and asymptotically approaches to a near-constant value at larger storms (CN_{∞}). None of our watersheds of study showed such a behavior. Figure 5.4 shows an example of the violent behavior in a watershed in Sicily, Italy (D'Asaro and Grillone, 2012).

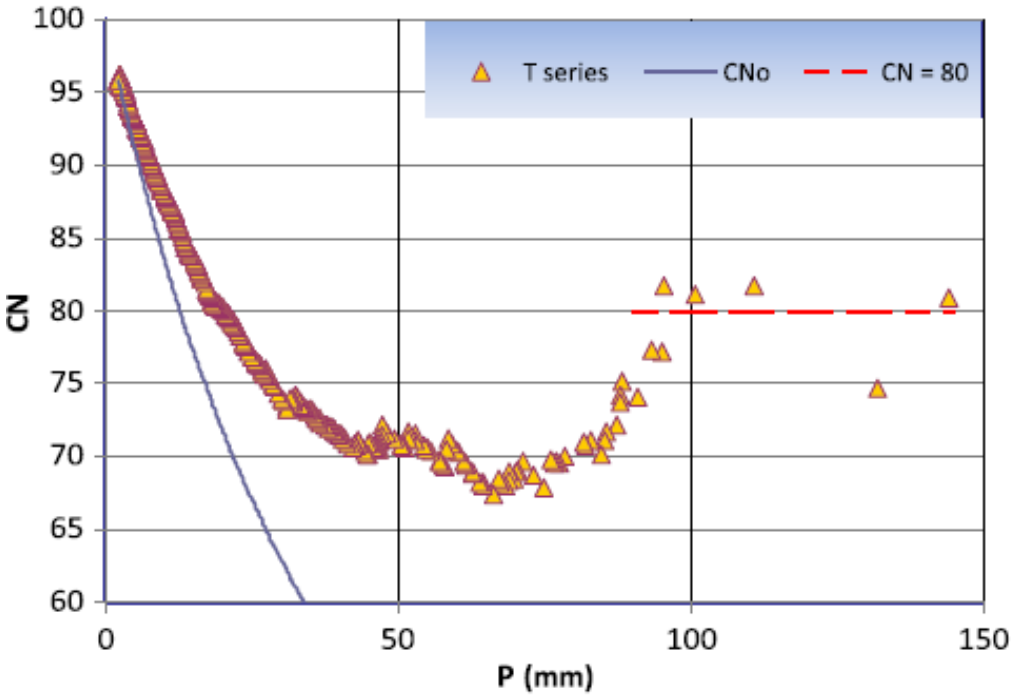

Figure 5.4 Example of the violent behavior in Delia watershed at Pozzillo station in Sicily, Italy (from D'Asaro and Grillone, 2012). CN_0 is the CN at which runoff starts and CN_∞ is determined as 80 in this watershed.

Hawkins (1993) and other researchers have used the asymptotic equation (5.8) to be fitted to P-CN data in standard pattern.

$$CN(P) = CN_\infty + (100 - CN_\infty)\, e^{-kP} \tag{5.8}$$

where *CN(P)* is the value of *CN* in rainfall depth *P*, and *k* is a fitting constant.

The aforementioned asymptotic fitting method was applied to all the watersheds of our study. Table 5.1 presents the CN_∞ and the *CN* pattern of the watersheds. Figure 5.5 shows the standard pattern asymptotic curves for the watersheds in CRWD, MN. The

plots of *CN* versus rainfall depth that show the type of *CN* behavior in each watershed are presented for all the watersheds of study in appendix "B". As seen in Table 5.1, the *CN* pattern in all the watersheds except Monroe and Hedburg is standard. Figure 5.2 shows a complacent response for Monroe watershed in Madison, WI; however, it should be noted that the maximum rainfall depth in the Monroe dataset is about 40 mm and by collecting more data (including large rainfall depths) in this watershed it is possible to have other *CN* patterns. Also, the monitoring data in Hedburg watershed is only for 1 year and the number of events is not adequate to make a judgment on the type of *CN* pattern in this watershed. Due to the above reasons neither of the two watersheds were further used in our analysis. The maximum rainfall depth in the Harper basin in Madison, WI is about 20 mm and larger rainfall events are needed to certify the standard behavior of the CN vs. P for this basin. In fact, by collecting adequate data on large rainfall events it is possible to have other CN patterns. Because of the above reason, we did not use this site in our analysis in this chapter. Table 5.1 shows a CN_{∞} of 38.7 for the Mall of America (MOA) site which obviously seems low for a commercial catchment with lots of parking lots and roads. Looking at the CN vs. P graph for this site (appendix "B") shows that there is only one data point with a large storm depth (123 mm) in MOA dataset which has caused the CN_{∞} to be such low. As discussed earlier in section 3.6, this large storm event has a smaller fraction of runoff than expected. Because of this issue, MOA site was not further considered in our analysis. Also as discussed in section 4.6, WBA catchment gave a ratio of EIA/TIA greater than one and hence, was excluded from the sites that were used in our analysis in this chapter. By excluding Hedburg and Monroe (complacent CN pattern),

Harper (lack of large rainfall data), MOA and WBA (runoff data issue), the total number of watersheds that were used in our analysis in this chapter was 35.

Table 5.1 Drainage area, actual CN and type of CN pattern in the 40 watersheds of study

Row	Watershed Name	Drainage Area (ha)	CN_∞	CN vs. Precip. Pattern
1	AHUG	15.9	55.8	Standard
2	GCP	51.8	62.3	Standard
3	Como 3	185.8	44.7	Standard
4	Sarita inlet	376.0	48.6	Standard
5	TBEB	377.2	70.6	Standard
6	EK	451.6	79.3	Standard
7	PC	579.9	76.1	Standard
8	SAP	1007.3	73.2	Standard
9	TBO	2034.8	77.6	Standard
10	MG1	5.5	82.5	Standard
11	MG2	3.5	71.9	Standard
12	P1	5.1	62.5	Standard
13	P2	6.8	63.9	Standard
14	P3	5.6	79.7	Standard
15	Hedburg	2.8	NA	Complacent
16	Tapestry	11.1	54.9	Standard
17	Smith Pond	55	75.1	Standard
18	MOA	202	38.7	Standard
19	Harper	16.4	83.7	Standard
20	Monroe	92.9	NA	Complacent
21	BW1	146.3	78.3	Standard
22	EBA	14.3	48.9	Standard
23	EHA	20.8	71.1	Standard
24	ERA	40.4	85.3	Standard
25	HI	1.2	92.3	Standard
26	HPA	17.4	64.5	Standard
27	LCA	84.9	60.2	Standard
28	LOA	5.4	87.1	Standard
29	LUA	5.5	95.1	Standard
30	MBA	82.1	90.9	Standard

Row	Watershed Name	Drainage Area (ha)	CN_{∞}	CN vs. Precip. Pattern
31	OFA	0.6	95.6	Standard
32	PP1	2.0	84.9	Standard
33	PP2	1.8	82.2	Standard
34	PP3	0.9	62.3	Standard
35	RRI	6.4	84.2	Standard
36	SCA	2.3	77.7	Standard
37	TBA	20.0	65.5	Standard
38	TCA	16.5	82.1	Standard
39	TPA	16.8	74.5	Standard
40	WBA	0.4	86.2	Standard

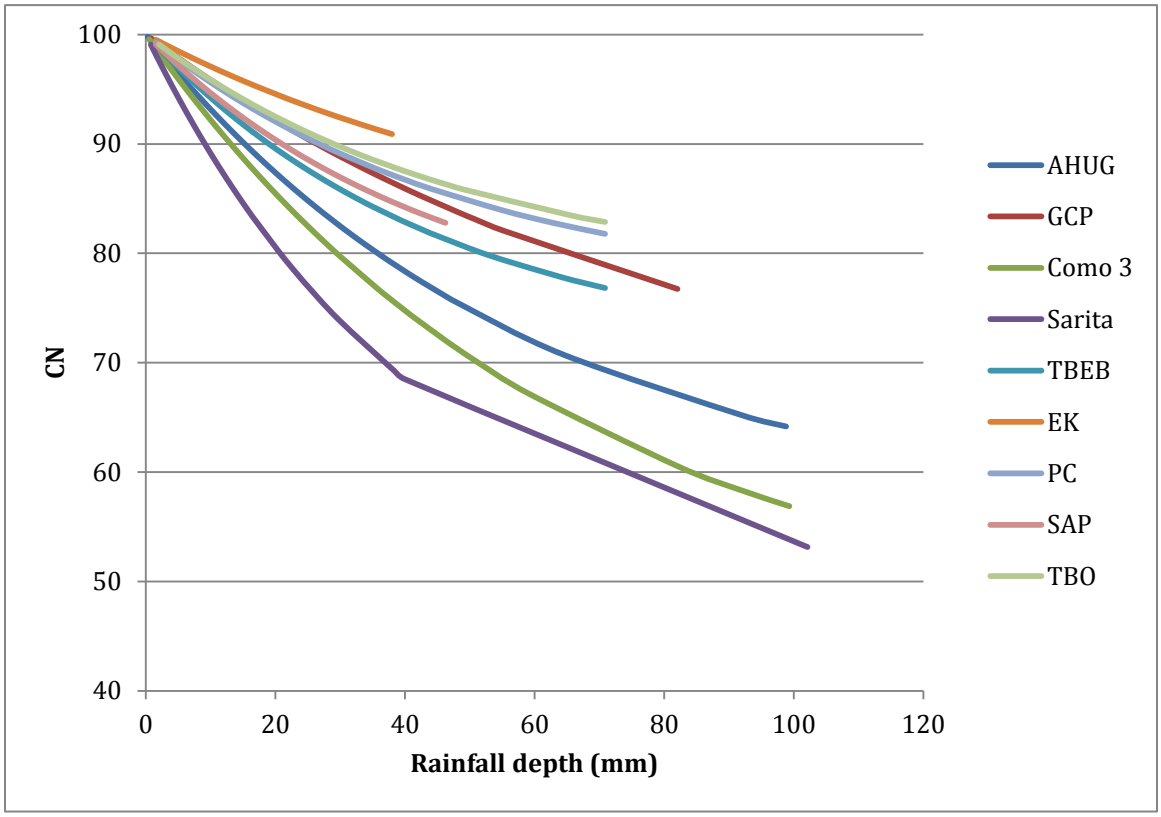

Figure 5.5 Curve Number versus rainfall depth in 9 drainage basins in the Capitol Region Watershed District (CRWD), Minnesota. All 9 drainage basins show a standard behavior for CN against rainfall depth.

5.4 Develop Relation between Actual Curve Number and EIA Fraction

Dividing the entire drainage area of a watershed into two categories, impervious and pervious area, the weighted average CN for a watershed can be found from Equation (5.9) (Pandit and Regan, 1998):

$$CN_w.A_t = CN_i.A_i + CN_p.A_p \quad (5.9)$$

where CN_w is the weighted average CN of the watershed, A_t =total drainage area of the watershed, CN_i =CN for the impervious area, A_i =area of impervious surfaces in the watershed, CN_p = CN for the pervious area, and A_p =area of the pervious surfaces watershed ($A_p = A_t - A_i$).

An important assumption in USDA TR-55 CN table for urban areas is that it considers only directly connected impervious areas (or effective impervious area) as impervious. So, the Equation (5.9) can be modified to (5.10).

$$CN_{act}.A_t = CN_{EIA}.A_{EIA} + CN_r.A_r \quad (5.10)$$

where CN_{act} is the actual CN of the watershed ($CN_{act} = CN_\infty$), CN_{EIA} = CN corresponding to effective impervious area, A_{EIA} = area of effective impervious surfaces in the watershed, CN_r = CN corresponding to remaining area in the watershed, and A_r = the remaining area of the watershed ($A_r = A_t - A_{EIA}$).

According to USDA TR-55, $CN_{EIA} = 98$. Hence, Equation (5.10) can be rewritten as (5.11).

$$CN_{\infty}.A_t = 98\,A_{EIA} + CN_r.(A_t - A_{EIA}) \quad (5.11)$$

And by dividing the both sides of Equation (5.11) by A_t:

$$CN_{\infty} = 98\,f_{EIA} + CN_r.(1 - f_{EIA}) \quad (5.12)$$

where f_{EIA} is fraction of effective impervious area in the watershed and is defined as:

$$f_{EIA} = A_{EIA}/A_t \quad (5.13)$$

In Equation (5.12), CN_{∞} is known but both f_{EIA} and CN_r are unknowns. So, in order to be able to solve Equation (5.12) we recognize that CN_r is a fraction of CN_{EIA}.

$$CN_r = \alpha\,CN_{EIA} \quad (0 < \alpha < 1) \quad (5.14)$$

Substituting Equation (5.14) into Equation (5.12) we have:

$$f_{EIA} = \frac{CN_{\infty} - 98\,\alpha}{98(1-\alpha)} \quad (5.15)$$

The CN_{∞} values for the watersheds of study are presented in Table 5.1. Also, we have already calculated f_{EIA} for the watersheds of study based on our proposed rainfall-runoff method (SWLS: Successive Weighted Least Square method) in chapter 3. So, the α values can be obtained by rewriting Equation (5.15) as:

$$\alpha = \frac{CN_{\infty} - 98\,f_{EIA}}{98(1-f_{EIA})} \quad (5.16)$$

Table 5.2 shows the f_{EIA} values from chapter 3 and the α values calculated based on Equation (5.16). Figure 5.6 is also a plot of α against CN_{∞} in the study sites. Weighted

least square (WLS) regression (similar to chapter 3) were used to estimate α in terms of CN_{∞}. When using the coefficient of determination (R^2) as a measure of goodness of fit in the WLS regression, in order to avoid "overly optimistic interpretation" of the frequently larger R^2_{WLS} values in comparison to R^2_{OLS} Willett and Singer (1988) recommend using a $pseudo\ R^2_{WLS}$ as Equation (5.17).

$$pseudo\ R^2_{WLS} = 1 - \left[\frac{(\mathbf{y}-\mathbf{x}\,\mathbf{b_{wls}})^{\mathrm{T}}(\mathbf{y}-\mathbf{x}\,\mathbf{b_{wls}})}{\mathbf{y}^{\mathrm{T}}\mathbf{y}-\mathrm{n}\bar{\mathrm{y}}^2}\right] \tag{5.17}$$

where **y** and **x** are original (untransformed) vector and matrix of variables as used in OLS method (Eq. 3.5) and $\mathbf{b_{wls}}$ is the WLS estimate of the regression parameters (Eq. 3.20).

There is a strong correlation between α and CN_{∞} in Figure 5.6, and α can be estimated as a function of CN_{∞}.

$$\alpha = 0.0116\ CN_{\infty} - 0.1601 \tag{5.18}$$

Substituting Equation (5.18) into Equation (5.15) makes it possible to estimate the fraction of EIA as a function of CN_{∞}.

$$f_{EIA} = \frac{16-0.14\ CN_{\infty}}{114-1.14\ CN_{\infty}} \tag{5.19}$$

Table 5.2 EIA and TIA fraction in the watersheds of study. The values of f_{TIA} are calculated based on GIS analysis of land cover layers in chapter 4. The f_{EIA} values are calculated based on SWLS method in chapter 3. α is the ratio of $CN_r/98$ and is calculated using equation 5.16

Row	Watershed Name	f_{TIA}	f_{EIA}	α
1	AHUG	0.507	0.137	0.5006
2	GCP	0.438	0.250	0.5144
3	Como 3	0.405	0.102	0.3945
4	Sarita inlet	0.367	0.030	0.4804
5	TBEB	0.447	0.193	0.6534
6	EK	0.562	0.376	0.6946
7	PC	0.587	0.310	0.6755
8	SAP	0.613	0.224	0.6745
9	TBO	0.473	0.284	0.7089
10	MG1	0.405	0.117	0.8215
11	MG2	0.388	0.151	0.6867
12	P1	0.380	0.204	0.5452
13	P2	0.351	0.089	0.6176
14	P3	0.273	0.096	0.7932
15	Tapestry	0.237	0.169	0.4706
16	Smith Pond	NA	0.076	0.7476
17	BW1	0.460	0.152	0.7630
18	EBA	0.404	0.093	0.4474
19	EHA	0.434	0.336	0.5865
20	ERA	0.460	0.179	0.8420
21	HI	0.500	0.281	0.9192
22	HPA	0.450	0.300	0.5116
23	LCA	0.225	0.064	0.5876
24	LOA	0.422	0.196	0.8620
25	LUA	0.974	0.484	0.9421
26	MBA	0.609	0.322	0.8939
27	OFA	0.862	0.452	0.9549
28	PP1	0.497	0.229	0.8271
29	PP2	0.511	0.270	0.7794
30	PP3	0.494	0.172	0.5605
31	RRI	0.305	0.107	0.8428

Row	Watershed Name	f_{TIA}	f_{EIA}	α
32	SCA	0.409	0.157	0.7536
33	TBA	0.452	0.106	0.6296
34	TCA	0.374	0.097	0.8203
35	TPA	0.415	0.142	0.7204

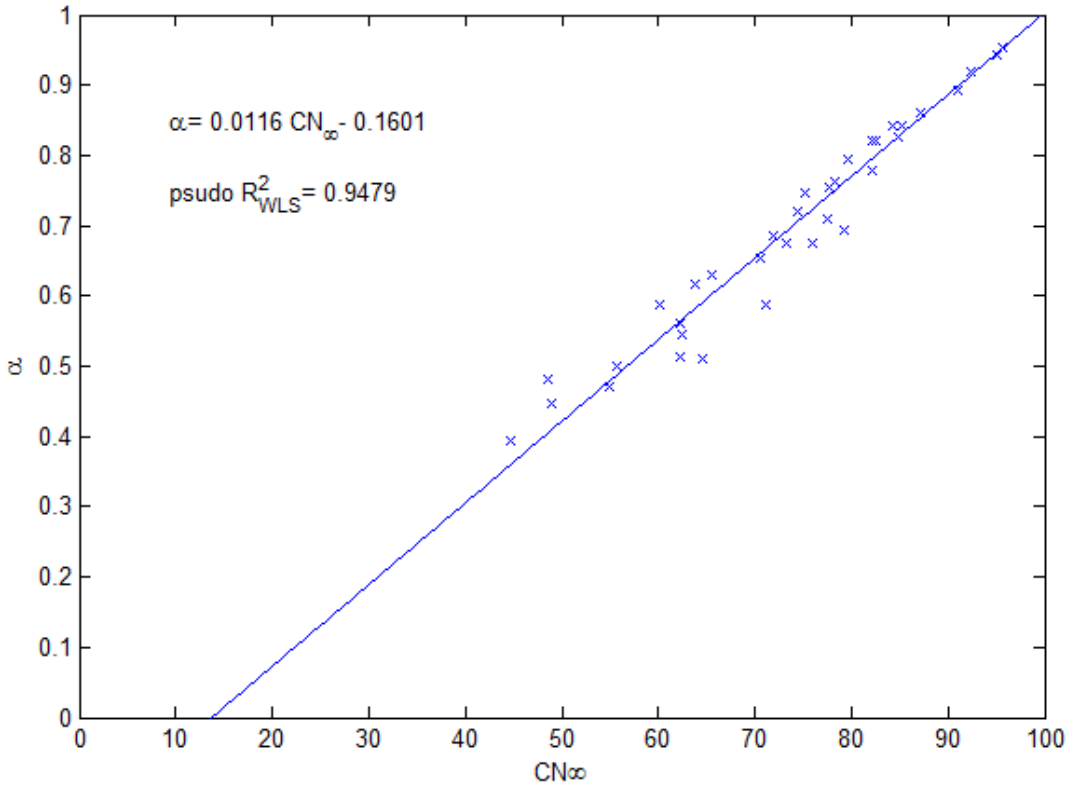

Figure 5.6 Plot of α versus CN_∞. Since α is the ratio of CN_r/98, the regression shows a strong correlation between CN_r and CN_∞ in the watersheds of study.

To investigate the applicability and limitations of the presented relation between f_{EIA} and CN_∞ we should note that Eq. (5.19) and Figure 5.6 are based on the assumption of linear correlation between α and CN_∞. On the other hand, Eq. (5.14) ($CN_r = 98\ \alpha$) should work in extreme conditions of f_{TIA}=0 and 1 in a watershed. When f_{TIA}=1, that means that

the watershed is fully impervious and $CN_r = 98$, so $\alpha = 1$. But f_{TIA}=0 means that the watershed is fully pervious and $CN_r = CN_p$. The minimum value of NRCS-CN in the Table 2-2a of TR-55 is 39 which is corresponding to open spaces with good condition. Therefore for the case of f_{TIA}=0, CN_r (or 98 α) should be greater than 39 which causes α to be greater than 39/98 or 0.4. Hence, the range of α values is [0.4,1].

$$0.4 \leq \alpha \leq 1 \tag{5.20}$$

Limiting α in the range of [0.4,1] in the Eq. (5.18) causes CN_∞ to be limited to the range of 49 and 100 (or 98 to be consistent with TR-55 CN values). This indicates that Eq. (5.19) is valid only for CN_∞ values greater than 49. However, for CN_∞ values less than 49 the α value is constant and equal to 0.4. In order to find the relationship between f_{EIA} and CN_∞ for $40 \leq CN_\infty \leq 49$, $\alpha = 0.4$ is replaced in Eq. (5.15) which leads to:

$$f_{EIA} = 0.0175\, CN_\infty - 0.6987 \quad if\ 40 \leq CN_\infty \leq 49 \tag{5.21}$$

Hence, EIA fraction for $40 \leq CN_\infty \leq 98$ can be estimated by a two criteria function as:

$$f_{EIA} = \begin{cases} 0.0175\, CN_\infty - 0.6987 & if\ 40 \leq CN_\infty \leq 49 \\ \frac{16 - 0.14\, CN_\infty}{114 - 1.14\, CN_\infty} & if\ 49 < CN_\infty \leq 98 \end{cases} \tag{5.22}$$

Figure 5.7 shows the plot of f_{EIA} vs. CN_∞ based on Eq. (5.22). It is seen that f_{EIA} has an increasing trend with the increase of CN_∞. However, rate of the change is very low while $49 < CN_\infty < 80$ and it increases dramatically when CN_∞ becomes greater than 80.

In order to see how compatible the presented f_{EIA} vs. CN_∞ plot is with the actual data, pairs of (CN_∞, f_{EIA}) for all the study sites with standard CN vs. rainfall depth pattern (35 sites) were added to Figure 5.7. The result is presented in Figure 5.8. The red points in Figure 5.8 represent the actual f_{EIA} and CN_∞ values for the study sites in which f_{EIA} is estimated based on the observed rainfall-runoff data using the proposed SWLS method (in chapter 3) and CN_∞ is calculated based on the ordered rainfall-runoff data using the Hawkins' asymptotic fitting method (Hawkins 1993) (Table 5.1).

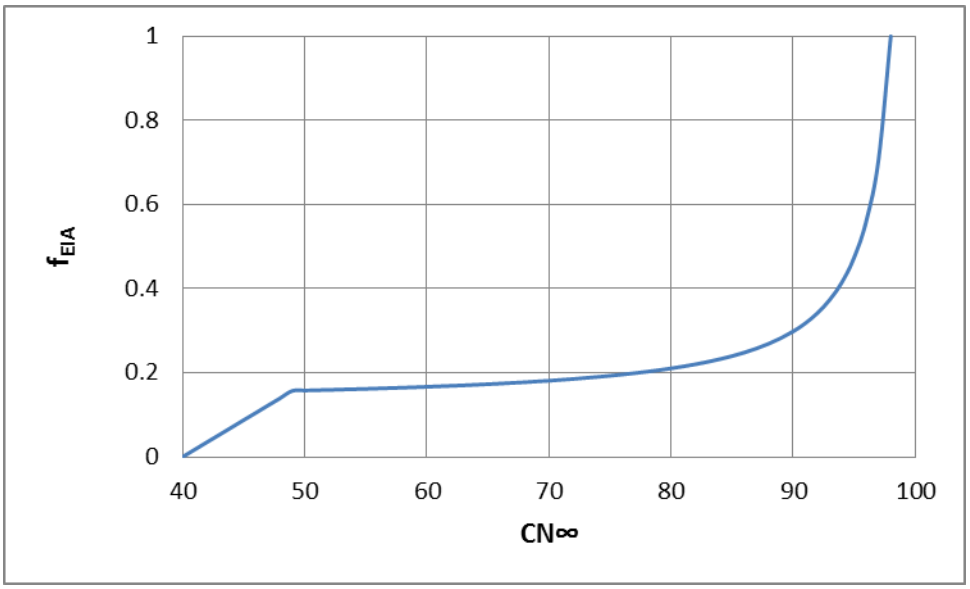

Figure 5.7 Plot of f_{EIA} versus CN_∞ based on Equation (5.22) for the estimation of f_{EIA} in ungauged urban watersheds in terms of CN_∞.

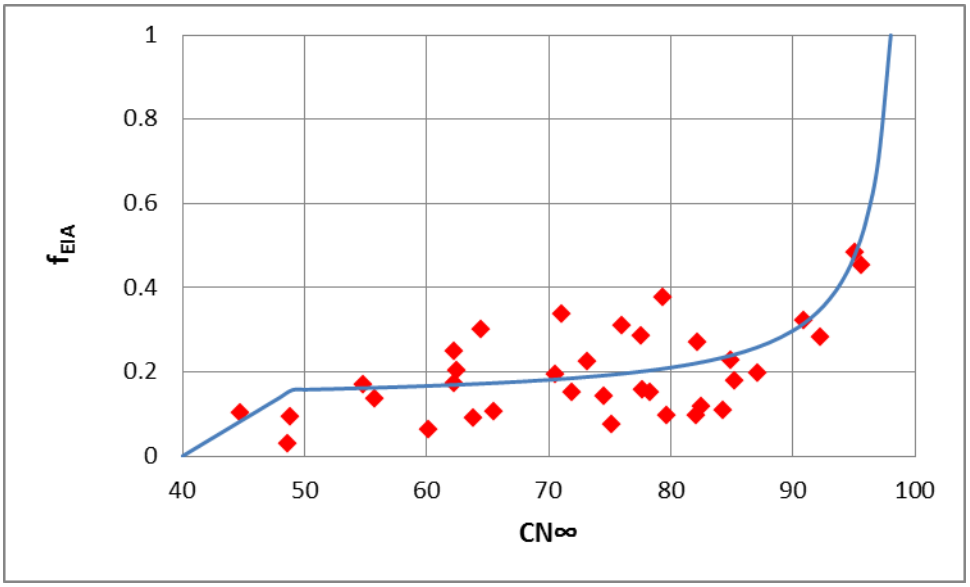

Figure 5.8 Comparison of the actual f_{EIA} and CN_∞ values in gauged watersheds with the presented curve for ungauged watersheds. The actual f_{EIA} values have been estimated based on the proposed SWLS method and the CN_∞ values have been calculated using the Hawkins' CN method (Hawkins 1993).

5.5 Develop Relationships between Watershed Characteristics and Actual Curve Number

The fraction of effective impervious area (f_{EIA}) has been shown in sections 5.4 and 5.5 to be a function of actual curve number (CN_∞). In order to be able to estimate f_{EIA} as a function of watershed characteristics in an ungauged watershed, one needs to have an estimate of CN_∞ in the watershed. In chapter 4 we analyzed land cover/land use and soil data for the study sites in GIS in order to calculate the composite CN (CN_{comp}) of watersheds using the CN table in TR-55. CN_{comp} was considered as the first watershed parameter to be examined to see if it has a correlation with CN_∞. However, no

significant correlation was observed between the actual and composite CN values by plotting CN_{∞}vs. CN_{comp} for the study sites.

5.5.1 Correlation between actual CN and TIA

In the next attempt, TIA was considered as a watershed parameter to be further examined. Plot of CN_{∞} versus f_{TIA} for all the study sites with available data in Table 5.2 is presented in Figure 5.9. Although the coefficient of determination for the regression line (R^2) does not show a strong correlation between CN_{∞} and f_{TIA} , we should note that in linear regression with a narrow range of y values (here CN_{∞} values) the data points can be close to their mean y value, causing a low value of R^2. The regression equation from Figure 5.9 (Eq. 5.23) is in a good agreement with the TR-55 CN table for urban watersheds in extreme conditions of f_{TIA}=0 and 1. Using Eq. (5.23), f_{TIA}=0 causes the CN_{∞} to be equal 54 and f_{TIA}=1 results in CN_{∞}=97 which correspond with TR-55 CN values for fully pervious and fully impervious watersheds, respectively.

$$CN_{\infty} = 42.928\, f_{TIA} + 53.886 \tag{5.23}$$

The TR-55 CN table for urban areas (Table 2-2a) uses the average percent impervious area in a watershed (i.e. %TIA) to develop the composite CN values for different land cover conditions. One basic assumption in TR-55 is that all impervious areas are directly connected to the drainage system so the CN value for all the impervious surfaces has been considered as 98. According to these assumptions, CN values for urban districts in the Table 2-2a of TR-55 are calculated based on the Eq. (5.24) which (by considering the

aforementioned assumptions) is similar to the Eq. (5.10) that we already used in order to derive the relationship between actual CN and EIA fraction in ungauged watersheds.

$$CN_{comp} = 98\, f_{TIA} + CN_p.(1 - f_{TIA}) \tag{5.24}$$

Eq. (5.24) can be rewritten as

$$CN_{comp} = CN_p + (98 - CN_p) f_{TIA} \tag{5.25}$$

Also in TR-55, pervious areas are assumed equivalent to open spaces in good hydrologic condition (grass cover > 75%). Based on this assumption, the CN values for fully pervious and impervious watersheds in different hydrologic soil groups (HSGs) in TR-55 are presented in Table 5.3. Based on this table and Eq. 5.25, the trend of TR-55 CN values in different hydrologic soil groups can be plotted and compared with the regression line for the estimation of CN_∞ in terms of f_{TIA}. Figure 5.10 presents this comparison. Solid lines in Figure 5.10 are corresponding to Eq. (5.25) in different HSGs and the dashed line is the regression line in Figure 5.9. The blue data points in Figure 5.10 are the observed (actual) data points for f_{TIA} and CN_∞.

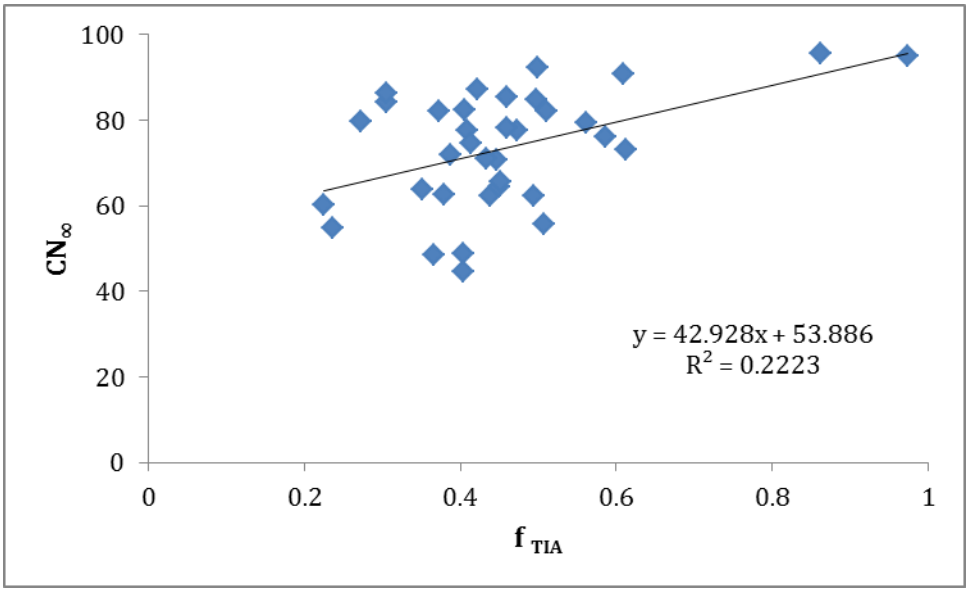

Figure 5.9 Plot of actual CN versus TIA fraction in the watersheds of study. Although the R^2 does not show a strong correlation, it can be explained by the narrow range of CN_∞ values and the regression equation is in a good agreement with the TR-55 CN table in extreme conditions of f_{TIA}=0 and 1.

Table 5.3 CN values in TR-55 for fully pervious and impervious watersheds in different hydrologic soil groups

HSG	f_{TIA}	TR-55 CN
A	0	39
	1	98
B	0	61
	1	98
C	0	74
	1	98
D	0	80
	1	98

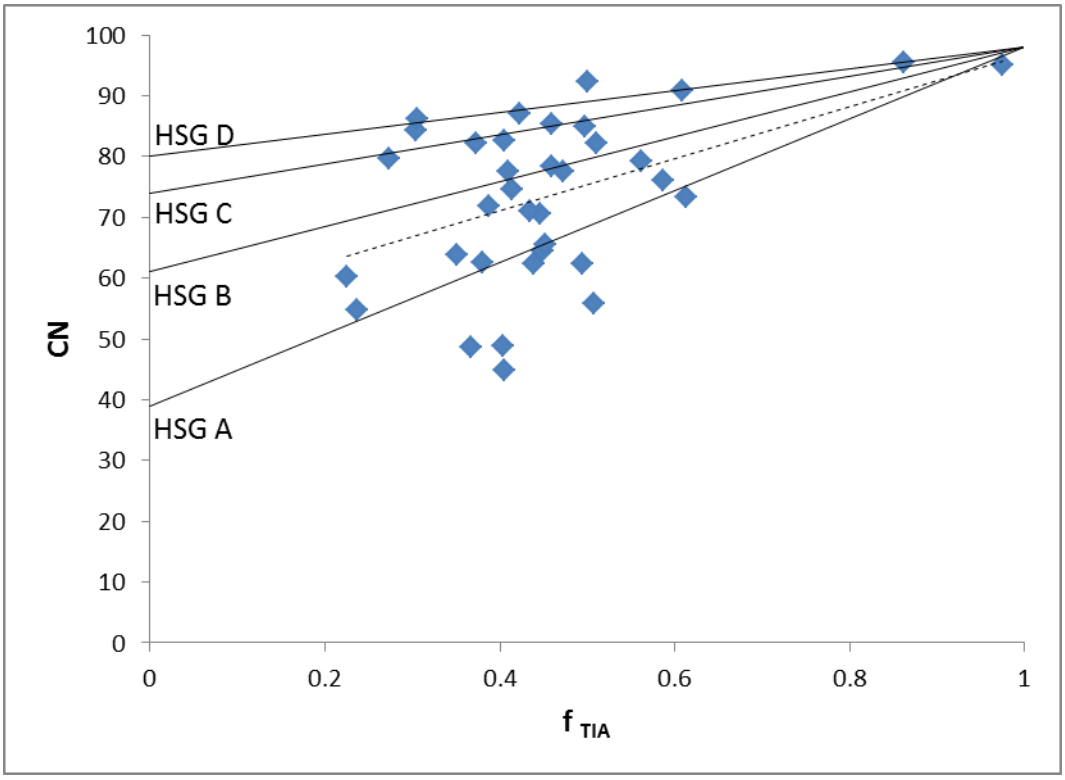

Figure 5.10 Comparison of the regression line for actual CN vs. TIA fraction (dashed line) with the TR-55 CN trends in different hydrologic soil groups (solid lines). The data points are as in Figure 5.9.

5.5.2 Hydrologic soil groups in the study sites

In order to improve the estimation of CN_∞ in ungauged watersheds, hydrologic soil group (HSG) was considered as another watershed characteristic to be used along with TIA in estimation of CN_∞. The spatial information on HSG is accessible through the NRCS Soil Survey Geographic database (SSURGO) in digital format. So, we determined the distribution of HSG in each study site in GIS using SSURGO. Table 5.4 and Figure 5.11 show the percentage of different HSGs in each watershed. To simply express the soil type in terms of HSG, we used the world "Mostly" in the "Remarks" column of the Table 5.4

where the percentage of an HSG is more than 70%. Table 5.4 reveals that the study sites in this study cover all the hydrologic soil groups. Figure 5.11 shows that while all of the study sites in the Twin Cities metro area of Minnesota and Madison, Wisconsin include HSG B and A, most of the study sites in Austin, Texas have HSG D and C. Generally, it means that the soils in Twin Cities metro and Madison watersheds have more infiltration capacity and less runoff generation potential than the soils in Austin, Texas. The HSG information of the study sites were added to the data points in Figure 5.10 and the result is presented in Figure 5.12. A general compatibility between the different HSGs and corresponding trend lines is seen for larger f_{TIA} values in Figure 5.12. However, the scatter around the lines for lower f_{TIA} values reveals that TR-55 CN values are not able to accurately represent the actual CN values in a watershed with different HSGs.

Table 5.4 Percentage of different hydrologic soil groups (HSGs) in the study sites using SSURGO national dataset. The study sites have covered almost all the different HSGs

Row	Site Name	HSG A	HSG B	HSG C	HSG D	Remarks
1	AHUG		100			B
2	GCP		100			B
3	Como 3		100			B
4	Sarita		100			B
5	TBEB	8.9	91.1			Mostly B-A
6	EK		100			B
7	PC	43.5	56.5			B-A
8	SAP		100			B
9	TBO	16.4	83.6			Mostly B-A
10	MG1		100			B
11	MG2		100			B
12	P1		100			B
13	P2		100			B
14	P3		100			B

Row	Site Name	HSG A	HSG B	HSG C	HSG D	Remarks
15	Hedburg		100			B
16	Tapestry		100			B
17	Harper		100			B
18	Monroe		94.6	5.4		Mostly B-C
19	BW1			100		C
20	EBA		71.8	28.2		Mostly B-C
21	EHA		100			B
22	ERA		90.9	9.1		Mostly B-C
23	HI			38.6	61.4	D-C
24	HPA			100		C
25	LCA		0.5	86.6	12.9	Mostly C-D
26	LOA				100	D
27	LUA				100	D
28	MBA			80.4	19.6	Mostly C-D
29	OFA			47.5	52.5	D-C
30	PP1				100	D
31	PP2				100	D
32	PP3				100	D
33	RRI				100	D
34	SCA			100		C
35	TBA			91.9	8.1	Mostly C-D
36	TCA				100	D
37	TPA				100	D
38	WBA			100		C

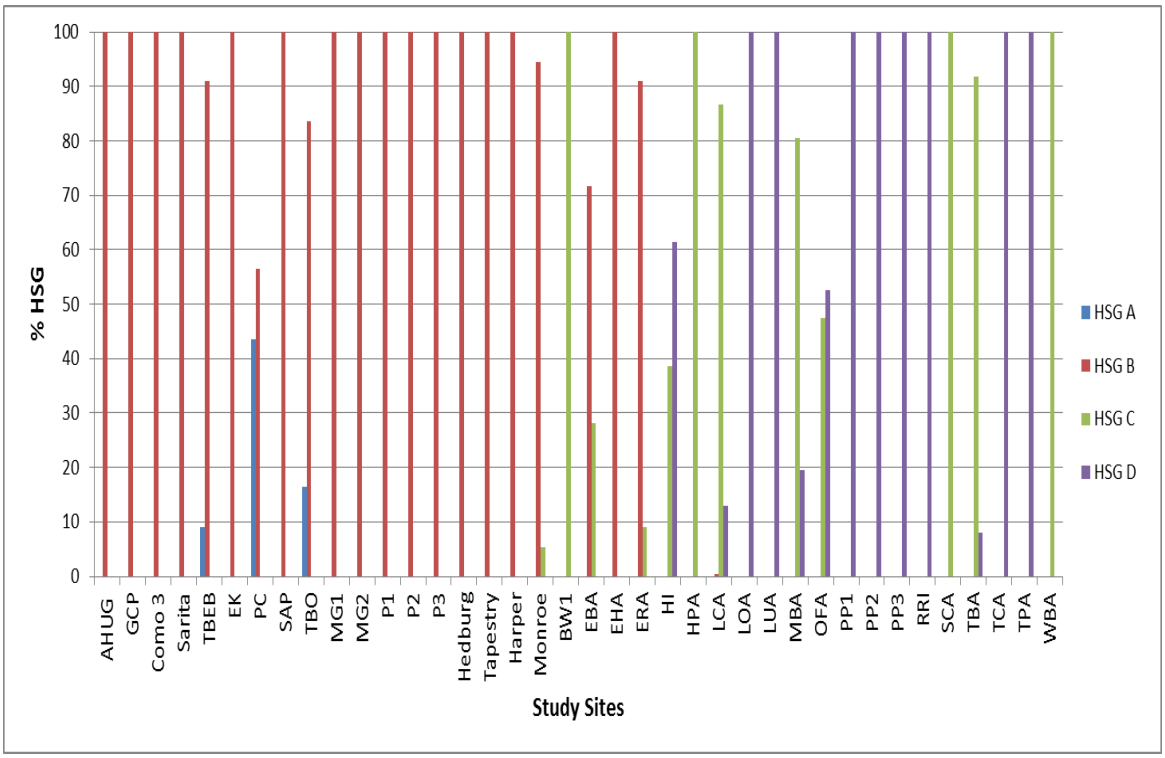

Figure 5.11 Distribution of hydrologic soil groups in the watersheds of study. While all of the study sites in Twin Cities metro area of MN and Madison, WI include HSG B and A, most of the study sites in Austin, TX have HSG D and C. The soils in Twin Cities metro and Madison watersheds have more infiltration capacity and less runoff generation potential in comparison to the soils in Austin.

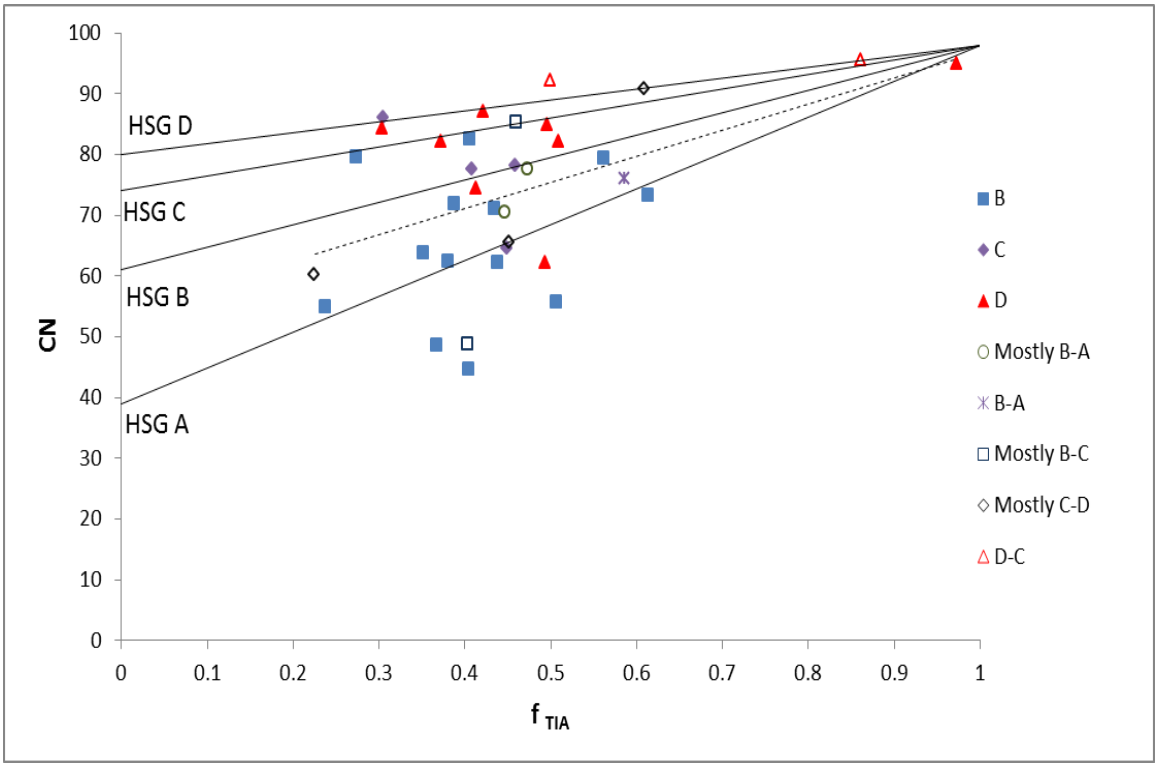

Figure 5.12 Comparison of the TR-55 CN trends in different hydrologic soil groups (solid lines) with the actual HSGs from SSURGO dataset. The data points are the same as Figure 5.10 and the dashed line is the regression line for actual CN vs. TA fraction. The scatter of the data around corresponding lines especially for lower f_{TIA} values indicates the inaccuracies of representing the actual CN values in a watershed with different HSGs and TR-55 CN values.

5.5.3 Saturated hydraulic conductivity of the soils in the study sites

In order to better represent the different soil types in the regression equation for estimating CN_∞ in terms of watershed characteristics, an average saturated hydraulic conductivity (K_{sat}) of the soil for each HSG was used in this study. A discussion about the impact of the K_{sat} on the TR 55 method can be found in Ahmed et al. (2014). Based

on NRCS (2007) for soils with a depth to a water impermeable layer and high water table of more than 100 cm (40 in), HSGs varies with K_{sat} according to Table 5.5.

Table 5.5 Saturated hydraulic conductivity (K_{sat}) for different hydrologic soil groups (HSGs) according to NRCS (2007)

Hydrologic Soil Group (HSG)	**Saturated Hydraulic Conductivity, K_{sat} (*in/hr*)**	**Saturated Hydraulic Conductivity, K_{sat} (*mm/hr*)**
A	> 1.42	> 36.07
B	> 0.57 to ≤ 1.42	> 14.48 to ≤ 36.07
C	> 0.06 to ≤ 0.57	> 1.52 to ≤ 14.48
D	≤ 0.06	≤ 1.52

Table 5.5 provides a range of K_{sat} for each HSG. Because of the high variability of K_{sat}, an arithmetic average is not a good measure to represent the entire range. Hence, an average of log of K_{sat} values for upper and lower limits in each range ($\log(K_{sat})_{average}$) were assigned to each HSG. In order to make a dimensionless parameter to be used in the regression analysis, we picked a reference HSG and considered the assigned value to each HSG as [average log (K_{sat})/average log(K_{sat_ref})] where K_{sat_ref} denotes the K_{sat} of HSG D. Then, the assigned values for HSGs A, B, C, and D are found as 1.37, 1.18, 0.49, and 0, respectively. For example, the calculation for HSG C is as follows.

$$\log[\frac{(K_{sat})_{average}}{(K_{sat\_ref})_{average}}] = \log(K_{sat})_{average} - \log(K_{sat_{ref}})_{average} = 0.67 - 0.18 = 0.49\ mm/hr \quad (5.26)$$

Using the obtained $\log[\frac{(K_{sat})_{average}}{(K_{sat_ref})_{average}}]$for each HSG, a weighted average $\log[\frac{(K_{sat})_{average}}{(K_{sat\_ref})_{average}}]$ for each study site was calculated based on the percentage of different HSGs in each site. The results are presented in Table 5.6. For simplicity, the calculated parameter is called $\log(\frac{K_{sat}}{K_{sat\_ref}})$ from now in this report.

Table 5.6 Dimensionless weighted average values of $log(\frac{K_{sat}}{K_{sat\_ref}})$ for all the study sites using the percentage of HSG in each site

Row	Site Name	HSG A	HSG B	HSG C	HSG D	Remarks	$\log(\frac{K_{sat}}{K_{sat\ ref}})$
1	AHUG		100			B	1.18
2	GCP		100			B	1.18
3	Como 3		100			B	1.18
4	Sarita		100			B	1.18
5	TBEB	8.9	91.1			Mostly B-A	1.19
6	EK		100			B	1.18
7	PC	43.5	56.5			B-A	1.26
8	SAP		100			B	1.18
9	TBO	16.4	83.6			Mostly B-A	1.21
10	MG1		100			B	1.18
11	MG2		100			B	1.18
12	P1		100			B	1.18
13	P2		100			B	1.18
14	P3		100			B	1.18
15	Hedburg		100			B	1.18
16	Tapestry		100			B	1.18
17	Harper		100			B	1.18
18	Monroe		94.6	5.4		Mostly B-C	1.14
19	BW1			100		C	0.49
20	EBA		71.8	28.2		Mostly B-C	0.98

Row	Site Name	HSG A	HSG B	HSG C	HSG D	Remarks	$\log(\frac{K_{sat}}{K_{sat\_ref}})$
21	EHA		100			B	1.18
22	ERA		90.9	9.1		Mostly B-C	1.11
23	HI			38.6	61.4	D-C	0.19
24	HPA			100		C	0.49
25	LCA		0.5	86.6	12.9	Mostly C-D	0.43
26	LOA				100	D	0.00
27	LUA				100	D	0.00
28	MBA			80.4	19.6	Mostly C-D	0.39
29	OFA			47.5	52.5	D-C	0.23
30	PP1				100	D	0.00
31	PP2				100	D	0.00
32	PP3				100	D	0.00
33	RRI				100	D	0.00
34	SCA			100		C	0.49
35	TBA			91.9	8.1	Mostly C-D	0.45
36	TCA				100	D	0.00
37	TPA				100	D	0.00
38	WBA			100		C	0.49

5.5.4 Selection of regression model for the estimation of actual CN

Sixteen regression models using CN_p, f_{TIA} and $\log(\frac{K_{sat}}{K_{sat\_ref}})$ as independent variables for the estimation of CN_∞ in ungauged watersheds as described in Table 5.7 were developed and investigated. As seen in Table 5.7, models 1-6 includes CN_p as independent variable. CN_p is calculated for each ungauged watershed as a weighted average CN corresponding to pervious area from TR-55 CN table for good hydrologic condition according to the percentage of different HSGs in the watershed. Models 3-6 and 9-16 have the term "(1-f_{TIA})" in order to ensure that the characteristics of pervious area (here CN_p or $\log(\frac{K_{sat}}{K_{sat\_ref}})$) has no effect in CN_∞ when $f_{TIA} = 1$.

Table 5.7 Description of the developed models for the estimation of CN_∞ in ungauged watersheds

Row	Model
1	$CN_\infty = b_0 + b_1 f_{TIA} + b_2 CN_p$
2	$CN_\infty = b_0 + b_1 f_{TIA} + b_2 CN_p + b_3 CN_p f_{TIA}$
3	$CN_\infty = b_0 + b_1 f_{TIA} + b_2 (1 - f_{TIA})^{0.1} CN_p$
4	$CN_\infty = b_0 + b_1 f_{TIA} + b_2 (1 - f_{TIA})^{0.5} CN_p$
5	$CN_\infty = b_0 + b_1 f_{TIA} + b_2 (1 - f_{TIA})\ CN_p$
6	$CN_\infty = b_0 + b_1 f_{TIA} + b_2 (1 - f_{TIA})^2 CN_p$
7	$CN_\infty = b_0 + b_1 f_{TIA}$
8	$CN_\infty = b_0 + b_1 f_{TIA} + b_2\ log\left(\frac{K_{sat}}{K_{sat_{Ref}}}\right)$
9	$CN_\infty = b_0 + b_1 f_{TIA} + b_2 (1 - f_{TIA})^{0.1}\ log\left(\frac{K_{sat}}{K_{sat_{Ref}}}\right)$
10	$CN_\infty = b_0 + b_1 f_{TIA} + b_2 (1 - f_{TIA})^{0.3}\ log\left(\frac{K_{sat}}{K_{sat_{Ref}}}\right)$
11	$CN_\infty = b_0 + b_1 f_{TIA} + b_2 (1 - f_{TIA})^{0.5}\ log\left(\frac{K_{sat}}{K_{sat_{Ref}}}\right)$

Row	Model
12	$CN_{\infty} = b_0 + b_1 f_{TIA} + b_2 (1 - f_{TIA})^{0.7} log\left(\frac{K_{sat}}{K_{sat_{Ref}}}\right)$
13	$CN_{\infty} = b_0 + b_1 f_{TIA} + b_2 (1 - f_{TIA})^{0.8} log\left(\frac{K_{sat}}{K_{sat_{Ref}}}\right)$
14	$CN_{\infty} = b_0 + b_1 f_{TIA} + b_2 (1 - f_{TIA})^{0.9} log\left(\frac{K_{sat}}{K_{sat_{Ref}}}\right)$
15	$CN_{\infty} = b_0 + b_1 f_{TIA} + b_2 (1 - f_{TIA}) log\left(\frac{K_{sat}}{K_{sat_{Ref}}}\right)$
16	$CN_{\infty} = b_0 + b_1 f_{TIA} + b_2 (1 - f_{TIA})^2 log\left(\frac{K_{sat}}{K_{sat_{Ref}}}\right)$

The results of the investigation are summarized in Table 5.8. The MSE, R^2, and F* statistics for each model is reported. Variables are evaluated for significance at the 5% level. The overall test statistic F* is defined as

$$F^* = \frac{MSR}{MSE} = \frac{VAR(\hat{y}_i - \bar{y})}{VAR(y_i - \hat{y}_i)} \tag{5.27}$$

A large F* means that at least one of the slope terms in the regression model is significantly different than zero. The significance of each parameter in a model is determined using a t-test. Table 5.8 shows that all variables in the models 1, and 3-13 are statistically significant at the 5% level. Model 12 seems to be the best model among the

others in Table 5.8, because it has the smallest MSE, largest R^2, and largest F*. However, it is only slightly better than models 10-15 in terms of the mentioned statistics. On the other hand, while model 11 has almost the same MSE, R^2, and F* as model 12, it better estimates the CN_∞ in the extreme condition of $f_{TIA} = 1$. Therefore, model 11 (Eq. 5.26) is selected for the estimation of CN_∞ in terms of TIA and K_{sat} in ungauged urban watersheds.

$$CN_\infty = 67.8 + 30.0\, f_{TIA} - 15.1\,(1 - f_{TIA})^{0.5} \log(\frac{K_{sat}}{K_{sat\_Ref}}) \quad (5.28)$$

Table 5.8 Significance and values of the estimated parameters in different models for the estimation of CN_∞ in ungauged watersheds. ✓ indicates that the variable was included in the model and was significant at the 5% level. × indicates that the variable was included in the model and was insignificant at the 5% level

Model No.	(1-fTIA)^ b3 CNp	CNp	fTIA	CNp fTIA	(1-fTIA)^b3 log(Ksat/ Ksat_Ref)	MSE	R^2	F*	b0	b1	b2	b3
1		✓	✓			123.20	0.367	9.270	16.88	36.39	0.58	0
2		×	×	×		125.12	0.377	6.254	-23.44	123.39	1.13	-1.18
3	✓		✓			122.68	0.370	9.378	9.55	51.03	0.64	0.1
4	✓		✓			124.59	0.360	8.987	-3.53	86.46	0.76	0.5
5	✓		✓			121.22	0.377	9.682	-20.89	117.50	1.10	1
6	✓		✓			130.32	0.330	7.890	-1.05	109.30	1.14	2
7			✓			146.73	0.222	9.434	53.89	42.93	0	0
8			✓		✓	119.82	0.384	9.984	65.66	34.14	-10.99	0
9			✓		✓	119.48	0.386	10.057	66.12	33.26	-11.75	0.1
10			✓		✓	118.96	0.389	10.170	66.99	31.57	-13.36	0.3
11			✓		✓	118.66	0.390	10.236	67.77	29.99	-15.08	0.5
12			✓		✓	118.57	0.391	10.256	68.46	28.54	-16.92	0.7

Model No.	(1-fTIA)^ b3 CNp	CNp	fTIA	CNp fTIA	(1-fTIA)^b3 log(Ksat/ Ksat_Ref)	MSE	R^2	F*	b0	b1	b2	b3
13			✓		✓	118.607	0.390	10.248	68.76	27.86	-17.87	0.8
14			×		✓	118.692	0.390	10.230	69.04	27.22	-18.85	0.9
15			×		✓	118.828	0.389	10.200	69.29	26.61	-19.85	1
16			×		✓	122.546	0.370	9.405	70.35	22.63	-30.58	2

5.5.5 Effect of initial abstraction on the estimation of actual CN

Eq. (5.28) describes the proposed model for estimating CN_∞ in terms of f_{TIA} and K_{sat} in ungauged urban watersheds. Other parameters (watershed characteristics) can be incorporated into the model to improve model performance in estimation actual CN. Slope is an important parameter in runoff calculations and intuitively seems to be important in the estimation of actual CN value in watershed. However, determining an average slope in urban watersheds where the storm sewers do not necessarily follow the slope of the streets is not simple. On the other hand, since slope affects the initial abstraction of rainfall (I_a) in an urban watershed, the significance of I_a in the estimation of CN_∞ was first investigated in this study. For this reason, model 17 including I_a as an independent variable was considered as Eq. (5.27).

$$CN_\infty = b_0 + b_1 f_{TIA} + b_2 (1 - f_{TIA})^{0.5} log\left(\frac{K_{sat}}{K_{sat_{Ref}}}\right) + b_3 I_a \quad (5.29)$$

f_{TIA} and $\log(\frac{K_{sat}}{K_{sat\_Ref}})$ are already obtained for all the study sites. Also, I_a values are already calculated for all the study sites using the proposed SWLS method and are

available in Table 3.1. By performing the regression analysis using the model (5.29), b_3 is not found to be significantly different than zero at the 5% level. Therefore, we conclude that the initial abstraction of rainfall is not statistically significant in the estimation of CN_∞based on the watersheds used in this study; hence, no further investigation was performed on the effect of slope on the actual CN.

5.6 Sensitivity of Runoff Depth to EIA Fraction

In order to evaluate the importance of the EIA fraction change on the runoff depth in an ungauged watershed, we developed graphs of runoff depth (Q) versus f_{EIA} for different amounts of rainfall depth (P). The NRCS Curve Number method has been used for the runoff calculation. To determine CN values for each rainfall depth in a watershed with a standard CN pattern from Eq. (5.8), one needs to have both CN_∞ and the exponential parameter *k*. These values for the watersheds of study with standard CN pattern are presented in Table 5.9. The mean, median, and standard deviation of *k* values are 0.0378, 0.0261, and 0.0295, respectively. In order to find a representative *k* value for ungauged watersheds, histograms of *k* was first plotted (Figure 5.13). Since the distribution of *k* appears to be closer to log-normal, the geometric mean of *k* values was used as the representative *k* value for ungauged watersheds. The geometric mean values of *k* was calculated as 0.03.

Table 5.9 CN_∞ and k values for the watersheds of study with a standard CN pattern. Parameter k is a fitting constant defined in Eq. 5.8

Row	Watershed Name	CN_∞	k
1	AHUG	55.8	0.0168
2	GCP	62.3	0.0117
3	Como 3	44.7	0.0153
4	Sarita	48.6	0.0238
5	TBEB	70.6	0.0219
6	EK	79.3	0.0153
7	PC	76.1	0.0202
8	SAP	73.2	0.0223
9	TBO	77.6	0.0204
10	MG1	82.5	0.0600
11	MG2	71.9	0.0264
12	P1	62.5	0.0219
13	P2	63.9	0.0261
14	P3	79.7	0.0569
15	Tapestry	54.9	0.0175
16	Smith Pond	75.1	0.0553
17	BW1	78.3	0.0387
18	EBA	48.9	0.0179
19	EHA	71.1	0.0132
20	ERA	85.3	0.0467
21	HI	92.3	0.0902
22	HPA	64.5	0.0096
23	LCA	60.2	0.0258
24	LOA	87.1	0.0474
25	LUA	95.1	0.0616
26	MBA	90.9	0.0898
27	OFA	95.6	0.1554
28	PP1	84.9	0.0403
29	PP2	82.2	0.0300
30	PP3	62.3	0.0178
31	RRI	84.2	0.0477
32	SCA	77.7	0.0318
33	TBA	65.5	0.0221
34	TCA	82.1	0.0721
35	TPA	74.5	0.0337

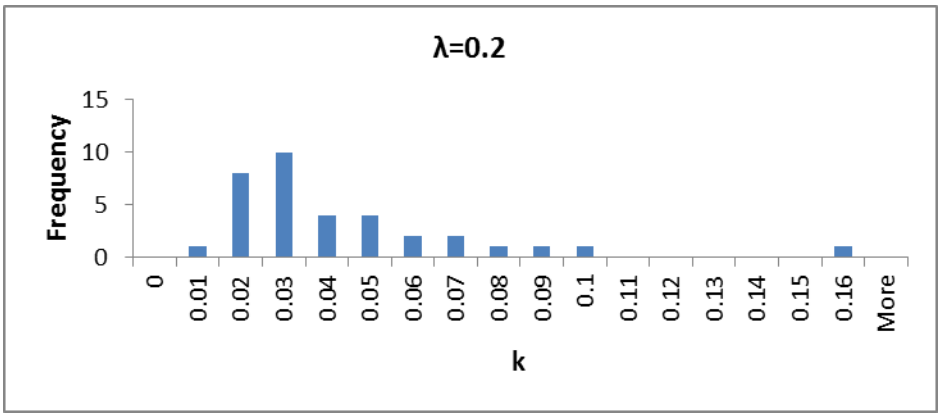

Figure 5.13 Histogram of the fitting parameter k for the watersheds of study with standard CN pattern.

Runoff depth (Q) in an ungauged watershed with a standard CN pattern was calculated in terms of EIA fraction (f_{EIA}) for 4 rainfall depths of 12.5, 25, 50 and 75 mm (i.e. 0.5, 1, 2, and 3 in). The results are presented in Table 5.10. Actual CN (CN_∞) in the second column of this table is calculated in terms of f_{EIA} based on Eq. (5.30) which is another form of Eq. (5.22).

$$CN_\infty = \begin{cases} 57.25\, f_{EIA} + 40 & if\ 0 \le f_{EIA} \le 0.157 \\ \frac{114\, f_{EIA} - 16}{1.14\, f_{EIA} - 0.14} & if\ 0.157 < f_{EIA} \le 1 \end{cases} \quad (5.30)$$

where $f_{EIA} = 0.157$ is corresponding to $CN_\infty = 49$ in Eq. (5.22).

CN values for each rainfall depth (P) are calculated based on Eq. (5.8). Based on the above discussion, the *k* parameter is considered as 0.03. The storage index S is then calculated from Eq. (5.6). Finally the runoff depth (Q) for each rainfall depth (P) is

calculated from Eq. (5.4) and (5.5). Since the actual f_{EIA} values in our study sites based on the proposed SWLS method were all less than 0.5, plot of runoff depth (Q) against EIA fraction (f_{EIA}) for different rainfall depths based on Table 5.10 is presented for f_{EIA} between zero and 0.5. This plot which is shown in Figure 5.14 can be utilized to show the sensitivity of runoff depth to EIA fraction for different rainfall depths in ungauged watersheds with standard CN pattern.

Table 5.10 Runoff depth in terms of EIA fraction in ungauged urban watersheds with a standard CN pattern

f_{EIA}	CN_∞	CN				S (mm)				Q (mm)			
		P= 12.5 mm	P= 25 mm	P= 50 mm	P= 75 mm	P= 12.5 mm	P= 25 mm	P= 50 mm	P= 75 mm	P= 12.5 mm	P= 25 mm	P= 50 mm	P= 75 mm
0	40	81.03	68.06	53.12	46.14	59.46	119.2	224.14	296.53	0.01	0.01	0.12	0.79
0.05	42.9	81.94	69.58	55.36	48.71	56.00	111.0	204.82	267.49	0.03	0.07	0.38	1.60
0.1	45.7	82.84	71.11	57.60	51.28	52.61	103.2	187.01	241.35	0.07	0.18	0.80	2.67
0.15	48.6	83.75	72.63	59.83	53.85	49.30	95.71	170.52	217.71	0.13	0.34	1.36	3.97
0.157	49	83.88	72.85	60.15	54.22	48.82	94.66	168.25	214.49	0.15	0.37	1.45	4.18
0.16	52.8	85.09	74.89	63.15	57.65	44.52	85.16	148.24	186.55	0.27	0.68	2.46	6.33
0.17	62.8	88.25	80.21	70.96	66.63	33.83	62.67	103.97	127.22	0.83	2.07	6.41	13.89
0.2	77.3	92.82	87.90	82.24	79.60	19.66	34.96	54.84	65.11	2.60	6.12	16.23	30.23
0.25	86.2	95.64	92.66	89.22	87.62	11.58	20.13	30.68	35.90	4.77	10.70	25.81	44.35
0.3	90.1	96.87	94.73	92.26	91.11	8.21	14.13	21.30	24.78	6.18	13.54	31.21	51.74
0.35	92.3	97.56	95.89	93.97	93.07	6.36	10.89	16.31	18.92	7.17	15.45	34.65	56.27
0.4	93.7	98.00	96.63	95.06	94.32	5.19	8.86	13.21	15.30	7.89	16.82	37.03	59.32
0.45	94.6	98.30	97.15	95.81	95.19	4.38	7.46	11.11	12.84	8.44	17.84	38.77	61.52
0.5	95.3	98.53	97.52	96.37	95.82	3.79	6.45	9.58	11.07	8.88	18.64	40.10	63.18
0.55	95.9	98.70	97.81	96.79	96.31	3.34	5.68	8.42	9.72	9.23	19.28	41.15	64.47
0.6	96.3	98.84	98.04	97.13	96.70	2.99	5.07	7.51	8.67	9.51	19.80	41.99	65.51

f_{EIA}	CN_∞	CN				S (mm)				Q (mm)			
		P= 12.5 mm	P= 25 mm	P= 50 mm	P= 75 mm	P= 12.5 mm	P= 25 mm	P= 50 mm	P= 75 mm	P= 12.5 mm	P= 25 mm	P= 50 mm	P= 75 mm
0.65	96.7	98.95	98.23	97.40	97.01	2.70	4.58	6.78	7.82	9.76	20.24	42.69	66.37
0.7	97.0	99.04	98.38	97.63	97.27	2.46	4.18	6.18	7.13	9.96	20.60	43.28	67.08
0.75	97.2	99.12	98.51	97.81	97.49	2.27	3.84	5.67	6.54	10.14	20.92	43.78	67.68
0.8	97.4	99.18	98.62	97.98	97.67	2.10	3.55	5.25	6.05	10.29	21.19	44.21	68.20
0.85	97.6	99.24	98.72	98.12	97.83	1.95	3.30	4.88	5.62	10.43	21.43	44.59	68.65

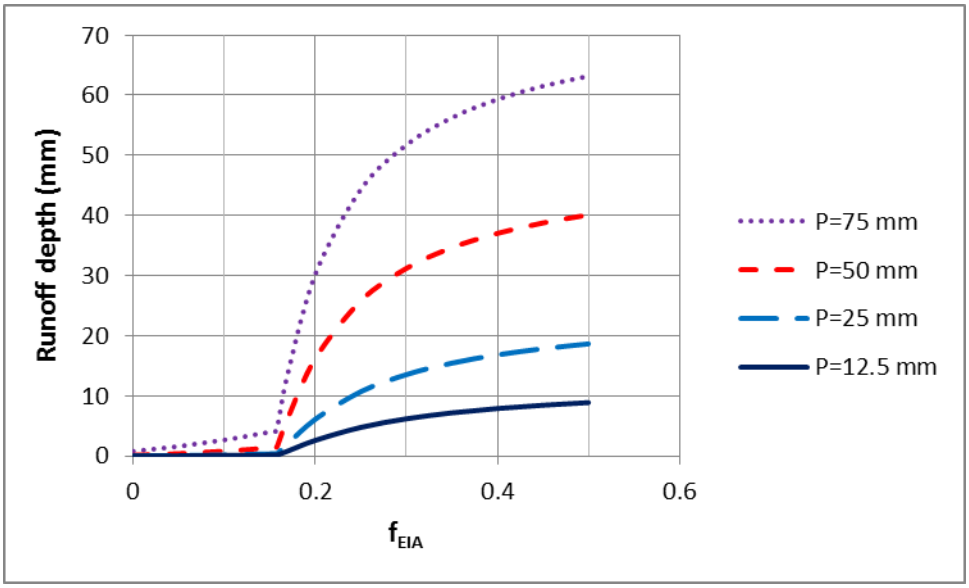

Figure 5.14 Runoff depth (Q) against EIA fraction (f_{EIA}) for different rainfall depths.

To compare the presented graph of Q vs. f_{EIA} with the observed values, runoff depth was calculated using the actual f_{EIA} , CN_∞ , and k values of study sites with standard CN pattern for the same rainfall depths in Figure 5.14. The results are presented in Table 5.11. For each watershed in Table 5.11, f_{EIA} is obtained from the proposed SWLS method (Table 5.2). Also, CN_∞ and k values can be found from Table 5.9. Then, CN for

each rainfall depth is calculated based on Eq. (5.8) using actual CN_∞ and k values of the watershed. Other steps for the runoff calculation are the same as Table 5.10. The obtained pairs of (f_{EIA} , Q) from Table 5.11 were added to the plot of Q vs. f_{EIA} to compare the developed curves for ungauged watersheds to the actual data. The result is presented in Figure 5.15. The curves for lower rainfalls are overestimating the runoff depth especially in higher f_{EIA} values. While the general trend of data agrees with the curves, more scatter is seen in higher rainfalls. This might be explained by the amount of contributing pervious area in a watershed. In other words, in higher rainfall depths (e.g. P=75 mm in Figure 5.15) more pervious area is expected to contribute to runoff generation. Hence, parameters such as soil type, infiltration capacity, and initial moisture content as well as initial abstraction of the pervious surfaces are added to the runoff generation process which make it more complex. To examine the effect of infiltration capacity of the soil on the amount of runoff depth in higher rainfall depths, weighted average hydrologic soil group (HSG) in the watersheds of study (as discussed in section 5.5.2 and Table 5.4) was used. As an example, Figure 5.16 displays different HSGs corresponding to the actual (f_{EIA},Q) data and compares them with the developed Q vs. f_{EIA} curve for ungauged watersheds at P=75 mm. As expected, Figure 5.16 depicts that the points including HSGs with higher infiltration capacity and lower runoff potential (e.g. HSGs A and B) are generally lower than the higher runoff potential HSGs in the plot. However, there are points (especially in lower f_{EIA} values which correspond to more pervious watersheds) that do not follow this pattern. As mentioned before, this might be explained by the other characteristics of contributing pervious area to runoff generation (e.g. initial moisture content of the soil and initial abstraction of the pervious surfaces).

Table 5.11 Actual runoff depth (Q) in the study sites with standard CN pattern for different rainfall depths using the actual f_{EIA} , CN_{∞} , and k values

Site Name	CN				S (mm)				Q (mm)			
	P= 12.5 mm	P= 25 mm	P= 50 mm	P= 75 mm	P= 12.5 mm	P= 25 mm	P= 50 mm	P= 75 mm	P= 12.5 mm	P= 25 mm	P= 50 mm	P= 75 mm
AHUG	91.6	84.8	74.8	68.3	23.25	45.46	85.35	117.87	1.98	4.12	9.17	15.62
GCP	94.9	90.4	83.3	78.0	13.73	26.85	50.90	71.72	4.05	8.29	17.48	27.79
Como 3	90.4	82.5	70.5	62.3	26.96	53.97	106.24	153.46	1.48	2.96	6.12	9.93
Sarita	86.8	77.0	64.3	57.2	38.69	76.03	141.30	189.69	0.52	1.12	2.90	6.06
TBEB	93.0	87.6	80.4	76.3	19.23	35.93	61.77	78.95	2.69	5.90	14.25	25.38
EK	96.4	93.4	89.0	85.9	9.47	17.84	31.53	41.69	5.60	11.70	25.38	41.01
PC	94.7	90.5	84.8	81.3	14.34	26.65	45.62	58.36	3.87	8.35	19.32	32.96
SAP	93.5	88.6	82.0	78.3	17.68	32.79	55.70	70.54	3.02	6.64	15.97	28.21
TBO	95.0	91.0	85.7	82.4	13.49	24.97	42.49	54.11	4.13	8.90	20.51	34.82
MG1	90.8	86.4	83.4	82.7	25.77	39.85	50.50	52.97	1.63	5.10	17.61	35.34
MG2	92.1	86.4	79.4	75.8	21.76	39.86	65.80	81.09	2.22	5.10	13.22	24.70
P1	91.0	84.2	75.1	69.8	25.04	47.66	84.39	110.02	1.73	3.79	9.34	17.23
P2	89.9	82.7	73.7	69.0	28.41	53.20	90.81	114.30	1.32	3.05	8.26	16.33
P3	89.7	84.6	80.9	80.0	29.30	46.32	60.13	63.65	1.23	3.99	14.70	30.79
Tapestry	91.1	84.0	73.6	67.0	24.76	48.45	90.88	125.21	1.76	3.68	8.25	14.25
Smith Pond	87.6	81.4	76.7	75.5	35.96	58.09	77.10	82.23	0.68	2.51	10.71	24.35
BW1	91.7	86.5	81.4	79.5	23.09	39.53	57.96	65.57	2.01	5.16	15.31	30.05
EBA	89.7	81.5	69.7	62.2	29.04	57.50	110.17	154.27	1.25	2.57	5.66	9.82
EHA	95.6	91.8	86.0	81.8	11.73	22.55	41.38	56.56	4.71	9.76	20.95	33.73
ERA	93.5	89.9	86.7	85.7	17.67	28.64	38.91	42.27	3.02	7.75	21.97	40.70
HI	94.8	93.1	92.4	92.3	13.93	18.78	20.91	21.13	3.99	11.28	31.46	54.50
HPA	96.0	92.4	86.5	81.8	10.61	20.78	39.69	56.51	5.13	10.44	21.64	33.75
LCA	89.0	81.1	71.2	65.9	31.29	59.26	102.98	131.21	1.04	2.39	6.53	13.21
LOA	94.2	91.1	88.3	87.5	15.51	24.94	33.57	36.33	3.55	8.91	24.38	44.09
LUA	97.4	96.1	95.3	95.1	6.90	10.23	12.53	13.03	6.86	15.88	37.58	61.35
MBA	93.9	91.9	91.0	91.0	16.53	22.38	24.98	25.26	3.29	9.82	28.94	51.39
OFA	96.2	95.7	95.6	95.6	10.00	11.50	11.75	11.75	5.38	15.07	38.23	62.54
PP1	94.0	90.4	86.9	85.7	16.10	26.86	38.14	42.49	3.39	8.29	22.30	40.57
PP2	94.4	90.6	86.2	84.1	14.97	26.31	40.72	48.05	3.69	8.46	21.22	37.69
PP3	92.5	86.4	77.8	72.2	20.68	39.83	72.63	97.76	2.41	5.10	11.64	20.07
RRI	92.9	89.0	85.7	84.7	19.33	31.30	42.39	45.93	2.67	7.02	20.55	38.76
SCA	92.7	87.7	82.2	79.7	20.09	35.48	54.97	64.65	2.52	6.00	16.19	30.40

Site Name	CN				S (mm)				Q (mm)			
	P= 12.5 mm	P= 25 mm	P= 50 mm	P= 75 mm	P= 12.5 mm	P= 25 mm	P= 50 mm	P= 75 mm	P= 12.5 mm	P= 25 mm	P= 50 mm	P= 75 mm
TBA	91.7	85.4	76.9	72.1	23.07	43.57	76.14	98.32	2.01	4.43	10.90	19.93
TCA	89.4	85.0	82.6	82.2	30.22	44.65	53.57	55.09	1.14	4.25	16.62	34.38
TPA	91.2	85.5	79.2	76.5	24.40	43.13	66.58	77.87	1.81	4.51	13.03	25.72

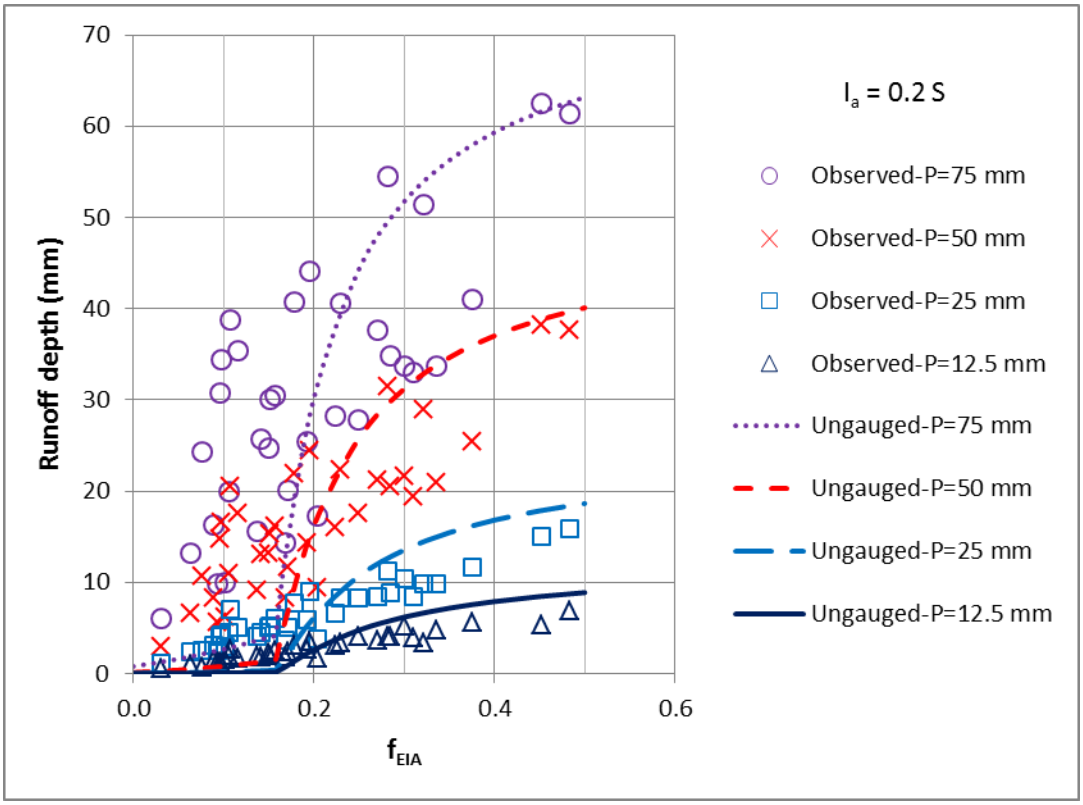

Figure 5.15 Comparison of the developed Runoff depth vs. EIA fraction curves for ungauged watersheds with the actual data.

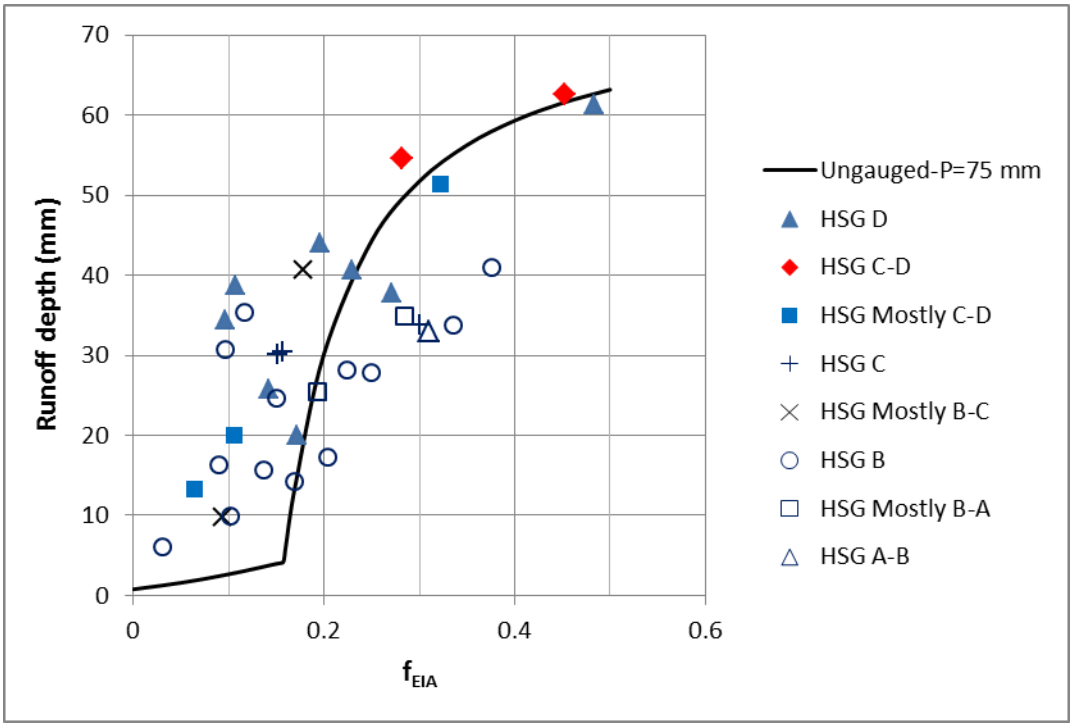

Figure 5.16 Using hydrologic soil group (HSG) to partially explain the scatter of the actual data in comparison to the developed Runoff depth vs. EIA fraction curve for ungauged watersheds with P=75 mm.

5.7 Summary

Our proposed GIS-CN method for estimating f_{EIA} in ungauged urban watersheds is summarized as the following steps:

1- Extract the spatial information of impervious area and hydrologic soil groups (HSGs) from the available land cover and soil GIS datasets and calculate fraction of total impervious area (f_{TIA}) and weighted average saturated hydraulic conductivity (K_{sat}) of the soil for the study site using Table 5.5 and section 5.5.3.

2- Estimate the actual curve number of the watershed (CN_∞) as a function of f_{TIA} and K_{sat} using Equation (5.28).

3- Determine the fraction of effective impervious area (f_{EIA}) as a function of CN_∞ using Equation (5.22).

Those three steps in the proposed GIS-CN method are shown in Figure 5.17.

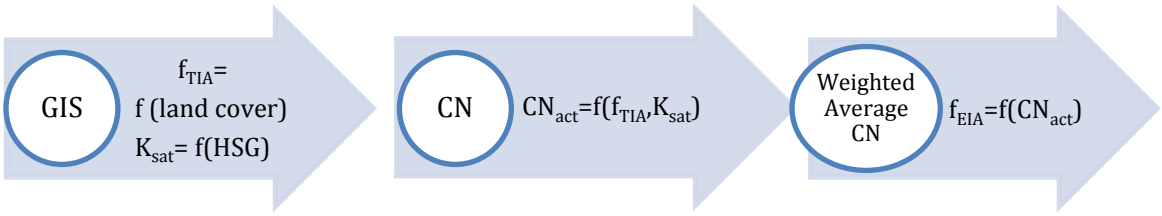

Figure 5.17 The process of determining f_{EIA} in ungauged urban watersheds in the proposed GIS-CN method.

The proposed GIS-CN method is relatively simple and can be applied to ungauged urban watersheds. It is simpler than the Han and Burian (2009) method, as it does not need the familiarity with GIS programming and spatial information on stormwater collection inlets. The required spatial data are land cover and hydrologic soil group which are both available in all watersheds through national datasets. The method does not need the digital elevation model (DEM) or the location of storm sewer network. A limitation of the method is that the results are valid only for EIA greater than 16%. The equations of the GIS-CN method presented in this report have been developed based on 40 urban watersheds with different sizes and characteristics in the Twin Cities metro area of

Minnesota, City of Madison, Wisconsin, and City of Austin, Texas. However, the presented general framework is capable of being applied to more urban watersheds in order to generalize the equations of the method.

CHAPTER 6: CONCLUSIONS

Two important parameters related to impervious surfaces in urban watersheds, total impervious area (TIA) and effective impervious area (EIA) were considered and discussed in this study. EIA is the most important watershed parameter in determining urban runoff. Knowledge of EIA is therefore critical in rainfall-runoff modeling. The incorrect use of TIA instead of EIA results in an overestimation of runoff volumes and rates and the overdesign of associated hydraulic structures. In addition, EIA is the primary contributing area for smaller storms and therefore the main concern for water quality. Design of stormwater control measures should therefore be based on EIA instead of TIA.

Proper methods for determining TIA and EIA were examined and proposed. The proposed methods were applied to 40 urban catchments of different sizes and various hydrologic conditions in the Twin Cities metro area of Minnesota, City of Madison, Wisconsin and City of Austin, Texas. The 18 catchments in the Twin Cities metro area have a range of sizes between 2.8 ha (Hedburg Drive, Minnetonka) and 2034.8 ha (Trout Brook outlet, Capitol Region Watershed District). The two catchments in Madison, Wisconsin, are 16.4 and 92.9 ha. The remaining 20 urban catchments are located in Austin, Texas and have a drainage area between 0.4 ha (WBA) and 146.3 ha (BW1). The main land use in the study sites were predominantly single-family residential, with a few catchments having predominantly commercial and institutional land use. The results of our GIS analysis on the spatial soil data showed that the infiltration rate of soils in the Twin Cities metro watersheds is generally higher than the watersheds in Austin, Texas.

The hydrologic soil group (HSG) in the Twin Cities metro watersheds was mostly B; this index for Austin watersheds was mostly C and D, which indicates a lower soil permeability and higher runoff potential in Austin watersheds.

The most accurate method for quantifying EIA in urban watersheds is the statistical analysis of observed rainfall-runoff data. Without a good comparison to EIA determined from rainfall and runoff data, the other techniques to measure EIA (e.g. GIS techniques) cannot be verified. Different issues about the current rainfall-runoff analysis method that reduce the accuracy of the EIA estimates (e.g. spatial variation of rainfall, runoff measurement error, and heteroscedasticity) were identified as:

1. Spatial variation of rainfall is an issue in larger watersheds. It was addressed by excluding the rainfall data with high spatial variability using a Modified Coefficient of Spatial Variation (MCSV) based on a Relative Root Mean Square Deviation (RRMSD) index.
2. Runoff measurement error is an inevitable issue in the flow monitoring process, which originates from various natural, human and instrument errors. This issue was addressed by proposing a new EIA criterion equal to the maximum of two times the standard error of runoff depth and 1 mm for categorizing EIA and combined events in the rainfall-runoff data of a watershed.
3. Heteroscedasticity is the problem of having non-constant variance of residuals in the regression process of runoff depth versus rainfall depth in a watershed that has a negative impact on the accuracy of the regression parameters (EIA fraction and initial abstraction). To decrease the uncertainty of EIA estimates and account for

heteroscedasticity in rainfall-runoff dataset, using weighted least square (WLS) instead of ordinary least square (OLS) in a successive regression process was proposed.

4. The proposed successive weighted least square (SWLS) method with the improved EIA criterion is recommended when the runoff measurement errors are uncorrelated. However, the successive ordinary least square (SOLS) method with the improved EIA criterion can also be used for homoscedastic problem where the runoff measurement errors have equal variances.

Analysis of rainfall-runoff data from the 40 mentioned urban catchments in this study revealed two general different runoff mechanisms: runoff from effective impervious surfaces (EIA events) and runoff from pervious and non-effective impervious surfaces (combined events). For the catchments with heteroscedastic data, using the SWLS method led to change in the categorization of the runoff events (i.e. EIA and combined events) so that fewer small rainfall depths were categorized as combined events. However, for other catchments no substantial change was seen in that categorization.

The EIA estimate in the method of statistical analysis of rainfall-runoff data is sensitive to the accuracy of monitoring data. On the other hand, stormwater runoff flow measurement is often a problematic process and monitoring results might be affected by various unexpected natural, human, and instrument-related errors. Thus, quality control on the rainfall-runoff dataset is recommended prior to the application of rainfall-runoff analysis method (specially the SOLS method).

To estimate the EIA fraction in ungauged watersheds, a new method based on the integration of GIS and Curve Number (CN) was developed. The proposed GIS-CN method is able to estimate the EIA fraction as a function of TIA and saturated hydraulic conductivity of the soil (K_{sat}) in an ungauged watershed. By making relationships between K_{sat} and HSG, and given that HSG spatial data are readily available through national datasets (e.g. SSURGO), we were able to use K_{sat} as an available parameter in ungauged watersheds. Our investigations on the CN behaviors against rainfall depth (P) in our urban watersheds showed the standard exponential pattern for CN-P plots in all of the watersheds of study except two, which both had a limited number of events in their monitoring dataset. By dividing the entire watershed into effective impervious area and the remaining portion, a strong correlation was found between the Curve Numbers associated with each portion that makes it possible to estimate CN for the remaining area. The presented GIS-CN technique was developed based on 40 urban watersheds with different sizes and characteristics in the Twin Cities metro area of Minnesota, City of Madison, Wisconsin, and City of Austin, Texas. All of the hydrologic soil groups were well-represented in these watersheds. In addition, the presented general framework is capable of being applied to more urban watersheds in order to further generalize the method.

TIA was another parameter related to impervious surfaces considered and discussed in this study. To use the proposed GIS-CN method and also estimate the portion of impervious surfaces in a watershed that is hydraulically connected to the drainage system (i.e. ratio of EIA/TIA), we need to calculate TIA from land cover data. Our proposed

procedure for modifying the spatial land cover data by un-shading the impervious surfaces obscured by tree canopy led to a notable increase (up to 29%) in the TIA of watersheds with high amount of tree canopy overhanging the streets and other impervious area in the watershed. Hence, the modification (un-shading) of land cover spatial data when the tree canopy classification is available in the land cover layers is recommended. The ratio of EIA/TIA in our study catchments reveals that only about half of the impervious surfaces in our residential watersheds are hydraulically connected to the drainage system.

The implementation opportunities of this study are immediate and not limited to a specific location. The end users of this research will be cities, counties, watershed districts, watershed management organizations, state departments of transportation, and the consultants who work for these entities in computing and modeling runoff from urban watersheds. The outcome and applications of the study will eventually lead to more cost-effective design of urban stormwater infrastructure. Proper identification of EIA will result in: more effective planning, locating and design of SCMs; identifying stormwater runoff pollution sources and environmental pollution control; cost savings; and more public consent due to the decreasing size of projects. A wide range of organizations involved in the design of stormwater management, pollution prevention, and transportation structures will benefit from this study.

REFERENCES

Ahmed, F., Natarajan, P., Gulliver, J. S., Weiss, P. T., & Nieber, J. L. (2014). *Assessing and Improving Pollution Prevention by Swales.* Final Report. Minnesota Department of Transportation. St. Paul, MN.

Ahmed, F., Gulliver, J. S., & Nieber, J. L. (2015). "Field infiltration measurements in grassed swales." *Journal of Hydrology,* Under review.

Alley, W. M., & Veenhuis, J. E. (1983). "Effective impervious area in urban runoff modeling." *Journal of Hydraulic Engineering, 109(2),* 313-319.

Asleson, B. C., Nestingen, R. S., Gulliver, J. S., Hozalski, R. M., & Nieber, J. L. (2009). "Performance assessment of rain gardens." *Journal of the American Water Resources Association,* 45(4), 1019-1031.

Barten, J., Vlach, B., Johnson, J., & Zachay, M. (2006) *Monitoring the Long-term Effectiveness of Metropolitan Cold Weather BMPs, Long-term Assessment of Phosphorus Free Fertilizers and Golf Course BMPs.* Final Report for the Grant Agreement CFMS NO. A56488, Three Rivers Park District, Plymouth, MN.

Bauer, M., Kilberg, D., Martin, M., & Tagar, Z. 2011. *Digital Classification and Mapping of Urban Tree Cover: City of Minneapolis.* Final Report. Department of Forest Resources, University of Minnesota, St. Paul, MN.

Beck, J. V., & Arnold, K. J. (1977). *Parameter estimation in engineering and science.* John Wiley & Sons, New York.

Bochis, C. & Pitt, R. (2005). "Impervious Surfaces in Urban Watersheds." *78th Annual Water Environment Federation Technical Exposition and Conference.* Washington, D.C. Oct. 29 – Nov. 2, 2005.

Bochis, C., Pitt, R., & Johnson, P. (2008). "Land development characteristics in Jefferson County, Alabama." In: *Stormwater and Urban Water Systems Modeling, Monograph 16.* (edited by W. James, E.A. McBean, R.E. Pitt and S.J. Wright). Computational Hydraulics International (CHI). Guelph, Ontario, pp. 249 – 282.

Boyd, M. J., Bufill, M. C., & Knee, R. M. (1993). "Pervious and impervious runoff in urban catchments." *Hydrological Sciences Journal, 38*(6), 463-478.

Boyd, M. J., Bufill, M. C., & Knee, R. M. (1994). "Predicting pervious and impervious storm runoff from urban drainage basins." *Hydrological Sciences Journal, 39*(4), 321-332.

Cablk, M. E., & Minor, T. B. (2003). "Detecting and discriminating impervious cover with high-resolution IKONOS data using principal component analysis and morphological operators." *International Journal of Remote Sensing, 24*(23), 4627–4645.

Capitol Region Watershed District (CRWD). (2012). *Capitol Region Watershed District 2011 Monitoring Report*, Capitol Region Watershed District, St. Paul, MN.

Chabaeva, A., Civco, D. L., & Hurd, J. D. (2009). "Assessment of impervious surface estimation techniques." *Journal of Hydrologic Engineering, 14*(4), 377-387.

Chiew, F. H. S., & McMahon, T. A. (1999). "Modelling runoff and diffuse pollution loads in urban areas." *Water Science and Technology, 39*(12), 241-248.

D'Asaro, F., & Grillone, G. (2012). "Empirical investigation of curve number method parameters in the Mediterranean area." *Journal of Hydrologic Engineering, 17(10),* 1141-1152.

D'Asaro, F., Grillone, G., & Hawkins, R. H. (2014). "Curve Number: Empirical evaluation and comparison with Curve Number handbook tables in Sicily." *Journal of Hydrologic Engineering, 19(12)*.

EPA. (2014). *Estimating Change in Impervious Area (IA) and Directly Connected Impervious Areas (DCIA) for New Hampshire Small MS4 Permit.* (Accessed June 2014), http://www.epa.gov/region1/npdes/stormwater/nh/NHDCIA.pdf

Fletcher, T. D., Andrieu, H., & Hamel, P. (2013). "Understanding, management and modelling of urban hydrology and its consequences for receiving waters: A state of the art." *Advances in Water Resources*, 51, 261-279.

Glick, R., Zhu, T., Bai, B., Hubka, J., Robinson, R., Mahmoud, S., Manning, S., Moezzi, A., & Selucky, J. (2009) *Stormwater Runoff Quality and Quantity from Small Watersheds in Austin, TX: Updated through 2008,* Report CM-09-03, City of Austin, Watershed Protection Department, Austin, TX.

Guo, J. C. (2008). "Volume-Based Imperviousness for Storm Water Designs." *Journal of Irrigation and Drainage Engineering, 134*(2), 193-196.

Guo, J. C., Blackler, G. E., Earles, T. A., & MacKenzie, K. (2010). "Incentive index developed to evaluate storm-water low-impact designs." *Journal of Environmental Engineering, 136*(12), 1341-1346.

Han, W. S., & Burian, S. J. (2009). "Determining effective impervious area for urban hydrologic modeling." *Journal of Hydrologic Engineering, 14*(2), 111-120.

Hatt, B. E., Fletcher, T. D., Walsh, C. J., & Taylor, S. L. (2004). "The influence of urban density and drainage infrastructure on the concentrations and loads of pollutants in small streams." *Environmental Management, 34*(1), 112-124.

Hawkins, R. H. (1993). "Asymptotic determination of runoff curve numbers from data." *Journal of Irrigation and Drainage Engineering, 119(2),* 334-345.

Hawkins, R. H., Ward, T. J., Woodward, D. E., & Van Mullem, J. A. (2009). *Curve number hydrology, State of the practice*. ASCE, Reston, VA.

Hawkins, R. H., Ward, T. J., Woodward, D. E., & Van Mullem, J. A. (2010). "Continuing evolution of rainfall-runoff and the curve number precedent." In Proceedings of the 4th Federal Interagency Hydrologic Modeling Conference, Las Vegas, June 27 – July 1, 2010.

Hernandez-Guzman, R., & Ruiz-Luna A. (2013). "SARA – an enhanced curve number-based tool for estimating direct runoff." *Journal of Hydroinformatics*, *15*(3), 881-887.

Hjelmfelt, A. T. (1980). "Empirical investigation of curve number technique." *Journal of the Hydraulics Division, 106(9),* 1471-1476.

Janke, B., Gulliver, J. S., & Wilson, B. N. (2011). *Development of Techniques to Quantify Effective Impervious Cover,* Report No. CTS 11-20, Center for Transportation Studies, University of Minnesota, Minneapolis, MN.

Judge, G. G., Hill, R. C., Griffiths, W. E., Lutkepohl, H., & Lee, T.- C. (1988). *Introduction to the theory and practice of econometrics.* John Wiley and Sons, New York.

Kilberg, D., Martin, M., & Bauer, M. (2011). *Digital Classification and Mapping of Urban Tree Cover: City of St. Paul.* Final Report. Department of Forest Resources, University of Minnesota, Minneapolis-St. Paul, MN.

Laenen, A. (1983). *Storm Runoff as Related to Urbanization Based on Data Collected in Salem and Portland and Generalized for the Willamette Valley, Oregon.* USGS Water Resources Investigations, Portland, OR.

Lee, J. G., & Heaney, J. P. (2003). "Estimation of urban imperviousness and its impacts on storm water systems." *Journal of Water Resources Planning and Management*, *129*(5), 419-426.

Nagarajan, N., & Poongothai, S. (2012). "Spatial mapping of runoff from a watershed using SCS-CN method with remote sensing and GIS." *Journal of Hydrologic Engineering*, *17*(11), 1268-1277.

Natural Resources Conservation Service (NRCS). (2004). *National Engineering Handbook, Part 630 Hydrology*, USDA, Washington, DC.

Natural Resources Conservation Service (NRCS). (2007). *National Engineering Handbook, Part 630 Hydrology*, "Hydrologic Soil Groups", USDA, Washington, DC.

NEMO, Center for Land Use Education and Research (CLEAR), College of Agriculture and Natural Resources, University of Connecticut, Internet. http://nemo.uconn.edu/tools/impervious_surfaces/measure.htm, (Accessed 1/18/2013).

Olson, N. C., Gulliver, J. S., Nieber, J. L., & Kayhanian, M. (2013). "Remediation to improve infiltration into compact soils." *Journal of environmental management*, *117*, 85-95.

Pandit, A., & Regan, J. (1998). "What is the impervious area curve number." *Advances in Modeling the Management of Stormwater Impacts*, *6*, 437-450.

Paus, K. H., Morgan, J., Gulliver, J. S., Leiknes, T., & Hozalski, R. M. (2014). "Assessment of the hydraulic and toxic metal removal capacities of Bioretention cells after 2 to 8 years of service." *Water, Air, & Soil Pollution*, *225*(1), 1-12.

Pitt, R. (2011). *Standard Land Use Characteristics and Pollutant Sources Report*. (Accessed May 2014), http://rpitt.eng.ua.edu/Publications/4_Stormwater_Characteristics_Pollutant_Sources_and_Land_Development_Characteristics/stormwater_characteristics.shtml

Ravagnani, F., Pellegrinelli, A., & Franchini, M. (2009). "Estimation of urban impervious fraction from satellite images and its impact on peak discharge entering a storm sewer system." *Water resources management*, *23*(10), 1893-1915.

Roso, S., Boyd, M. J., & Chisholm, L. A. (2006). "Assessment of Spatial Analysis Techniques for Estimating Impervious Cover." In Proceedings of the 30th Hydrology and Water Resources Symposium, Launceston, Tasmania, Dec. 4-7, 2006.

Roy, A. H., & Shuster, W. D. (2009). "Assessing Impervious Surface Connectivity and Applications for Watershed Management." *Journal of the American Water Resources Association*, *45*(1), 198-209.

Schueler, T. R. (1994). "The importance of imperviousness." *Watershed protection techniques*, 1(3), 100-111.

Shuster, W. D., Bonta, J., Thurston, H., Warnemuende, E., & Smith, D. R. (2005). "Impacts of impervious surface on watershed hydrology: A review." *Urban Water Journal, 2*(4), 263-275.

Soil Conservation Service. (1964). "Section 4 Hydrology", *National Engineering Handbook,* USDA, Washington, DC.

Soil Conservation Service. (1972). "Section 4 Hydrology", *National Engineering Handbook,* USDA, Washington, DC.

Soil Conservation Service. (1985). "Section 4 Hydrology", *National Engineering Handbook,* USDA, Washington, DC.

Sutherland, R. C. (1995). "Methodology for estimating the effective impervious area of urban watersheds." *Watershed Protection Techniques, 2*(1), 282-284.

Tetra Tech Inc. (2010). *Stormwater Best Management Practices (BMP) Performance Analysis.* Internet. www.epa.gov/region1/npdes/stormwater/assets/pdfs/BMP-Performance-Analysis-Report.pdf (Accessed June 2014).

Thiessen, A.H. (1911). "Precipitation averages for large areas." *Monthly Weather Review,* 39, 1082–1084.

United States Department of Agriculture (USDA). 1986. *Urban Hydrology for Small Watersheds.* Technical Release 55. 2nd Edition. Natural Resource Conservation Service (NRCS). Washington, D.C.

Waschbusch, R., Selbig, W., & Bannerman, R. (1999). *Sources of Phosphorus in Stormwater and Street Dirt from Two Urban Residential Basins In Madison, Wisconsin, 1994–95, Water Resources Investigations Report 99–4021,* U.S. Geological Survey, Middleton, Wisconsin.

Wenger, S. J. W. S., Peterson, J. T. P. J., Freeman, M. C. F. M., Freeman, B. J. F. B., & Homans, D. D. H. D. (2008). "Stream fish occurrence in response to impervious cover, historic land use, and hydrogeomorphic factors." *Canadian Journal of Fisheries and Aquatic Sciences, 65*(7), 1250-1264.

Willett, J. B., & Singer, J. D. (1988). "Another cautionary note about R^2: Its use in weighted least-squares regression analysis." *The American Statistician,* 42(3), 236-238.

Wilson, B. N., Hansen, B., Schmidt, T., & Zearling, T., (2007). *An Evaluation of Stormwater Management in a Watershed of the Minnesota Valley National Wildlife*

Refuge. Technical report. Department of Bioproducts and Biosystems Engineering. University of Minnesota. St. Paul, MN.

Woodward, D. E., Van Mullem, J. A., Hawkins, R. H., & Plummer, A. (2010). *Curve number completion study.* Consultant's Report to USDA, NRCS, Beltsville, MD.

Zhan, X., & Huang, M-L. (2004). "ArcCN-Runoff: an ArcGIS tool for generating curve number and runoff maps." *Environmental Modelling & Software, 19*, 875-879.

APPENDIX A: PLOTS OF RUNOFF DEPTH VERSUS RAINFALL DEPTH

Plots of runoff depth versus rainfall depth at the final step of the two discussed methods, SOLS (1 mm), and SWLS (max [2 SE, 1 mm]), for all the watersheds of study are presented in this appendix. The storm events in each plot are categorized into “EIA” and “Combined” events. The order of figures from top to bottom is SOLS (1 mm), and SWLS (max [2 SE, 1 mm]), respectively. The location, drainage area, land use, and monitoring years for each watershed are presented in section 2.2 of the report.

Capitol Region Watershed District, MN

AHUG

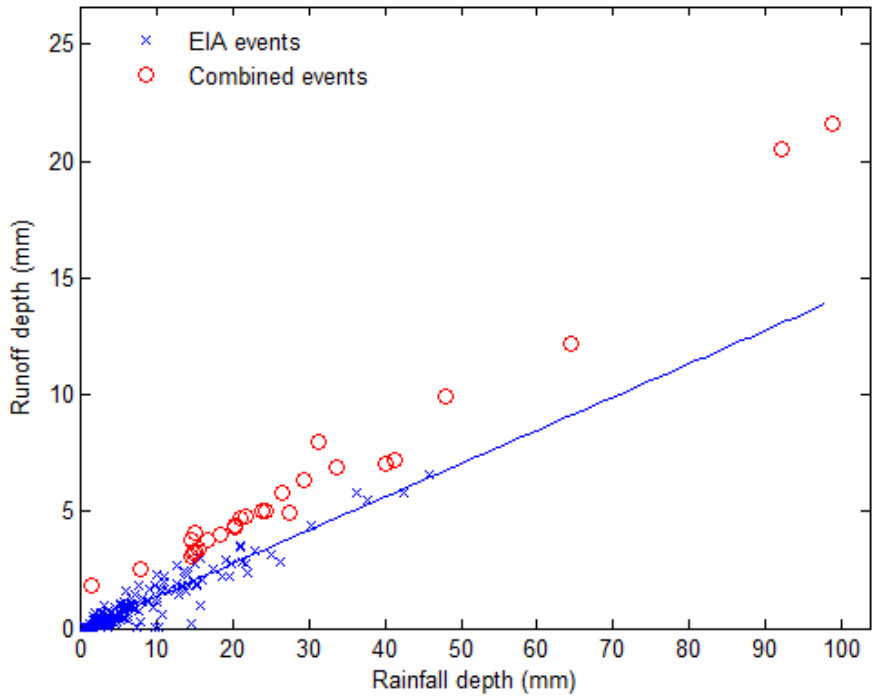

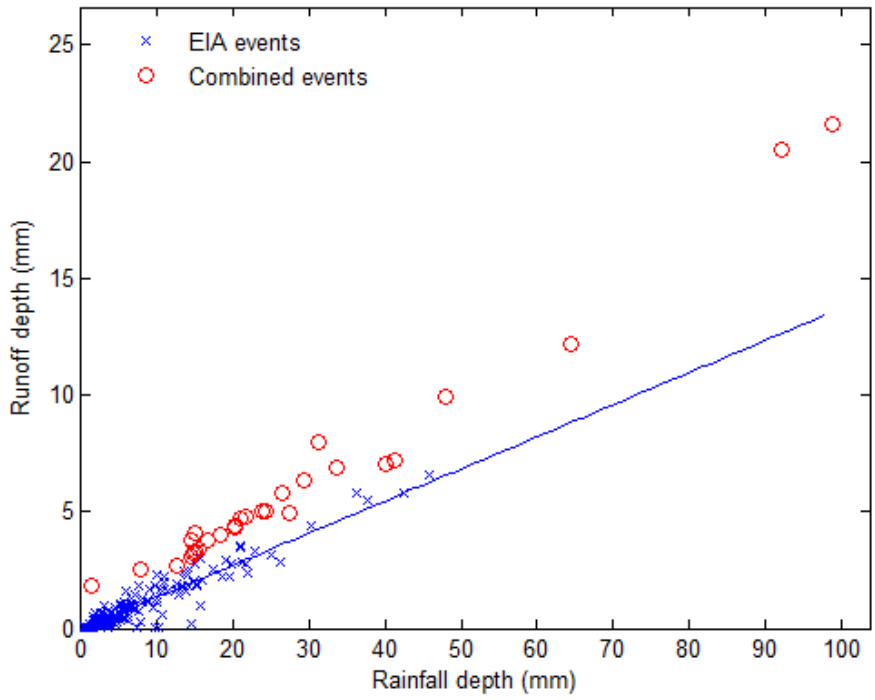

GCP

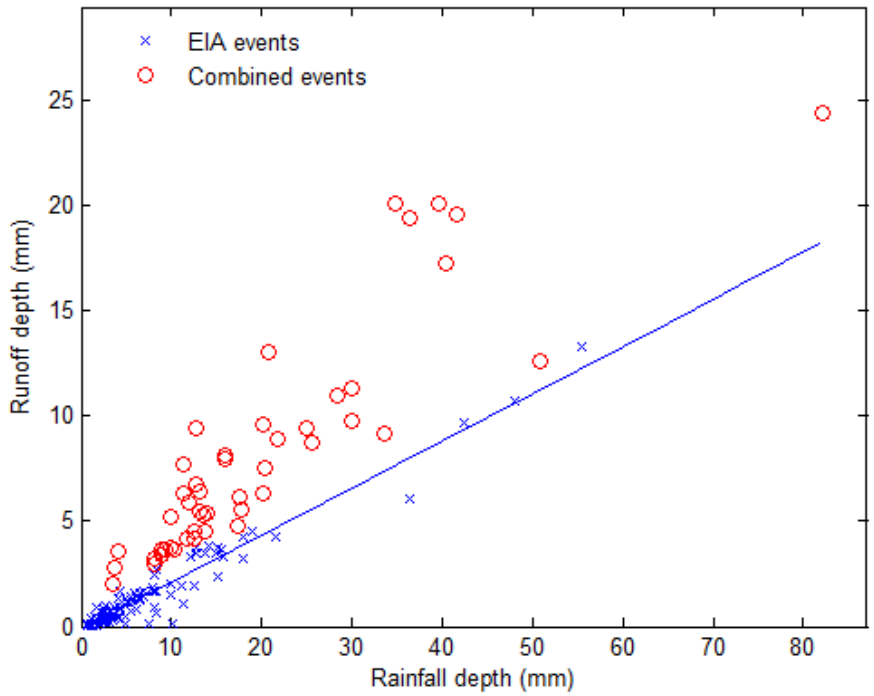
EIA events
Combined events
Runoff depth (mm)
Rainfall depth (mm)
0
5
10
15
20
25
0
10
20
30
40
50
60
70
80

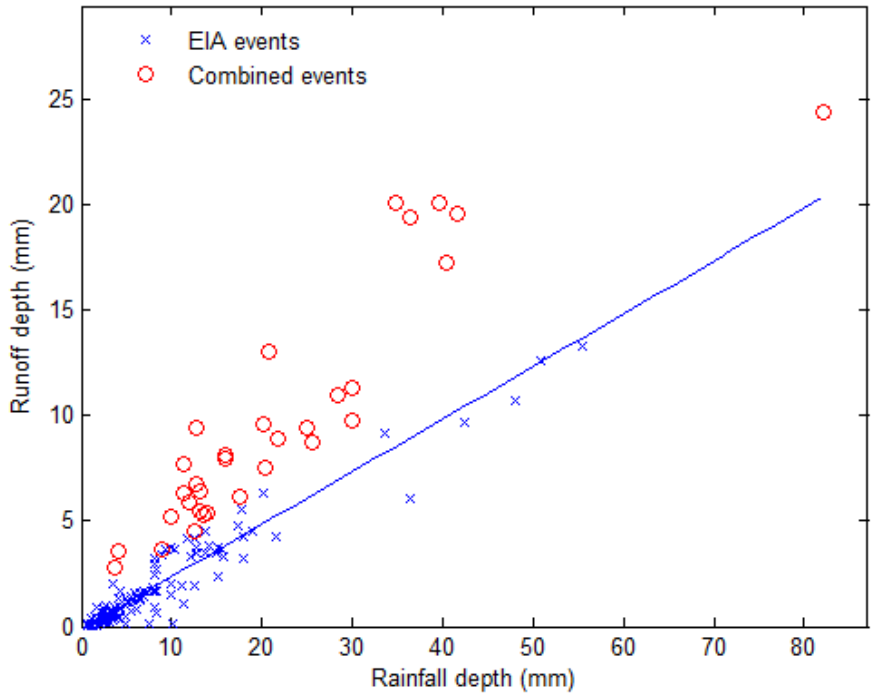
EIA events
Combined events
Runoff depth (mm)
Rainfall depth (mm)
0
5
10
15
20
25
0
10
20
30
40
50
60
70
80

Como 3

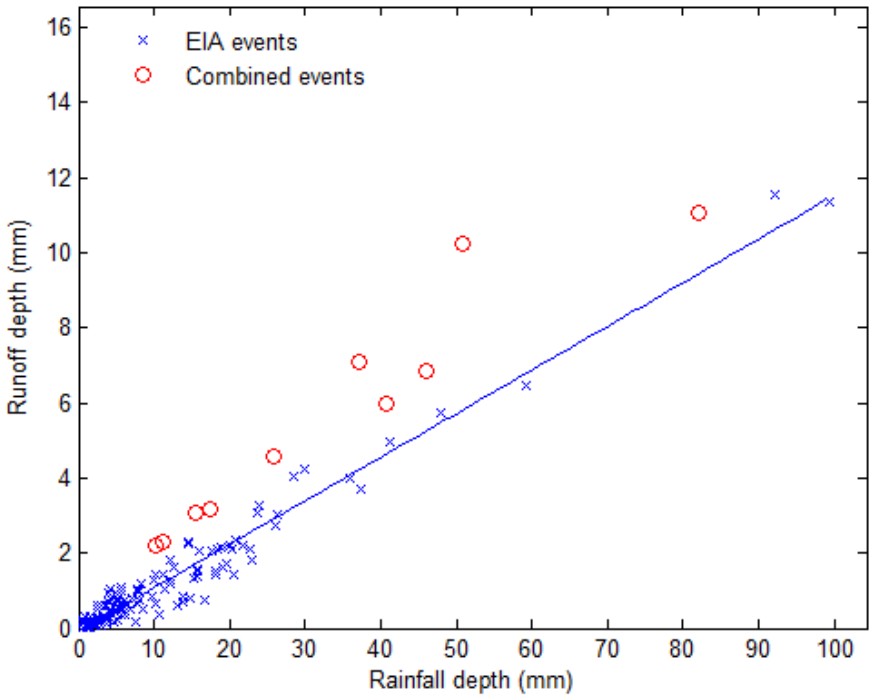
EIA events
Combined events
Runoff depth (mm)
Rainfall depth (mm)
0
2
4
6
8
10
12
14
16
0
10
20
30
40
50
60
70
80
90
100

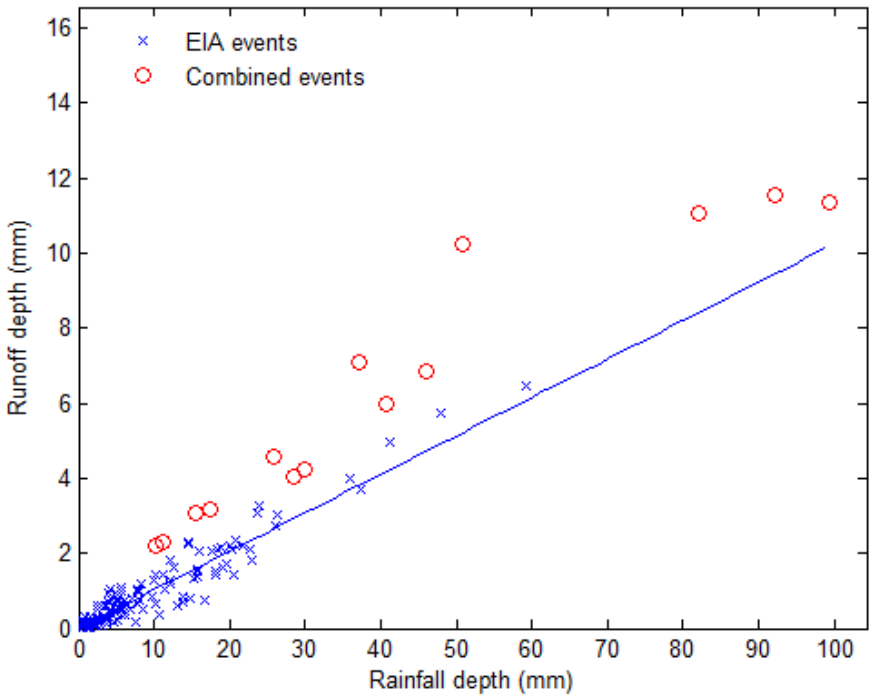
EIA events
Combined events
Runoff depth (mm)
Rainfall depth (mm)
0
2
4
6
8
10
12
14
16
0
10
20
30
40
50
60
70
80
90
100

Sarita

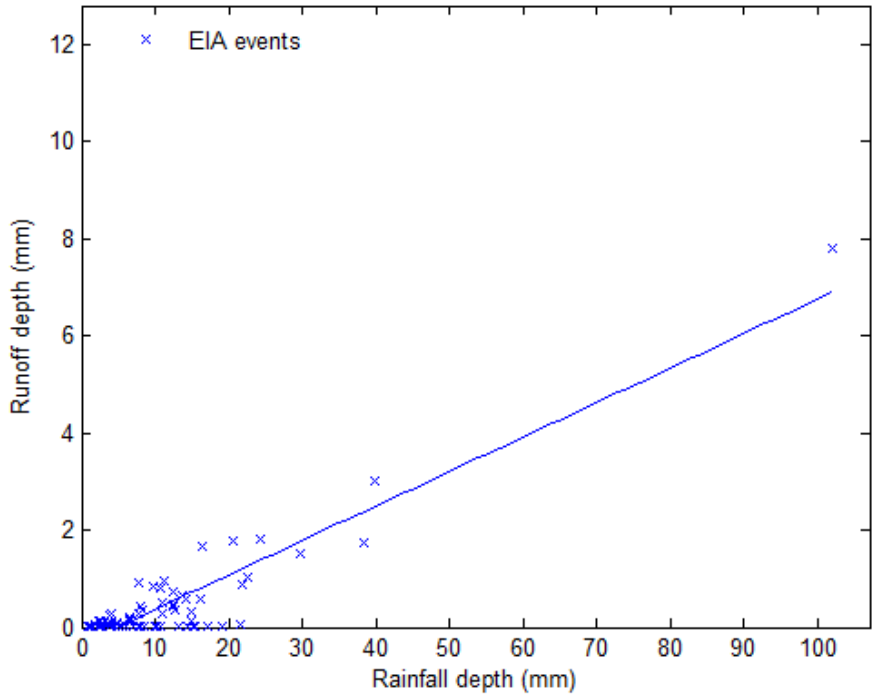
EIA events
Runoff depth (mm)
Rainfall depth (mm)
0
2
4
6
8
10
12
0
10
20
30
40
50
60
70
80
90
100

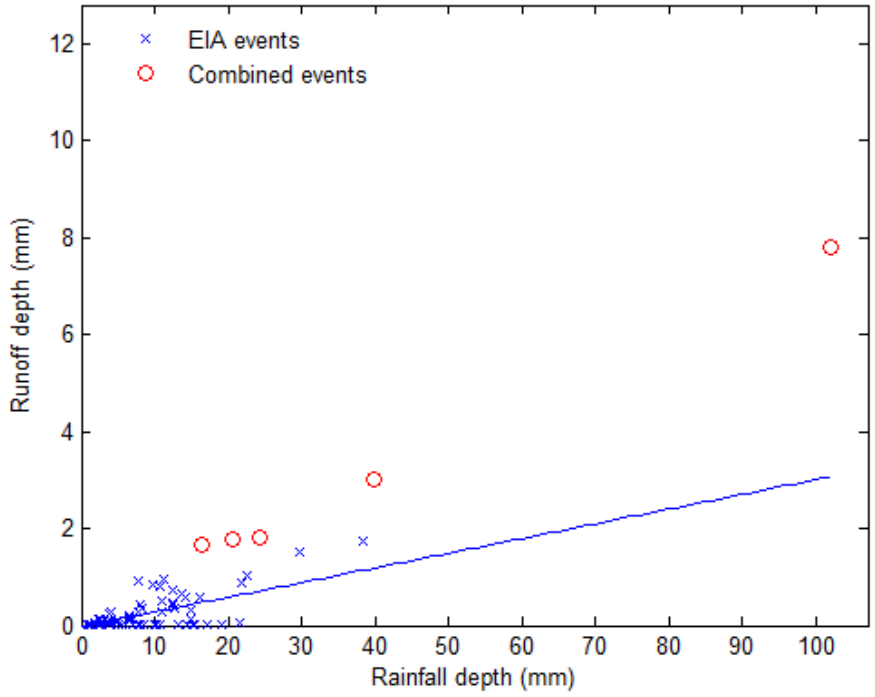
EIA events
Combined events
Runoff depth (mm)
Rainfall depth (mm)
0
2
4
6
8
10
12
0
10
20
30
40
50
60
70
80
90
100

TBEB

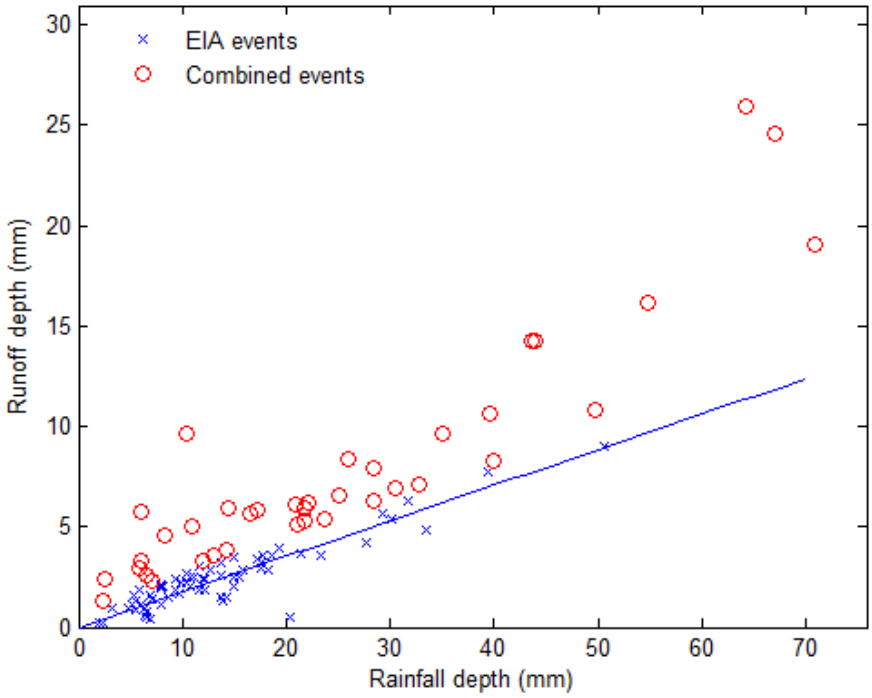
EIA events
Combined events
Runoff depth (mm)
Rainfall depth (mm)
0
5
10
15
20
25
30
0
10
20
30
40
50
60
70

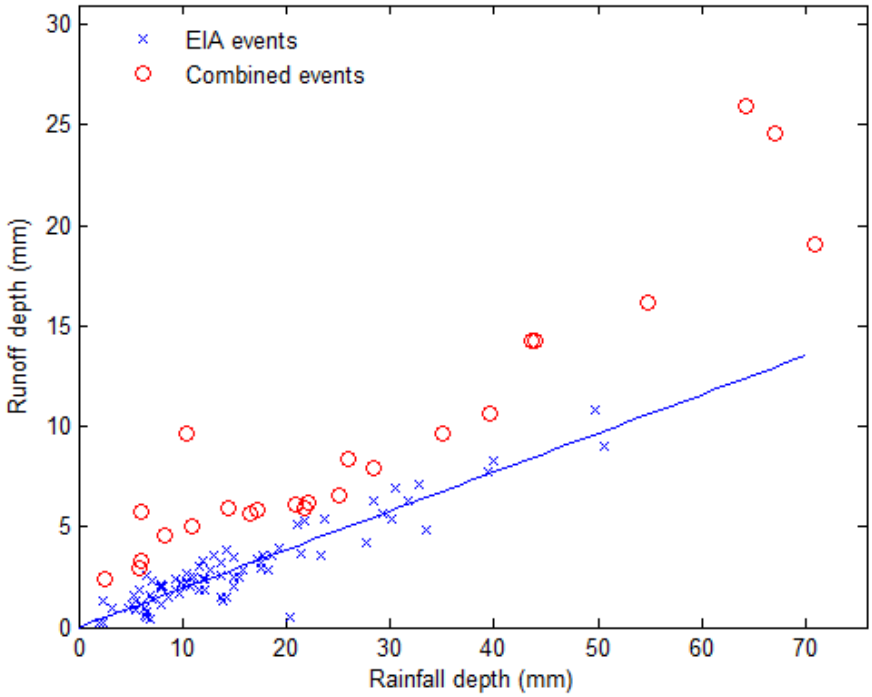
EIA events
Combined events
Runoff depth (mm)
Rainfall depth (mm)
0
5
10
15
20
25
30
0
10
20
30
40
50
60
70

EK

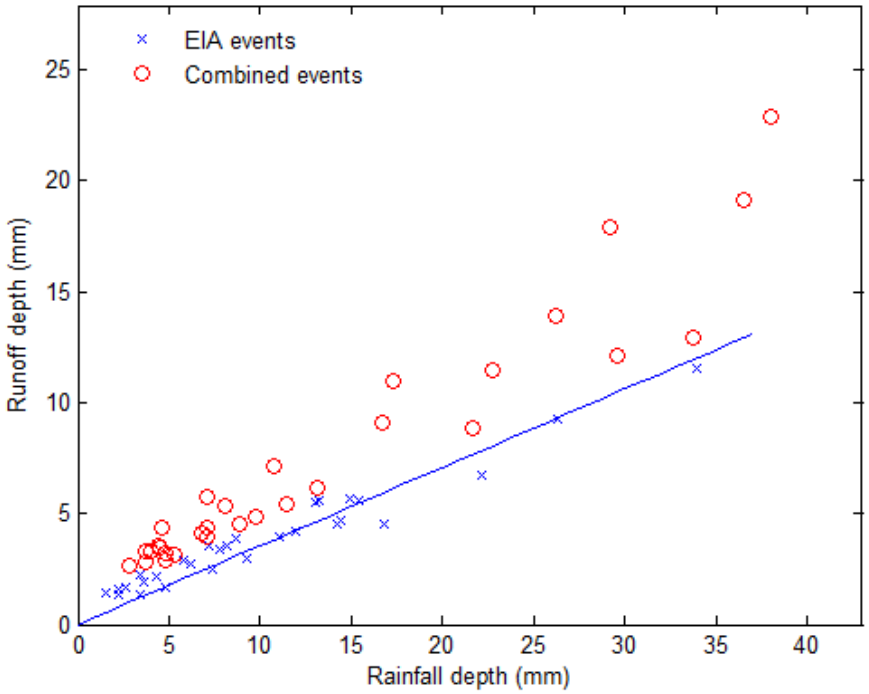
EIA events
Combined events
Runoff depth (mm)
Rainfall depth (mm)
0
5
10
15
20
25
30
35
40

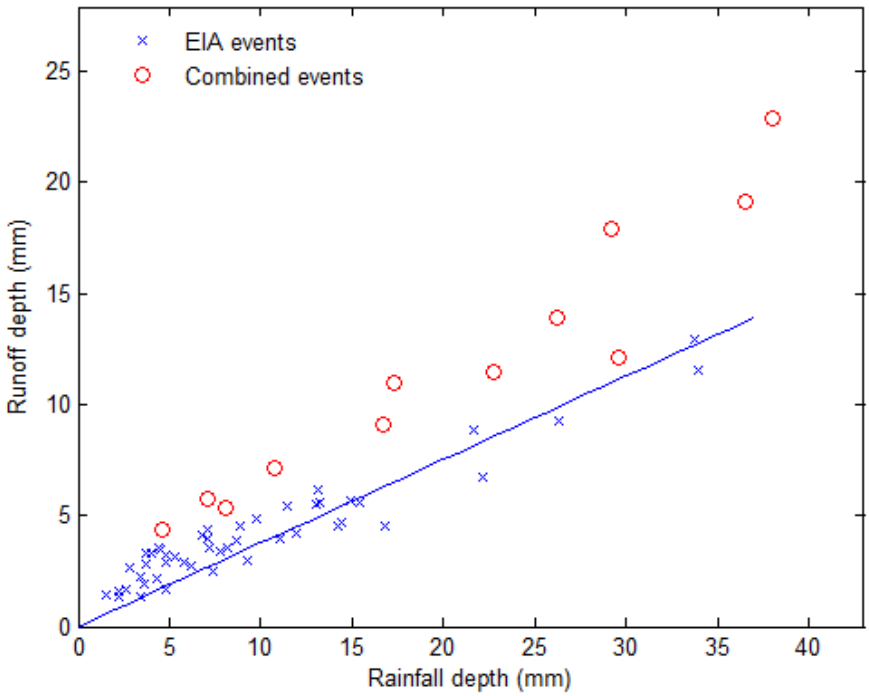
EIA events
Combined events
Runoff depth (mm)
Rainfall depth (mm)
0
5
10
15
20
25
30
35
40

PC

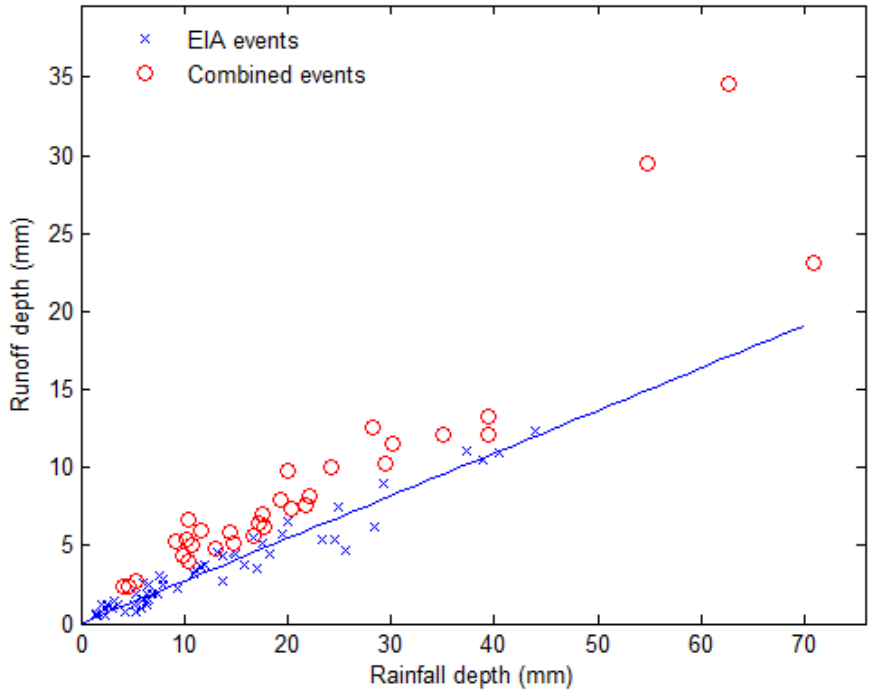
EIA events
Combined events
Runoff depth (mm)
Rainfall depth (mm)
0
5
10
15
20
25
30
35
0
10
20
30
40
50
60
70

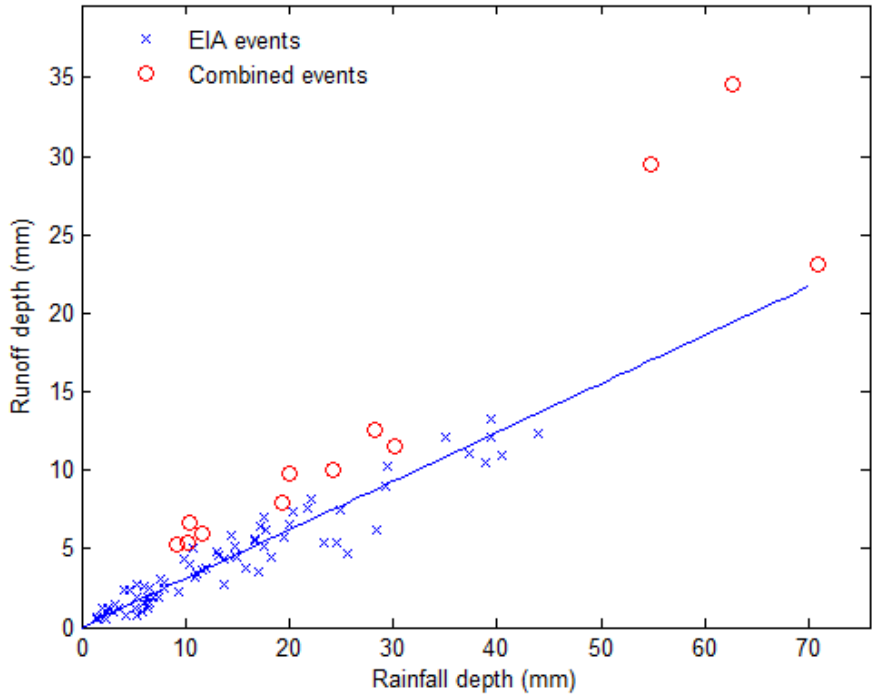
EIA events
Combined events
Runoff depth (mm)
Rainfall depth (mm)
0
5
10
15
20
25
30
35
0
10
20
30
40
50
60
70

SAP

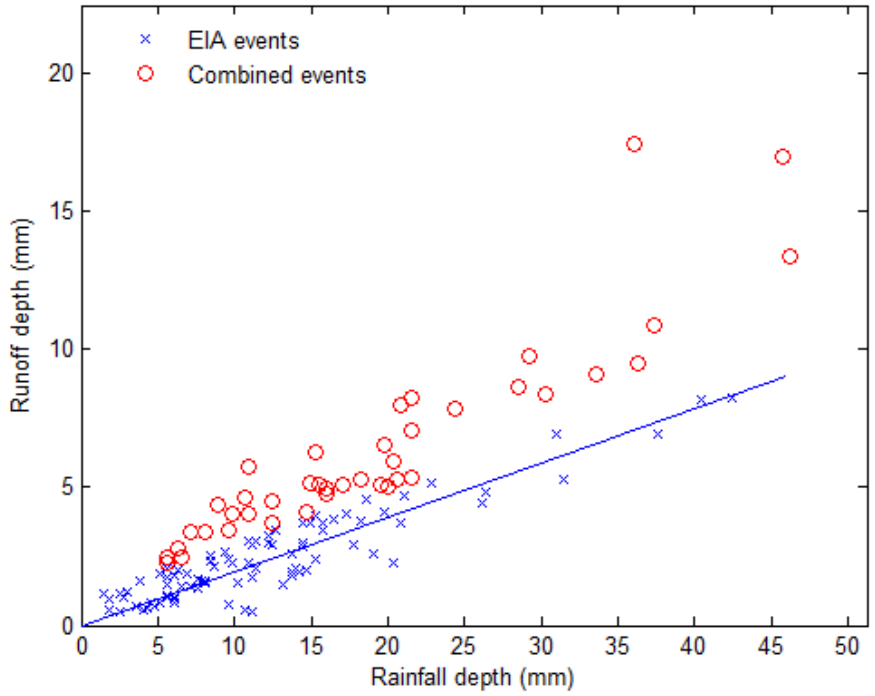
EIA events
Combined events
Runoff depth (mm)
Rainfall depth (mm)
0
5
10
15
20
25
30
35
40
45
50

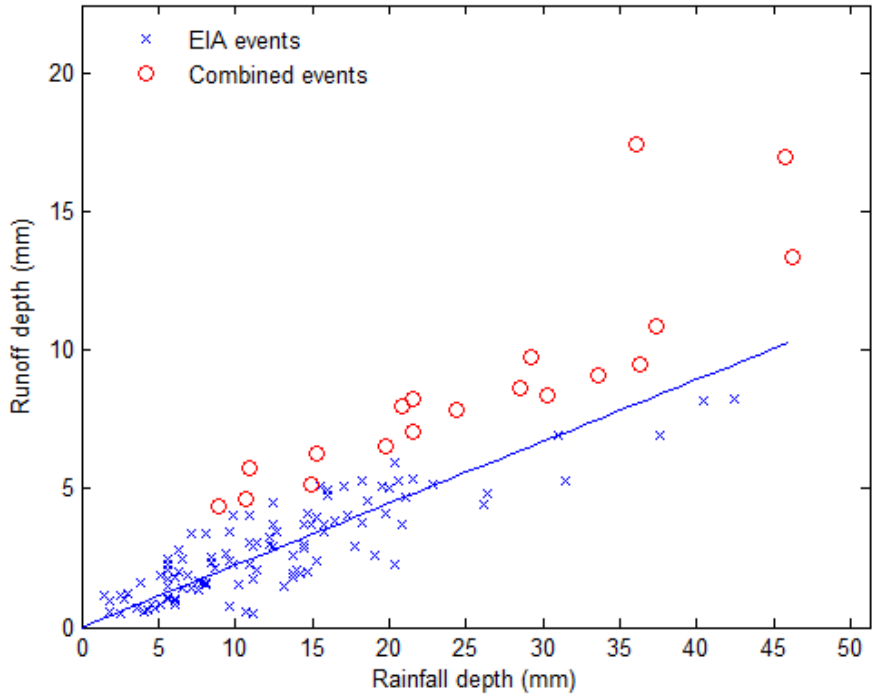
EIA events
Combined events
Runoff depth (mm)
Rainfall depth (mm)
0
5
10
15
20
25
30
35
40
45
50

TBO

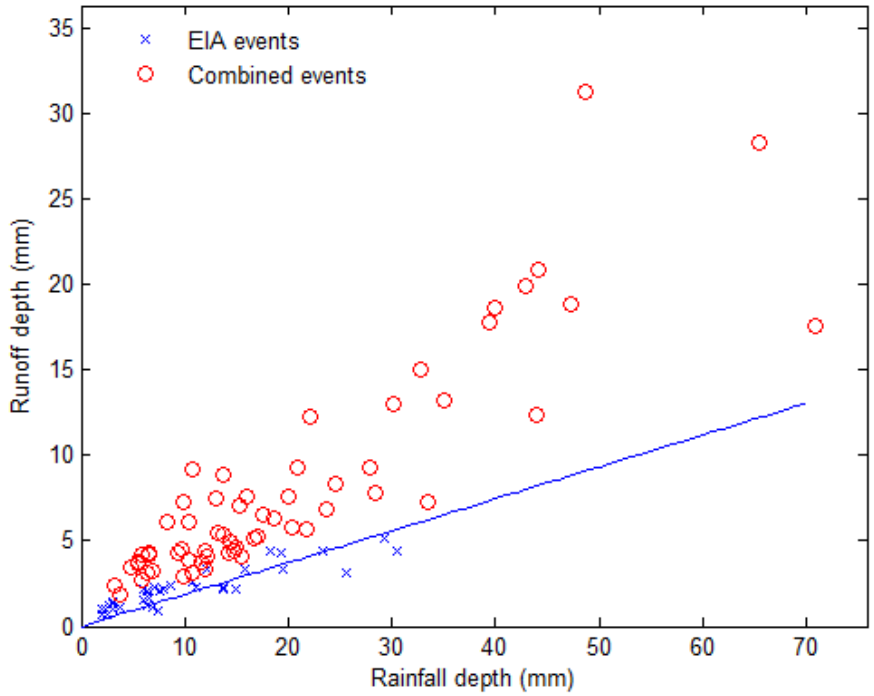
EIA events
Combined events
Runoff depth (mm)
Rainfall depth (mm)
0
5
10
15
20
25
30
35
0
10
20
30
40
50
60
70

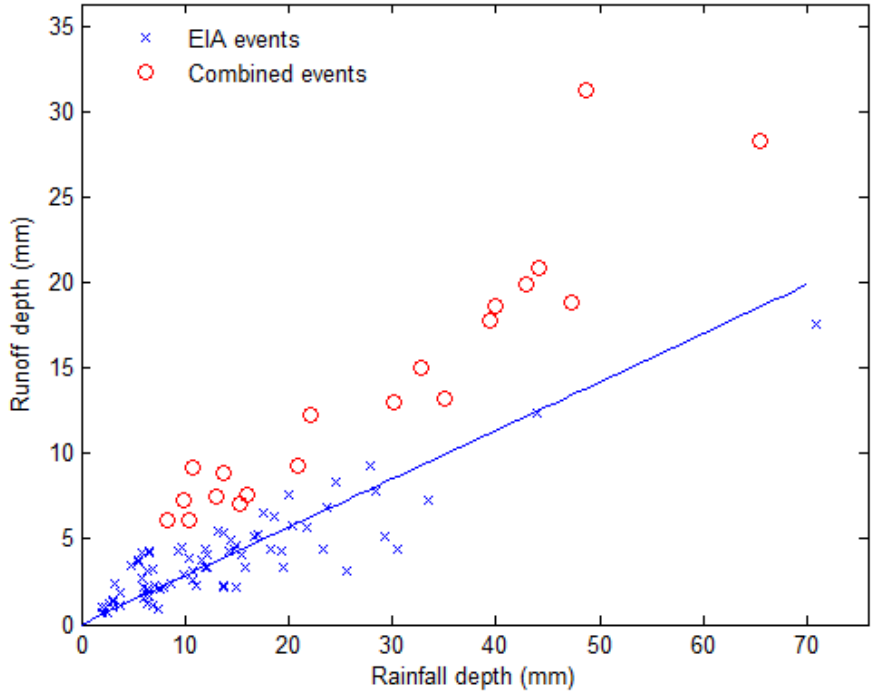
EIA events
Combined events
Runoff depth (mm)
Rainfall depth (mm)
0
5
10
15
20
25
30
35
0
10
20
30
40
50
60
70

Three Rivers Park District, MN

MG1

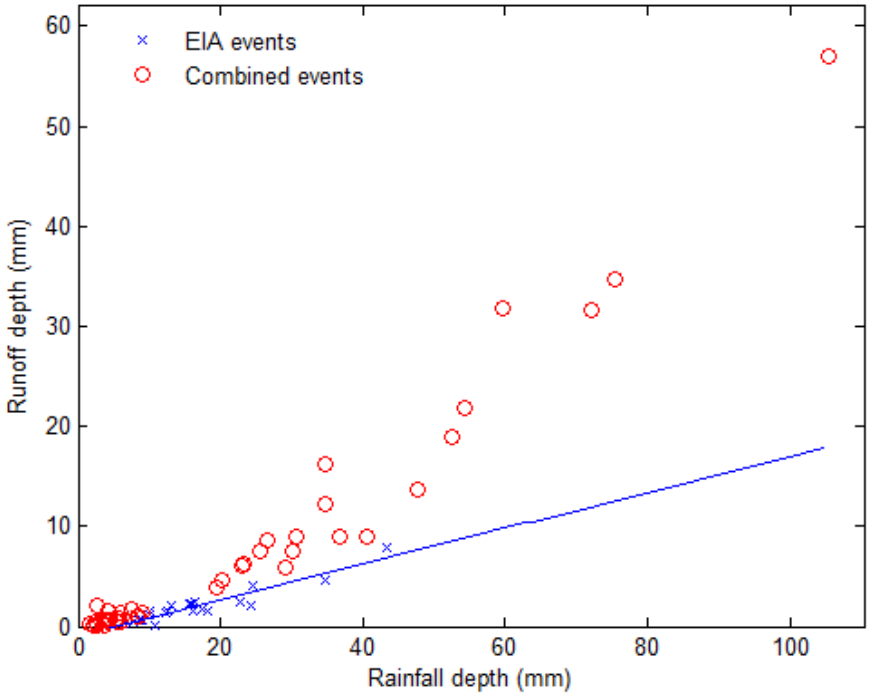

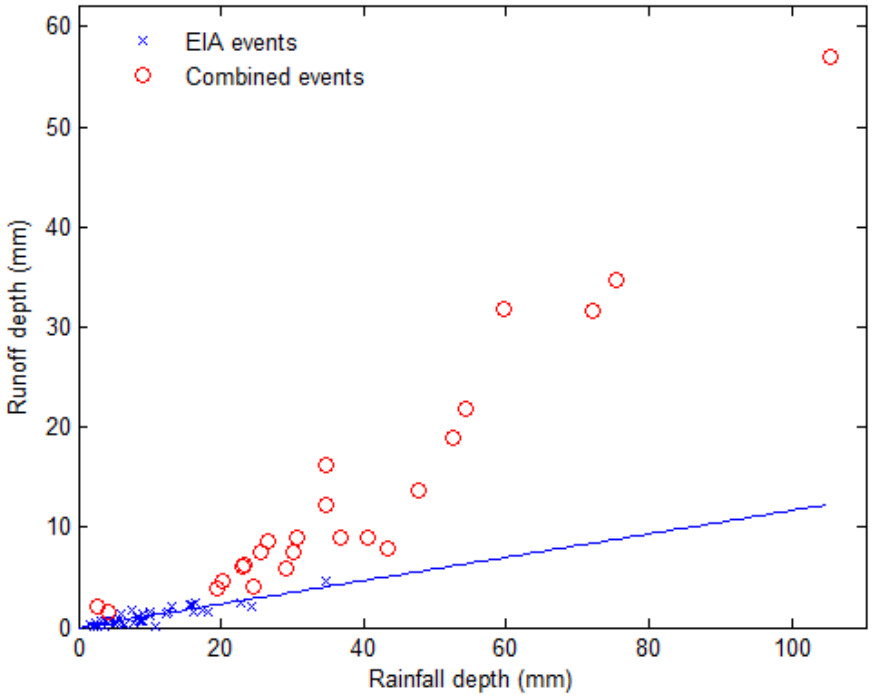

MG2

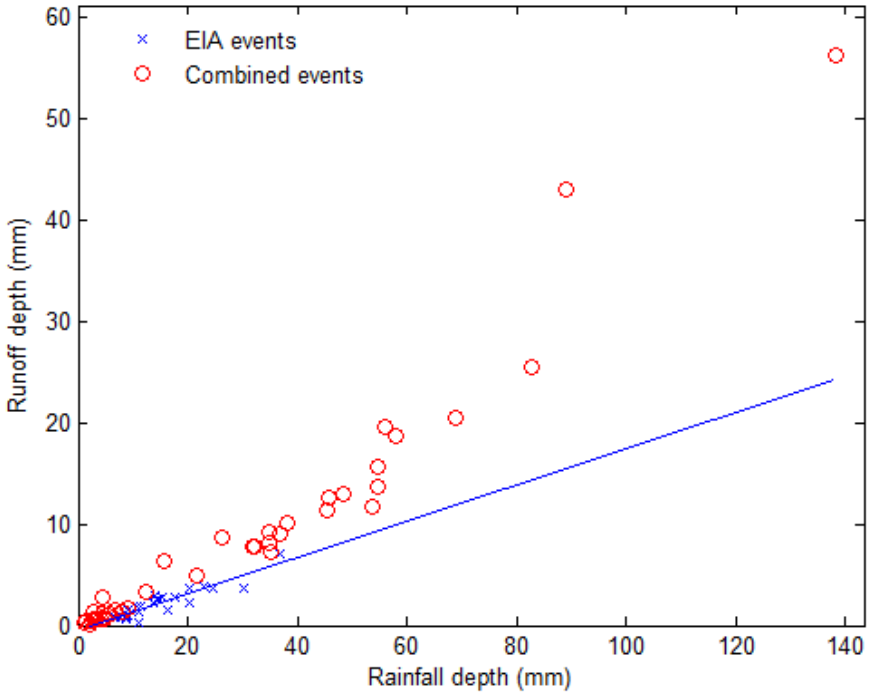
EIA events
Combined events
Runoff depth (mm)
Rainfall depth (mm)
0
10
20
30
40
50
60
0
20
40
60
80
100
120
140

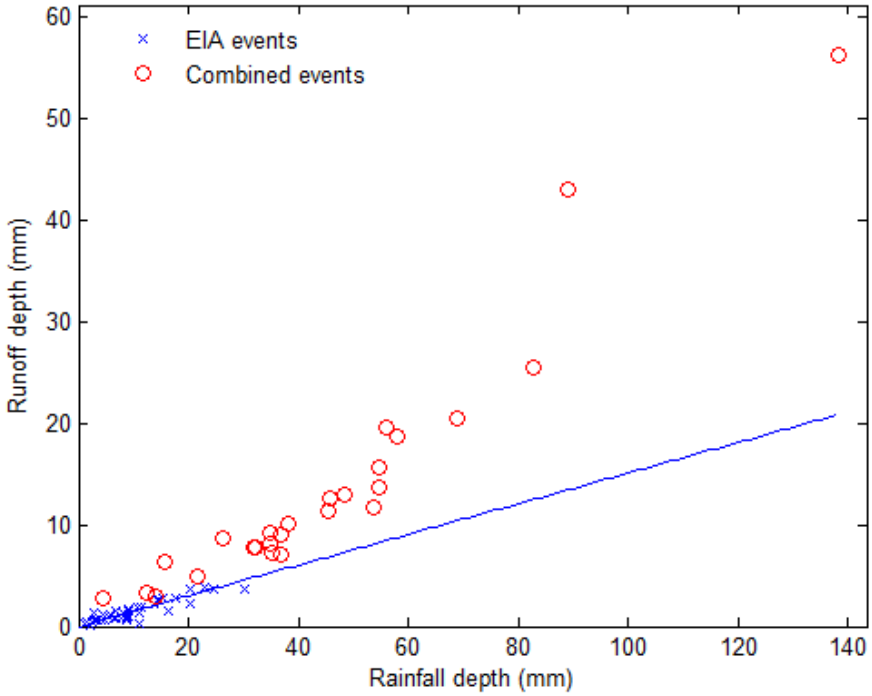
EIA events
Combined events
Runoff depth (mm)
Rainfall depth (mm)
0
10
20
30
40
50
60
0
20
40
60
80
100
120
140

P1

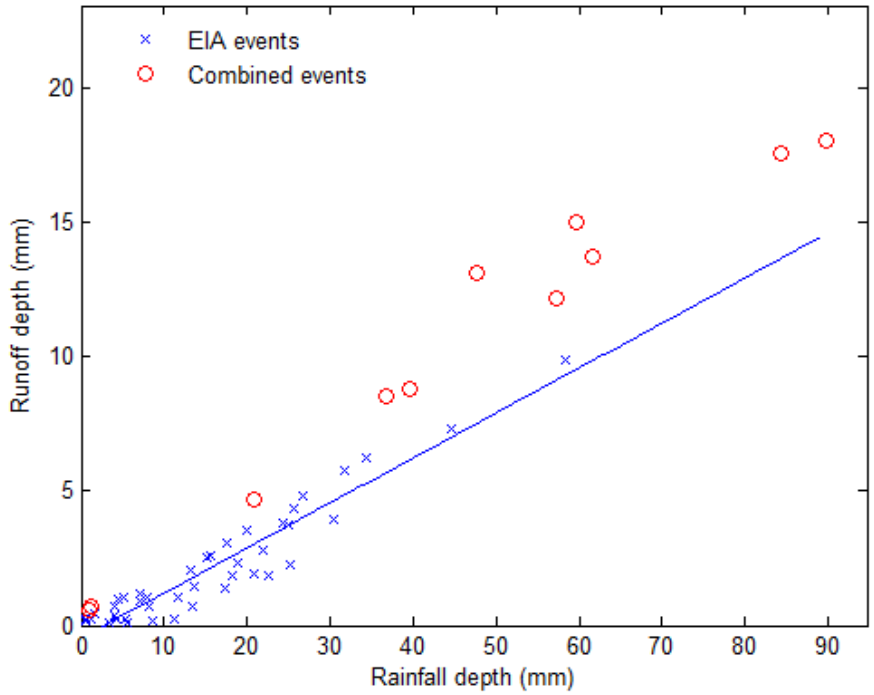
EIA events
Combined events
Runoff depth (mm)
Rainfall depth (mm)
0
5
10
15
20
0
10
20
30
40
50
60
70
80
90

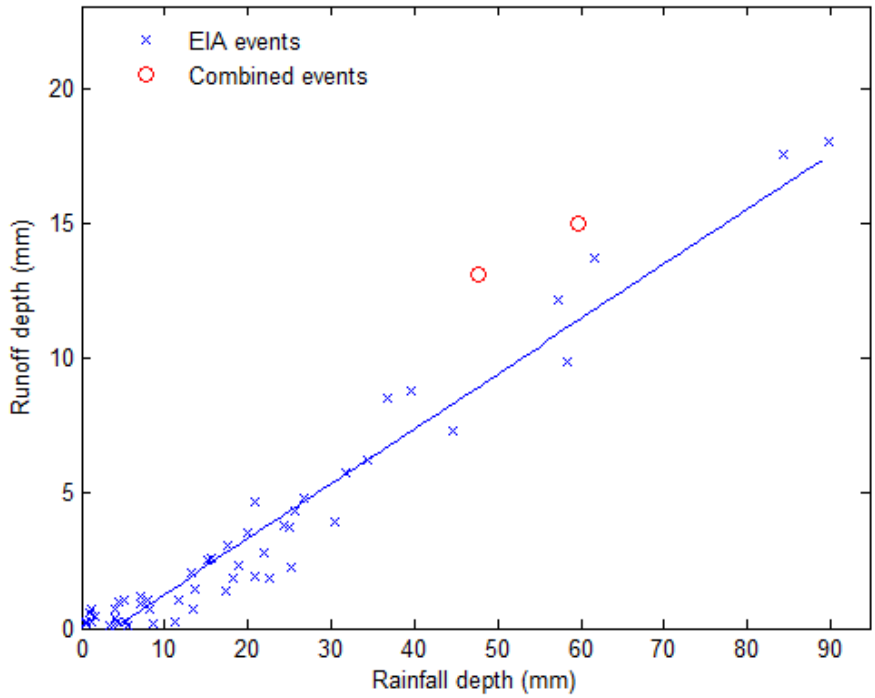
EIA events
Combined events
Runoff depth (mm)
Rainfall depth (mm)
0
5
10
15
20
0
10
20
30
40
50
60
70
80
90

P2

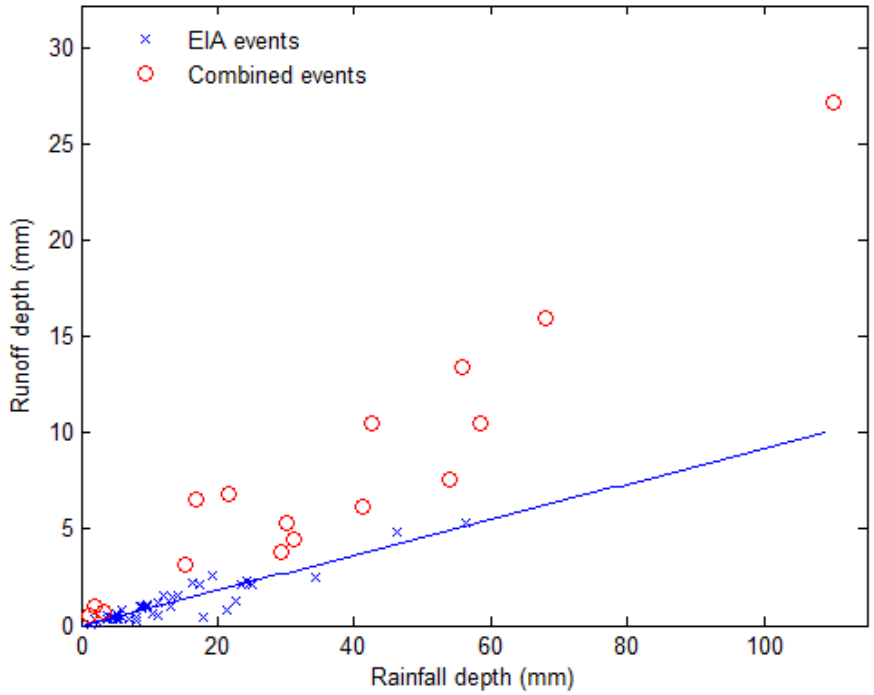
EIA events
Combined events
Runoff depth (mm)
Rainfall depth (mm)
0
5
10
15
20
25
30
0
20
40
60
80
100

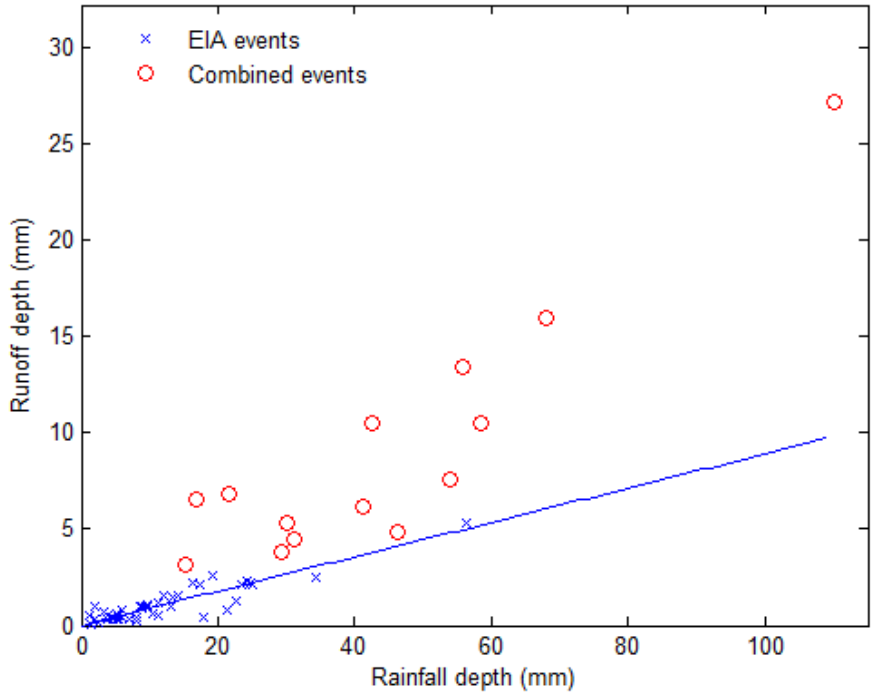
EIA events
Combined events
Runoff depth (mm)
Rainfall depth (mm)
0
5
10
15
20
25
30
0
20
40
60
80
100

P3

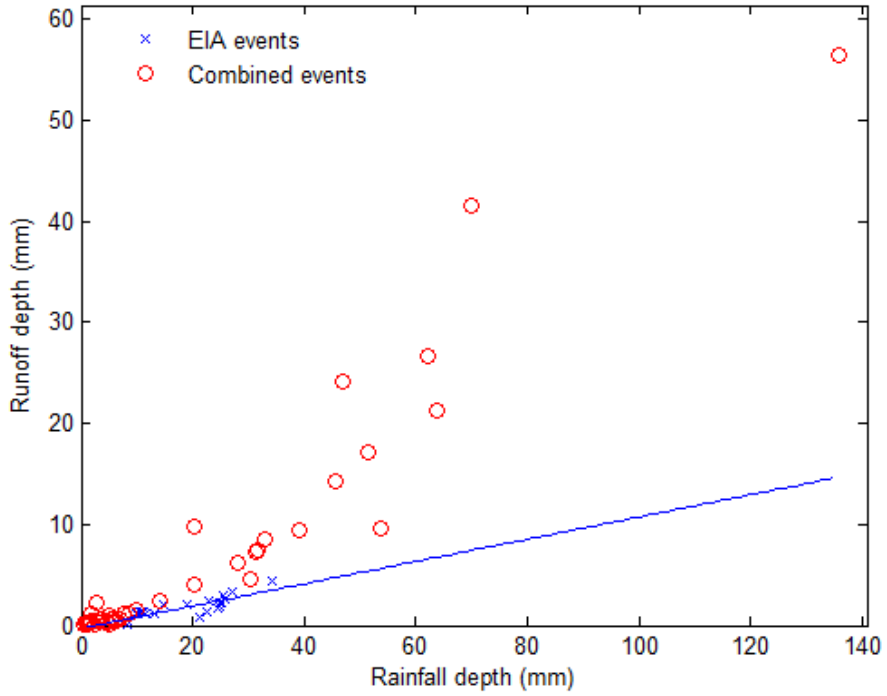
EIA events
Combined events
Runoff depth (mm)
Rainfall depth (mm)
0
10
20
30
40
50
60
0
20
40
60
80
100
120
140

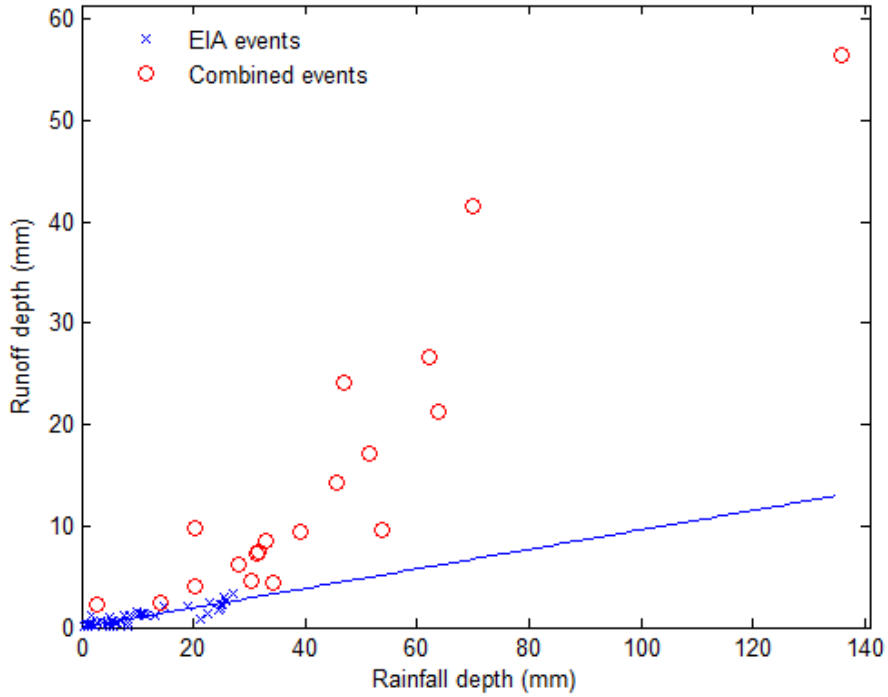
EIA events
Combined events
Runoff depth (mm)
Rainfall depth (mm)
0
10
20
30
40
50
60
0
20
40
60
80
100
120
140

City of Bloomington, MN

Smith Pond

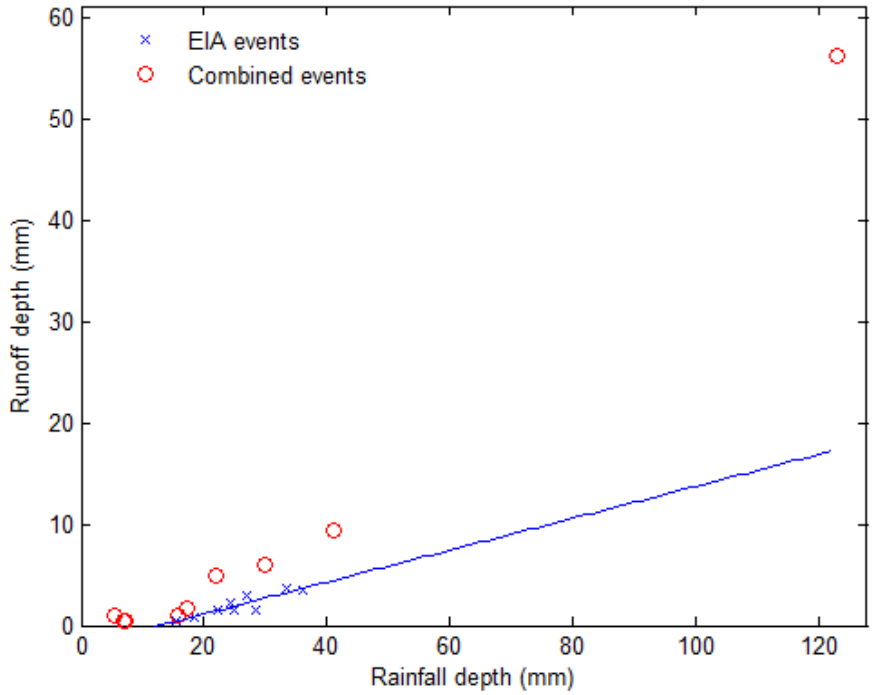

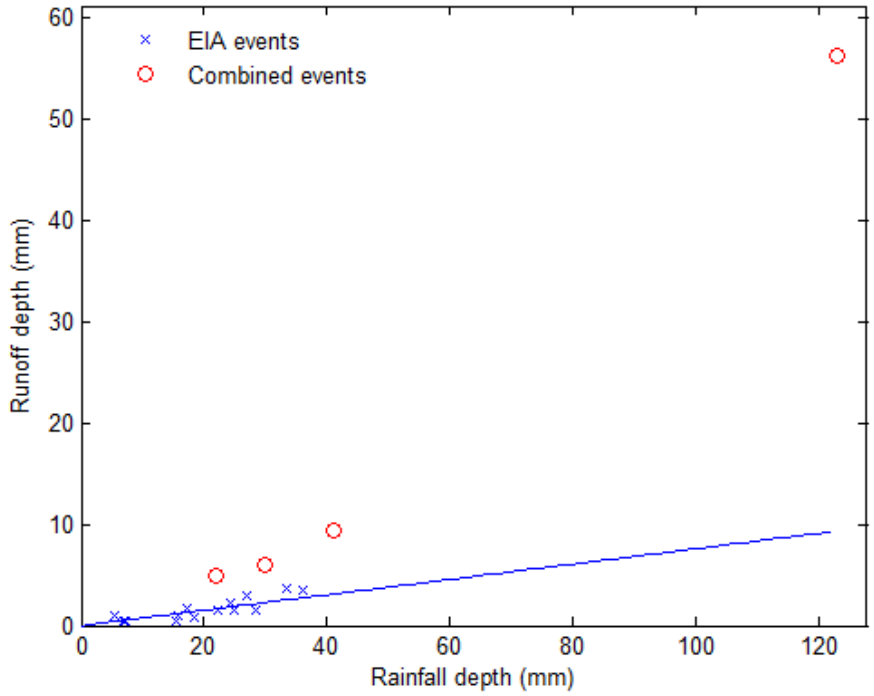

Mall of America (MOA)

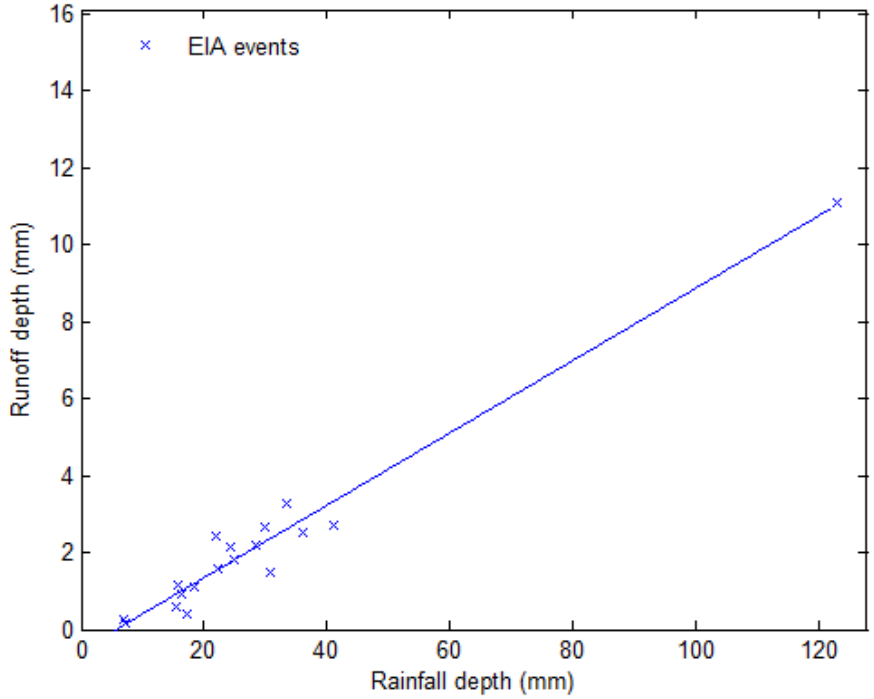

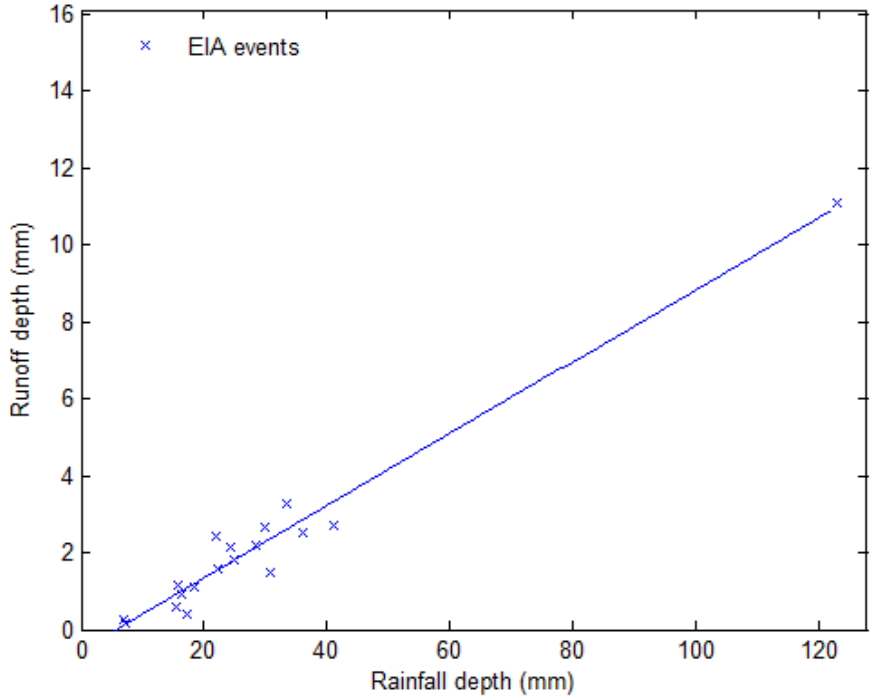

City of Minnetonka, MN

Hedburg Drive

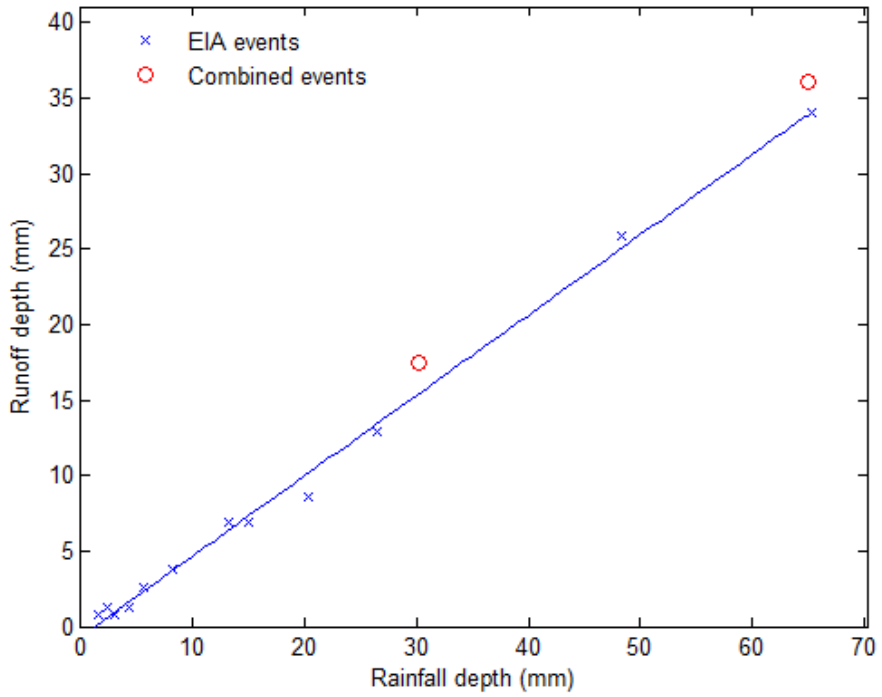

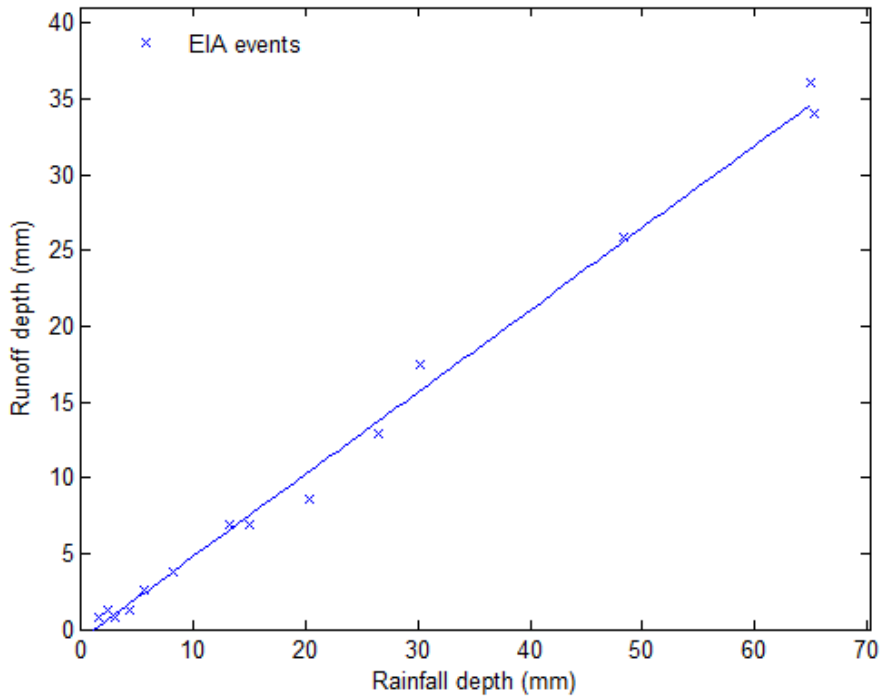

Mayflower Ave (Tapestry)

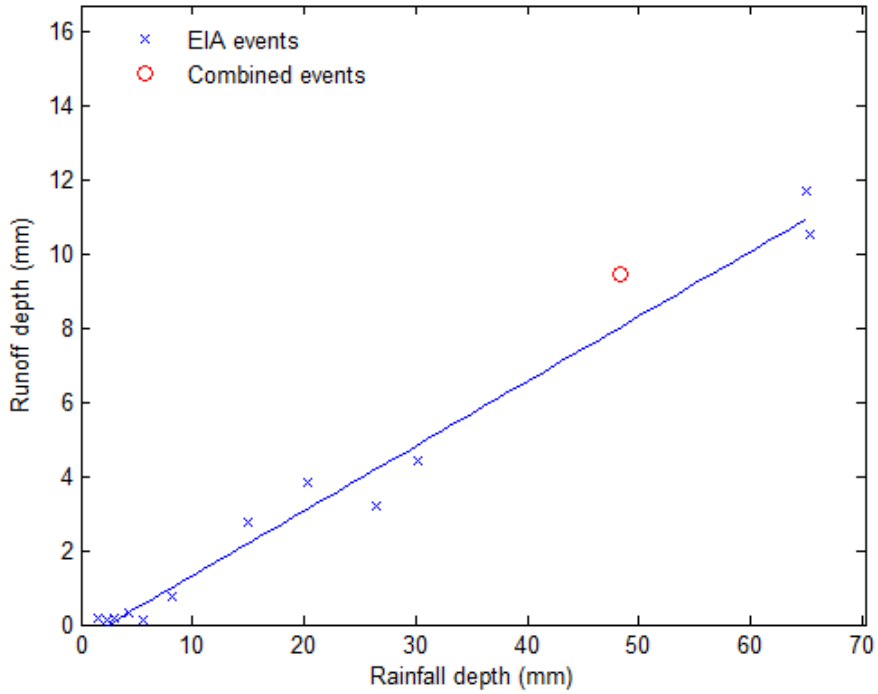

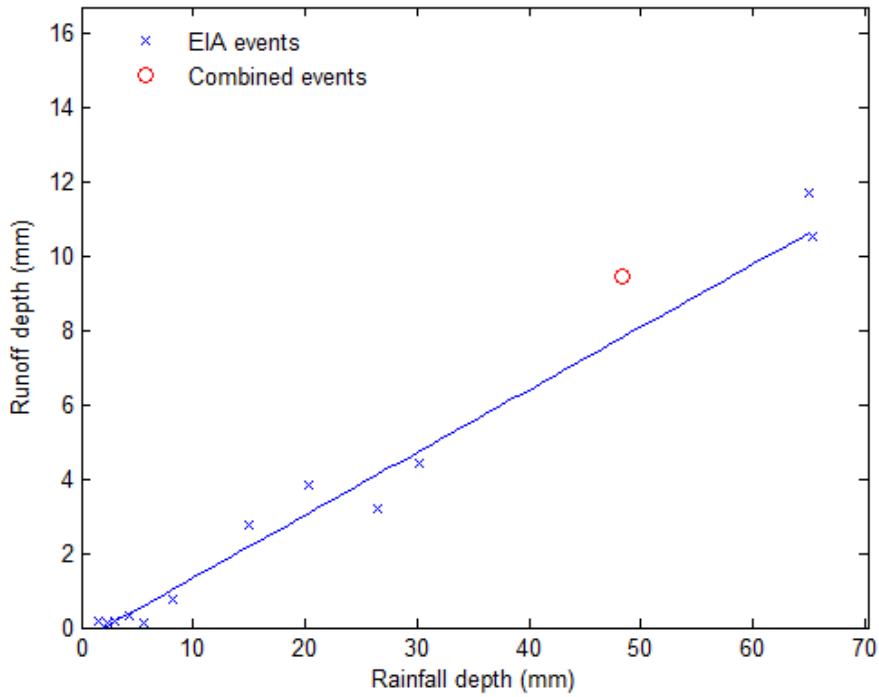

City of Madison, WI

Harper

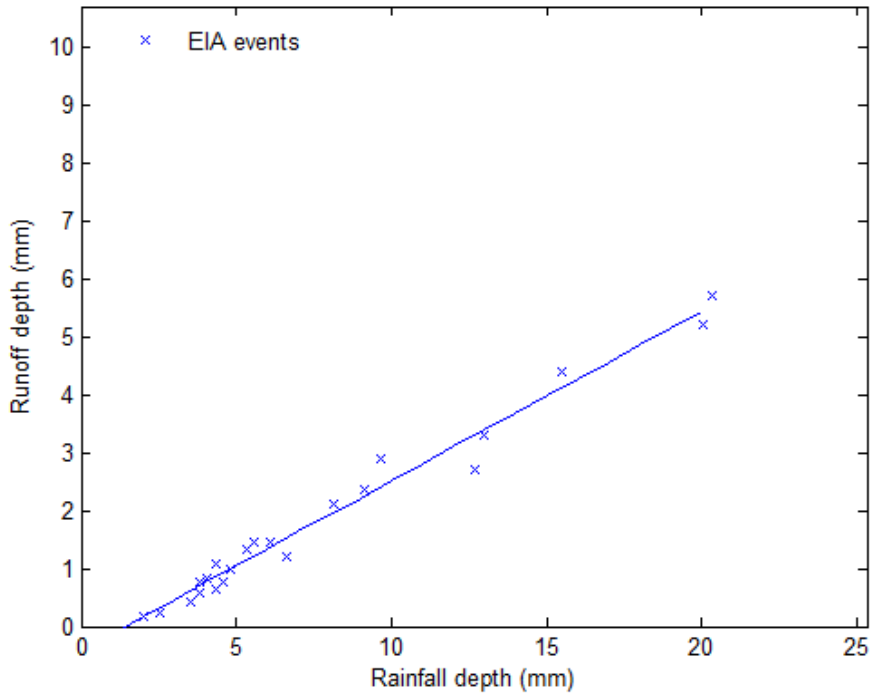

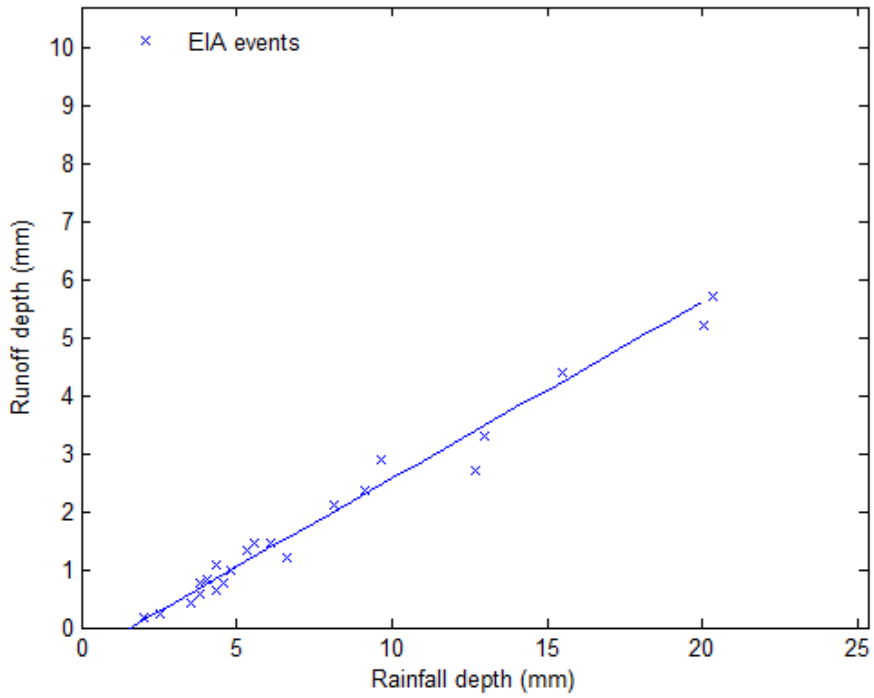

Monroe

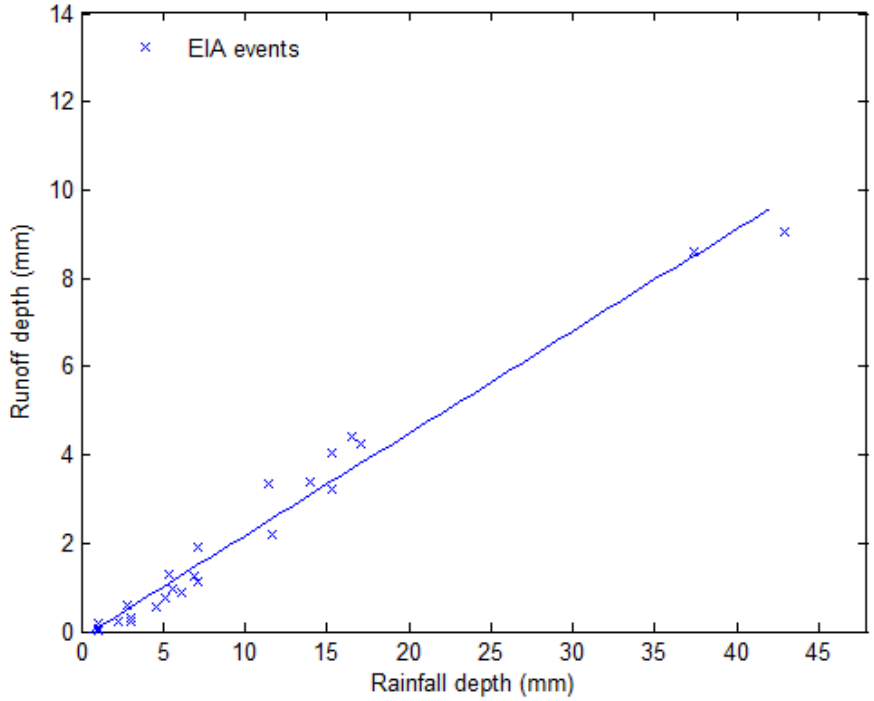
EIA events
Runoff depth (mm)
Rainfall depth (mm)
0
2
4
6
8
10
12
14
0
5
10
15
20
25
30
35
40
45

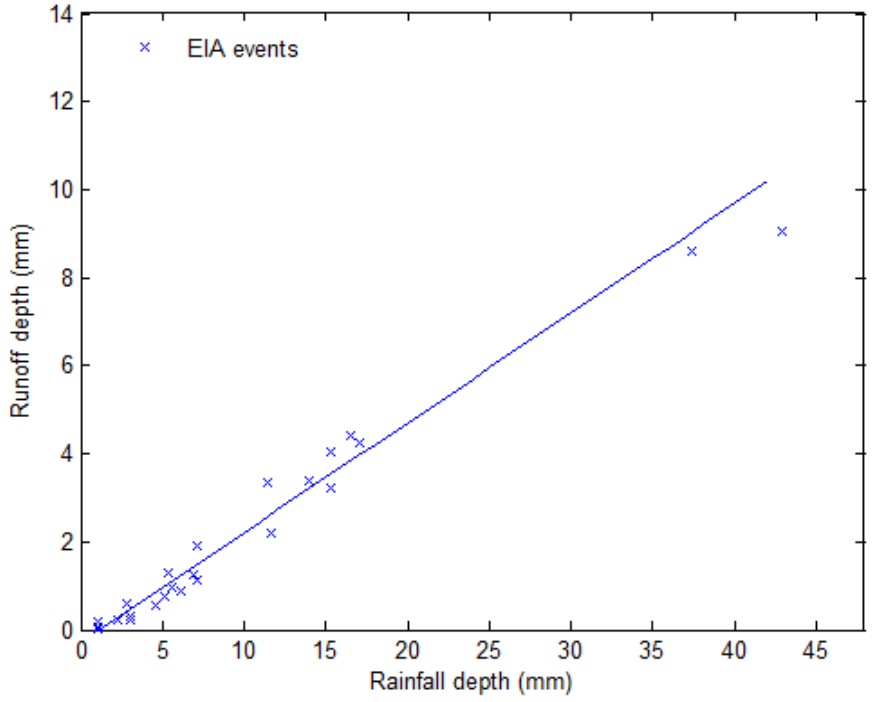
EIA events
Runoff depth (mm)
Rainfall depth (mm)
0
2
4
6
8
10
12
14
0
5
10
15
20
25
30
35
40
45

City of Austin, TX

BW1

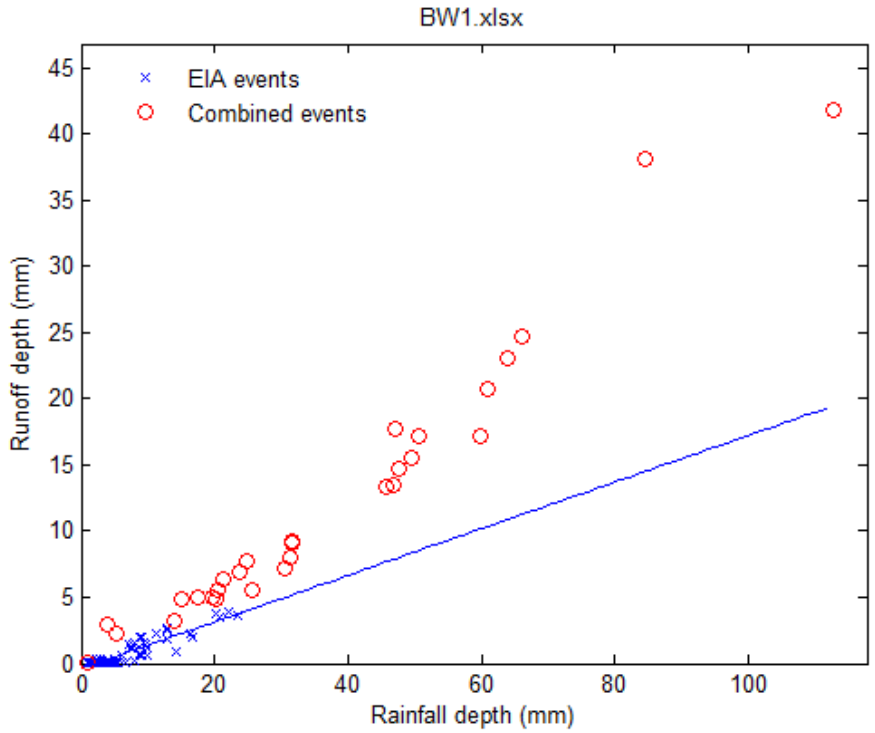

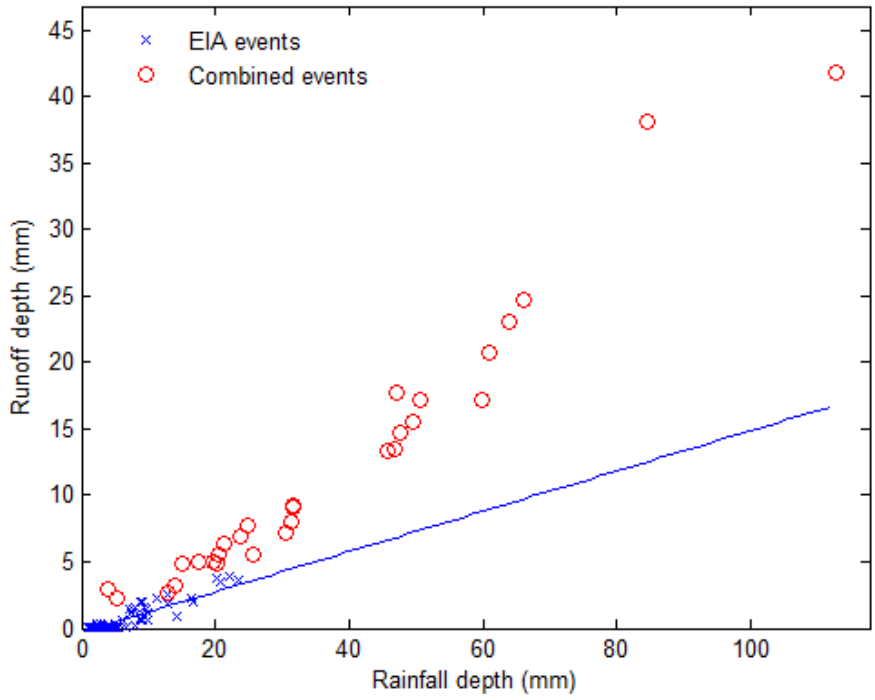

EBA

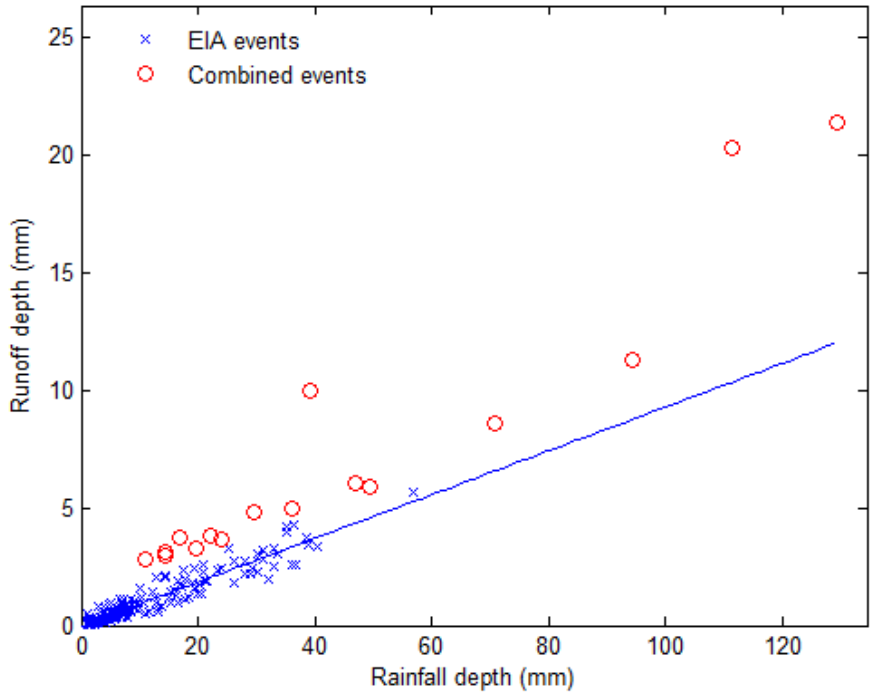
EIA events
Combined events
Runoff depth (mm)
Rainfall depth (mm)
0
5
10
15
20
25
0
20
40
60
80
100
120

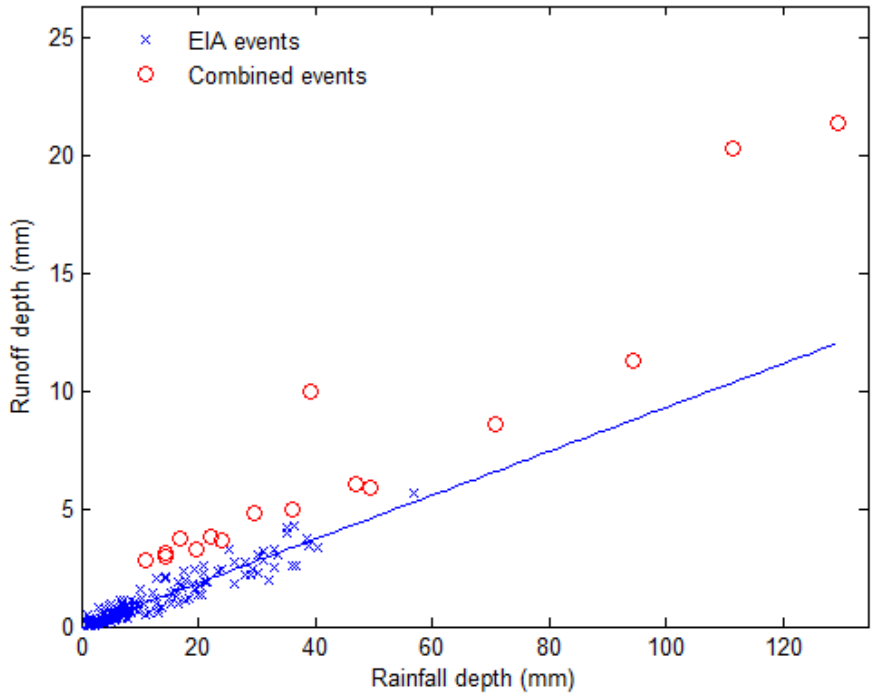
EIA events
Combined events
Runoff depth (mm)
Rainfall depth (mm)
0
5
10
15
20
25
0
20
40
60
80
100
120

EHA

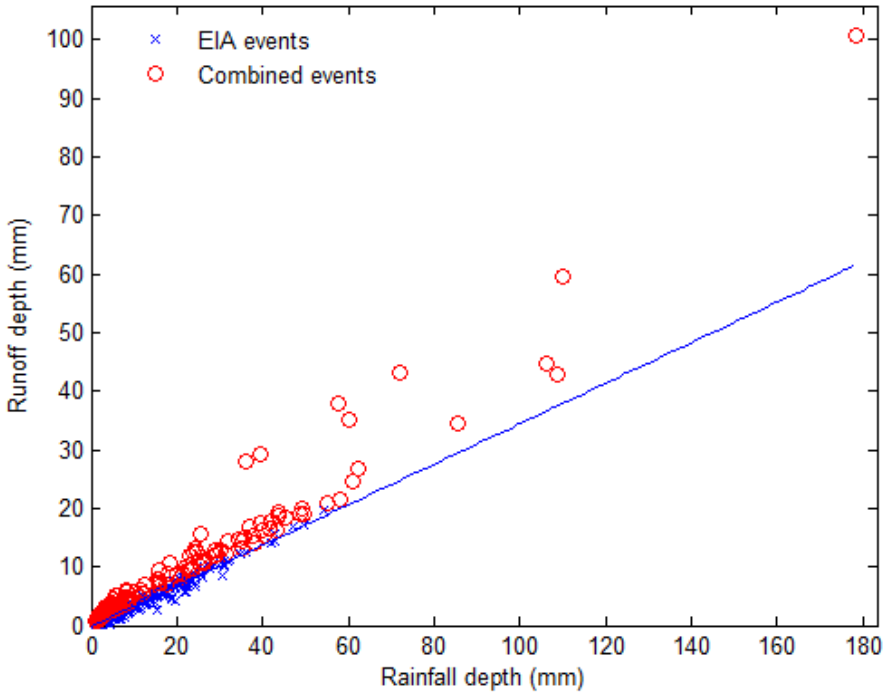
EIA events
Combined events
Runoff depth (mm)
Rainfall depth (mm)
0
10
20
30
40
50
60
70
80
90
100
0
20
40
60
80
100
120
140
160
180

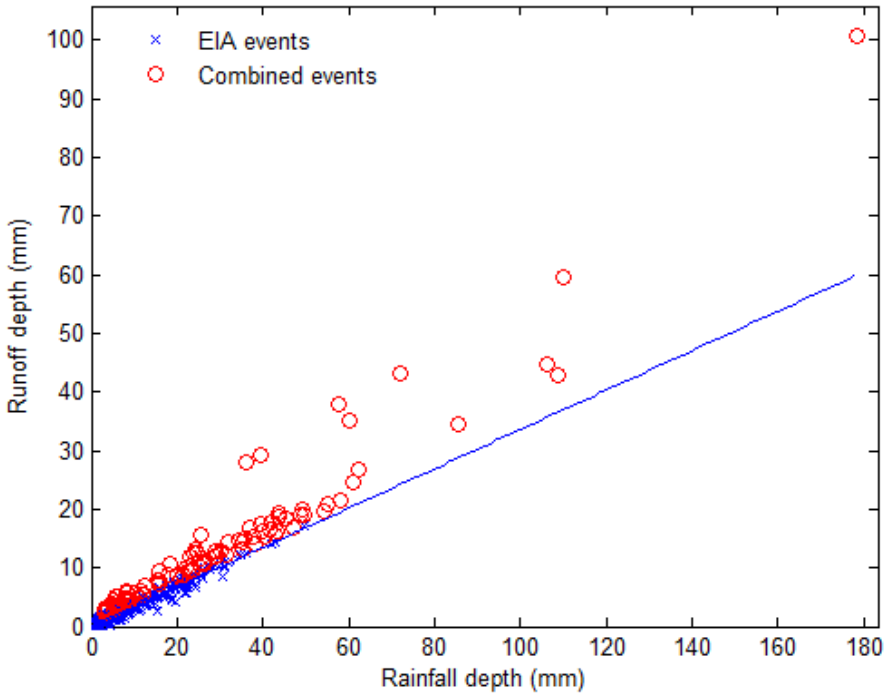
EIA events
Combined events
Runoff depth (mm)
Rainfall depth (mm)
0
10
20
30
40
50
60
70
80
90
100
0
20
40
60
80
100
120
140
160
180

ERA

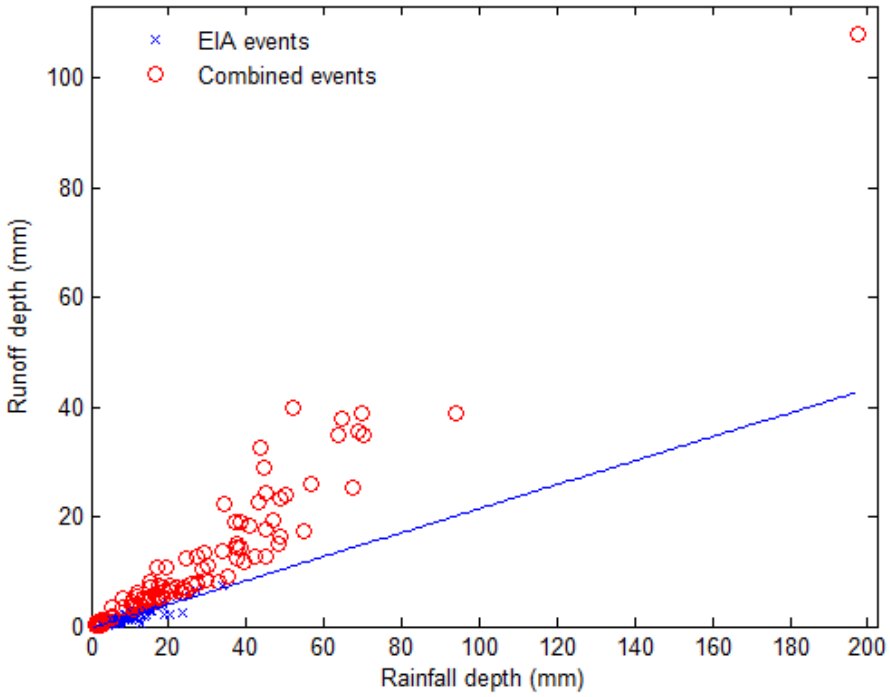
EIA events
Combined events
Runoff depth (mm)
Rainfall depth (mm)
0
20
40
60
80
100
120
140
160
180
200

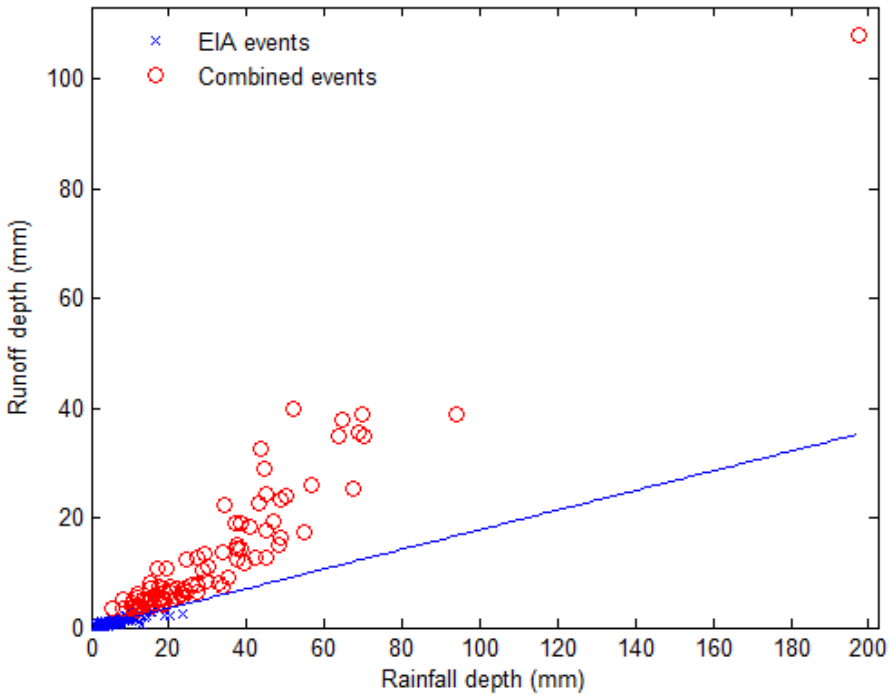
EIA events
Combined events
Runoff depth (mm)
Rainfall depth (mm)
0
20
40
60
80
100
120
140
160
180
200

HI

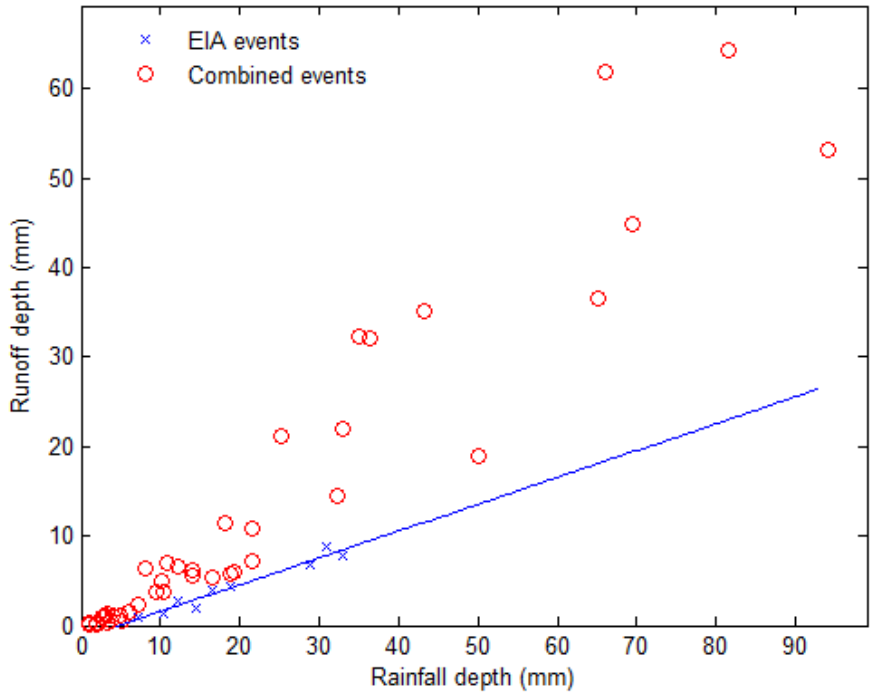
EIA events
Combined events
Runoff depth (mm)
Rainfall depth (mm)
0
10
20
30
40
50
60
70
80
90

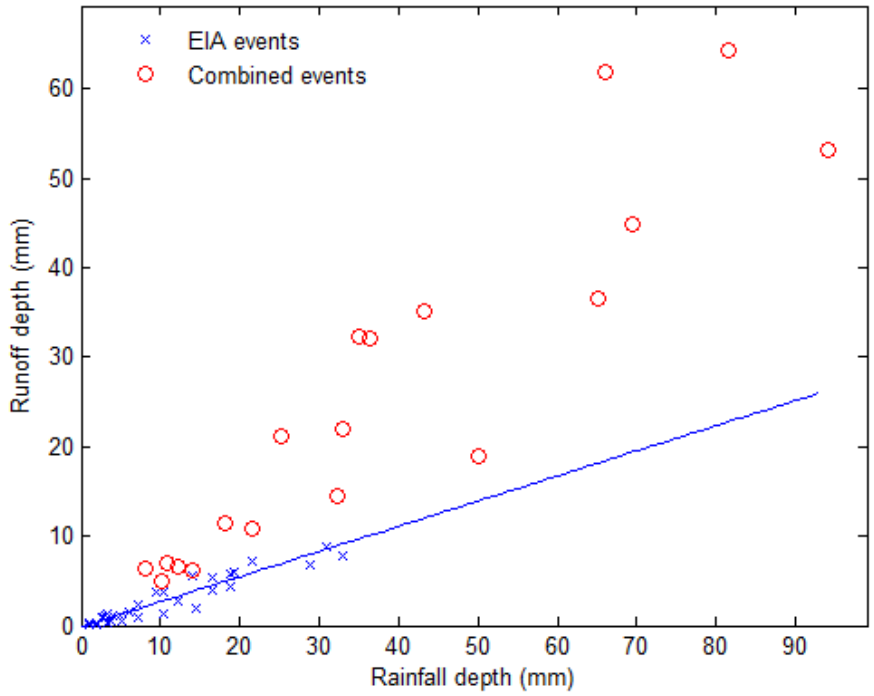
EIA events
Combined events
Runoff depth (mm)
Rainfall depth (mm)
0
10
20
30
40
50
60
70
80
90

HPA

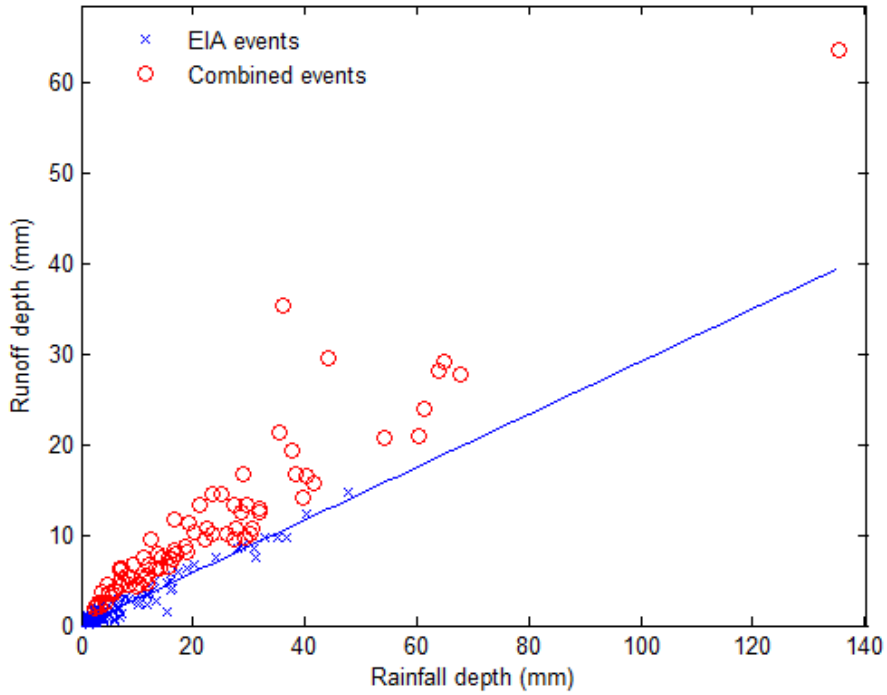
EIA events
Combined events
Runoff depth (mm)
Rainfall depth (mm)
0
10
20
30
40
50
60
0
20
40
60
80
100
120
140

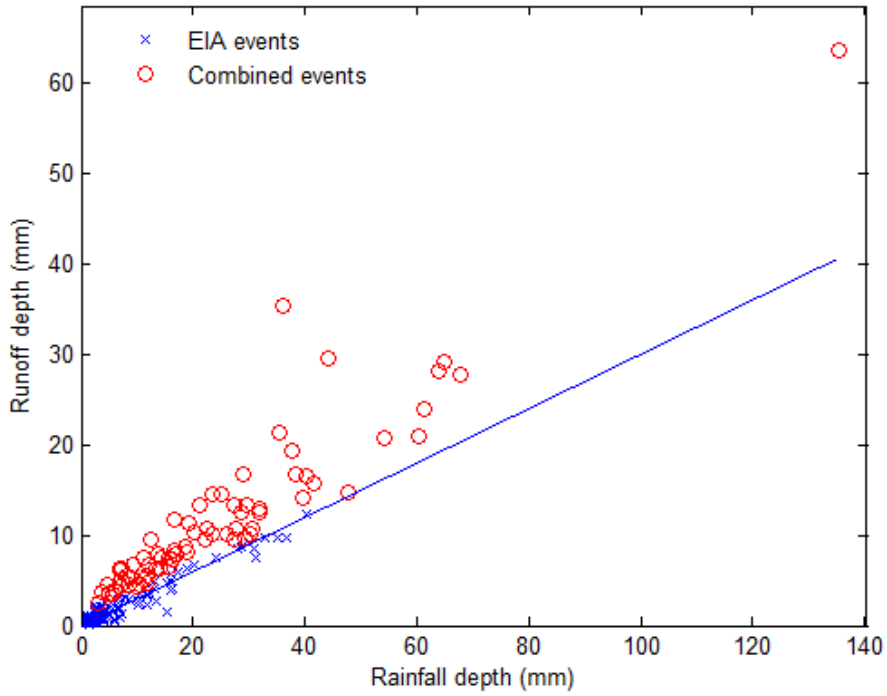
EIA events
Combined events
Runoff depth (mm)
Rainfall depth (mm)
0
10
20
30
40
50
60
0
20
40
60
80
100
120
140

LCA

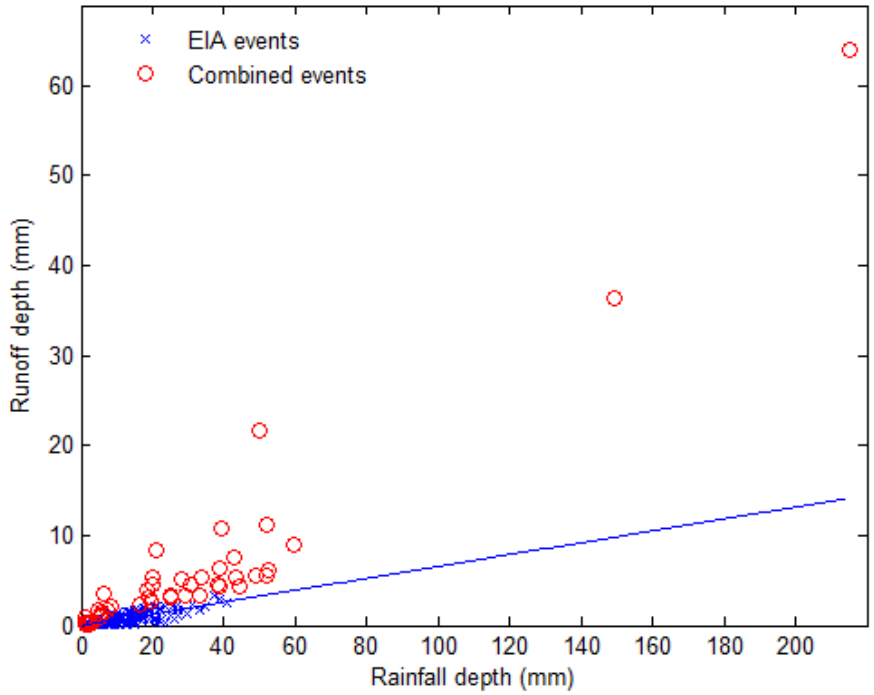
EIA events
Combined events
Runoff depth (mm)
Rainfall depth (mm)
0
10
20
30
40
50
60
0
20
40
60
80
100
120
140
160
180
200

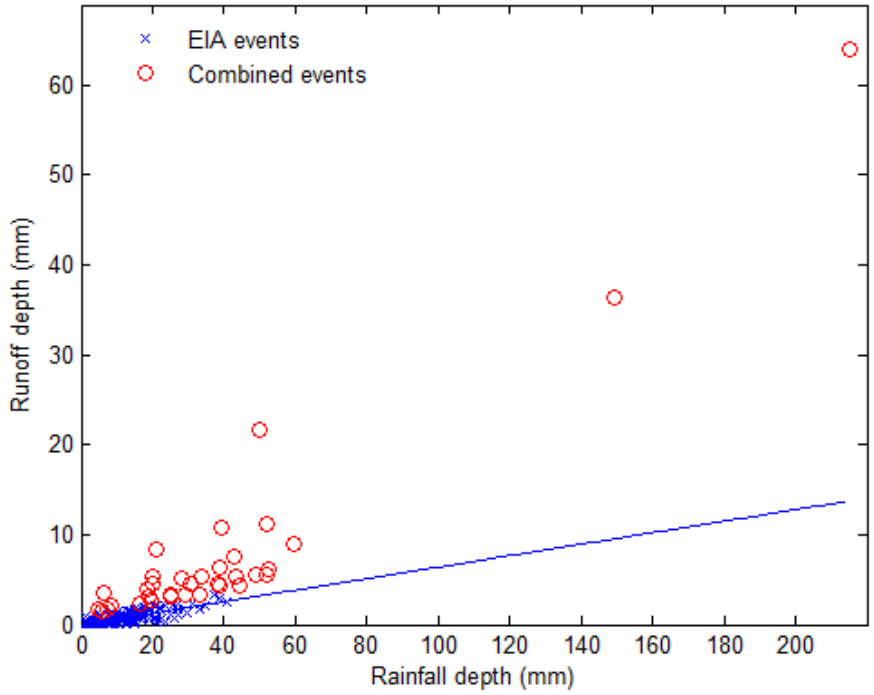
EIA events
Combined events
Runoff depth (mm)
Rainfall depth (mm)
0
10
20
30
40
50
60
0
20
40
60
80
100
120
140
160
180
200

LOA

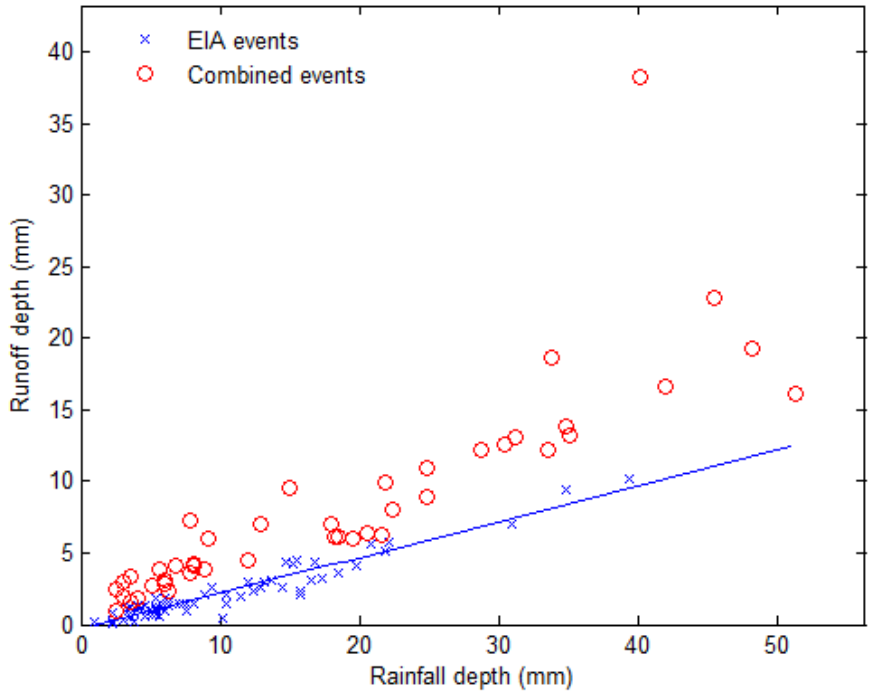
EIA events
Combined events
Runoff depth (mm)
Rainfall depth (mm)
0
5
10
15
20
25
30
35
40
0
10
20
30
40
50

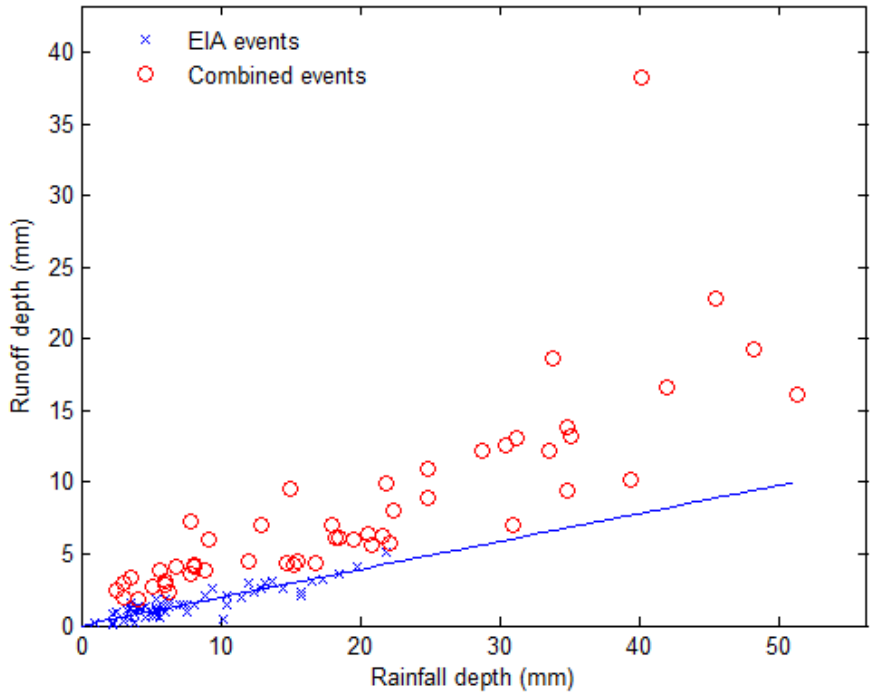
EIA events
Combined events
Runoff depth (mm)
Rainfall depth (mm)
0
5
10
15
20
25
30
35
40
0
10
20
30
40
50

LUA

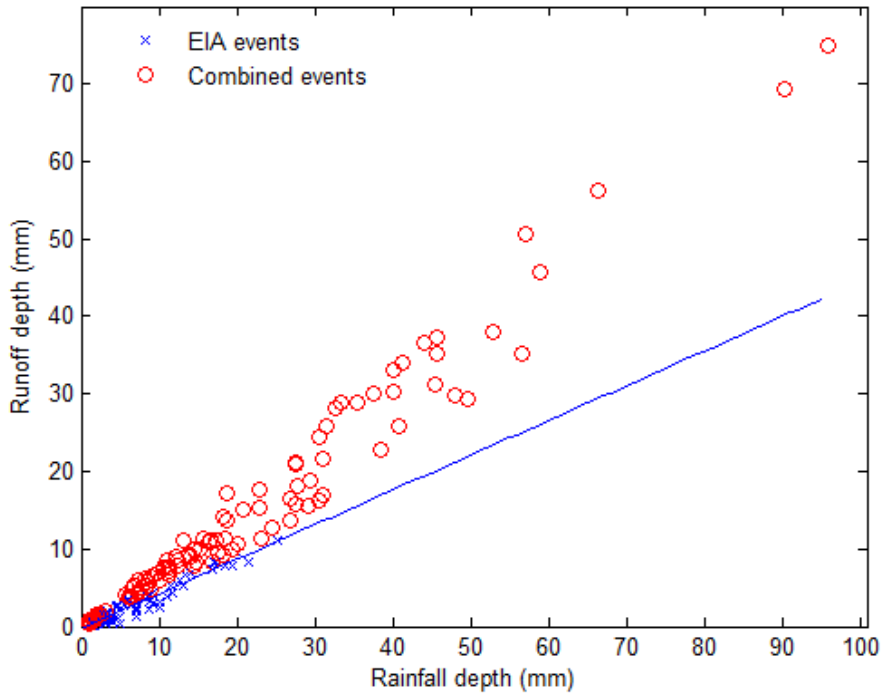
EIA events
Combined events
Runoff depth (mm)
Rainfall depth (mm)
0
10
20
30
40
50
60
70
80
90
100

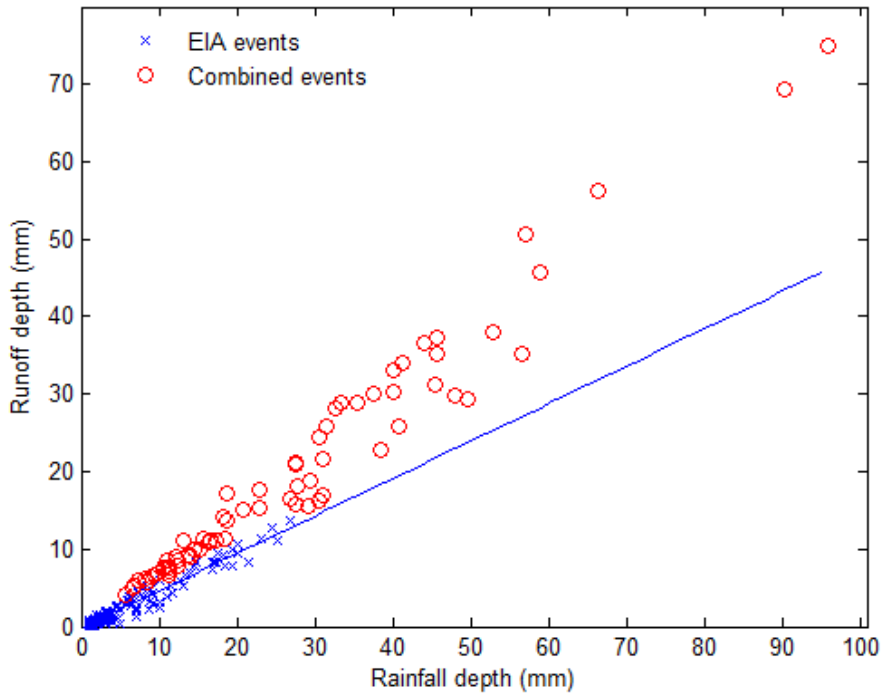
EIA events
Combined events
Runoff depth (mm)
Rainfall depth (mm)
0
10
20
30
40
50
60
70
80
90
100

MBA

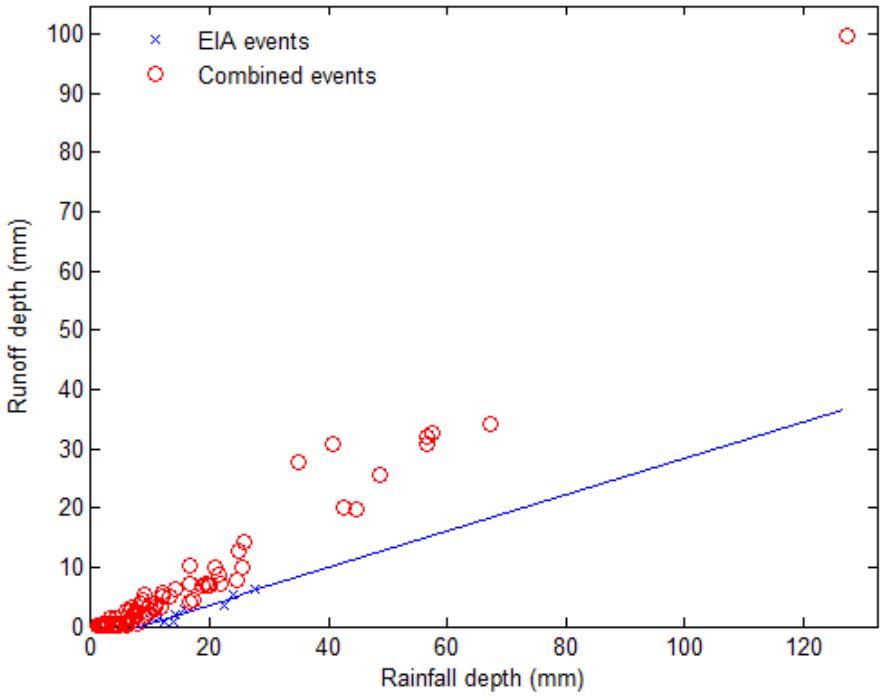
EIA events
Combined events
Runoff depth (mm)
Rainfall depth (mm)
0
10
20
30
40
50
60
70
80
90
100
0
20
40
60
80
100
120

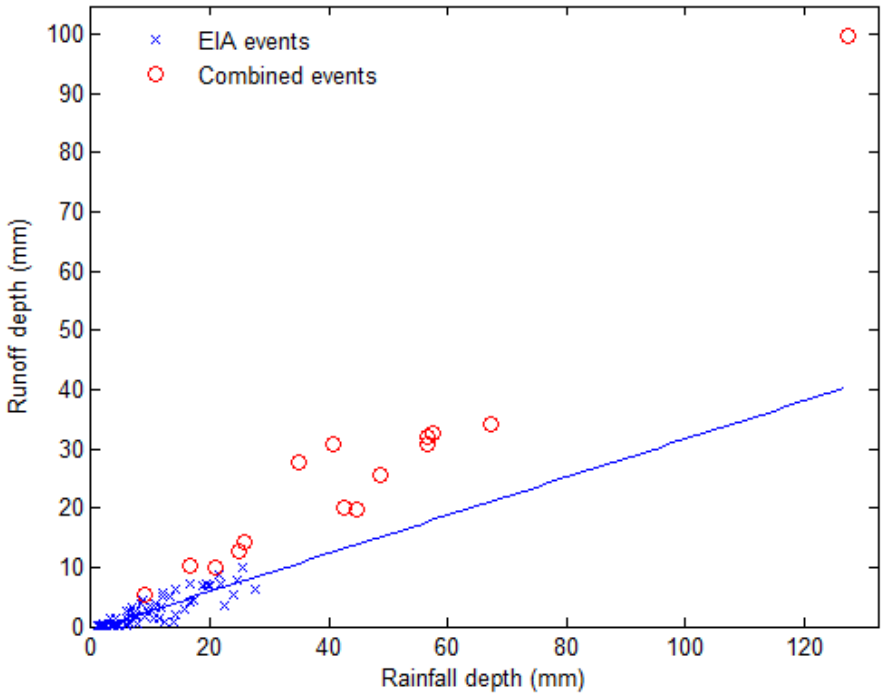
EIA events
Combined events
Runoff depth (mm)
Rainfall depth (mm)
0
10
20
30
40
50
60
70
80
90
100
0
20
40
60
80
100
120

OFA

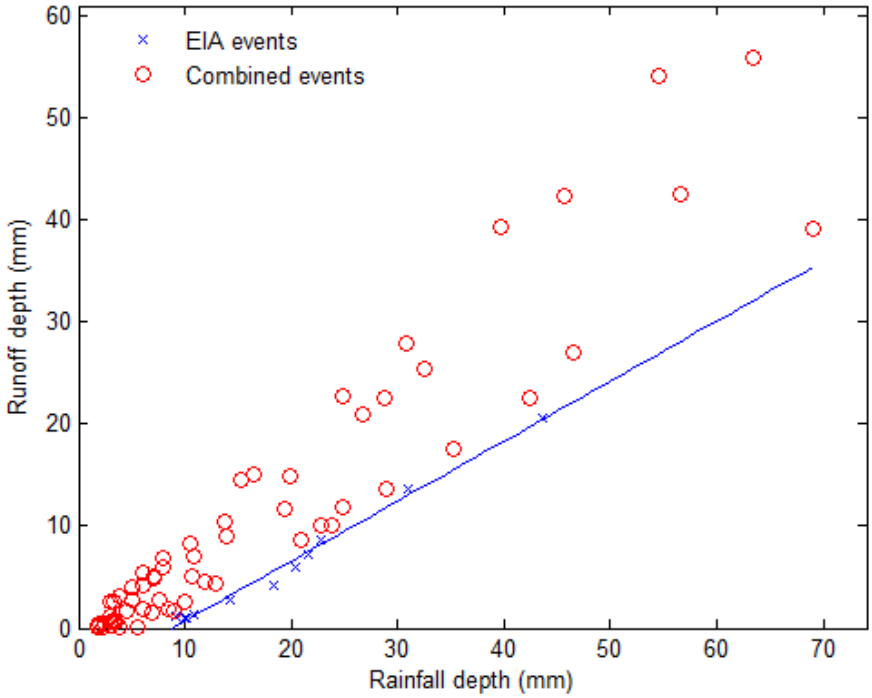
EIA events
Combined events
Runoff depth (mm)
Rainfall depth (mm)
0
10
20
30
40
50
60
70

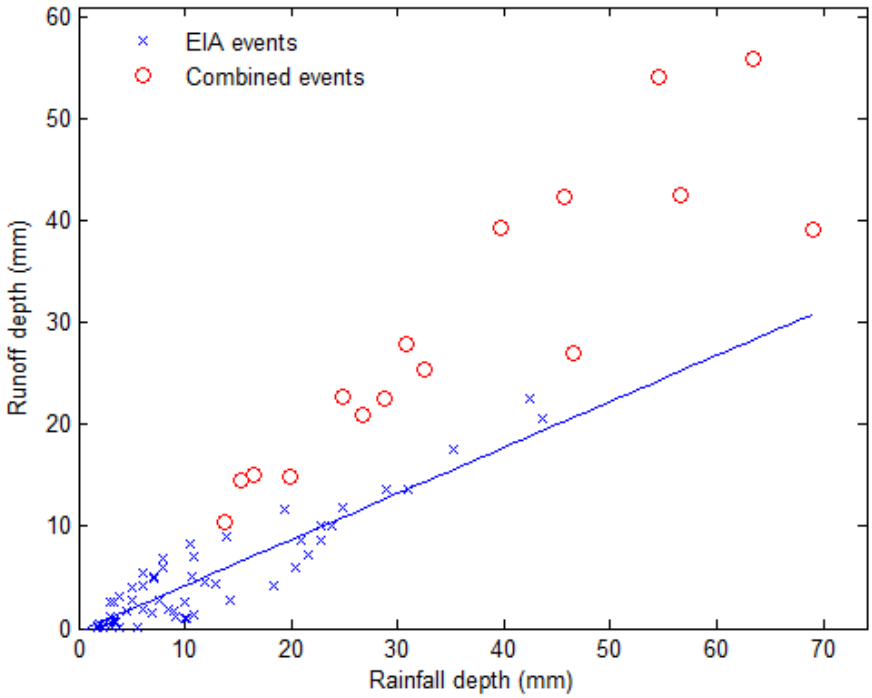
EIA events
Combined events
Runoff depth (mm)
Rainfall depth (mm)
0
10
20
30
40
50
60
70

PP1

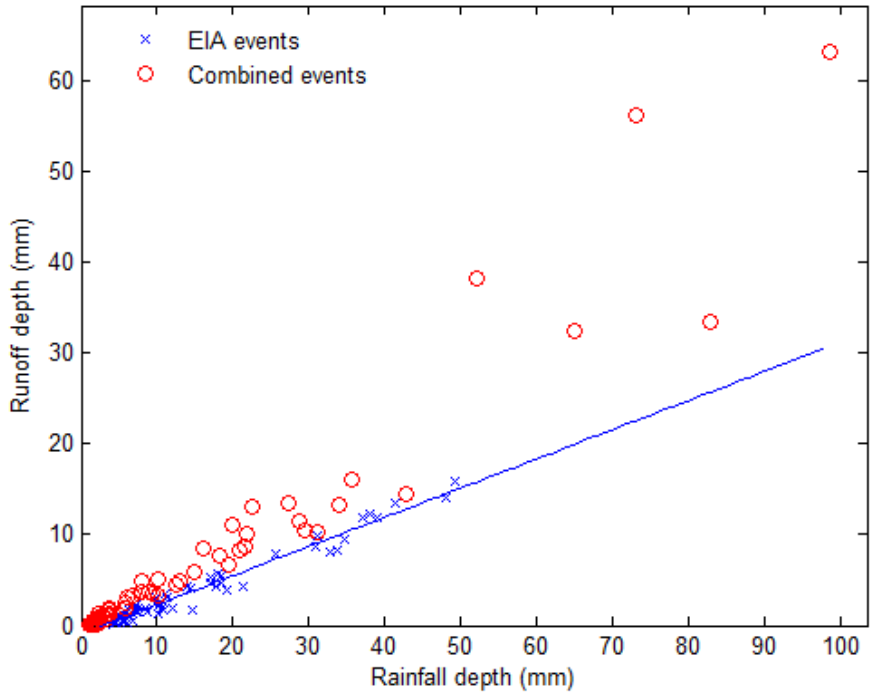
EIA events
Combined events
Runoff depth (mm)
Rainfall depth (mm)
0
10
20
30
40
50
60
70
80
90
100

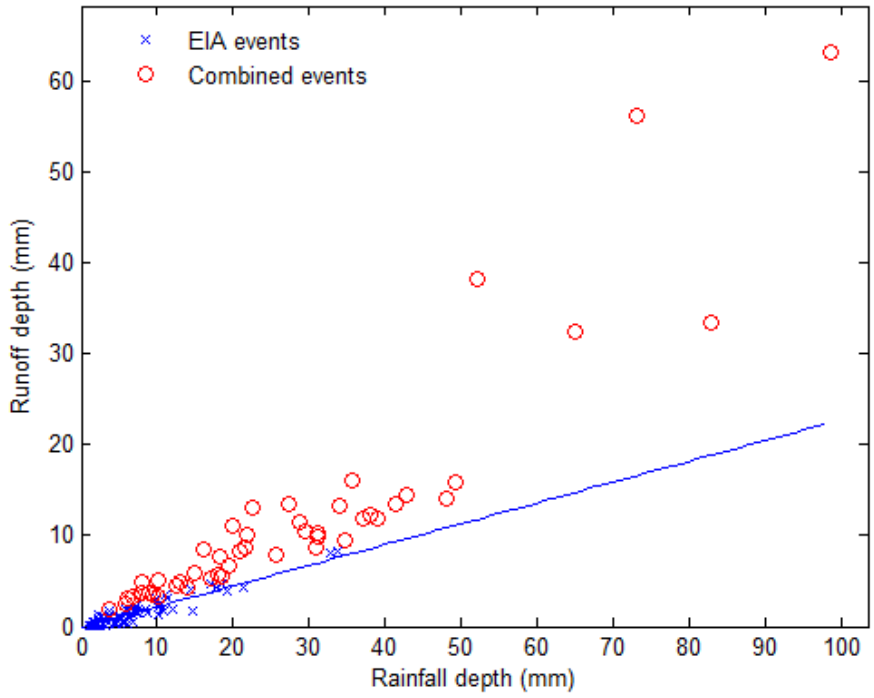
EIA events
Combined events
Runoff depth (mm)
Rainfall depth (mm)
0
10
20
30
40
50
60
70
80
90
100

PP2

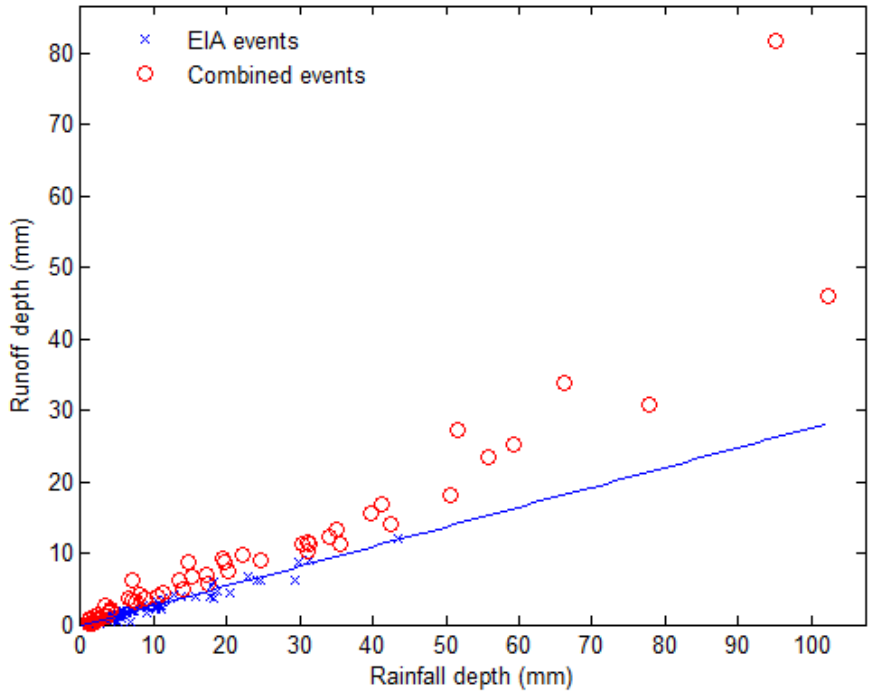
EIA events
Combined events
Runoff depth (mm)
Rainfall depth (mm)
0
10
20
30
40
50
60
70
80
90
100

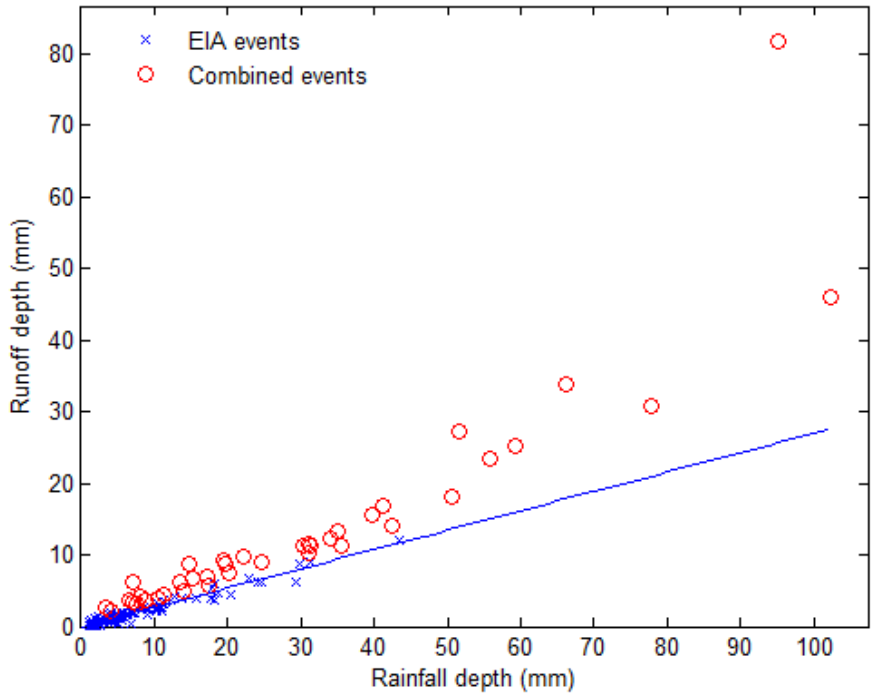
EIA events
Combined events
Runoff depth (mm)
Rainfall depth (mm)
0
10
20
30
40
50
60
70
80
90
100

PP3

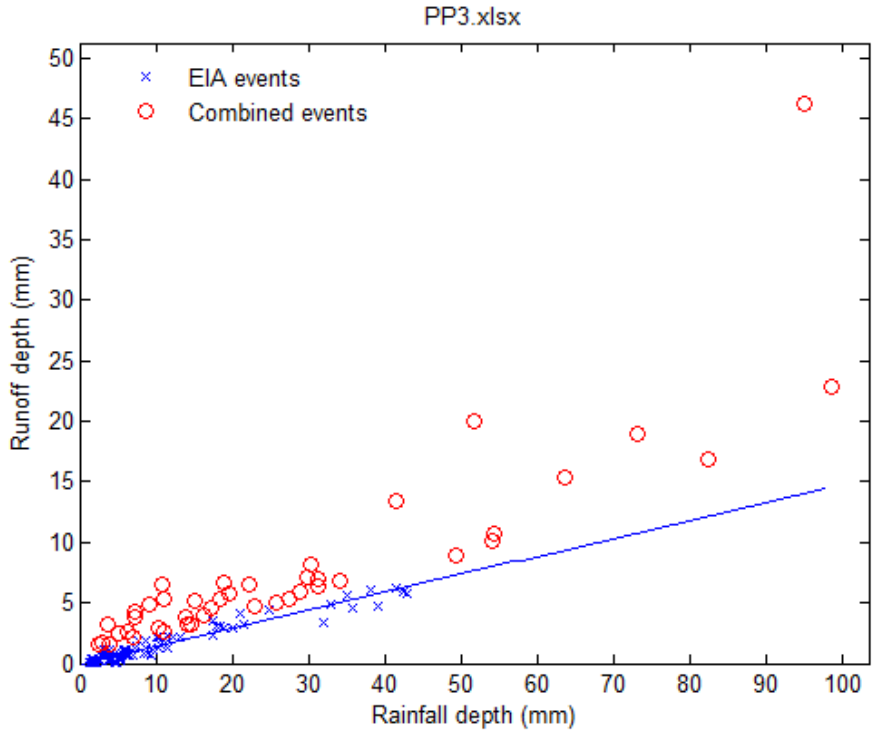
PP3.xlsx
EIA events
Combined events
Runoff depth (mm)
Rainfall depth (mm)
0
5
10
15
20
25
30
35
40
45
50
0
10
20
30
40
50
60
70
80
90
100

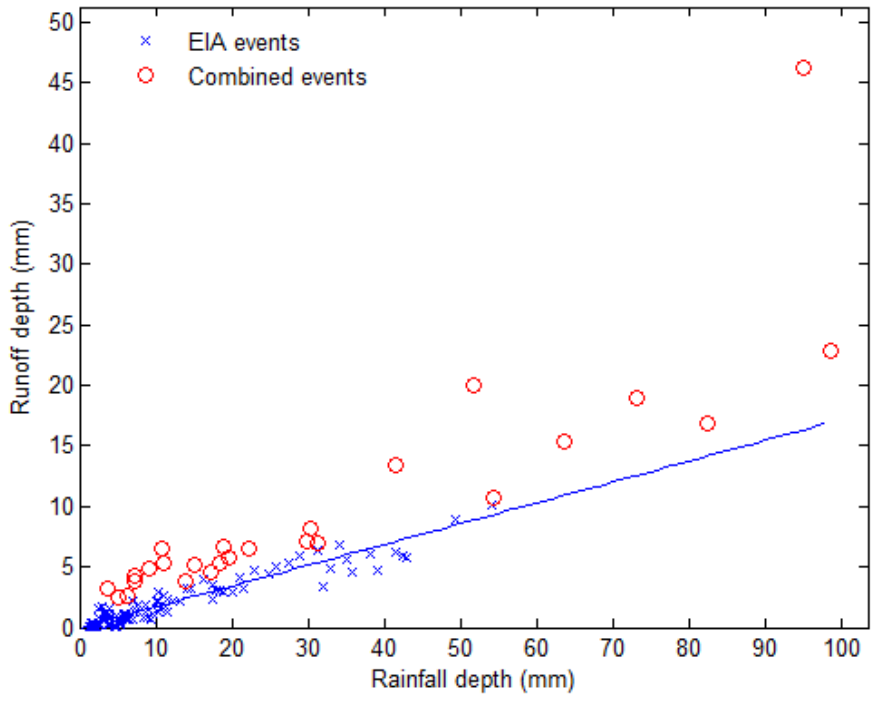
EIA events
Combined events
Runoff depth (mm)
Rainfall depth (mm)
0
5
10
15
20
25
30
35
40
45
50
0
10
20
30
40
50
60
70
80
90
100

RRI

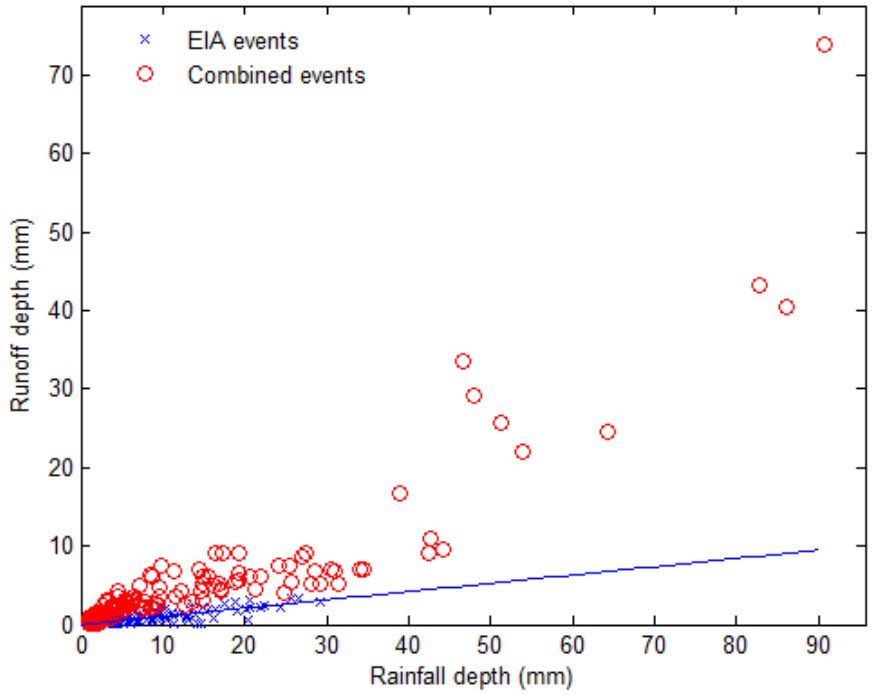
EIA events
Combined events
Runoff depth (mm)
Rainfall depth (mm)
0
10
20
30
40
50
60
70
80
90

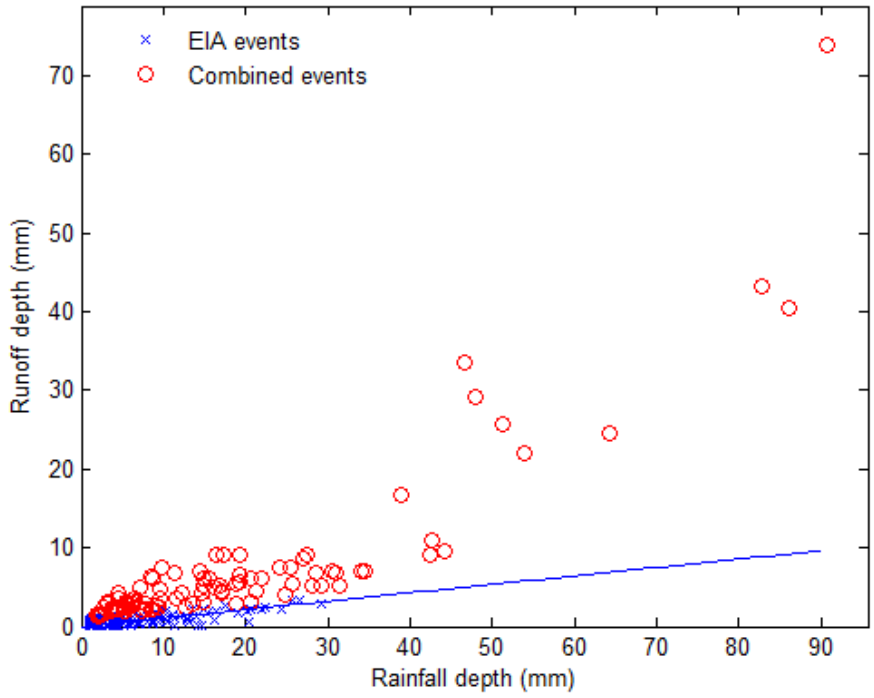
EIA events
Combined events
Runoff depth (mm)
Rainfall depth (mm)
0
10
20
30
40
50
60
70
80
90

SCA

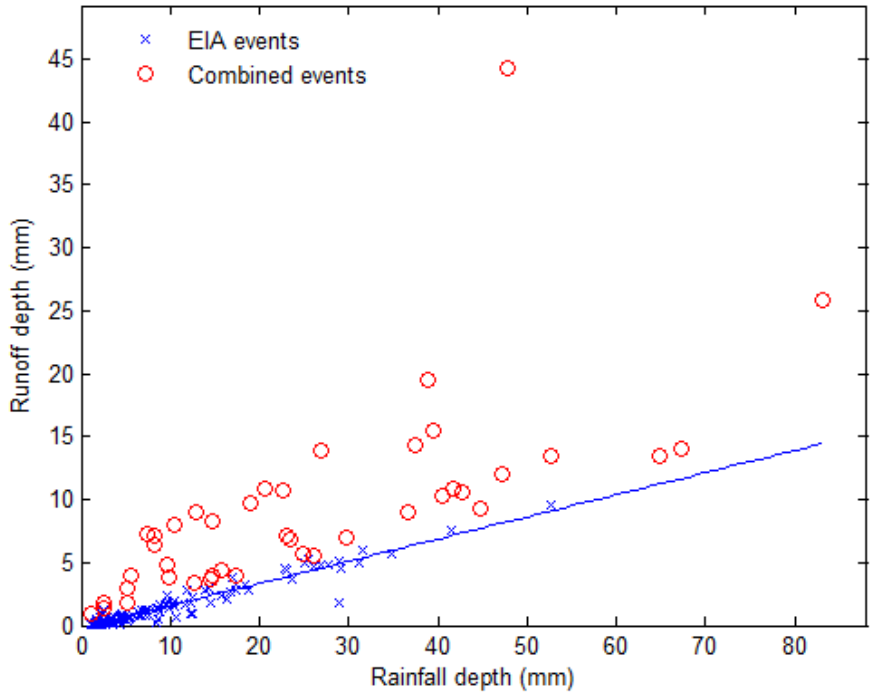
EIA events
Combined events
Runoff depth (mm)
Rainfall depth (mm)
0
5
10
15
20
25
30
35
40
45
0
10
20
30
40
50
60
70
80

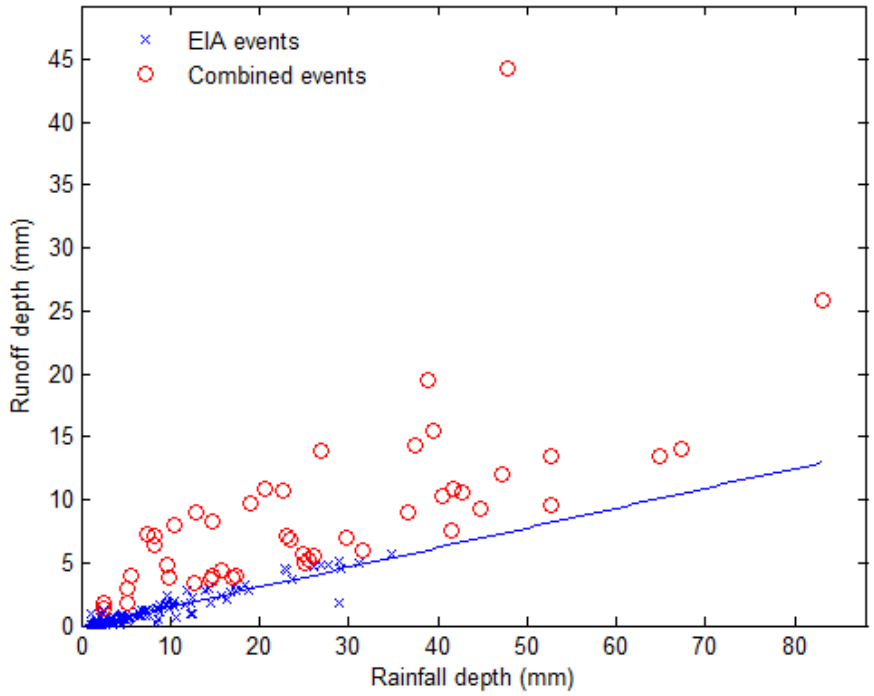
EIA events
Combined events
Runoff depth (mm)
Rainfall depth (mm)
0
5
10
15
20
25
30
35
40
45
0
10
20
30
40
50
60
70
80

TBA

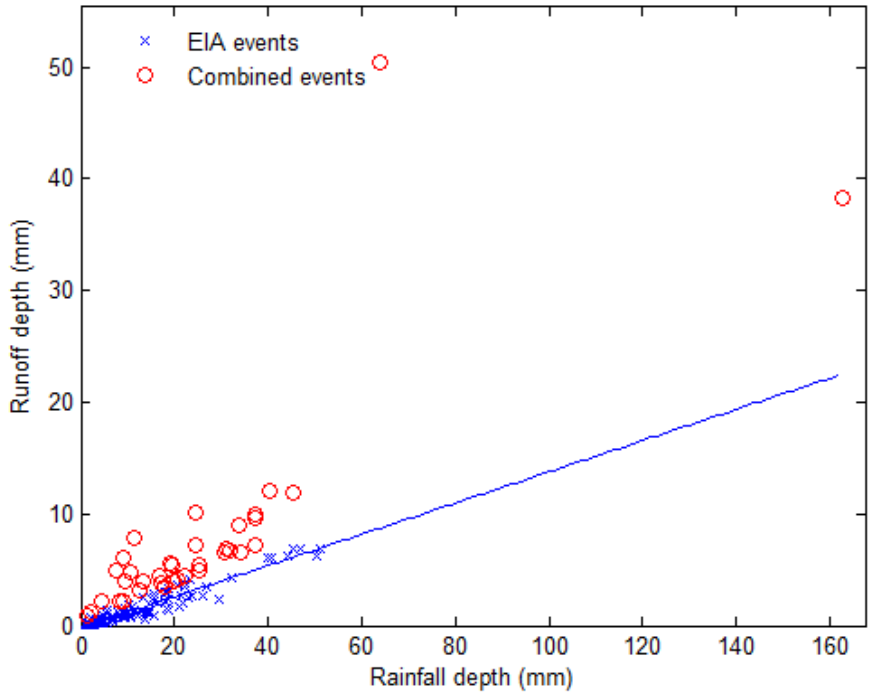
EIA events
Combined events
Runoff depth (mm)
Rainfall depth (mm)
0
10
20
30
40
50
0
20
40
60
80
100
120
140
160

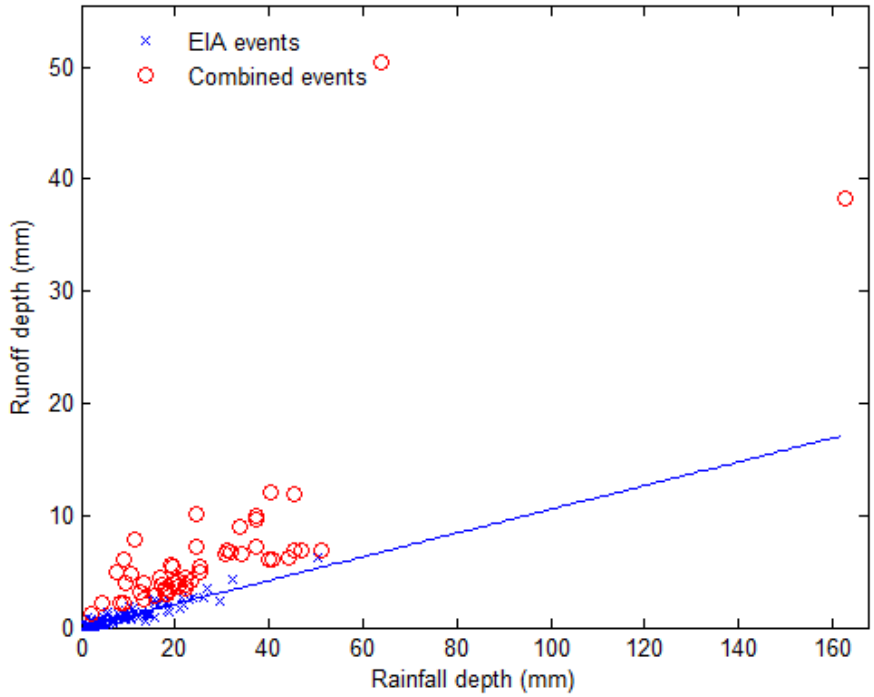
EIA events
Combined events
Runoff depth (mm)
Rainfall depth (mm)
0
10
20
30
40
50
0
20
40
60
80
100
120
140
160

TCA

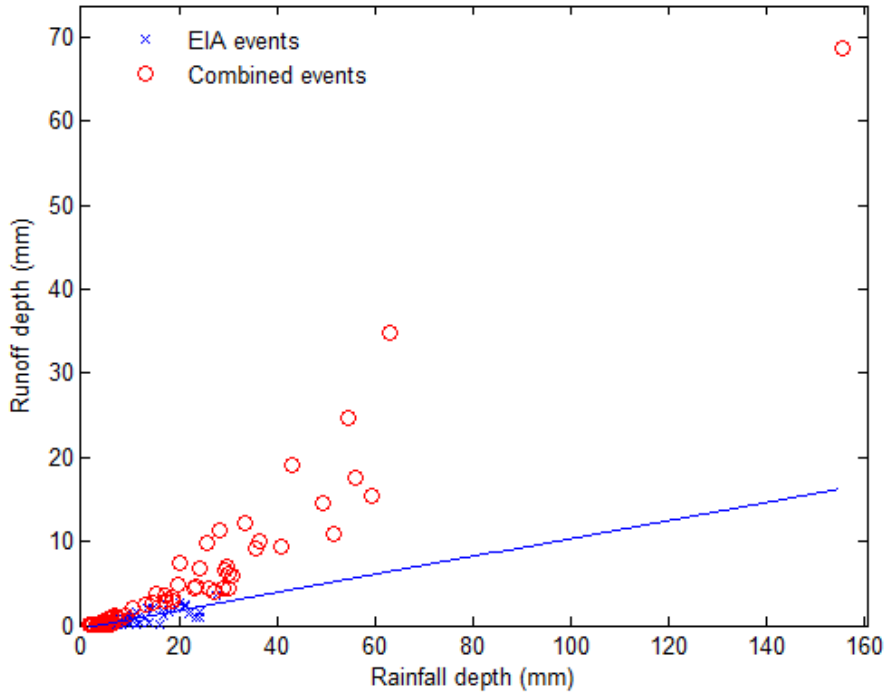
EIA events
Combined events
Runoff depth (mm)
Rainfall depth (mm)
0
10
20
30
40
50
60
70
0
20
40
60
80
100
120
140
160

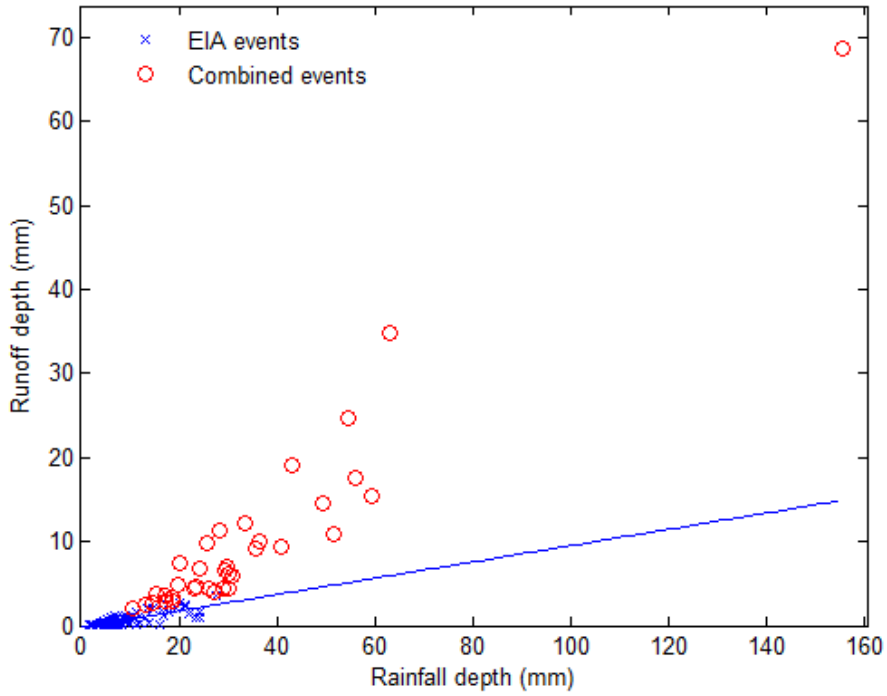
EIA events
Combined events
Runoff depth (mm)
Rainfall depth (mm)
0
10
20
30
40
50
60
70
0
20
40
60
80
100
120
140
160

TPA

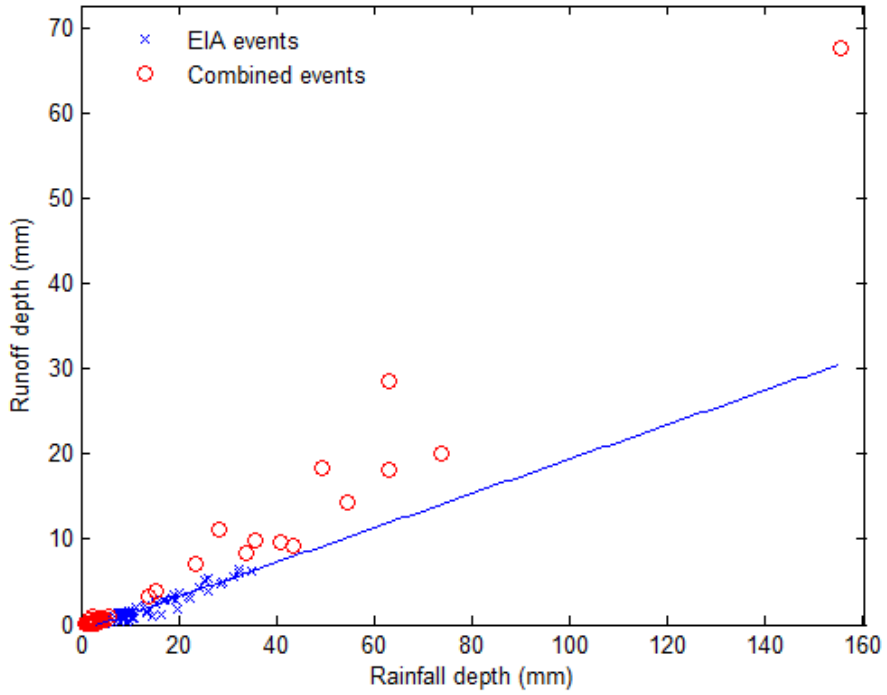
EIA events
Combined events
Runoff depth (mm)
Rainfall depth (mm)
0
10
20
30
40
50
60
70
0
20
40
60
80
100
120
140
160

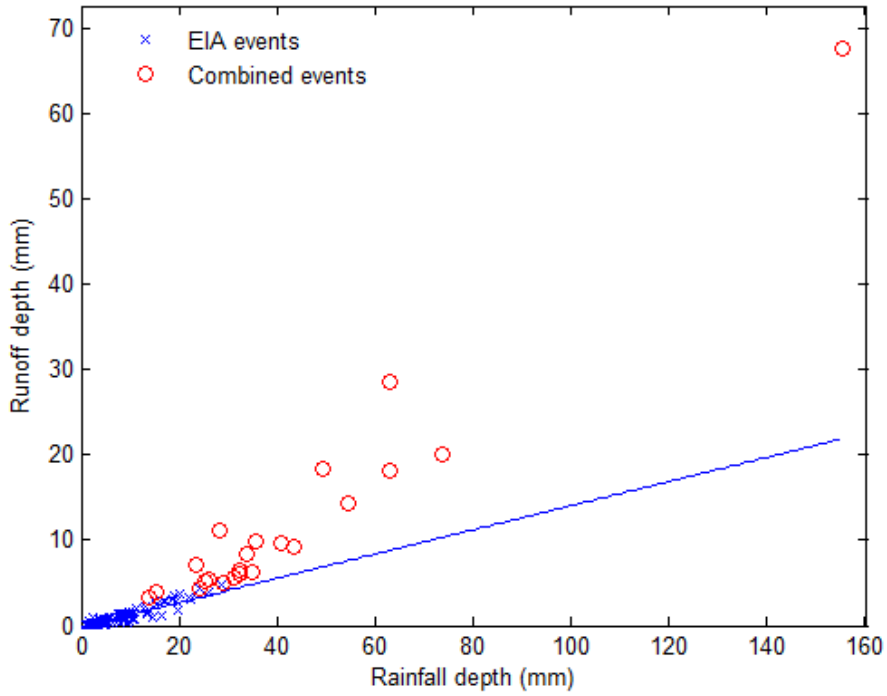
EIA events
Combined events
Runoff depth (mm)
Rainfall depth (mm)
0
10
20
30
40
50
60
70
0
20
40
60
80
100
120
140
160

WBA

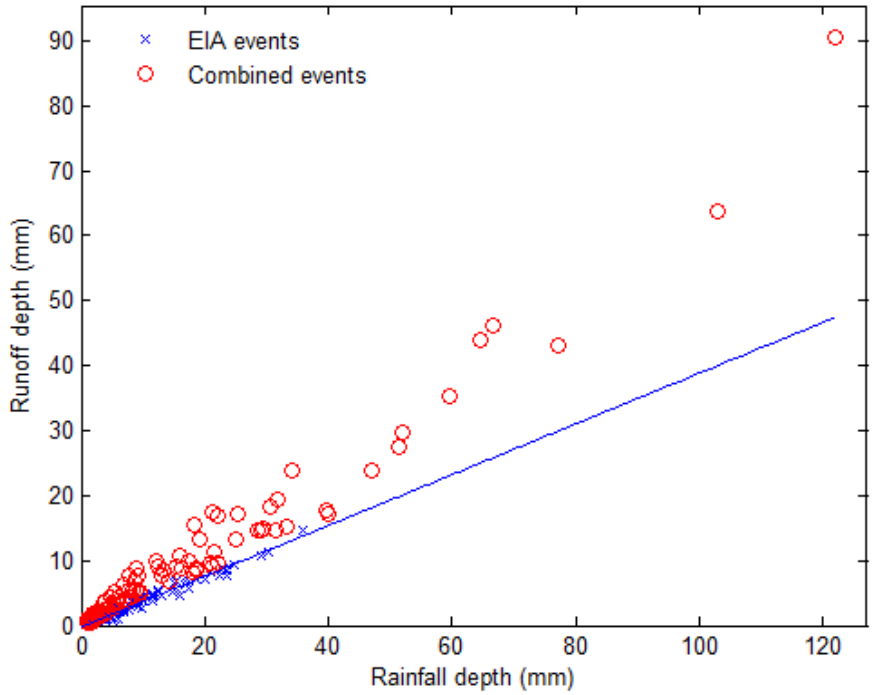
EIA events
Combined events
Runoff depth (mm)
Rainfall depth (mm)
0
10
20
30
40
50
60
70
80
90
0
20
40
60
80
100
120

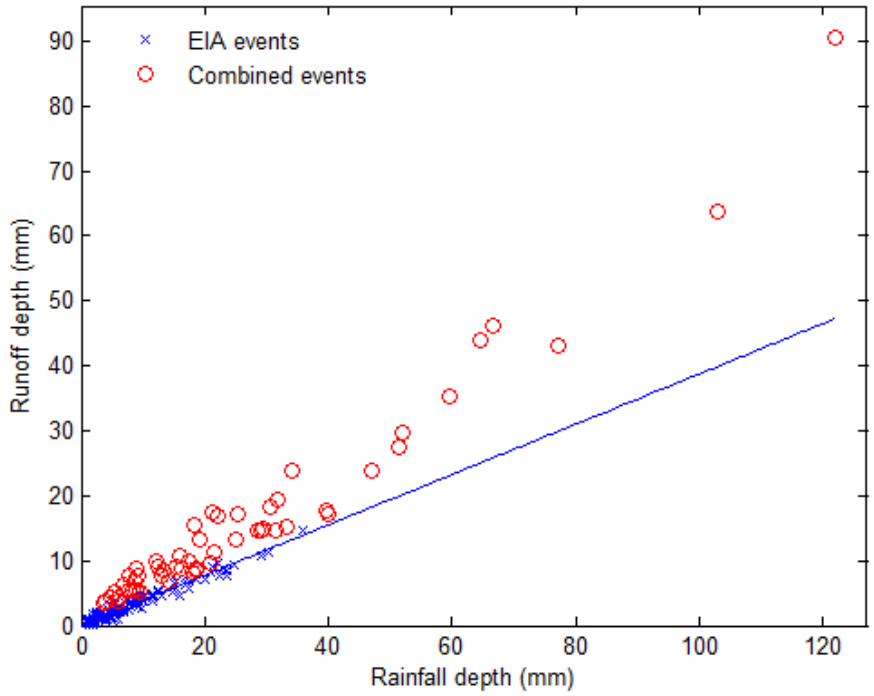
EIA events
Combined events
Runoff depth (mm)
Rainfall depth (mm)
0
10
20
30
40
50
60
70
80
90
0
20
40
60
80
100
120

APPENDIX B: PLOTS OF CURVE NUMBER VERSUS RAINFALL DEPTH

Plots of Curve Number (CN) versus rainfall depth (P) which shows the type of CN pattern for each watershed are presented for all the watersheds of study and different cases of initial abstraction ratio (λ) in this appendix. For each watershed, the order of figures from top to bottom is λ=0.2 and λ=0.05, respectively. The location, drainage area, land use, and monitoring years for each watershed are presented in section 2.2 of the report.

Capitol Region Watershed District (CRWD), MN

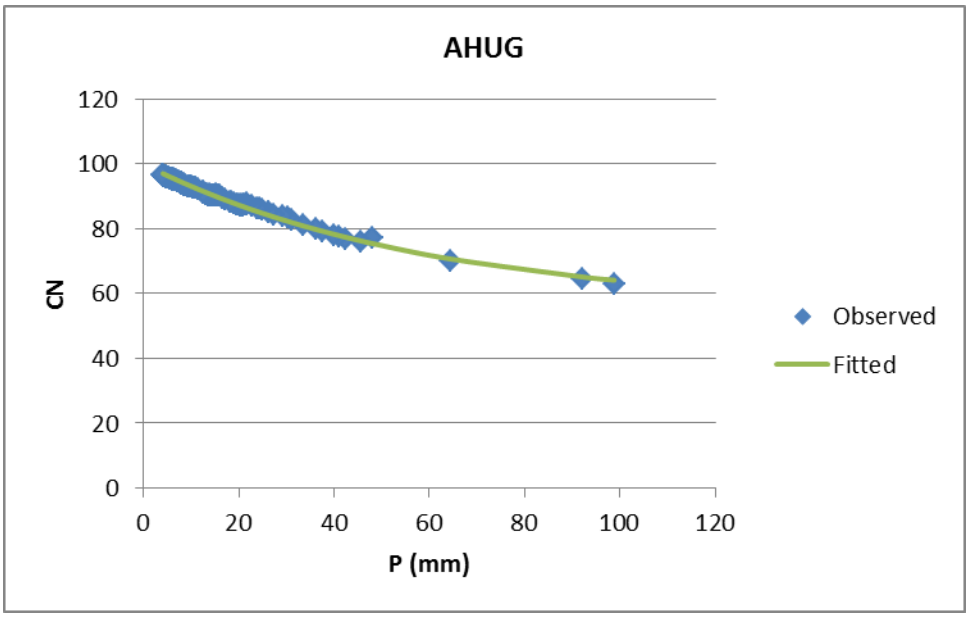

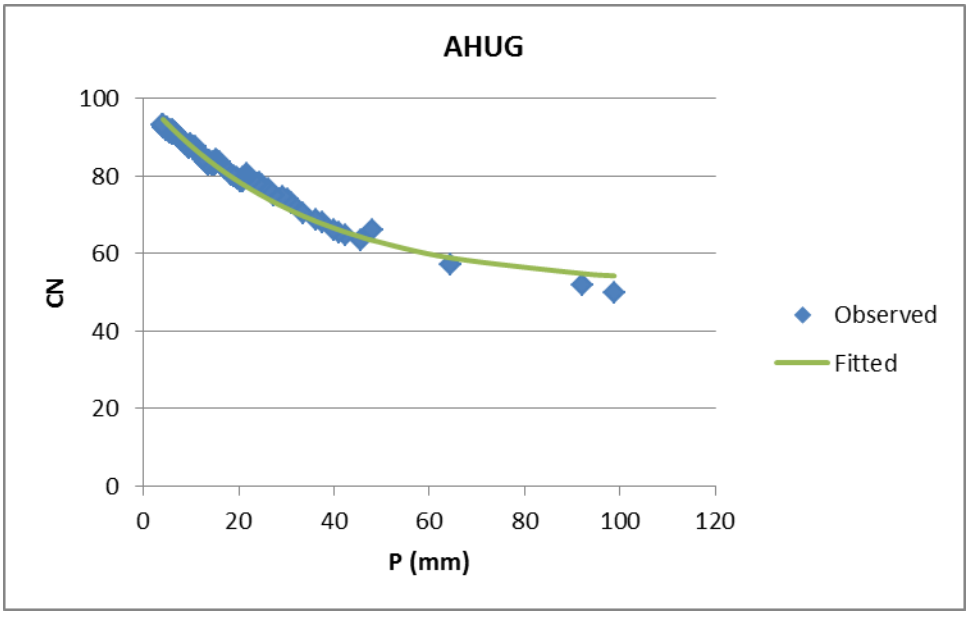

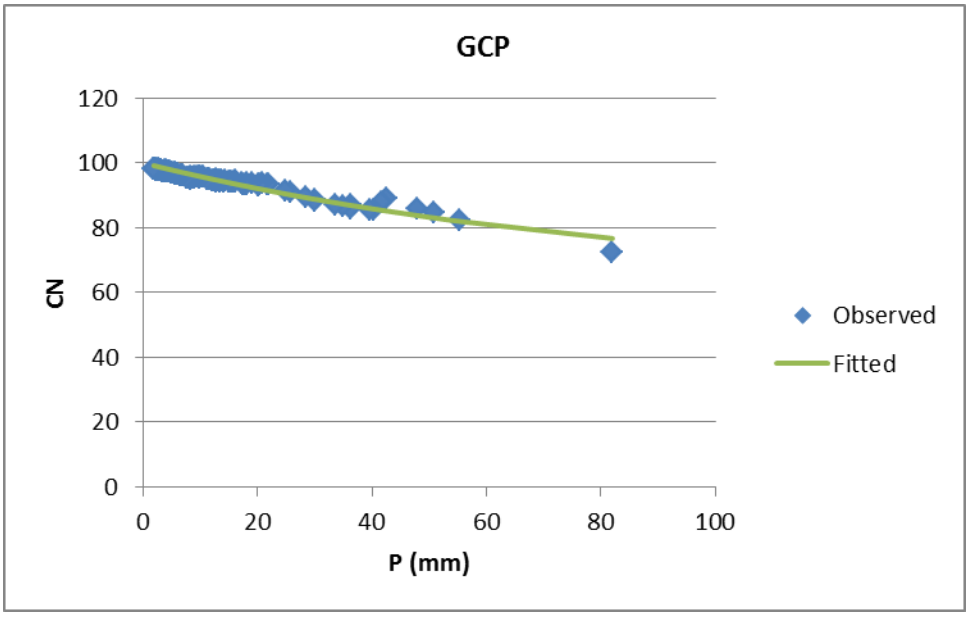
GCP
120
100
80
60
40
20
0
CN
0
20
40
60
80
100
P (mm)
Observed
Fitted

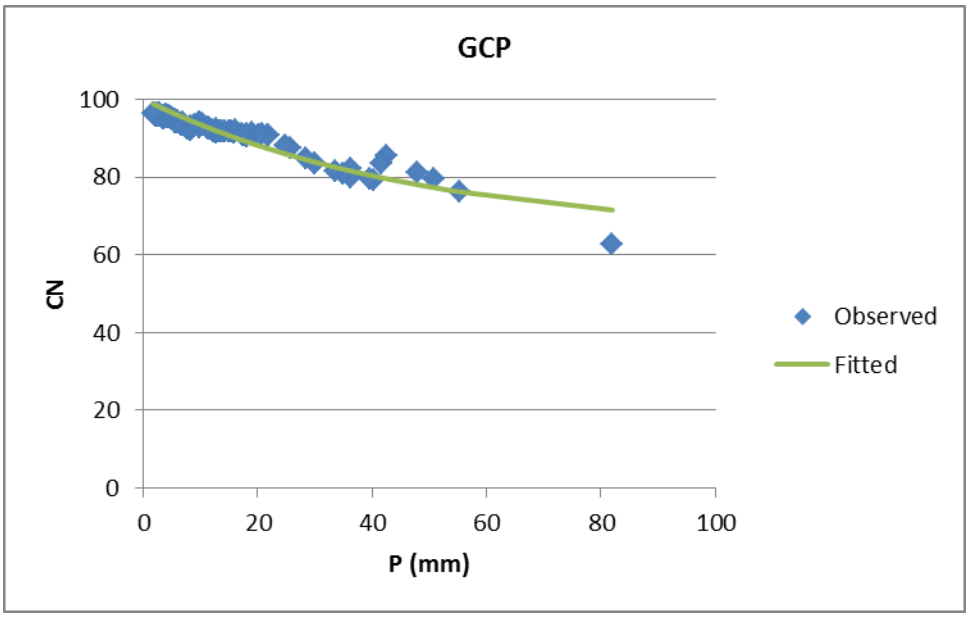
GCP
100
80
60
40
20
0
CN
0
20
40
60
80
100
P (mm)
Observed
Fitted

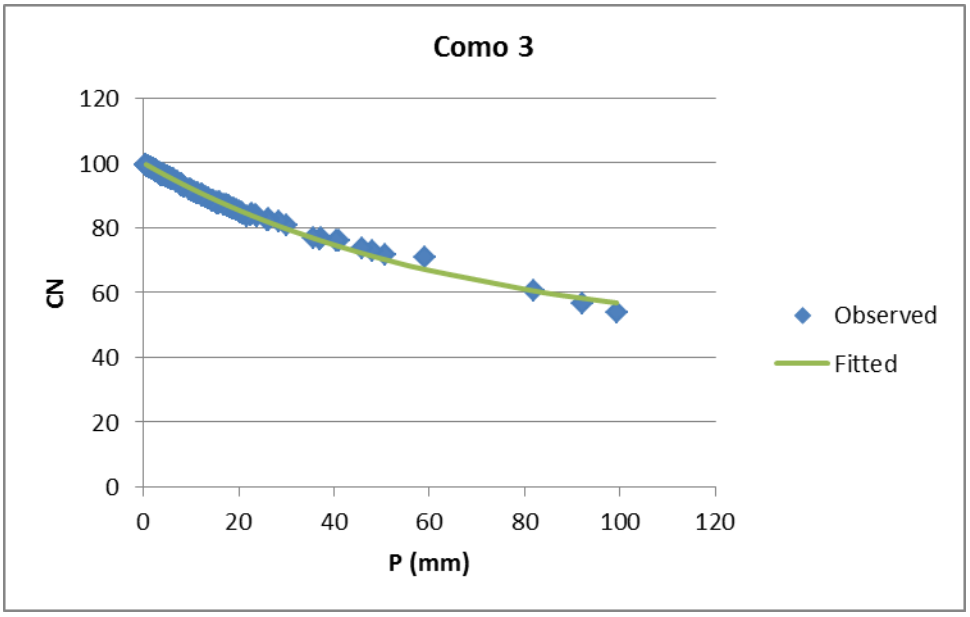
Como 3
120
100
80
60
40
20
0
CN
0
20
40
60
80
100
120
P (mm)
Observed
Fitted

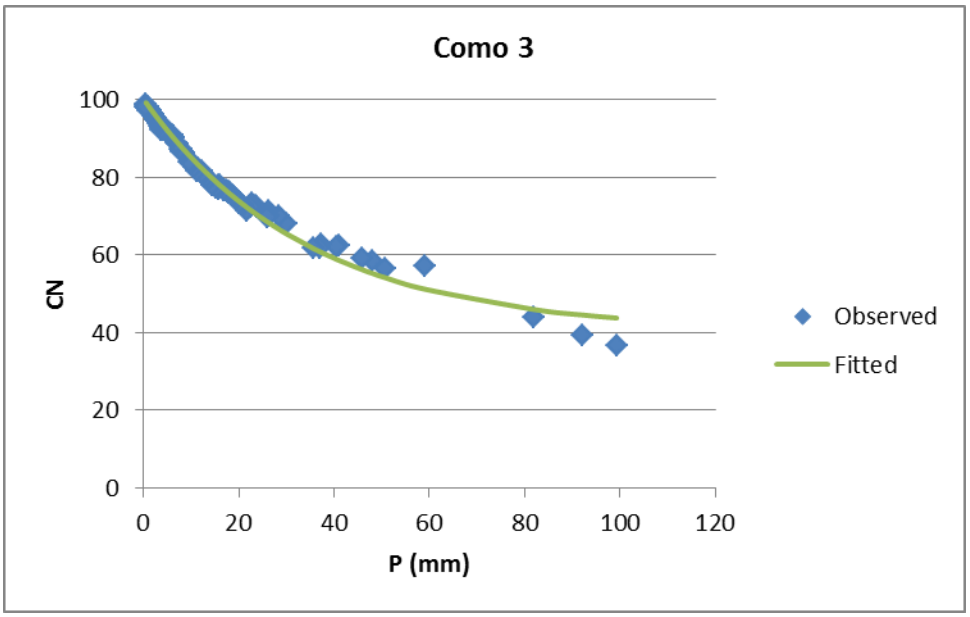
Como 3
100
80
60
40
20
0
CN
0
20
40
60
80
100
120
P (mm)
Observed
Fitted

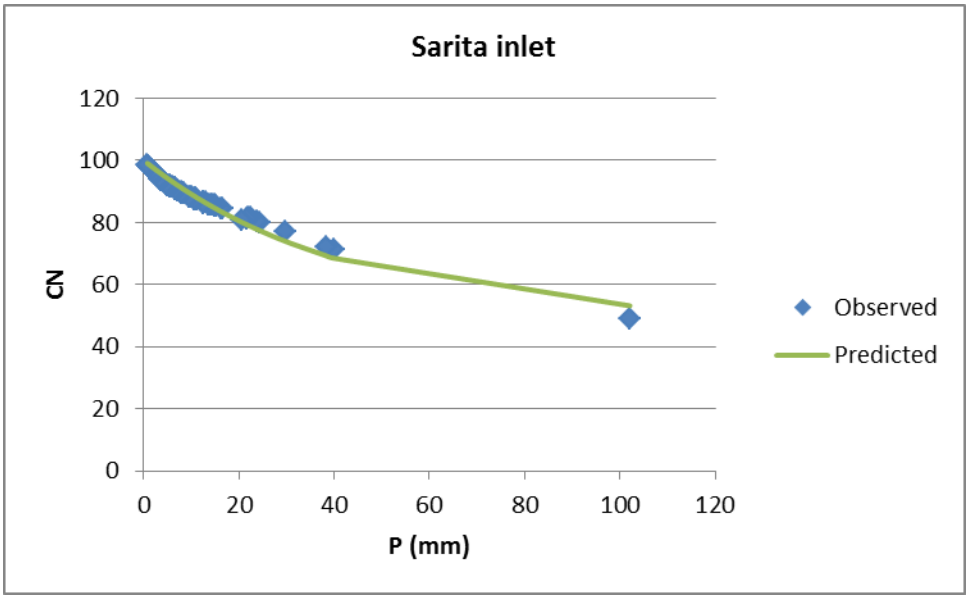
Sarita inlet
120
100
80
60
40
20
0
CN
0
20
40
60
80
100
120
P (mm)
Observed
Predicted

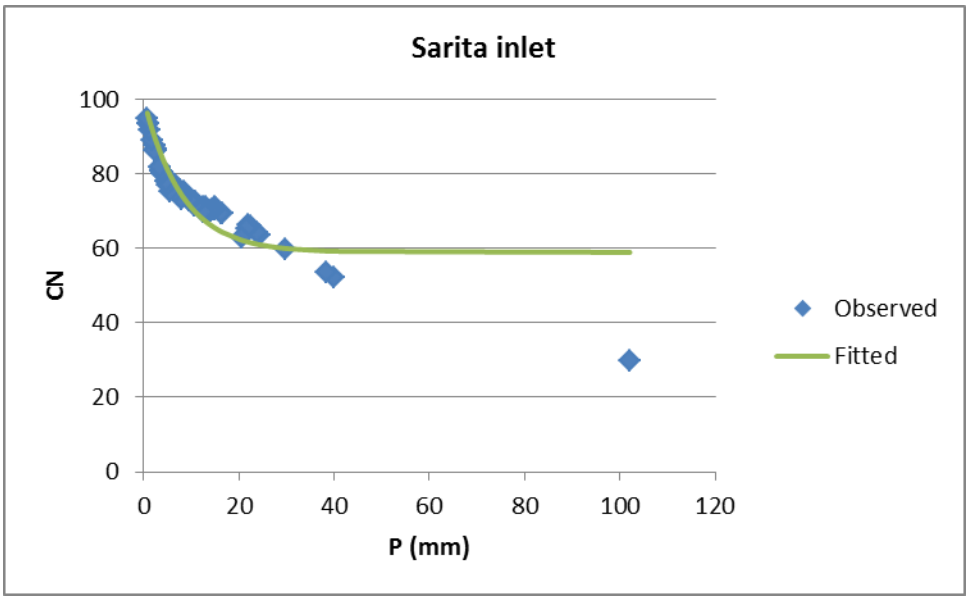
Sarita inlet
100
80
60
40
20
0
CN
0
20
40
60
80
100
120
P (mm)
Observed
Fitted

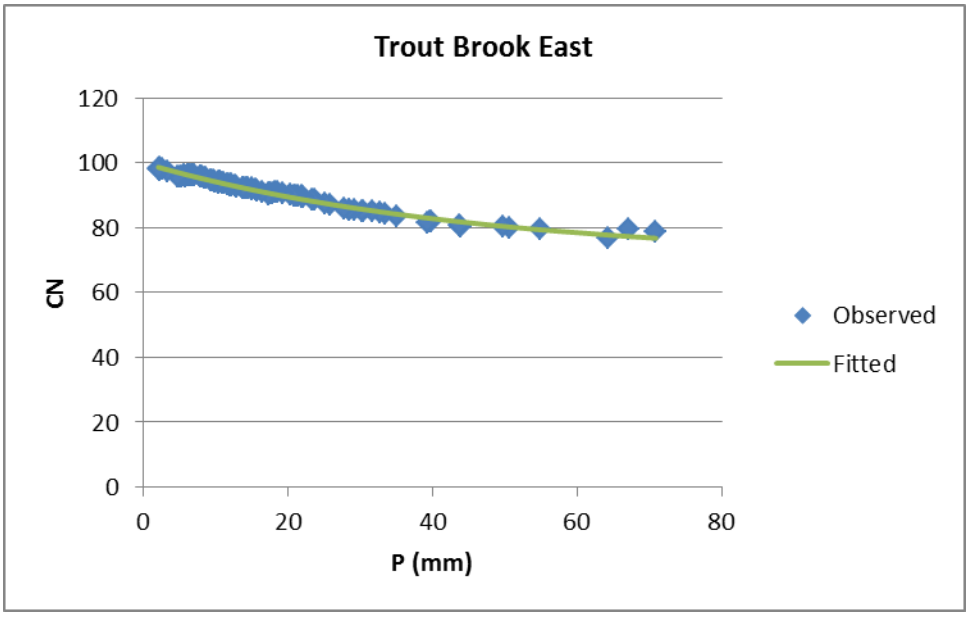
Trout Brook East
120
100
80
60
40
20
0
CN
0
20
40
60
80
P (mm)
Observed
Fitted

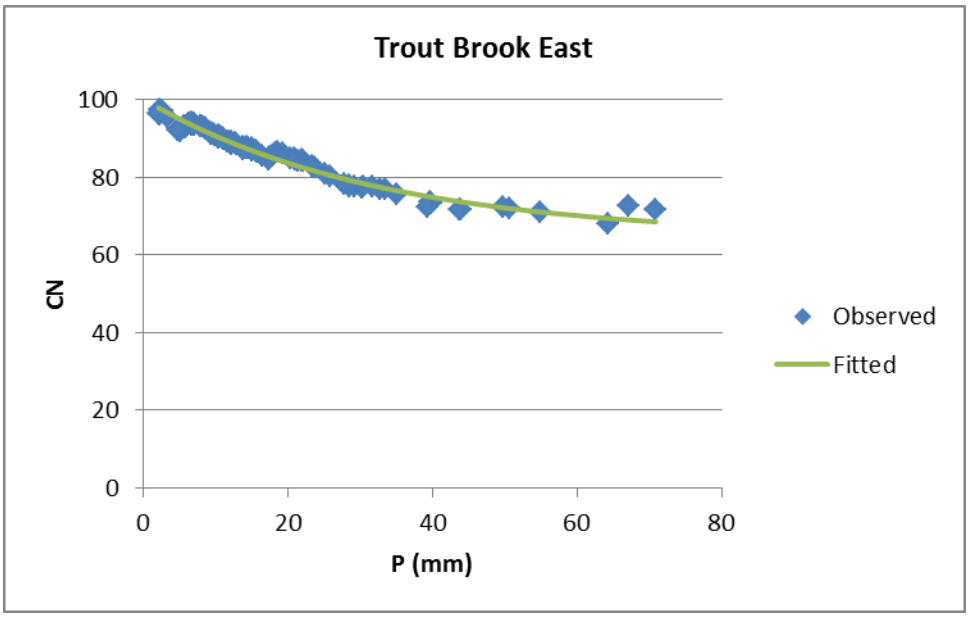
Trout Brook East
100
80
60
40
20
0
CN
0
20
40
60
80
P (mm)
Observed
Fitted

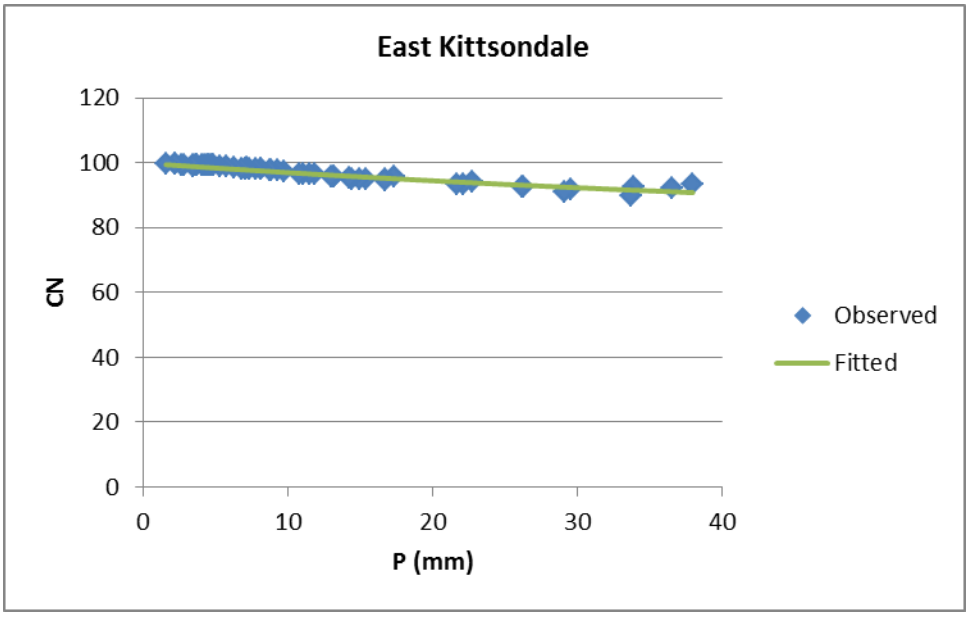
East Kittsondale
120
100
80
60
40
20
0
CN
0
10
20
30
40
P (mm)
Observed
Fitted

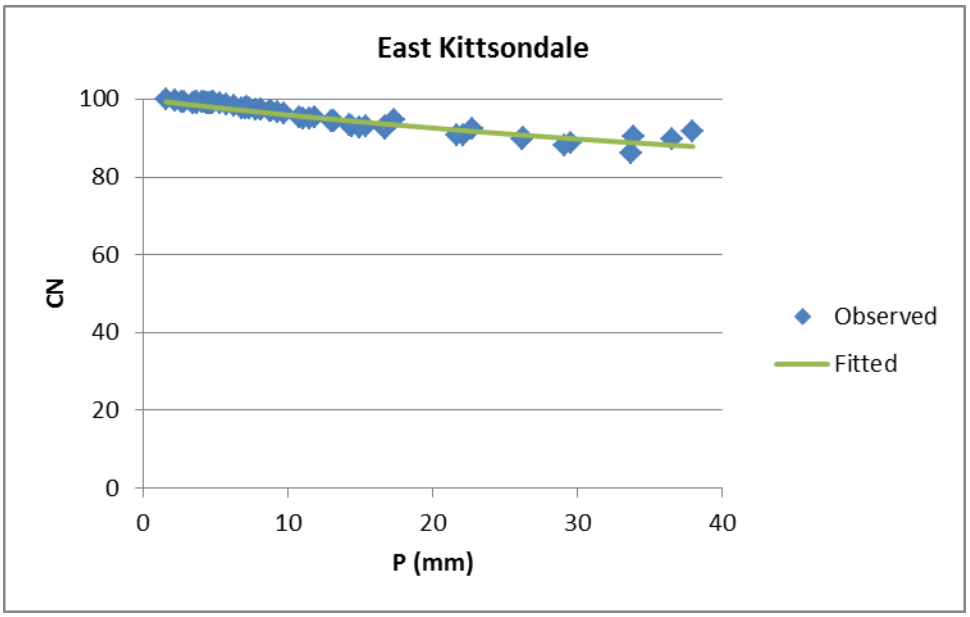
East Kittsondale
100
80
60
40
20
0
CN
0
10
20
30
40
P (mm)
Observed
Fitted

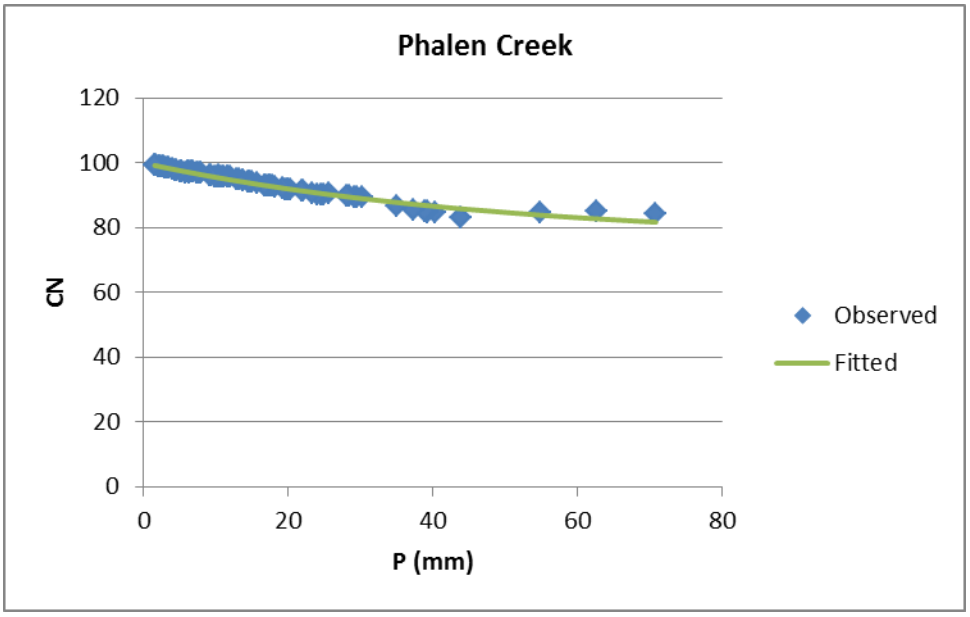
Phalen Creek
120
100
80
60
40
20
0
CN
0
20
40
60
80
P (mm)
Observed
Fitted

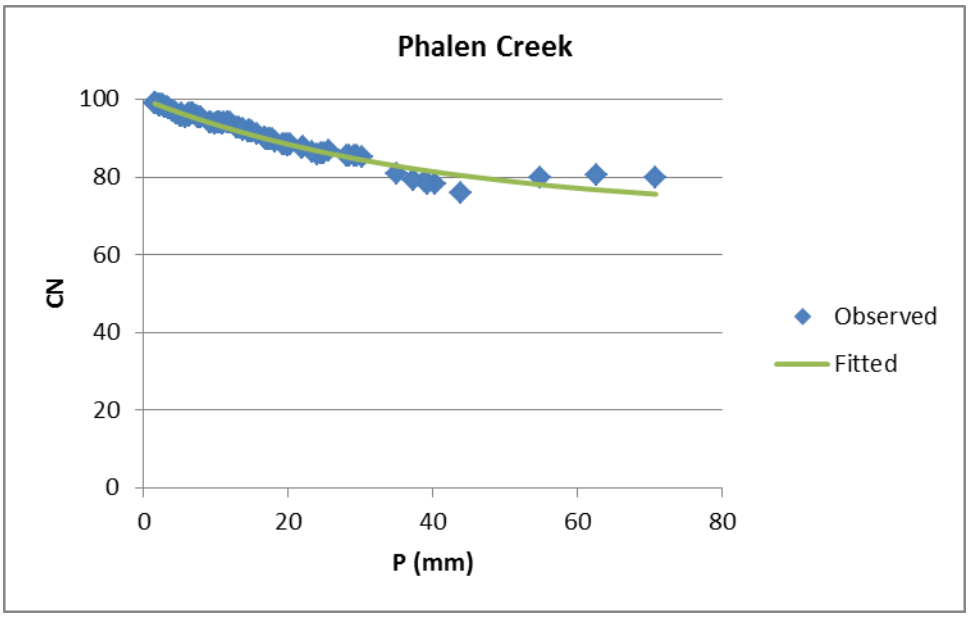
Phalen Creek
100
80
60
40
20
0
CN
0
20
40
60
80
P (mm)
Observed
Fitted

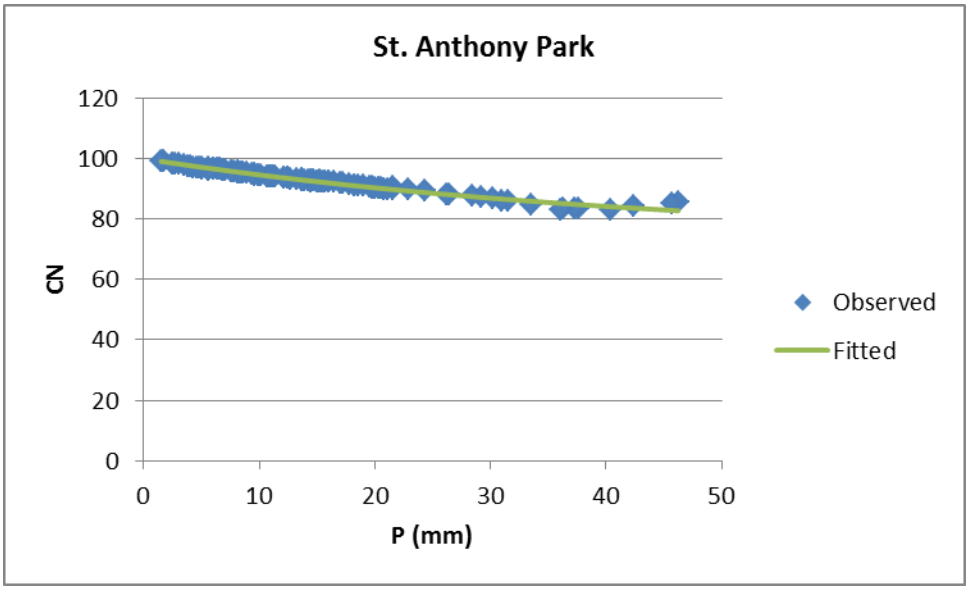
St. Anthony Park
120
100
80
60
40
20
0
CN
0
10
20
30
40
50
P (mm)
Observed
Fitted

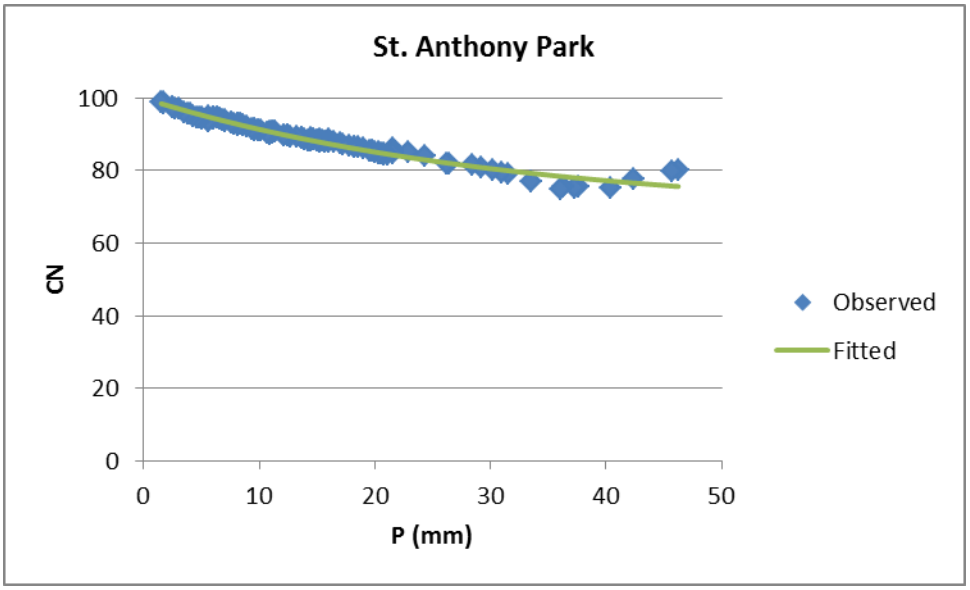
St. Anthony Park
100
80
60
40
20
0
CN
0
10
20
30
40
50
P (mm)
Observed
Fitted

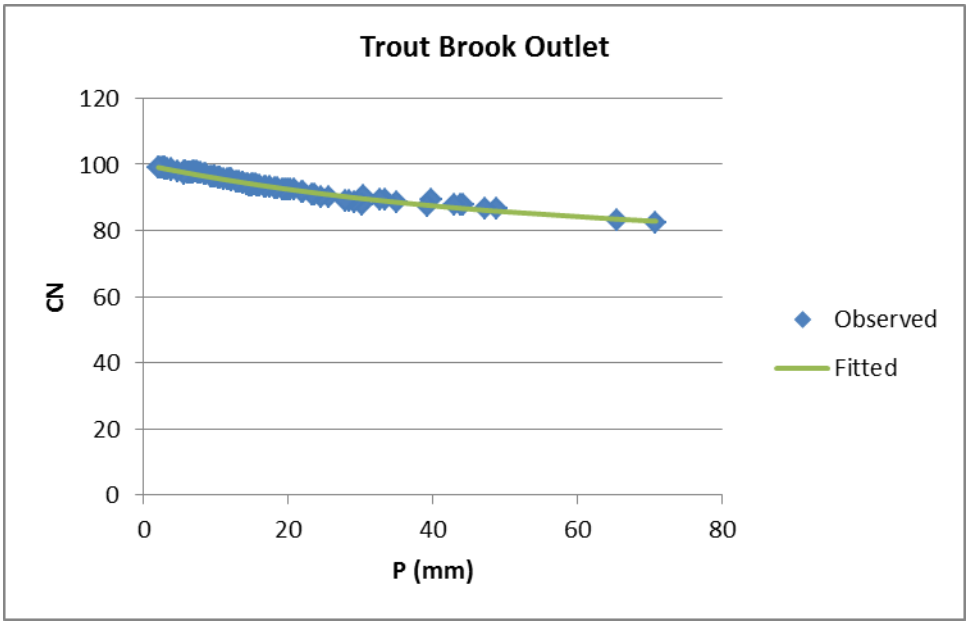
Trout Brook Outlet
120
100
80
60
40
20
0
CN
0
20
40
60
80
P (mm)
Observed
Fitted

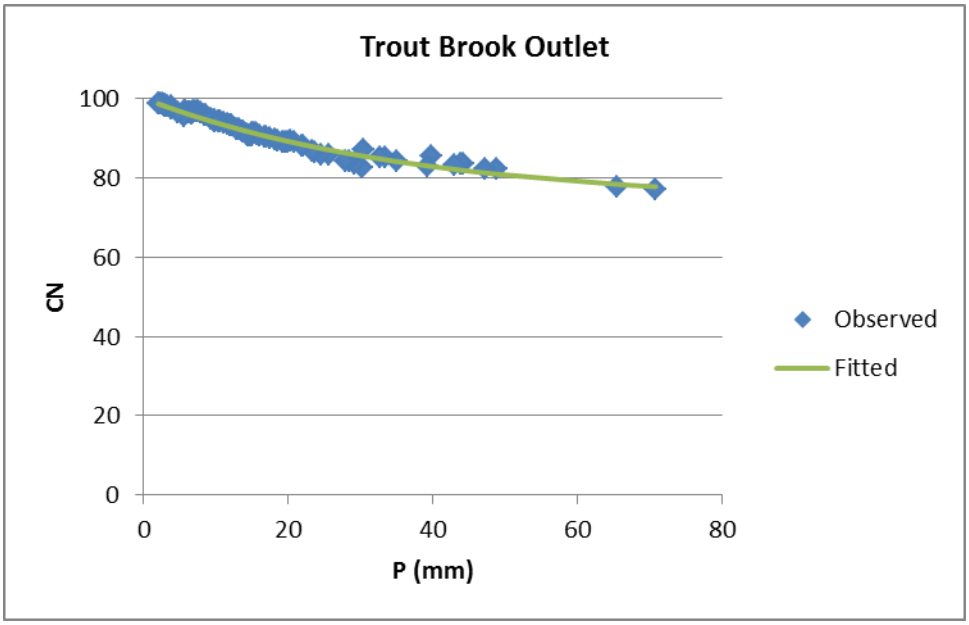
Trout Brook Outlet
100
80
60
40
20
0
CN
0
20
40
60
80
P (mm)
Observed
Fitted

Three Rivers Park District (TRPD), MN

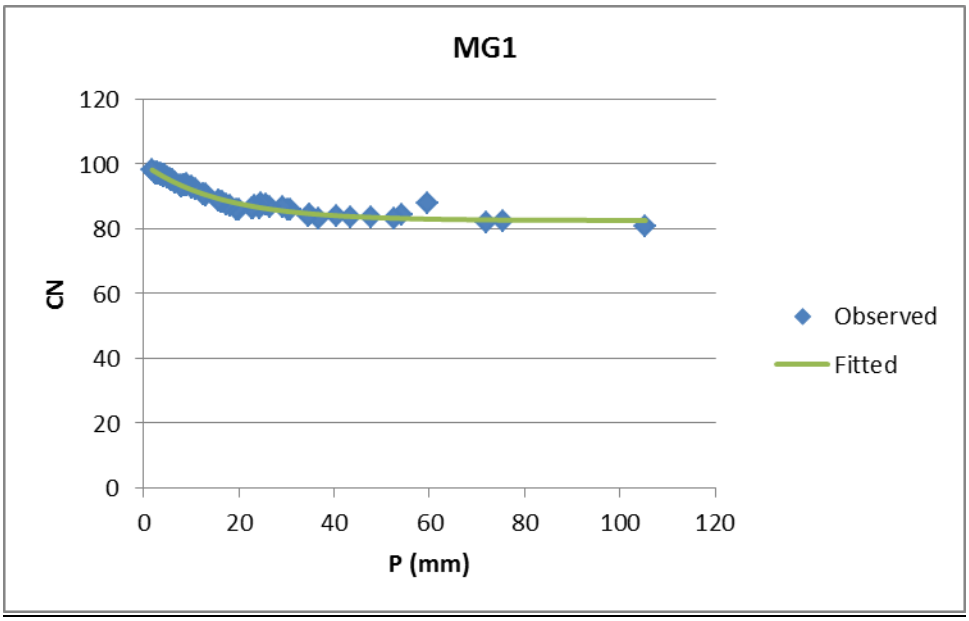

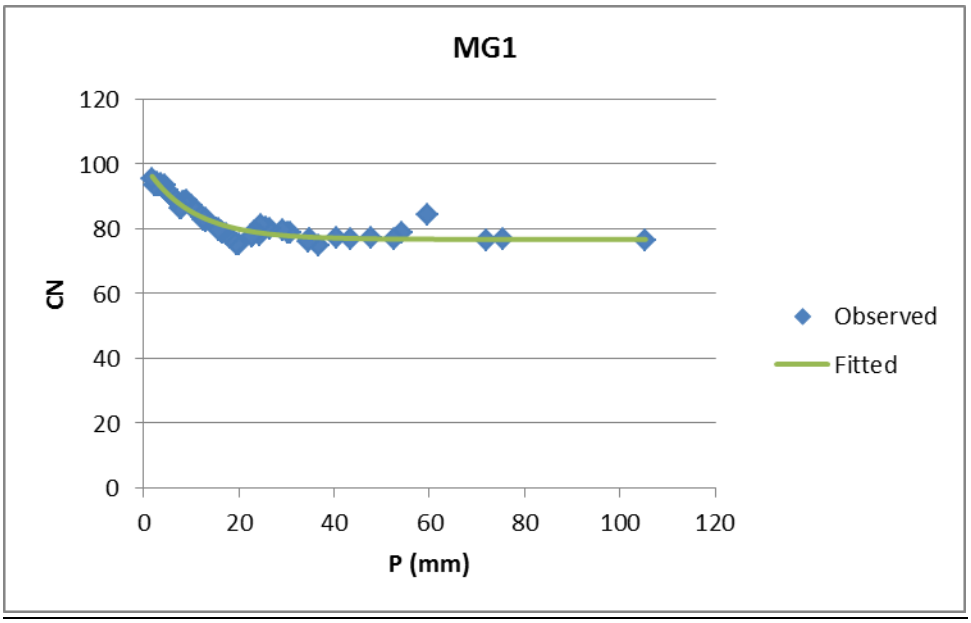

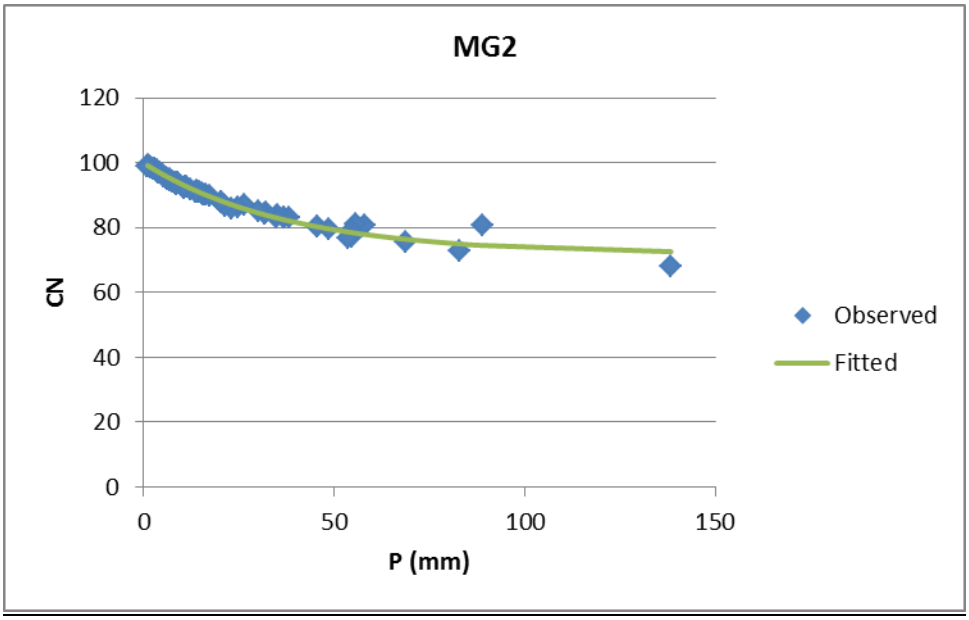
MG2
120
100
80
60
40
20
0
CN
0
50
100
150
P (mm)
Observed
Fitted

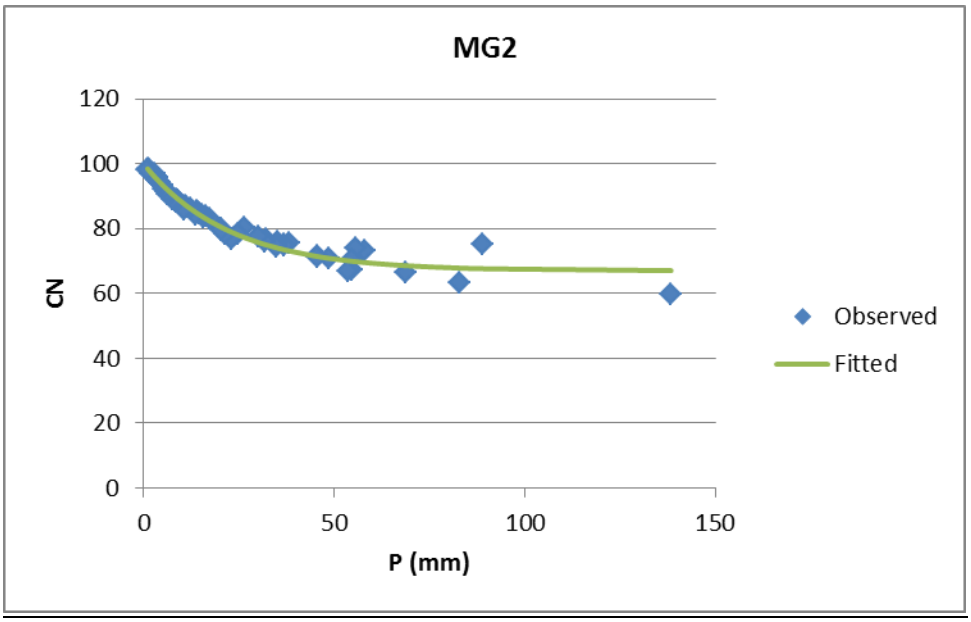
MG2
120
100
80
60
40
20
0
CN
0
50
100
150
P (mm)
Observed
Fitted

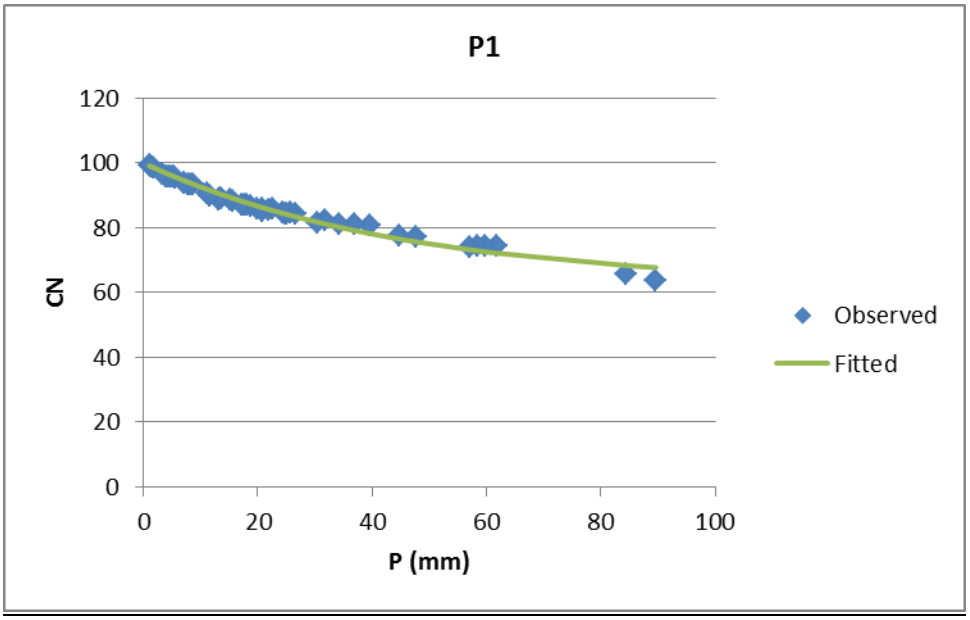
P1
120
100
80
60
40
20
0
CN
0
20
40
60
80
100
P (mm)
Observed
Fitted

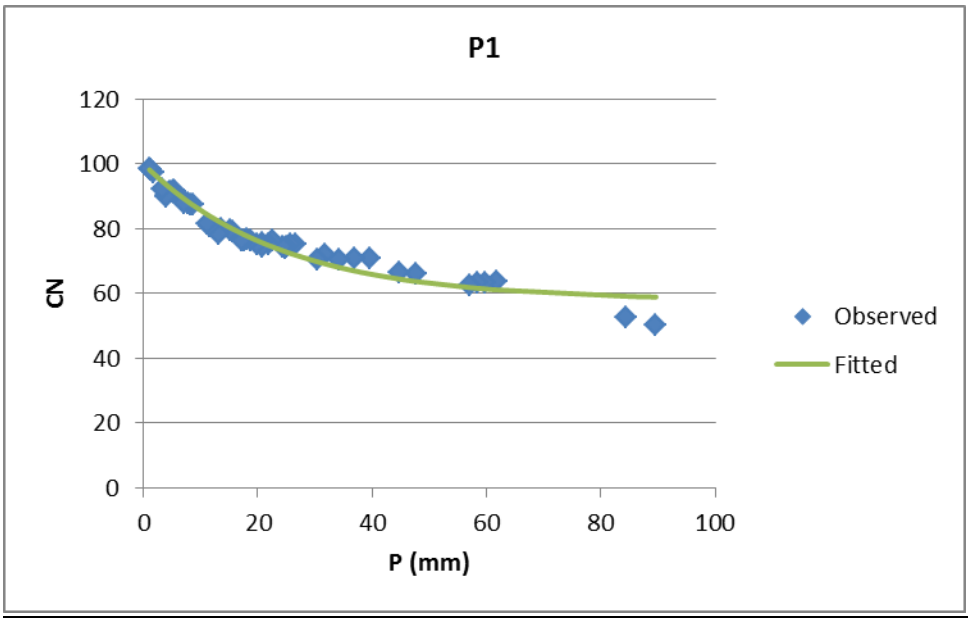
P1
120
100
80
60
40
20
0
CN
0
20
40
60
80
100
P (mm)
Observed
Fitted

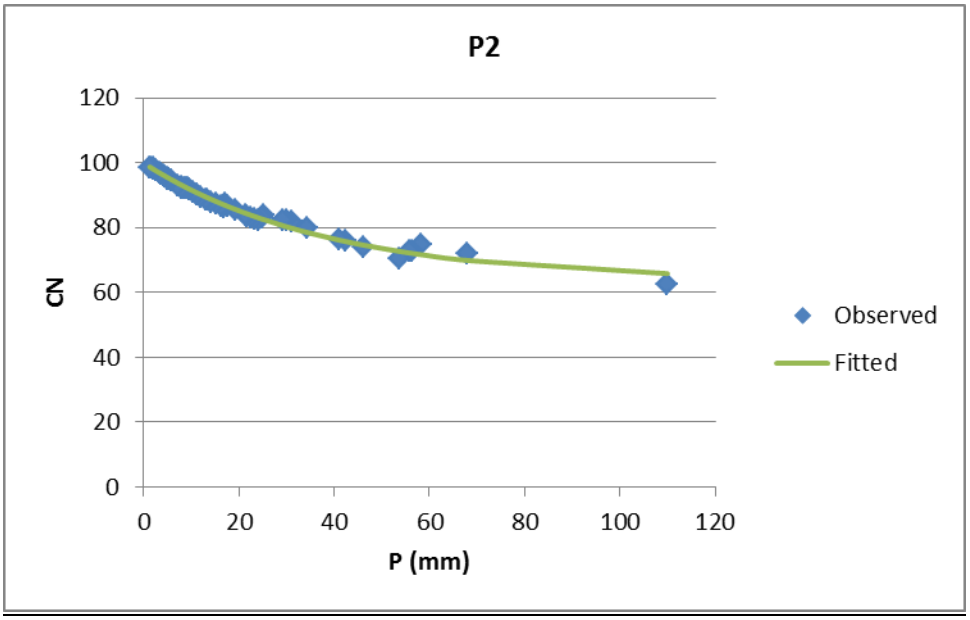
P2
120
100
80
60
40
20
0
CN
0
20
40
60
80
100
120
P (mm)
Observed
Fitted

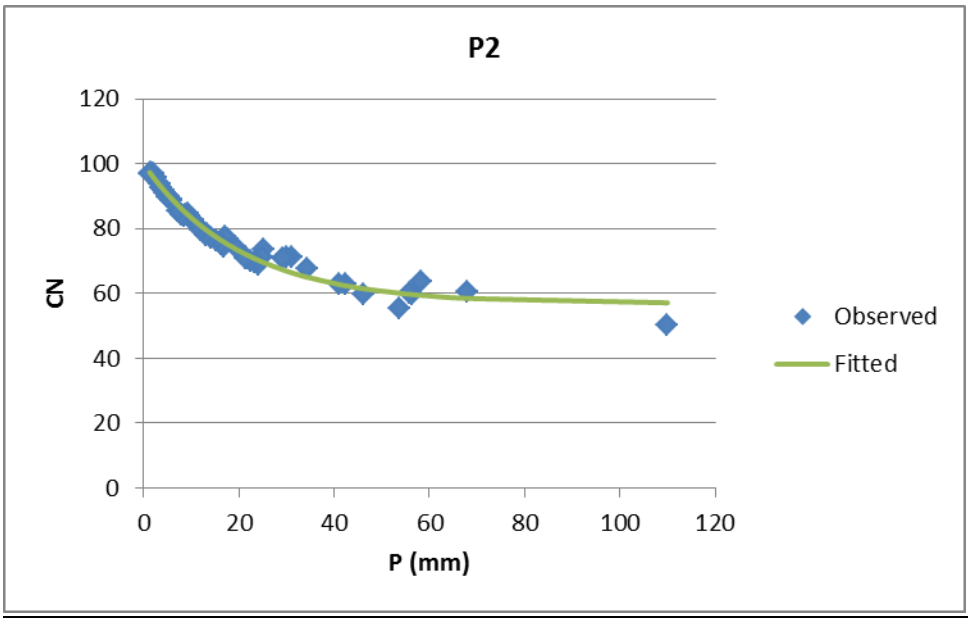
P2
120
100
80
60
40
20
0
CN
0
20
40
60
80
100
120
P (mm)
Observed
Fitted

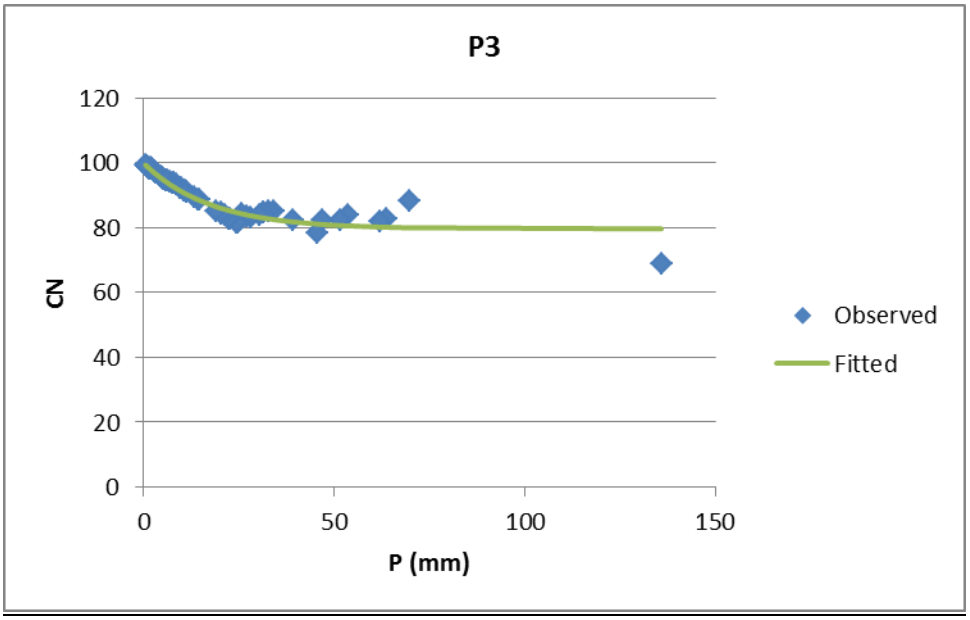
P3
120
100
80
60
40
20
0
CN
0
50
100
150
P (mm)
Observed
Fitted

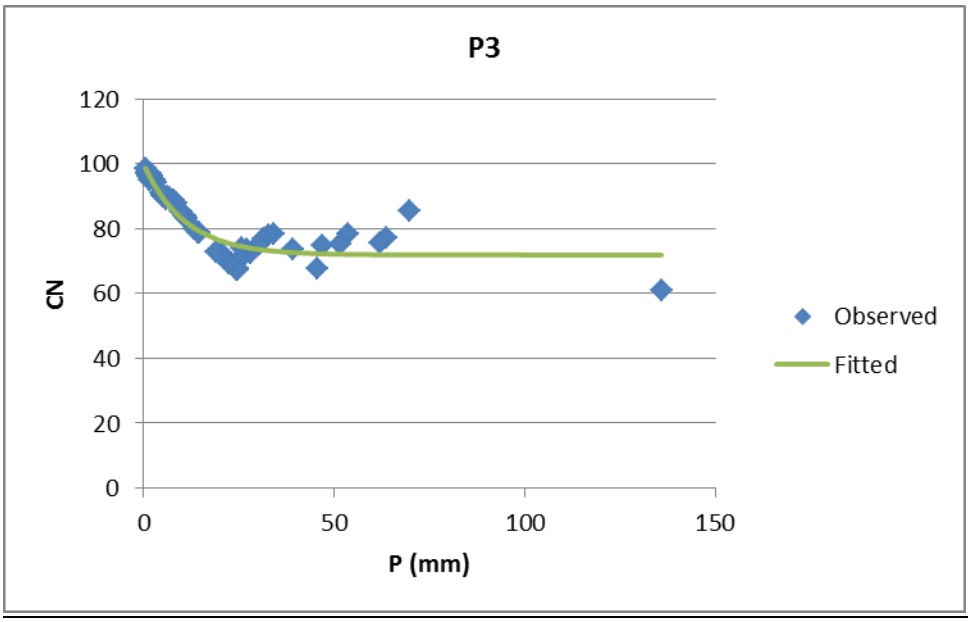
P3
120
100
80
60
40
20
0
CN
0
50
100
150
P (mm)
Observed
Fitted

City of Bloomington, MN

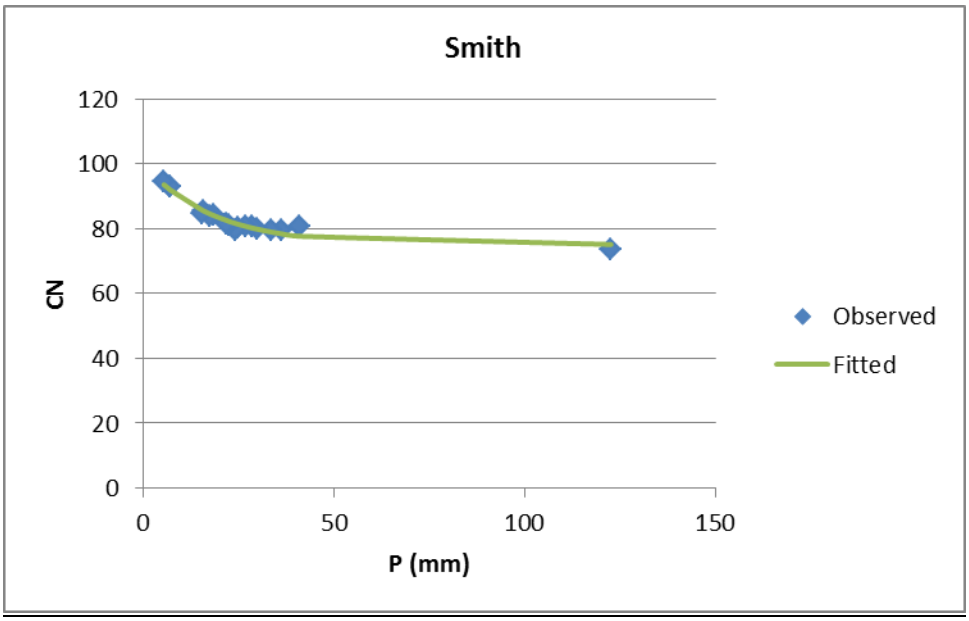

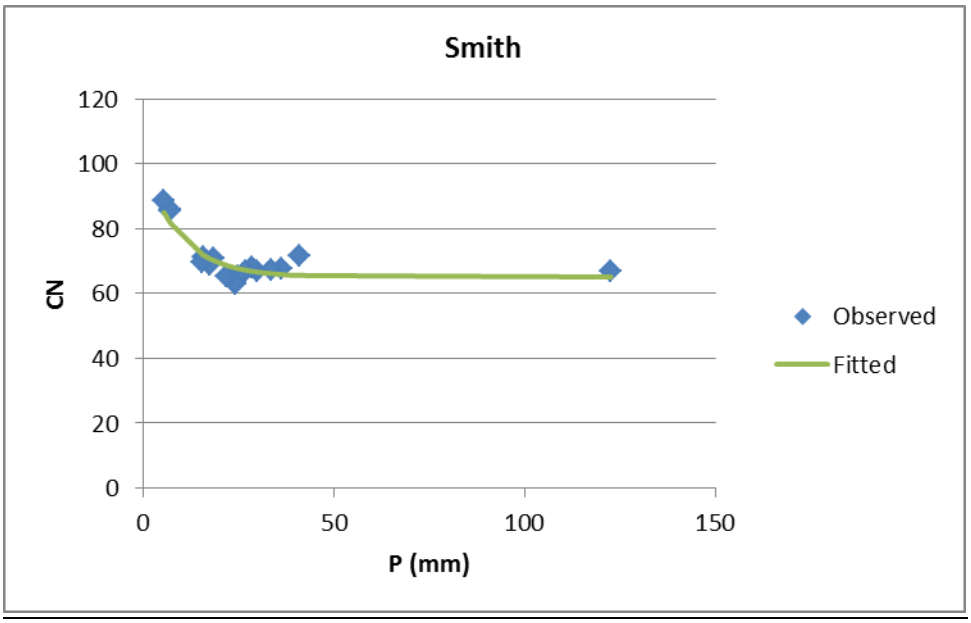

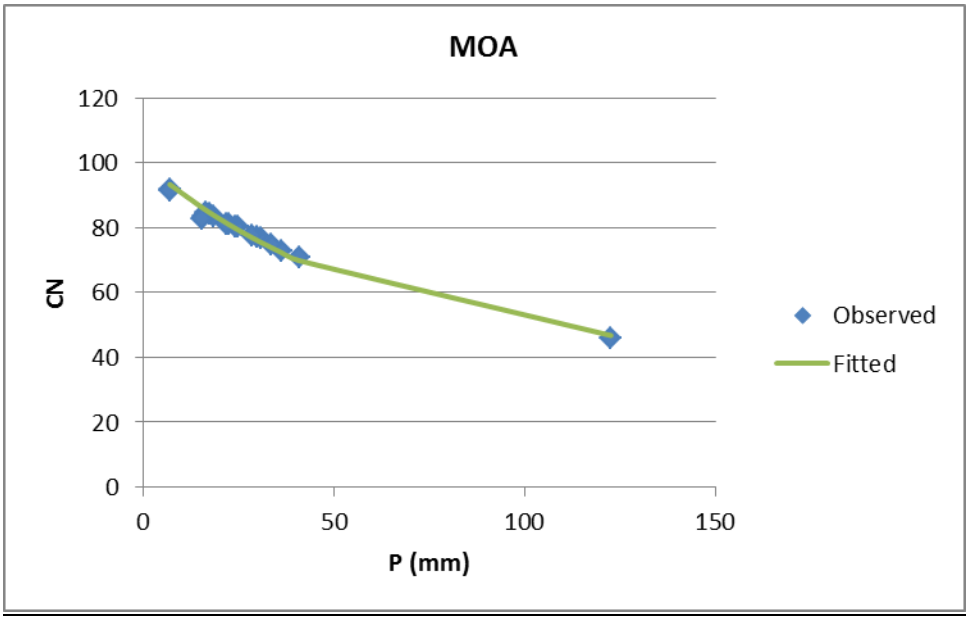
MOA
120
100
80
60
40
20
0
CN
0
50
100
150
P (mm)
Observed
Fitted

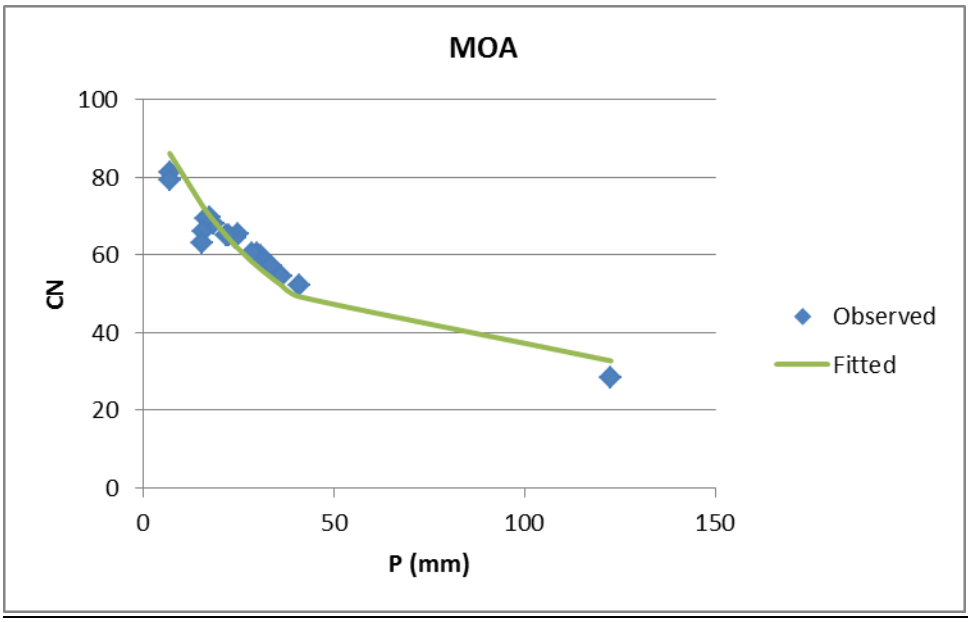
MOA
100
80
60
40
20
0
CN
0
50
100
150
P (mm)
Observed
Fitted

City of Minnetonka, MN

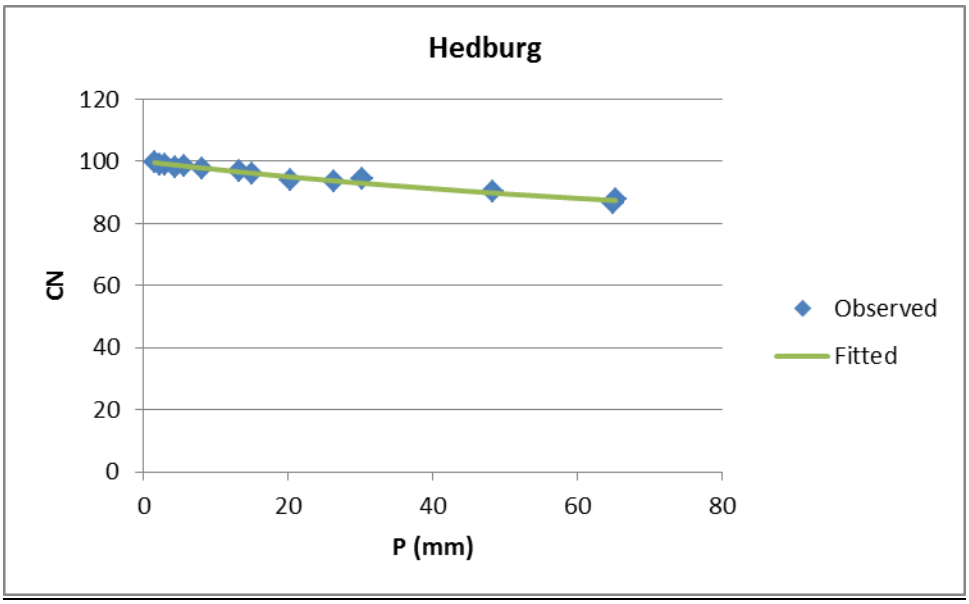

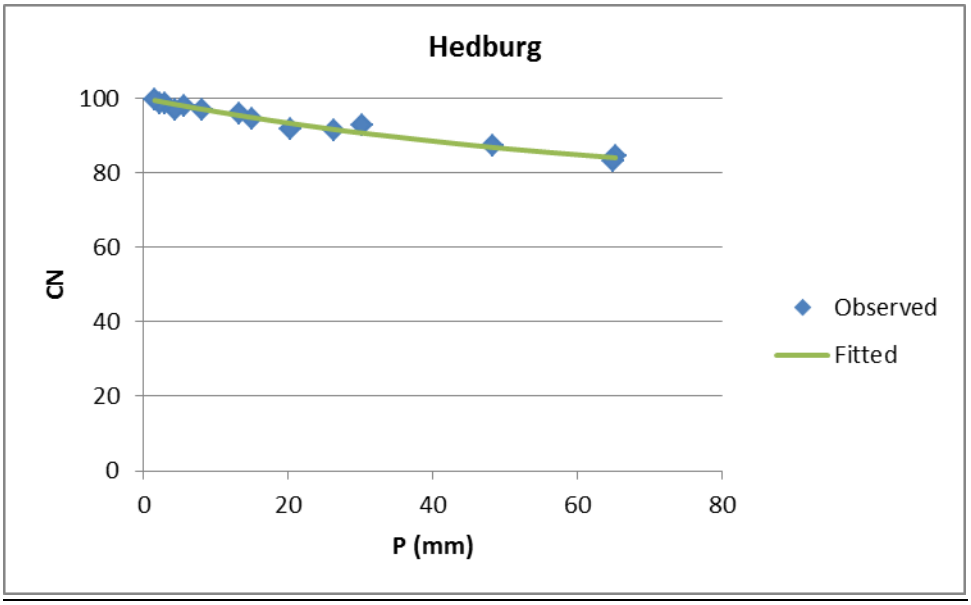

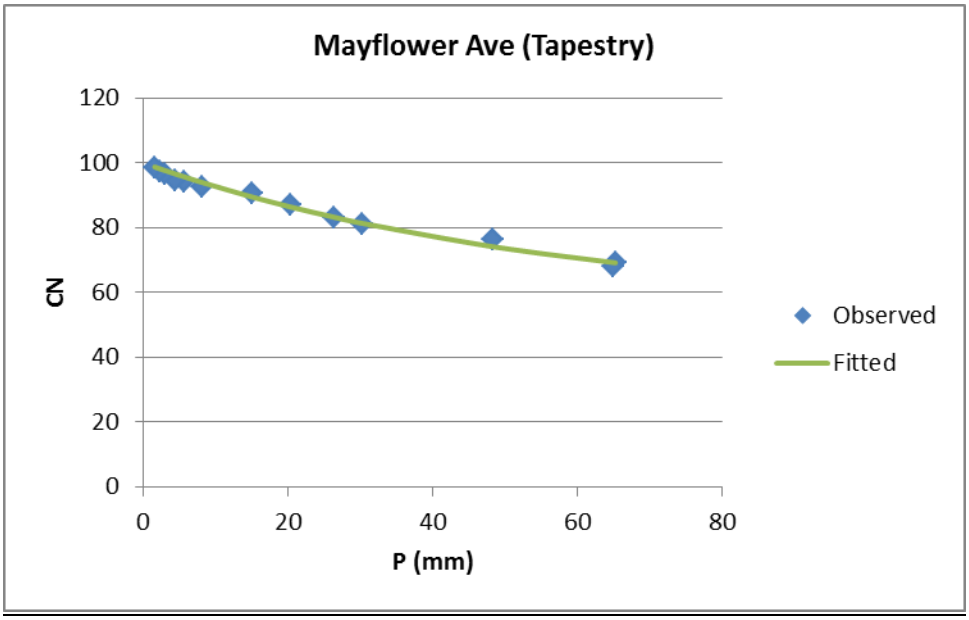
Mayflower Ave (Tapestry)
120
100
80
60
40
20
0
CN
0
20
40
60
80
P (mm)
Observed
Fitted

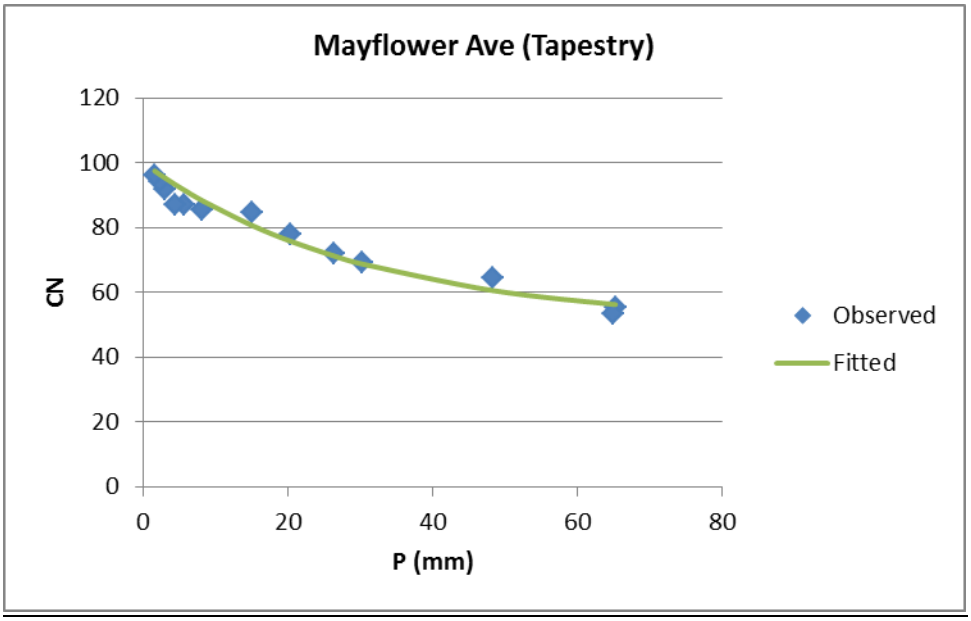
Mayflower Ave (Tapestry)
120
100
80
60
40
20
0
CN
0
20
40
60
80
P (mm)
Observed
Fitted

City of Madison, WI

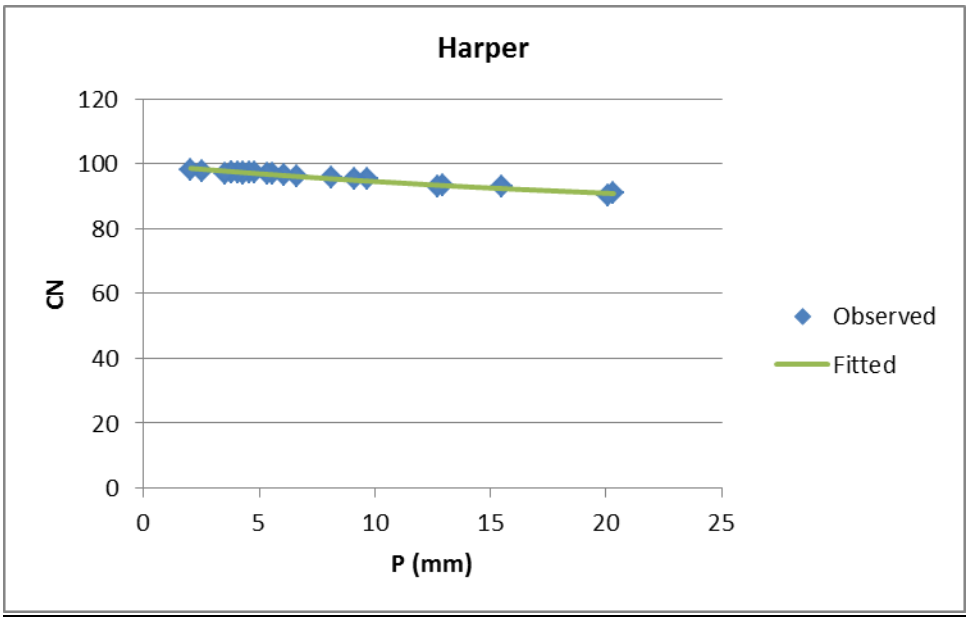

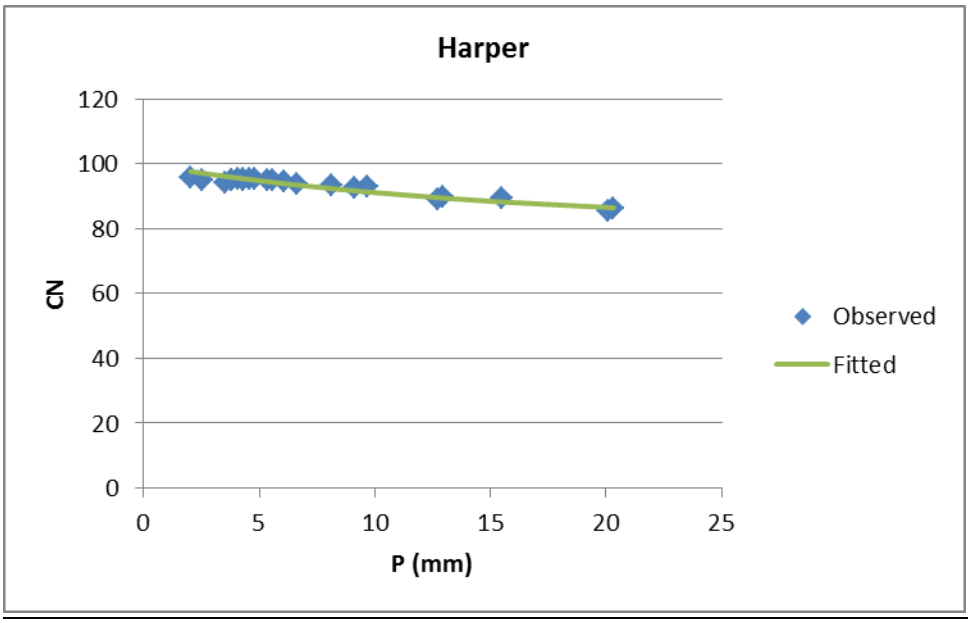

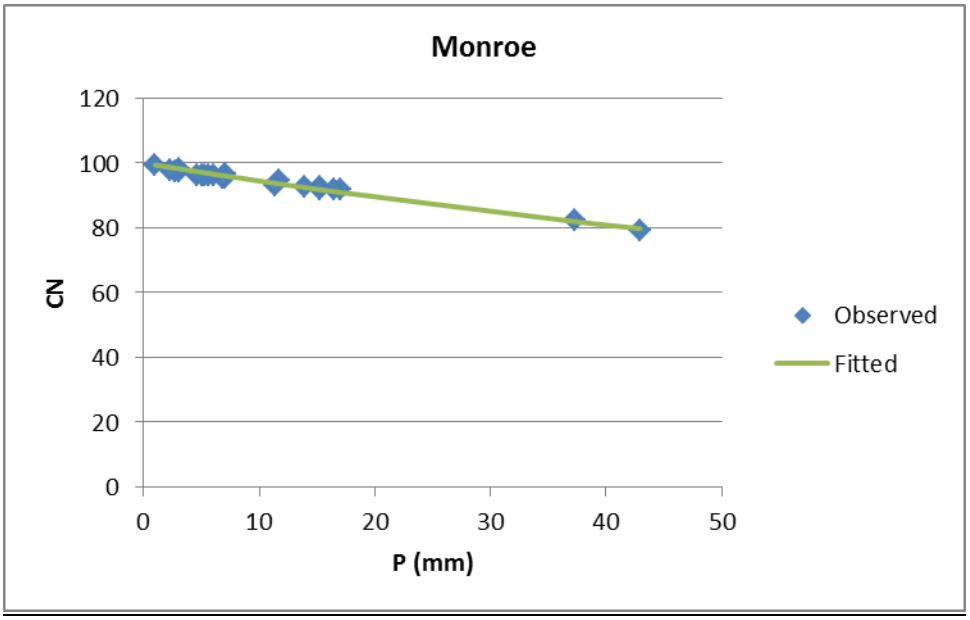
Monroe
120
100
80
60
40
20
0
CN
0
10
20
30
40
50
P (mm)
Observed
Fitted

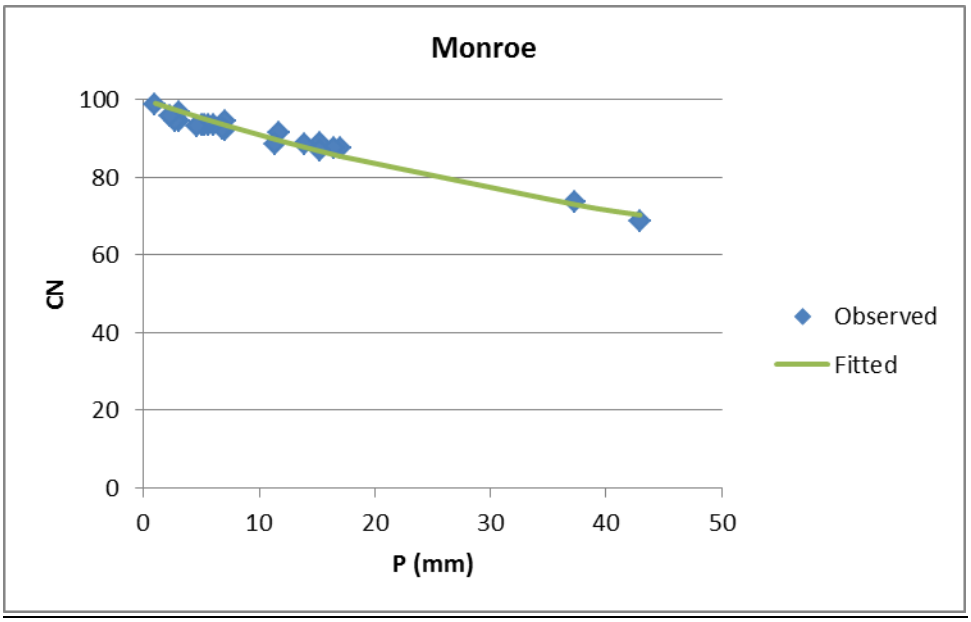
Monroe
100
80
60
40
20
0
CN
0
10
20
30
40
50
P (mm)
Observed
Fitted

City of Austin, TX

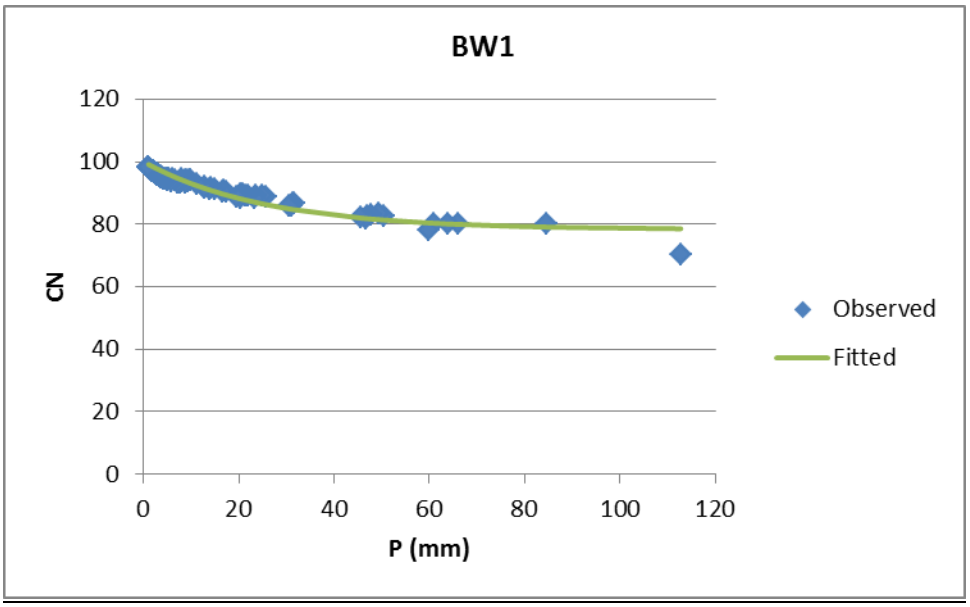

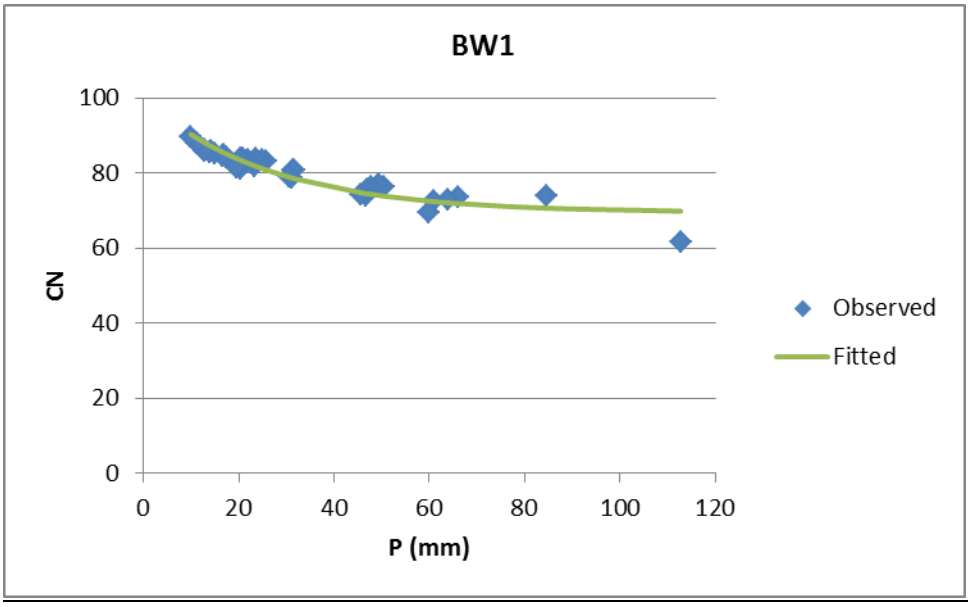

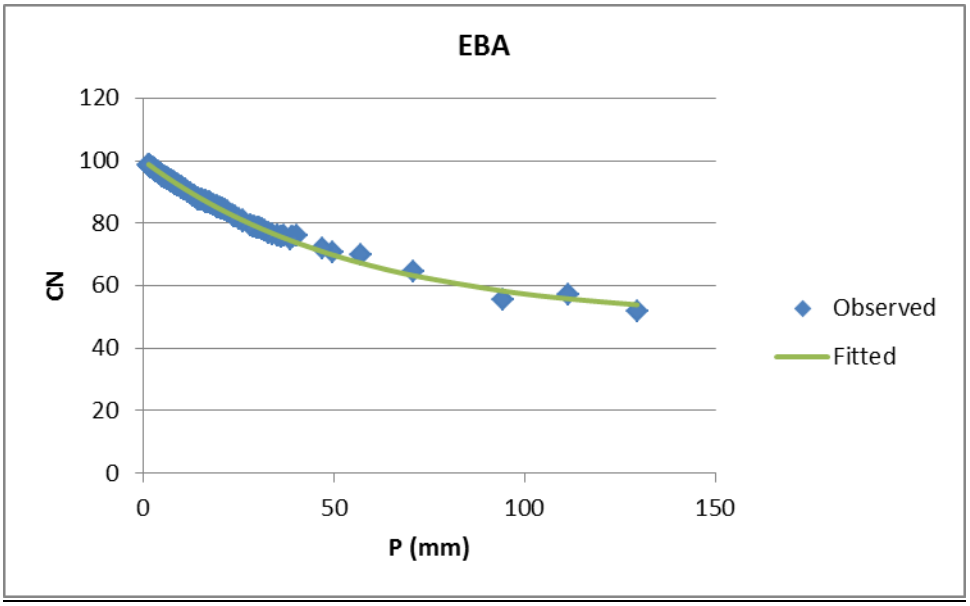
EBA
120
100
80
60
40
20
0
CN
0
50
100
150
P (mm)
Observed
Fitted

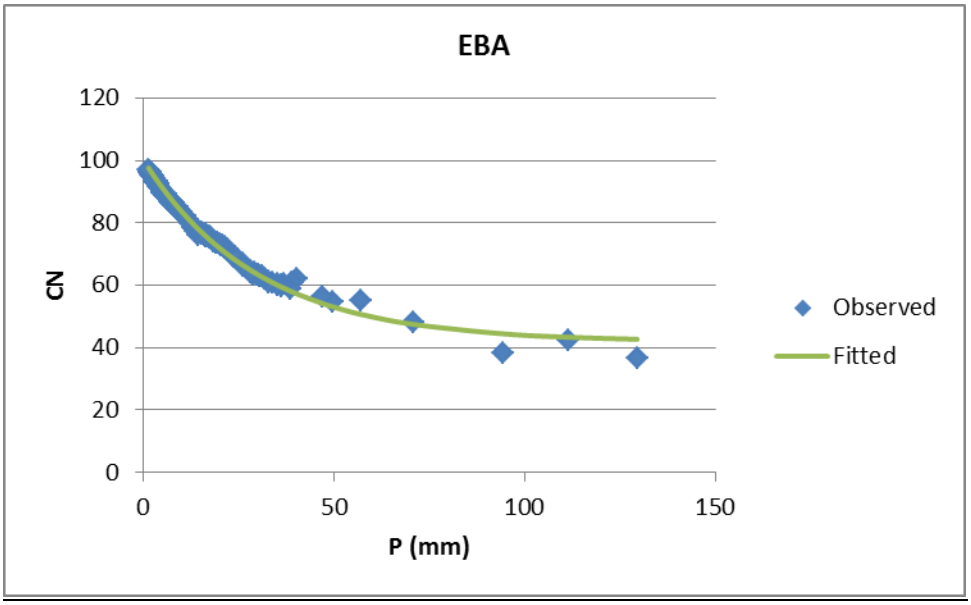
EBA
120
100
80
60
40
20
0
CN
0
50
100
150
P (mm)
Observed
Fitted

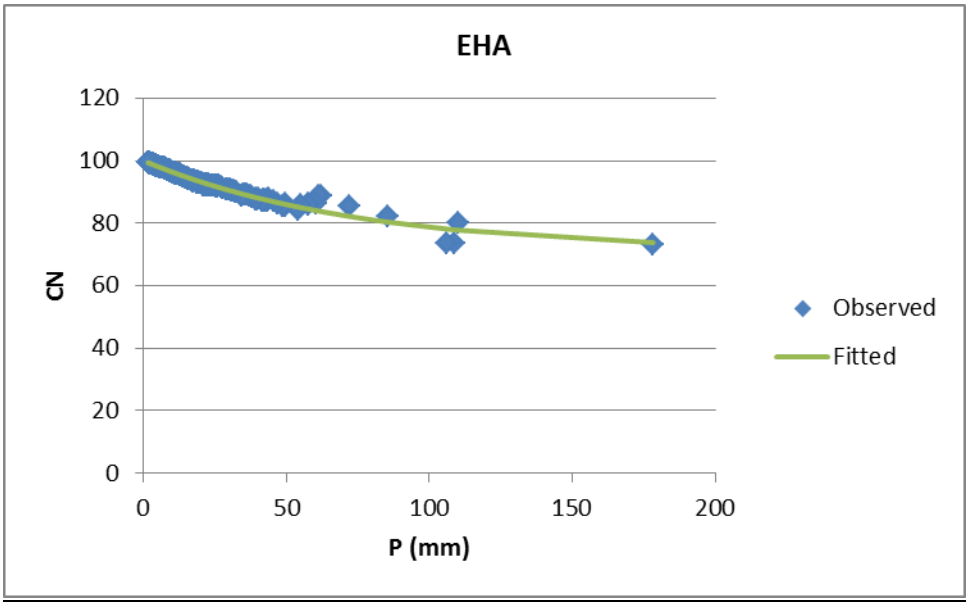
EHA
120
100
80
60
40
20
0
CN
0
50
100
150
200
P (mm)
Observed
Fitted

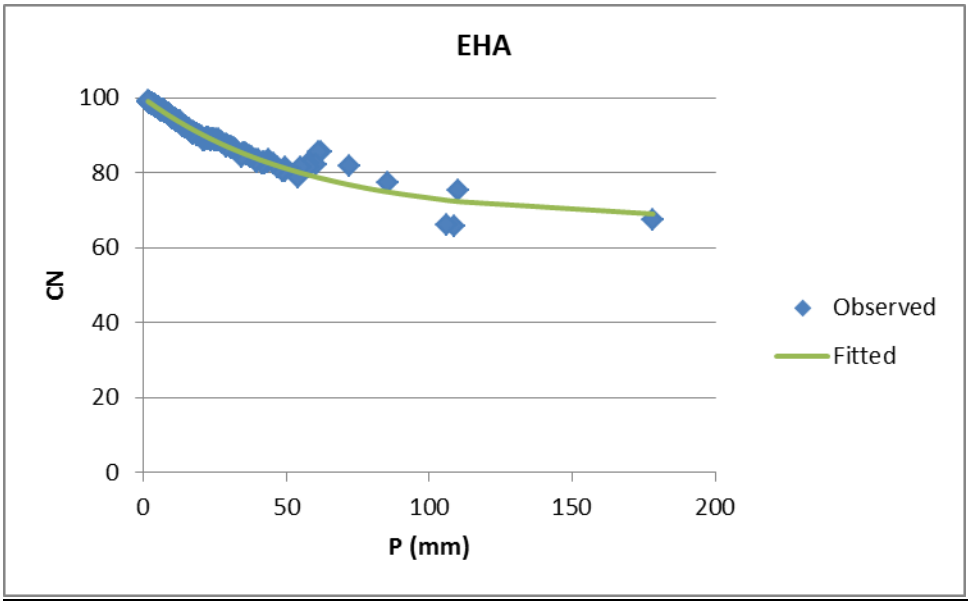
EHA
100
80
60
40
20
0
CN
0
50
100
150
200
P (mm)
Observed
Fitted

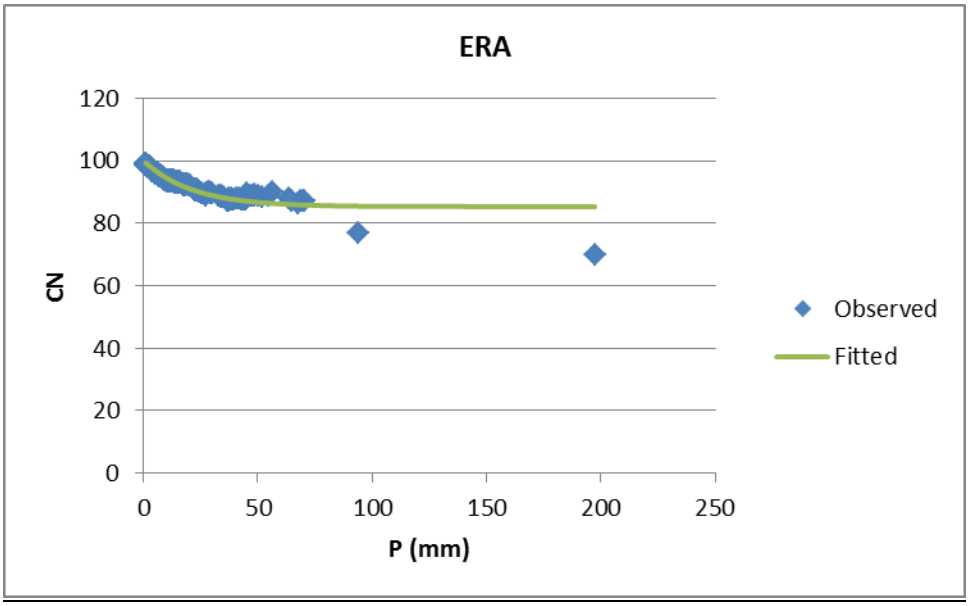
ERA
120
100
80
60
40
20
0
CN
0
50
100
150
200
250
P (mm)
Observed
Fitted

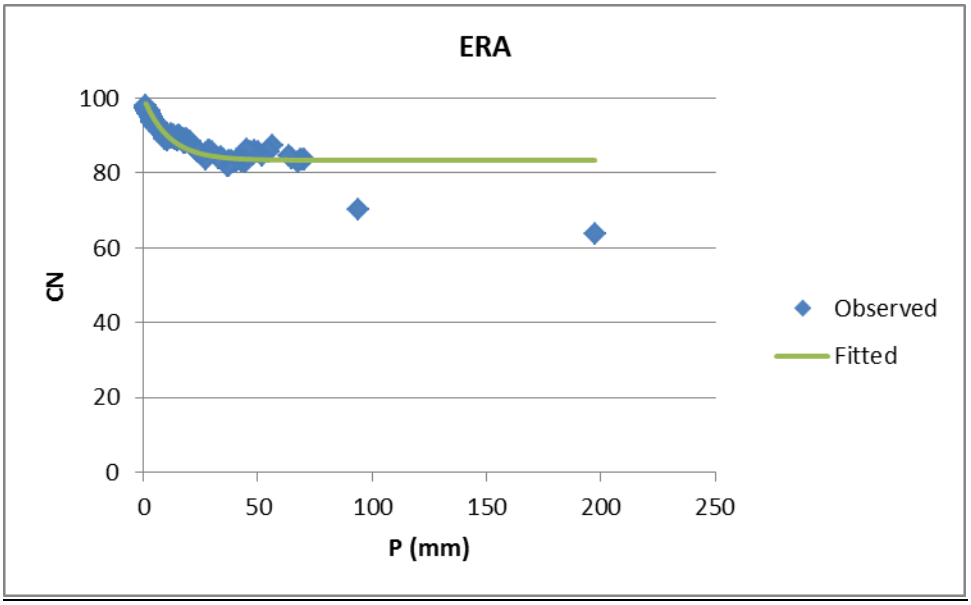
ERA
100
80
60
40
20
0
CN
0
50
100
150
200
250
P (mm)
Observed
Fitted

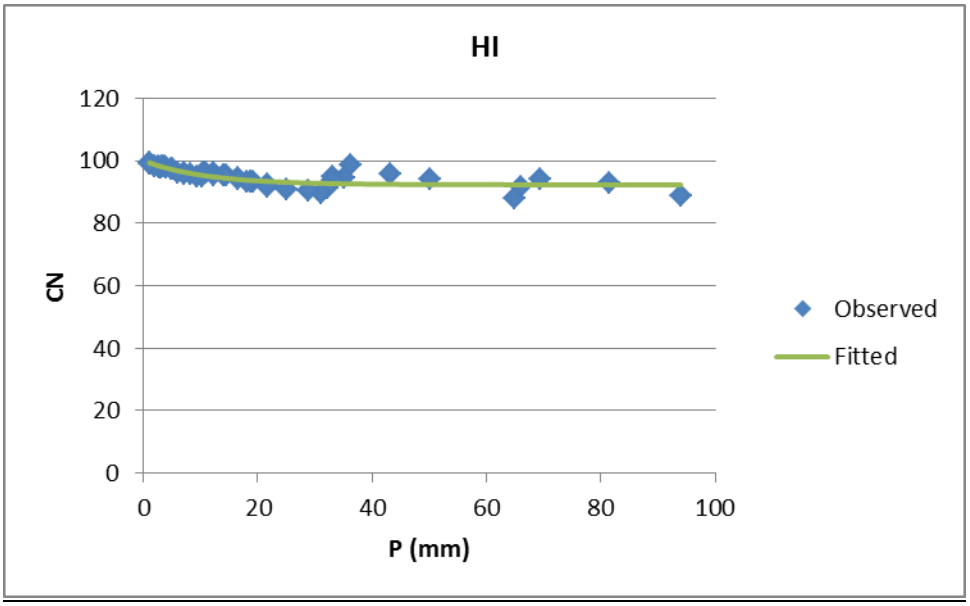
HI
120
100
80
60
40
20
0
CN
0
20
40
60
80
100
P (mm)
Observed
Fitted

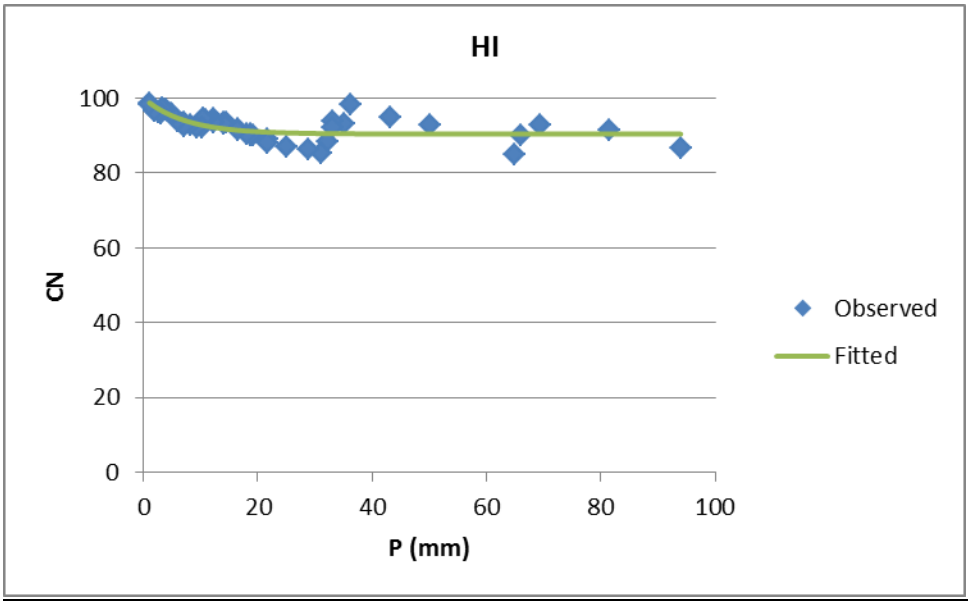
HI
100
80
60
40
20
0
CN
0
20
40
60
80
100
P (mm)
Observed
Fitted

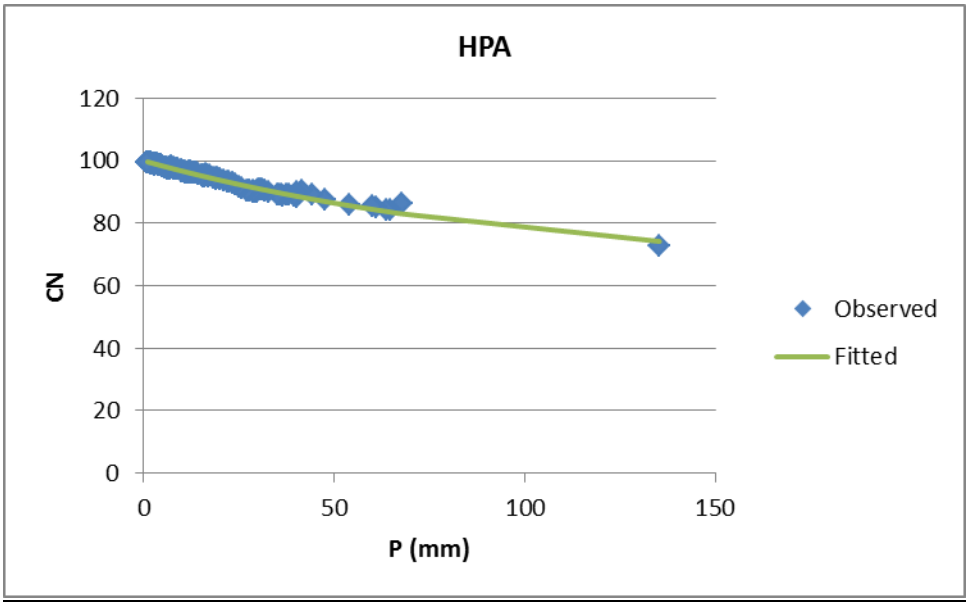
HPA
120
100
80
60
40
20
0
CN
0
50
100
150
P (mm)
Observed
Fitted

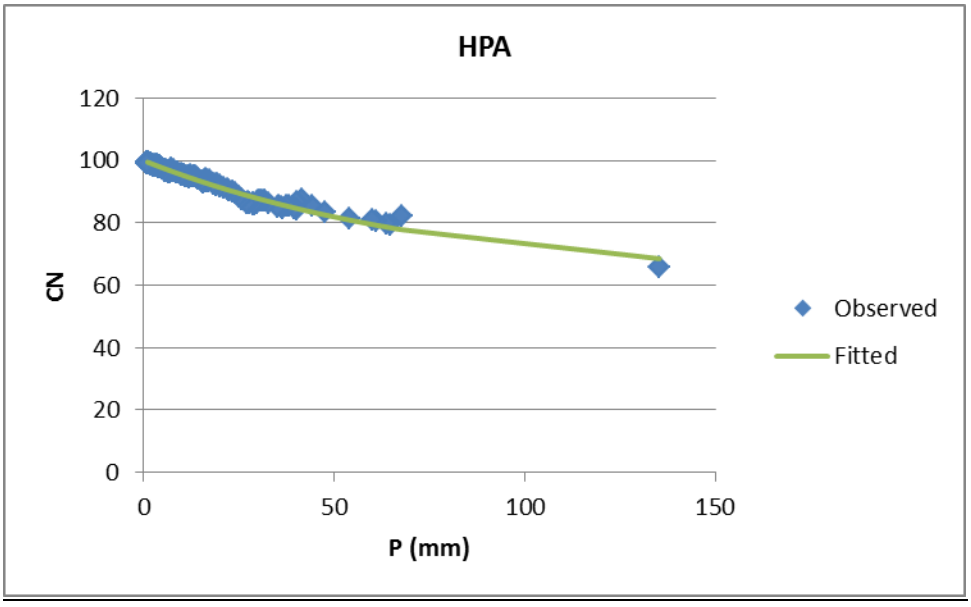
HPA
120
100
80
60
40
20
0
CN
0
50
100
150
P (mm)
Observed
Fitted

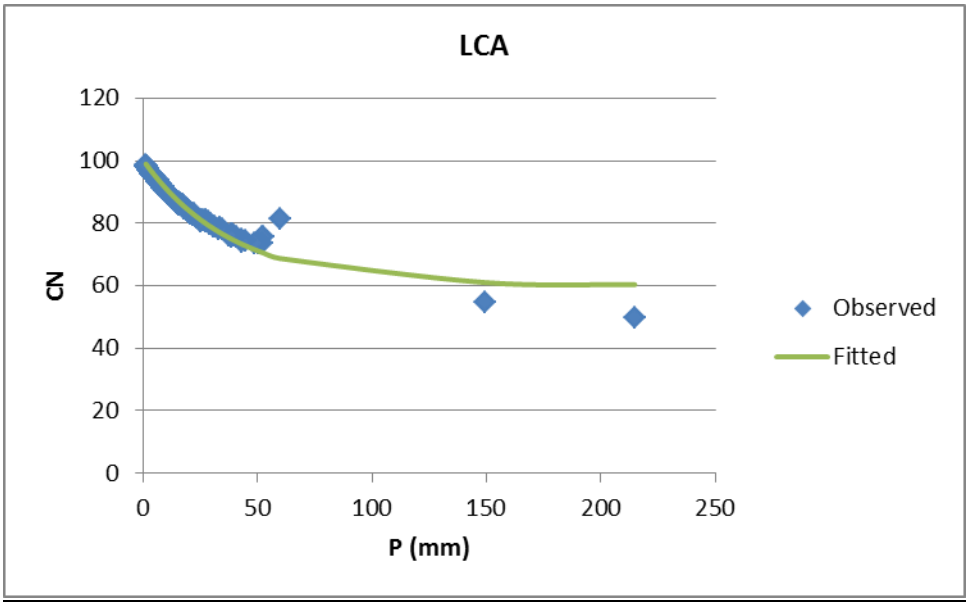
LCA
120
100
80
60
40
20
0
CN
0
50
100
150
200
250
P (mm)
Observed
Fitted

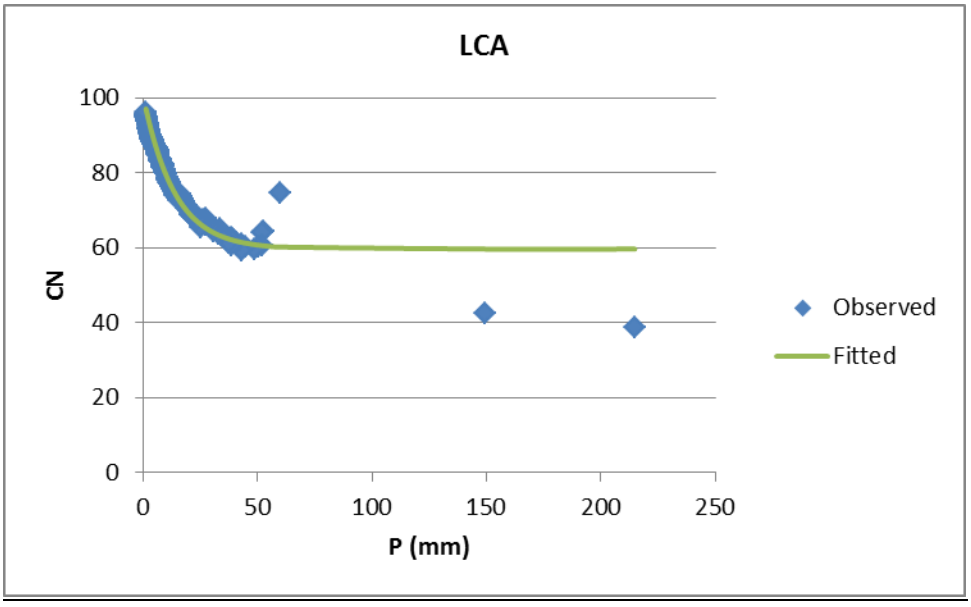
LCA
100
80
60
40
20
0
CN
0
50
100
150
200
250
P (mm)
Observed
Fitted

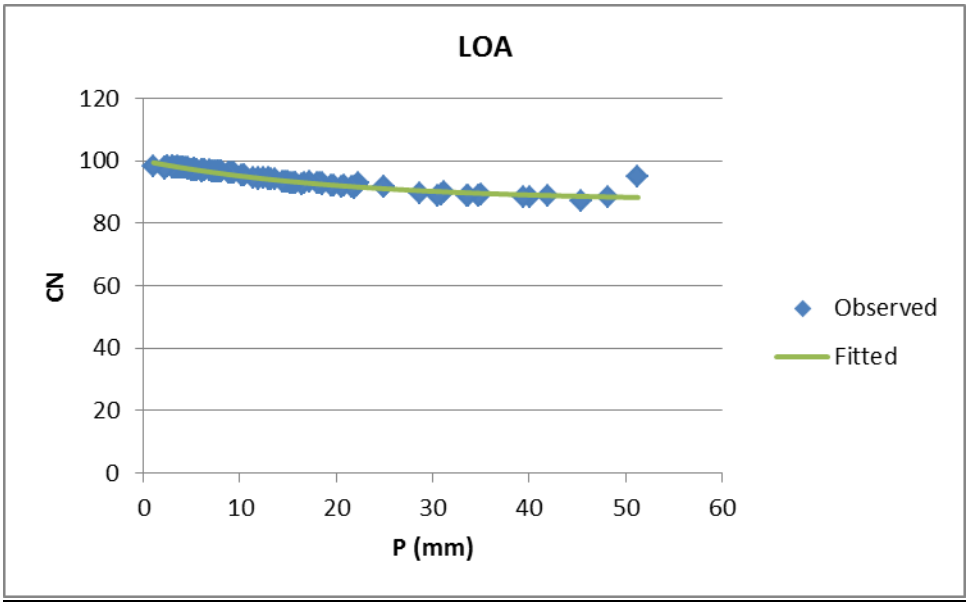
LOA
120
100
80
60
40
20
0
CN
0
10
20
30
40
50
60
P (mm)
Observed
Fitted

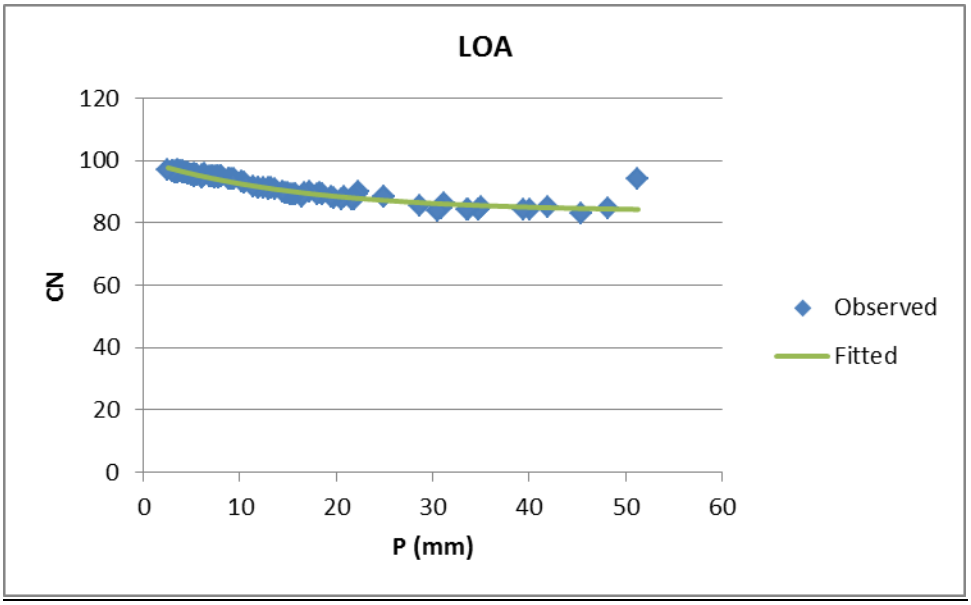
LOA
120
100
80
60
40
20
0
CN
0
10
20
30
40
50
60
P (mm)
Observed
Fitted

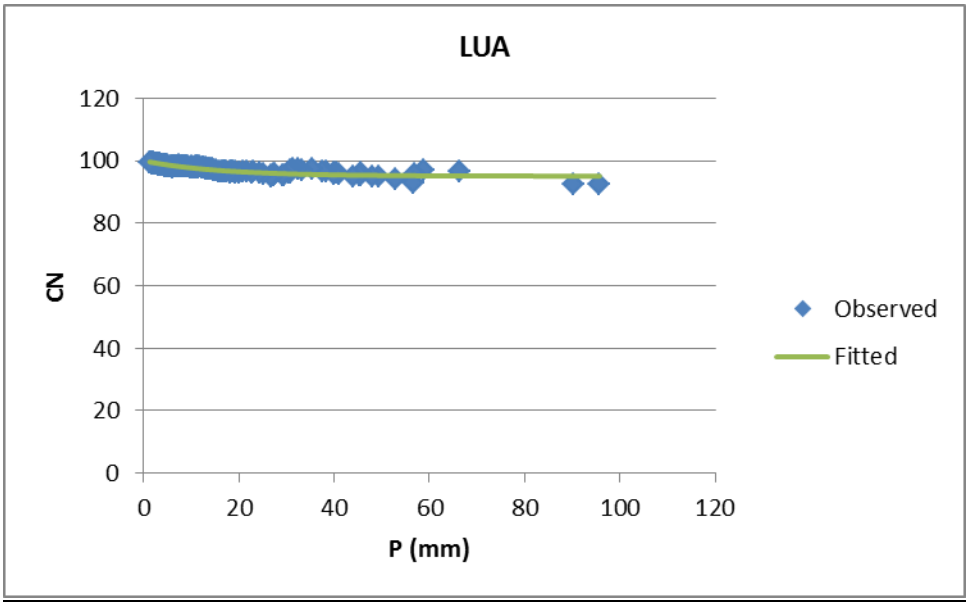
LUA
120
100
80
60
40
20
0
CN
0
20
40
60
80
100
120
P (mm)
Observed
Fitted

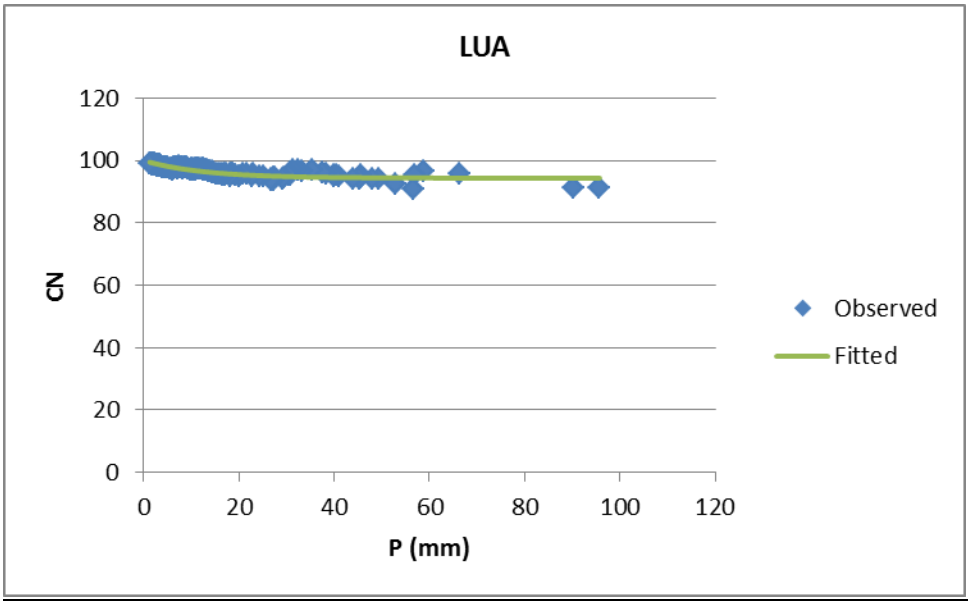
LUA
120
100
80
60
40
20
0
CN
0
20
40
60
80
100
120
P (mm)
Observed
Fitted

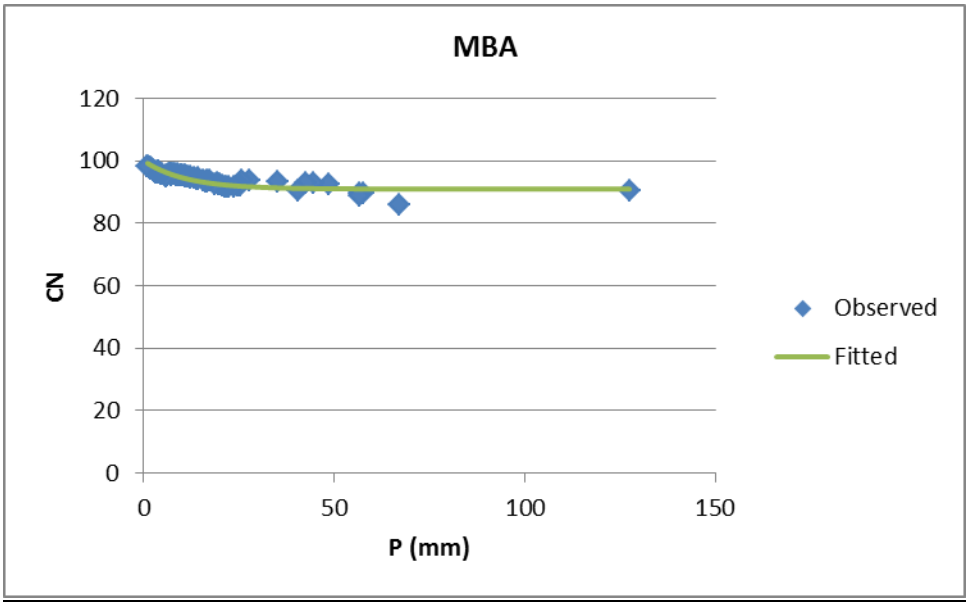
MBA
120
100
80
60
40
20
0
CN
0
50
100
150
P (mm)
Observed
Fitted

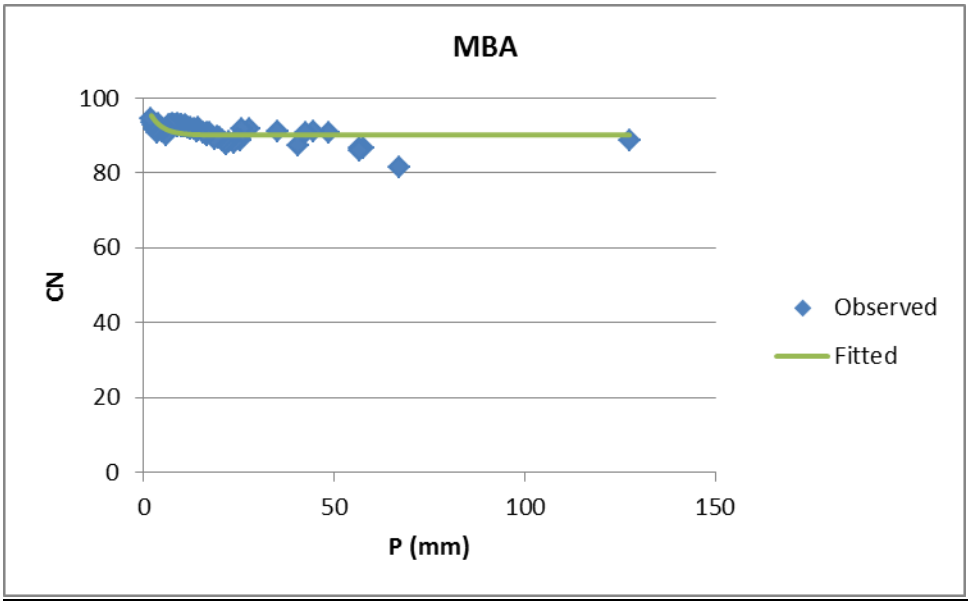
MBA
100
80
60
40
20
0
CN
0
50
100
150
P (mm)
Observed
Fitted

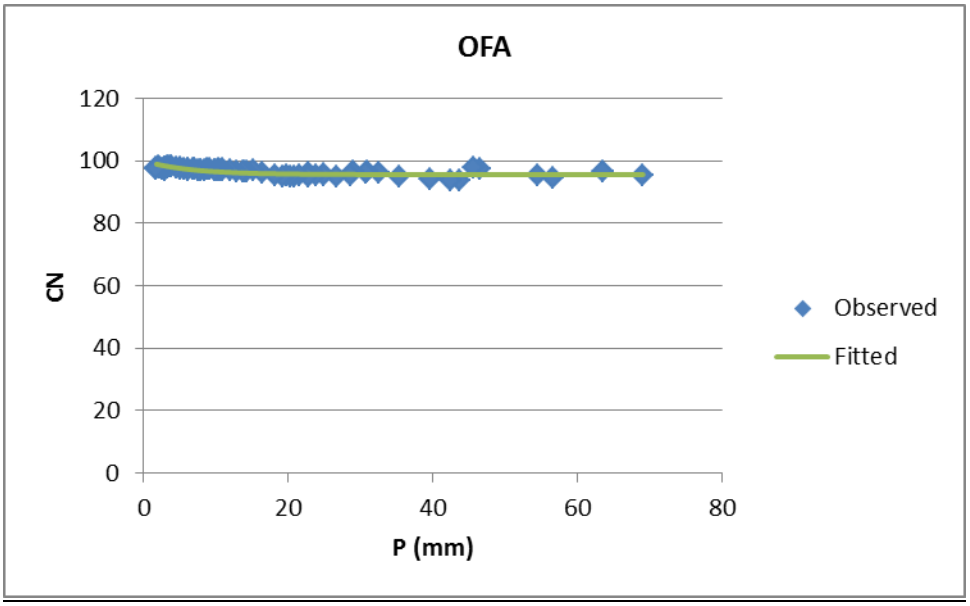
OFA
120
100
80
60
40
20
0
CN
0
20
40
60
80
P (mm)
Observed
Fitted

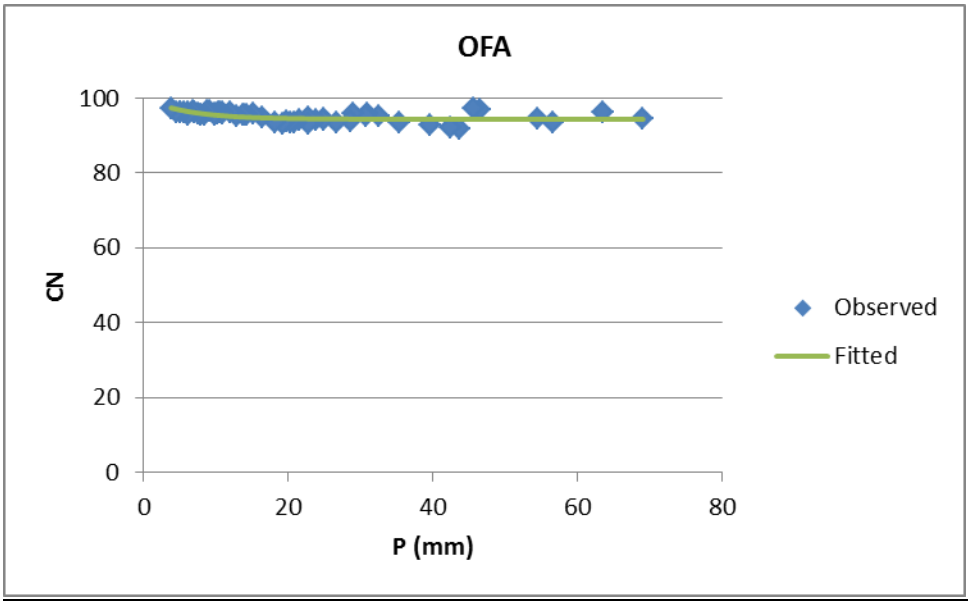
OFA
100
80
60
40
20
0
CN
0
20
40
60
80
P (mm)
Observed
Fitted

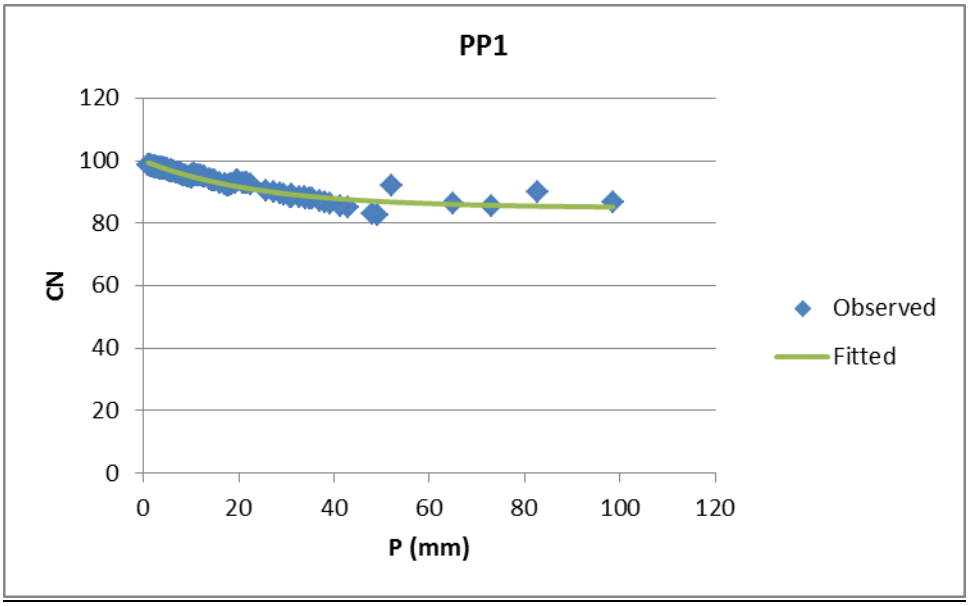
PP1
120
100
80
60
40
20
0
CN
0
20
40
60
80
100
120
P (mm)
Observed
Fitted

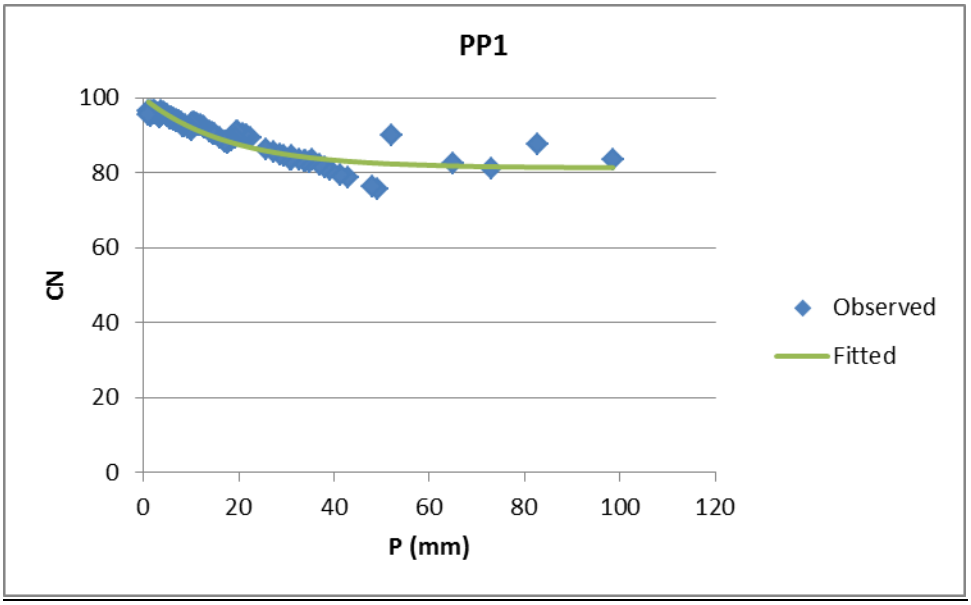
PP1
100
80
60
40
20
0
CN
0
20
40
60
80
100
120
P (mm)
Observed
Fitted

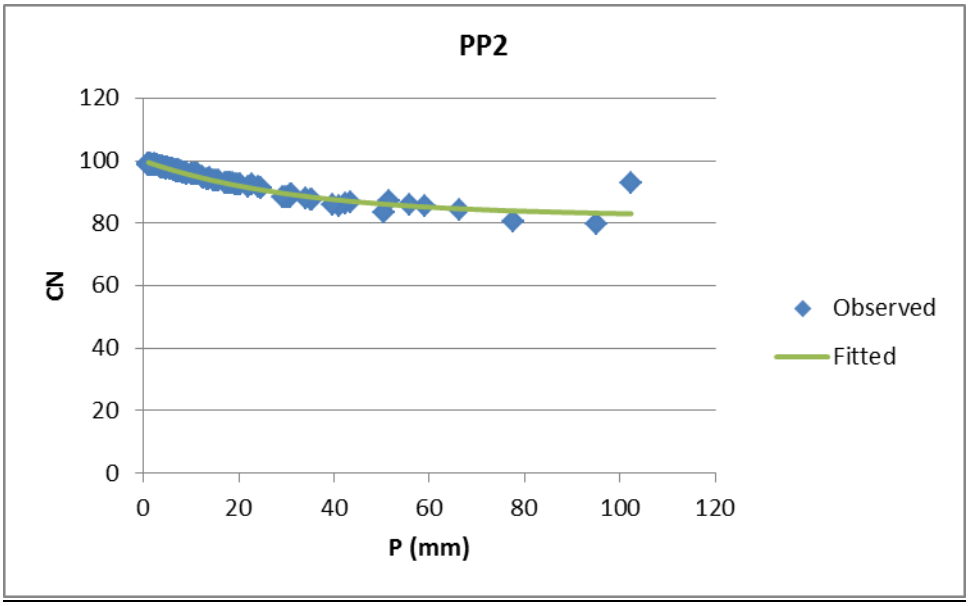
PP2
120
100
80
60
40
20
0
CN
0
20
40
60
80
100
120
P (mm)
Observed
Fitted

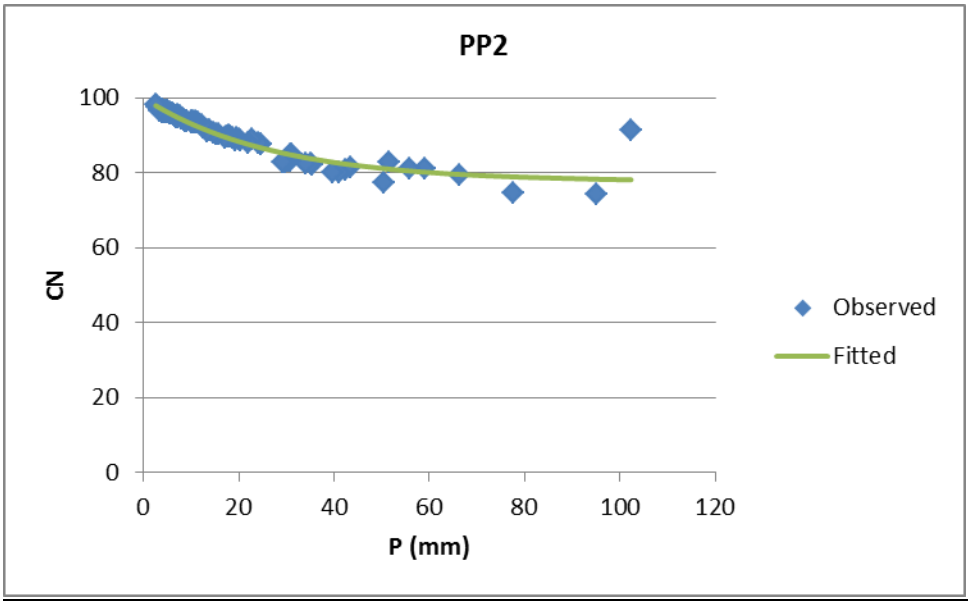
PP2
100
80
60
40
20
0
CN
0
20
40
60
80
100
120
P (mm)
Observed
Fitted

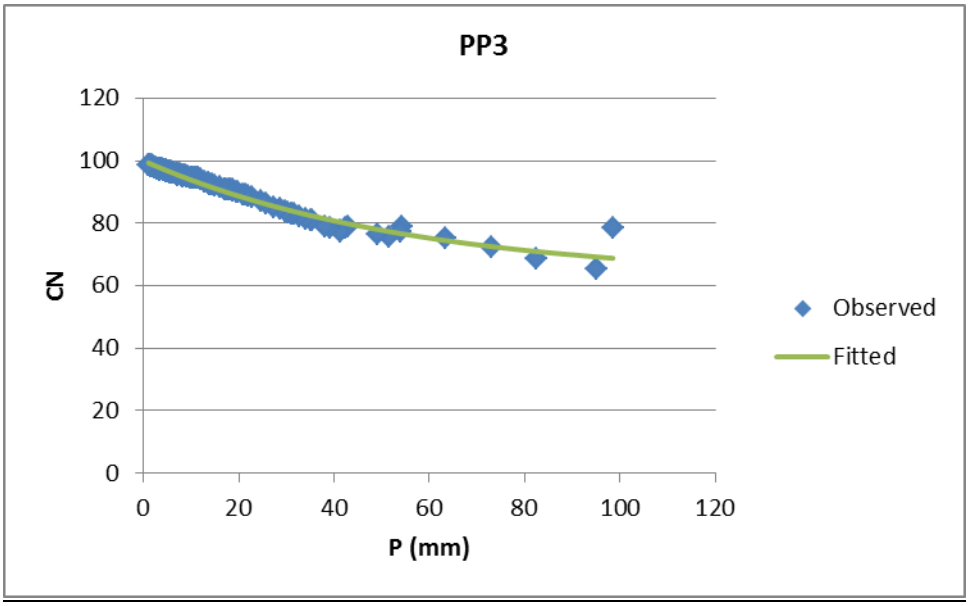
PP3
120
100
80
60
40
20
0
CN
0
20
40
60
80
100
120
P (mm)
Observed
Fitted

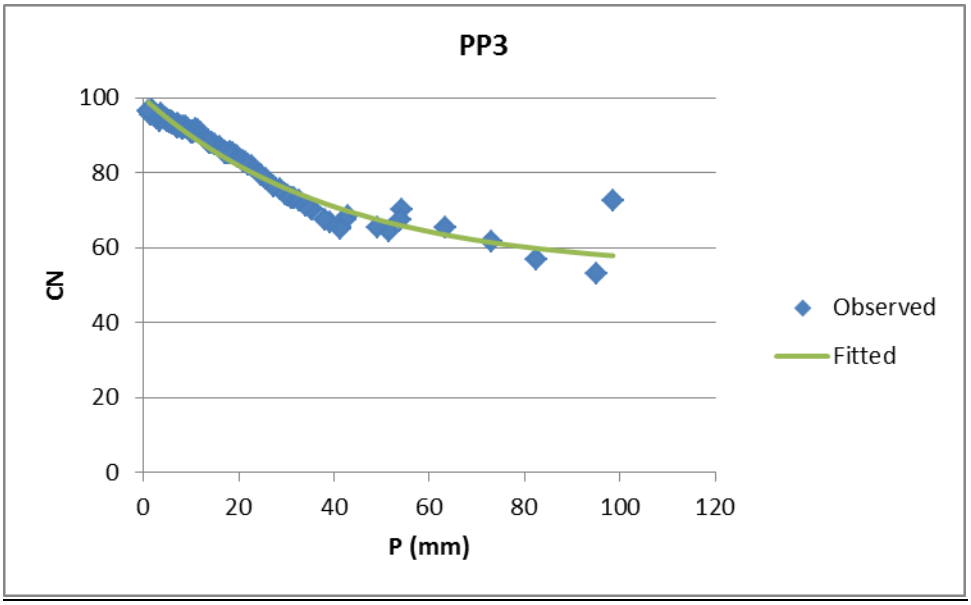
PP3
100
80
60
40
20
0
CN
0
20
40
60
80
100
120
P (mm)
Observed
Fitted

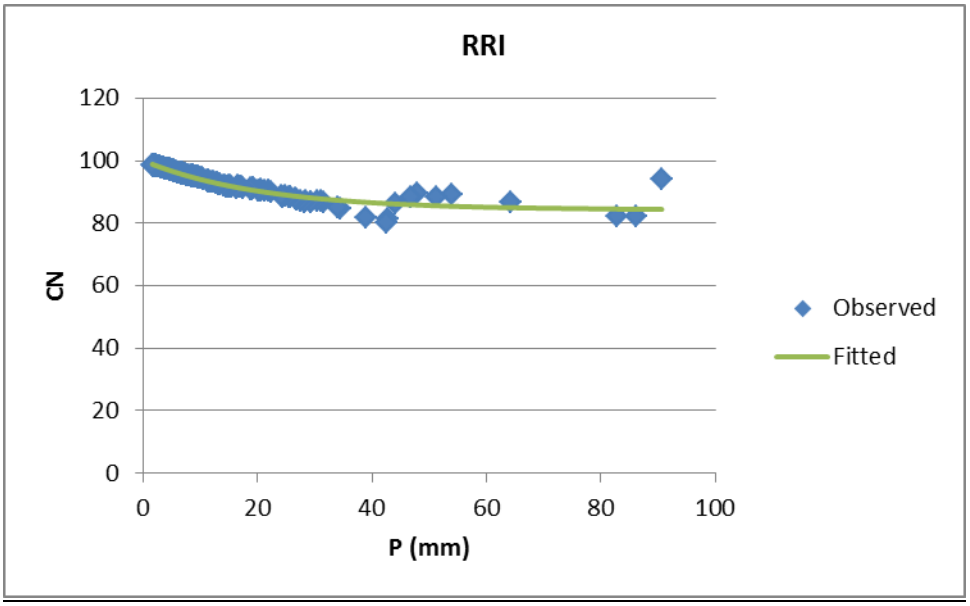
RRI
120
100
80
60
40
20
0
CN
0
20
40
60
80
100
P (mm)
Observed
Fitted

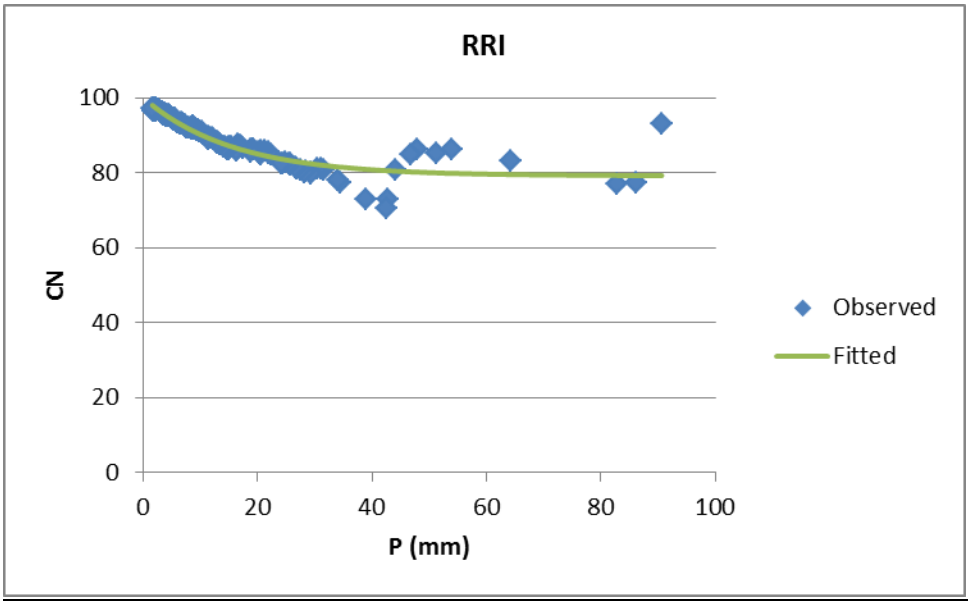
RRI
100
80
60
40
20
0
CN
0
20
40
60
80
100
P (mm)
Observed
Fitted

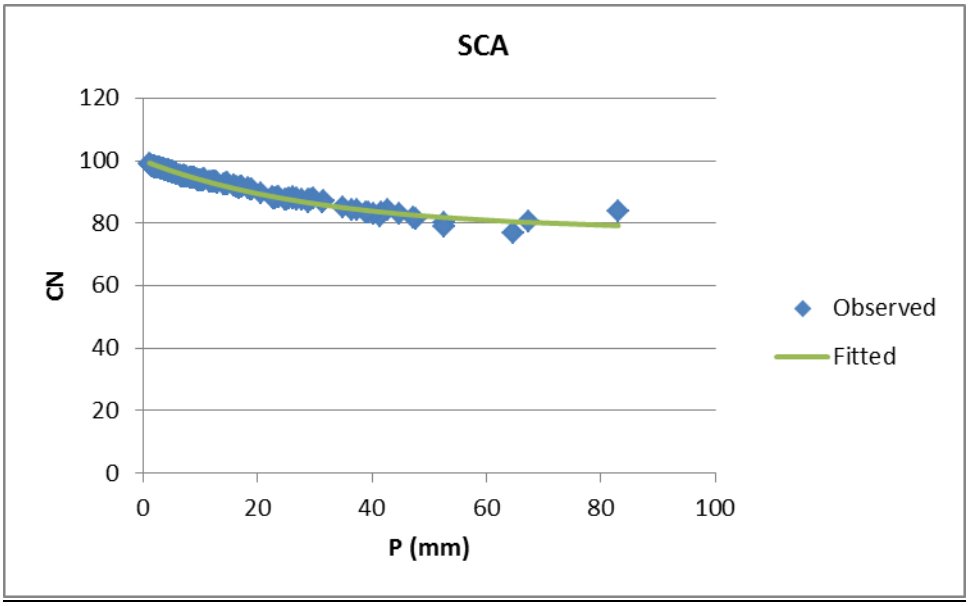
SCA
120
100
80
60
40
20
0
CN
0
20
40
60
80
100
P (mm)
Observed
Fitted

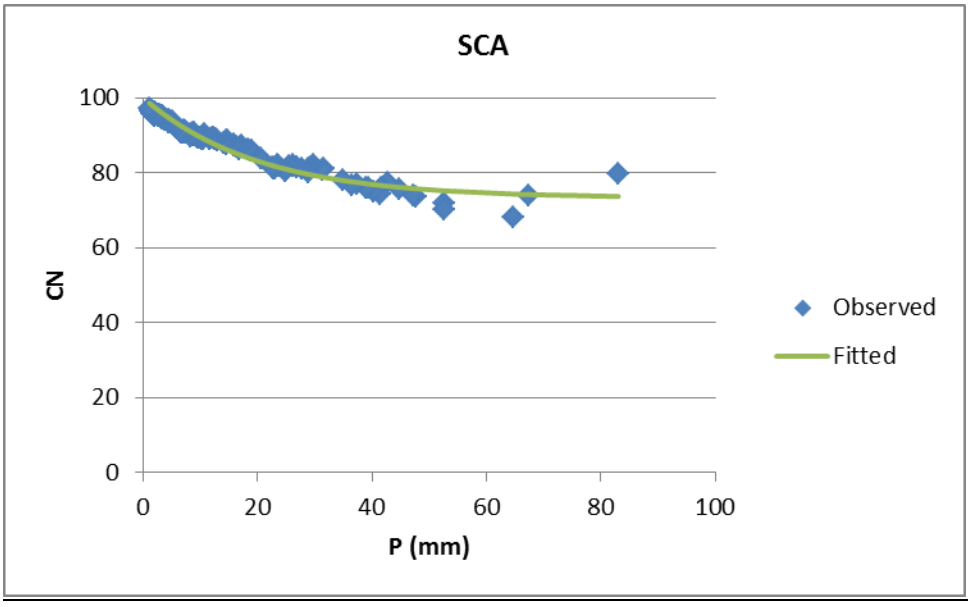
SCA
100
80
60
40
20
0
CN
0
20
40
60
80
100
P (mm)
Observed
Fitted

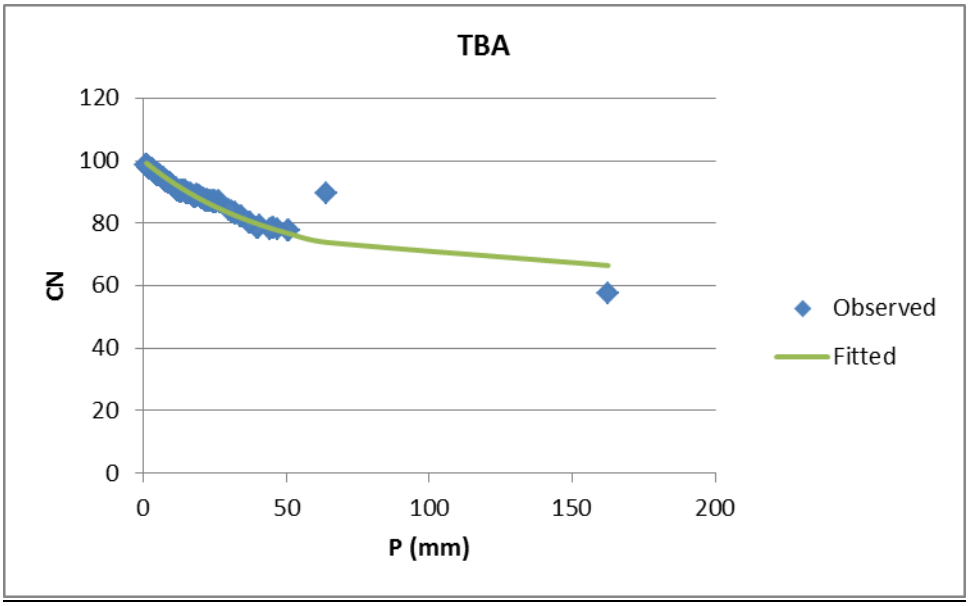
TBA
120
100
80
60
40
20
0
CN
0
50
100
150
200
P (mm)
Observed
Fitted

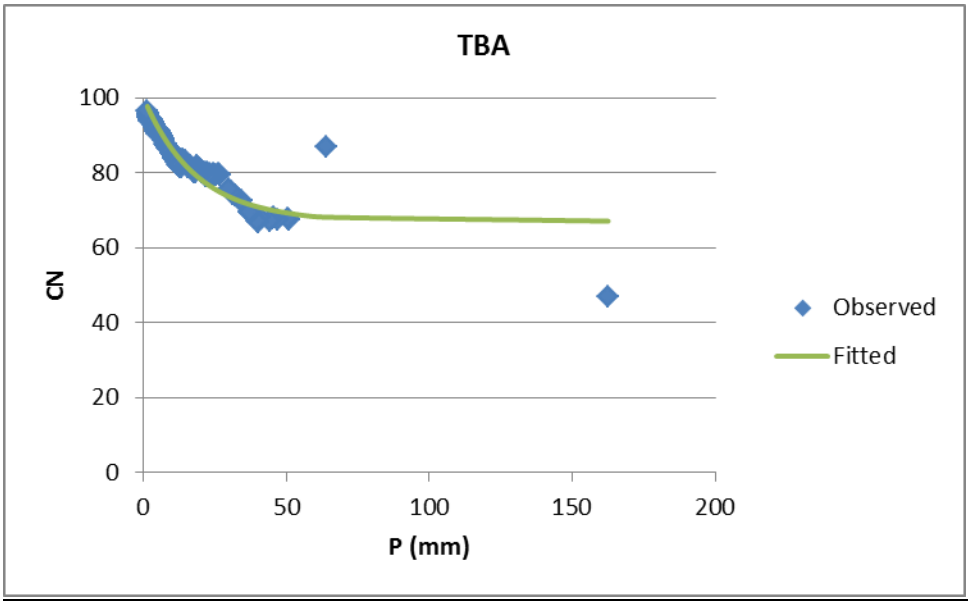
TBA
100
80
60
40
20
0
CN
0
50
100
150
200
P (mm)
Observed
Fitted

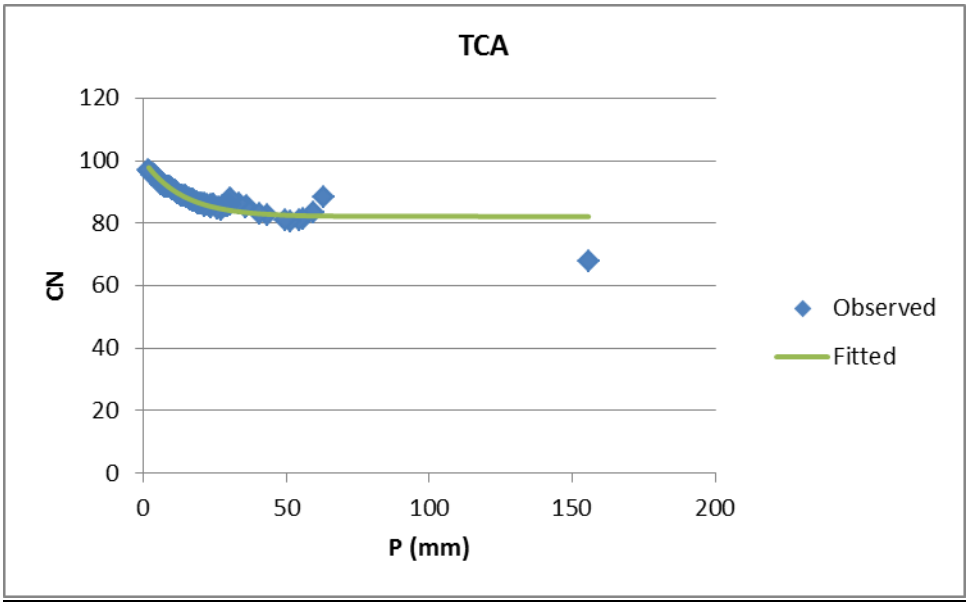
TCA
120
100
80
60
40
20
0
CN
0
50
100
150
200
P (mm)
Observed
Fitted

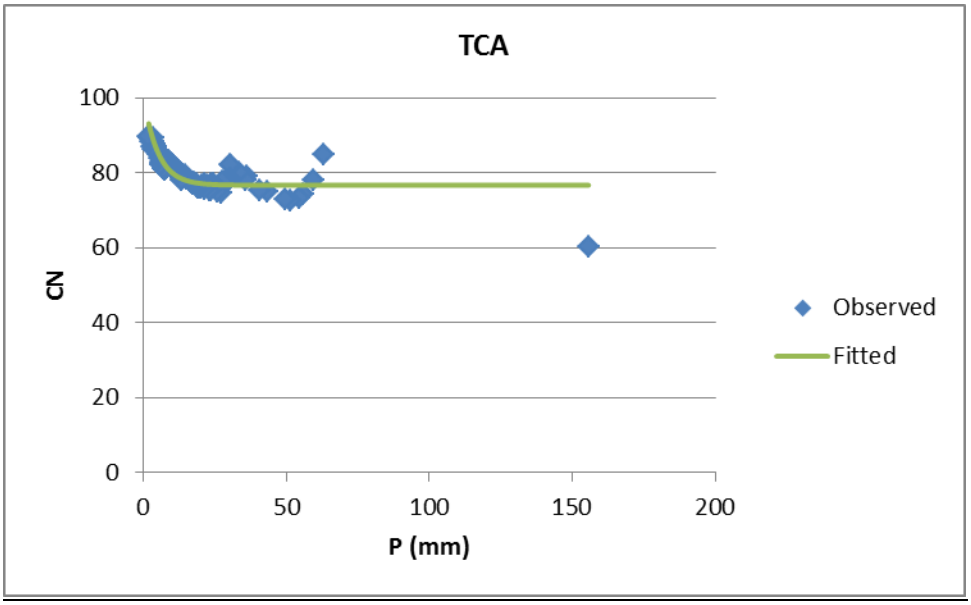
TCA
100
80
60
40
20
0
CN
0
50
100
150
200
P (mm)
Observed
Fitted

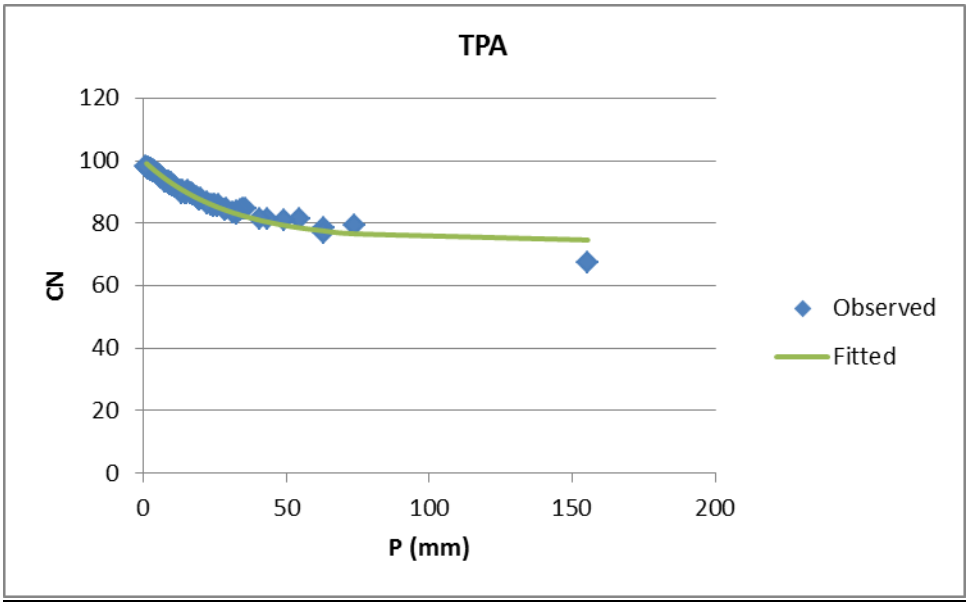
TPA
120
100
80
60
40
20
0
CN
0
50
100
150
200
P (mm)
Observed
Fitted

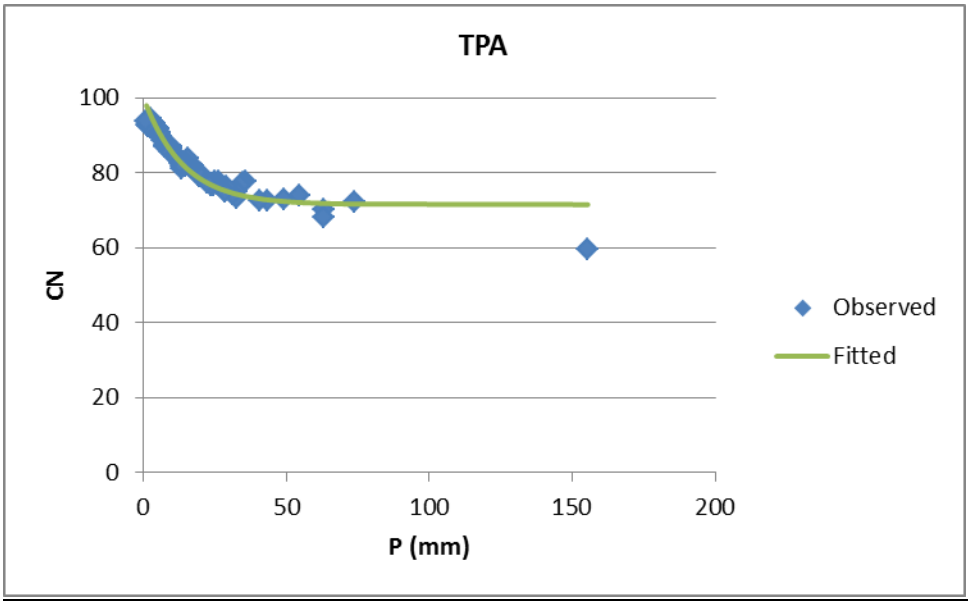
TPA
100
80
60
40
20
0
CN
0
50
100
150
200
P (mm)
Observed
Fitted

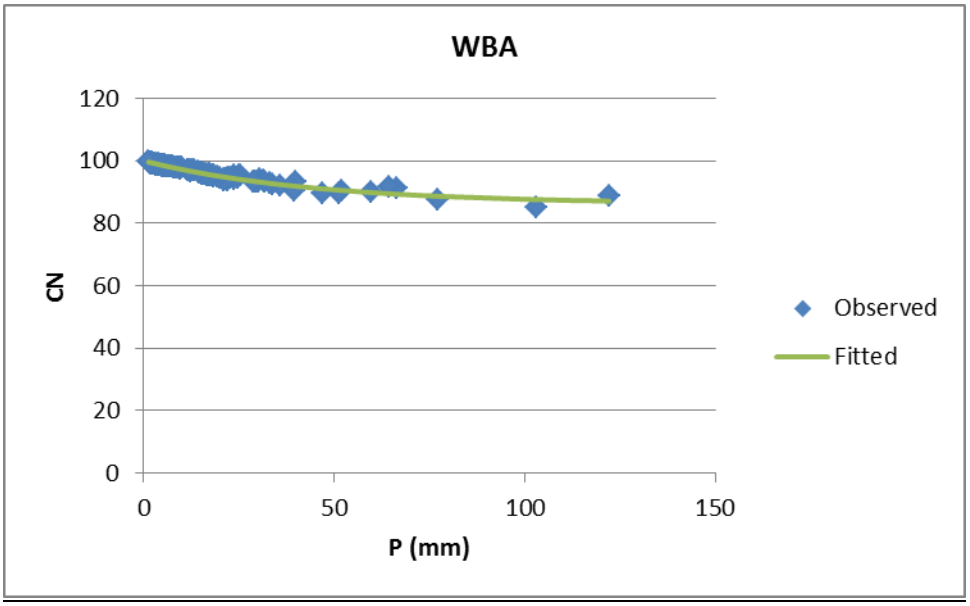
WBA
120
100
80
60
40
20
0
CN
0
50
100
150
P (mm)
Observed
Fitted

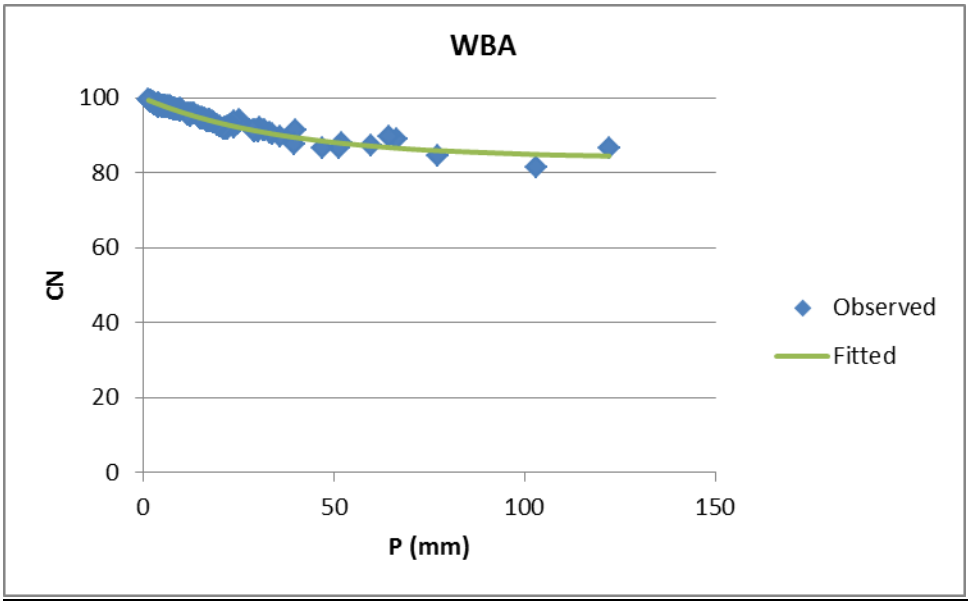
WBA
100
80
60
40
20
0
CN
0
50
100
150
P (mm)
Observed
Fitted

APPENDIX C: GIS-CN RESULTS FOR THE INITIAL ABSTRACTION RATIO OF 0.05

The original value of the initial abstraction ratio (I_a/S) or λ has been established by SCS (now NRCS) as 0.2. This value has been investigated by many researchers and determined to be higher than the actual λ value in most of the watersheds (Hawkins et al. 2009,2010). So, investigating the role of λ in the CN studies is recently emphasized (Hawkins et al. 2009, D'Asaro and Grillone 2012, D'Asaro et al. 2014). Based on the results of several studies, Hawkins et al. (2009) states λ=0.05 as a more appropriate assumption for general application. Also, Woodward et al. (2010) recommends λ=0.05 to NRCS for agency use. As an effort to examine the effect of initial abstraction ratio on the results of the proposed GIS-CN method in chapter 5, we investigated the effect of using the initial abstraction ratio of 0.05 (λ=0.05) on the presented f_{EIA} versus CN_∞ curve for ungauged watersheds (Eq. 5.22) and actual CN_∞ values. The general equations of the NRCS-CN method are as Equations (5.1) to (5.3).

Assuming λ=0.05, the original NRCS-CN equations become

$$Q = \frac{(P-0.05\,S)^2}{P+0.95\,S} \qquad for\ P \geq 0.05\,S \tag{C.1}$$

$$Q = 0 \qquad for\ P < 0.05\,S \tag{C.2}$$

where P, Q, and S are the same parameters as Equation (5.1).

The storage parameter S can be obtained from Eq. (C.1) as

$$S_{0.05} = 10\left[2P + 19Q - \sqrt{361Q^2 + 80PQ}\right] \quad \text{(C.3)}$$

where $S_{0.05}$ is the maximum potential retention with using the assumption of λ=0.05. Therefore by using λ=0.05, $S_{0.05}$ is obtained from Eq. (C.3) and a unique *CN* is then determined for each storm event in the ordered dataset using equations (5.5) or (5.6). The actual CN (CN_∞) for each watershed is then calculated using a similar method as for λ=0.2. Table C.1 presents the CN_∞ and the *CN* pattern of the watersheds in the case of λ=0.05.

Table C.1 Actual CN (CN_∞), type of CN pattern and α (ratio of CN_r/98) in the case of λ=0.05 for the 40 watersheds of study

Row	Watershed Name	CN_∞	CN vs. Precip. Pattern	α
1	AHUG	51.6	Standard	0.4509
2	GCP	65.2	Standard	0.5541
3	Como 3	40.4	Standard	0.3450
4	Sarita inlet	NA	Complacent	NA
5	TBEB	64.6	Standard	0.5771
6	EK	75.5	Standard	0.6324
7	PC	70.6	Standard	0.5950
8	SAP	68.3	Standard	0.6095
9	TBO	73.8	Standard	0.6544
10	MG1	76.7	Standard	0.7545
11	MG2	67.0	Standard	0.6281
12	P1	58.0	Standard	0.4868
13	P2	57.0	Standard	0.5406
14	P3	71.9	Standard	0.7057
15	Hedburg	NA	Complacent	NA
16	Tapestry	50.5	Standard	0.4176
17	Smith Pond	65.2	Standard	0.6372
18	MOA	31.5	Standard	NA
19	Harper	81.7	Standard	NA
20	Monroe	NA	Complacent	NA
21	BW1	69.5	Standard	0.6572

Row	Watershed Name	CN_∞	CN vs. Precip. Pattern	α
22	EBA	41.9	Standard	0.3686
23	EHA	67.6	Standard	0.5332
24	ERA	83.4	Standard	0.8185
25	HI	90.4	Standard	0.8920
26	HPA	61.7	Standard	0.4712
27	LCA	59.7	Standard	0.5823
28	LOA	83.6	Standard	0.8168
29	LUA	94.3	Standard	0.9276
30	MBA	90.1	Standard	0.8817
31	OFA	94.3	Standard	0.9320
32	PP1	81.3	Standard	0.7795
33	PP2	77.7	Standard	0.7156
34	PP3	53.9	Standard	0.4566
35	RRI	79.2	Standard	0.7856
36	SCA	73.3	Standard	0.7010
37	TBA	67.1	Standard	0.6479
38	TCA	76.7	Standard	0.7597
39	TPA	71.6	Standard	0.6854
40	WBA	83.9	Standard	NA

As seen in the Table C.1, Sarita catchment showed a complacent CN pattern in this case. Hedburg and Monroe basins still have complacent CN patterns as well. Harper, MOA and WBA also have the same issues as before. Therefore by excluding Sarita, Hedburg and Monroe (complacent CN pattern), Harper (lack of large rainfall data), MOA and WBA (runoff data issue), the total number of watersheds that were used in our analysis in the case of λ=0.05 was 34. Using f_{EIA} values from the proposed SWLS method (same as Table 5.2) and CN_∞ values from Table C.1, the α values for the case of λ=0.05 can be obtained using Eq. (5.16). The last column of Table C.1 shows the α values for the case of λ=0.05. Similar to Eq. (5.18), α is estimated in terms of CN_∞ using a weighted least square (WLS) regression.

$$\alpha = 0.0116\, CN_{\infty} - 0.1660 \qquad \text{(C.4)}$$

Similar to the original case (λ=0.2), Figure C.1 shows a strong correlation between α and CN_{∞} with a $pseudo\ R^2_{WLS}$ of 0.9429 in the case of λ=0.05 as well. Since the obtained equation for α in terms of CN_{∞} in the case of λ=0.05 (Eq. C.4) is almost the same equation as the original case of λ=0.2 (Eq. 5.18) and by using the same discussion as on Eq. (5.20) (range of α), f_{EIA} is estimated in terms of CN_{∞} using the same equation as the original case (Eq. 5.22).

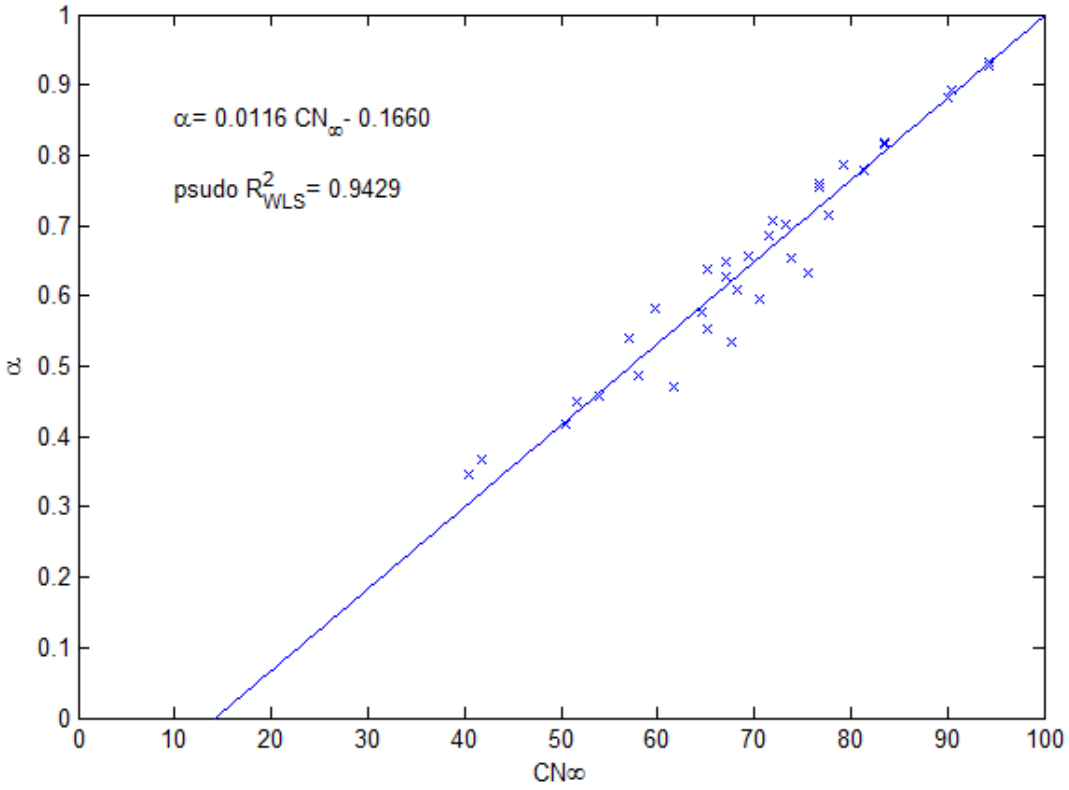

Figure C.1 Plot of α versus CN_{∞} for the case of λ=0.05. Since α is the ratio of CN_r/98, the regression shows a strong correlation between CN_r and CN_{∞} in the watersheds of study.

Figure C.2 presents the plot of f_{EIA} vs. CN_∞ for the case of λ=0.05 (which is the same as the original case) and the actual CN_∞ and f_{EIA} data (red points) for all the study sites with standard CN pattern (34 sites). The actual f_{EIA} values are the same as Figure 5.8 but the actual CN_∞values are corresponding to the case of λ=0.05 (Table C.1).

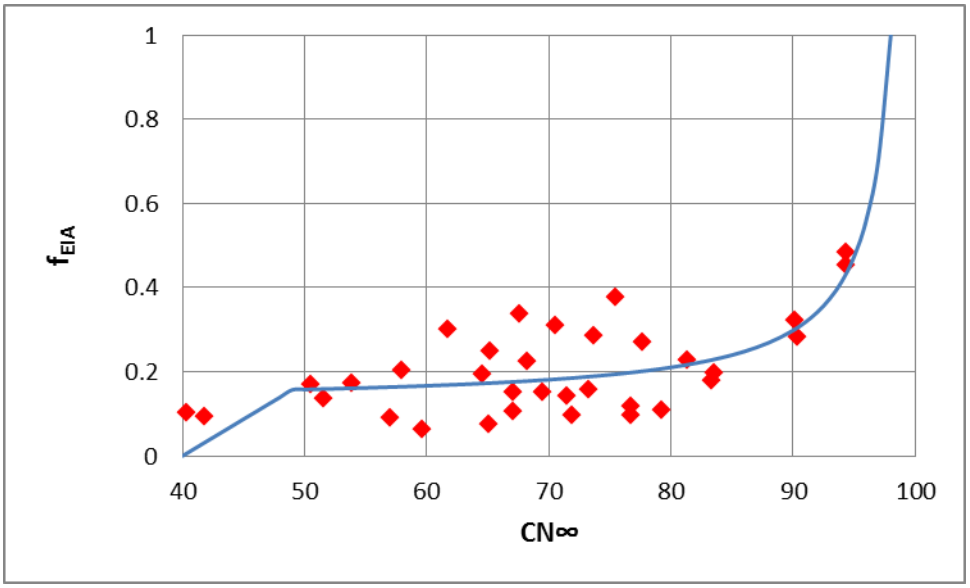

Figure C.2 Comparison of the actual f_{EIA} and CN_∞ values in gauged watersheds with the presented curve for ungauged watersheds in the case of λ=0.05. The actual f_{EIA} values have been estimated based on the proposed SWLS method and the actual CN_∞ values have been calculated using the Hawkins' asymptotic CN method (Hawkins 1993) and the assumption of $I_a = 0.05S$.

The agreement between the actual data points and presented curve in the one extreme value of CN_∞ (i.e. 98) is better as seen in Figure C.2. This good agreement can be explained by the fact that CN_∞equal to 98 in Figure C.3 is corresponding to fully

impervious (i.e. f_{TIA}=1) watersheds, respectively. In these extremes, there is no interaction between impervious and pervious surfaces in runoff generation, so the EIA fraction can be better estimated using the CN index, which in principle includes land cover and soil parameters. However, by having interaction between pervious and impervious surfaces in a watershed the runoff generation mechanism becomes more complex and perhaps more parameters than CN (e.g. spatial distribution of impervious surfaces and tree cover) are needed to explain this process.

Sensitivity of Runoff Depth to EIA Fraction

In order to evaluate the importance of the EIA fraction change on the runoff depth in an ungauged watershed, we developed graphs of runoff depth (Q) versus f_{EIA} for different amounts of rainfall depth (P). The Curve Number method with the assumption of λ=0.05 has been used for the runoff calculation. To determine CN values for each rainfall depth in a watershed with a standard CN pattern from Eq. (5.8), one needs to have both CN_{∞} and the exponential parameter *k*. These values for the watersheds of study with standard CN pattern are presented in Table C.2. The mean, median, and standard deviation of *k* values for λ=0.05 are 0.0658, 0.0463, and 0.0606, respectively. In order to find a representative *k* value for ungauged watersheds, histogram of *k* was first plotted (Figures C.4). The histogram depicts that both range and standard deviation of *k* values have increased in comparison to the original case of λ=0.2 (Figure 5.13). Since the distribution of *k* appears to be closer to log-normal, the geometric mean of *k* values was used as the representative *k* value for ungauged watersheds. The geometric mean value of *k* were calculated as 0.05 for the cases of λ= 0.05.

Table C.2 CN_∞ and k values for the watersheds of study with a standard CN pattern in the case of λ=0.05. Parameter k is a fitting constant defined in Eq. 5.8

Row	Watershed Name	CN_∞	k
1	AHUG	51.6	0.0294
2	GCP	65.2	0.0208
3	Como 3	40.4	0.0289
4	TBEB	64.6	0.0311
5	EK	75.5	0.0180
6	PC	70.6	0.0250
7	SAP	68.3	0.0315
8	TBO	73.8	0.0266
9	MG1	76.7	0.0994
10	MG2	67.0	0.0439
11	P1	58.0	0.0415
12	P2	57.0	0.0486
13	P3	71.9	0.0916
14	Tapestry	50.5	0.0329
15	Smith Pond	65.2	0.1046
16	BW1	69.5	0.0383
17	EBA	41.9	0.0331
18	EHA	67.6	0.0174
19	ERA	83.4	0.0895
20	HI	90.4	0.1353
21	HPA	61.7	0.0128
22	LCA	59.7	0.0726
23	LOA	83.6	0.0601
24	LUA	94.3	0.0786
25	MBA	90.1	0.3136
26	OFA	94.3	0.1621
27	PP1	81.3	0.0546
28	PP2	77.7	0.0366
29	PP3	53.9	0.0248
30	RRI	79.2	0.0635
31	SCA	73.3	0.0498
32	TBA	67.1	0.0540
33	TCA	76.7	0.1946
34	TPA	71.6	0.0714

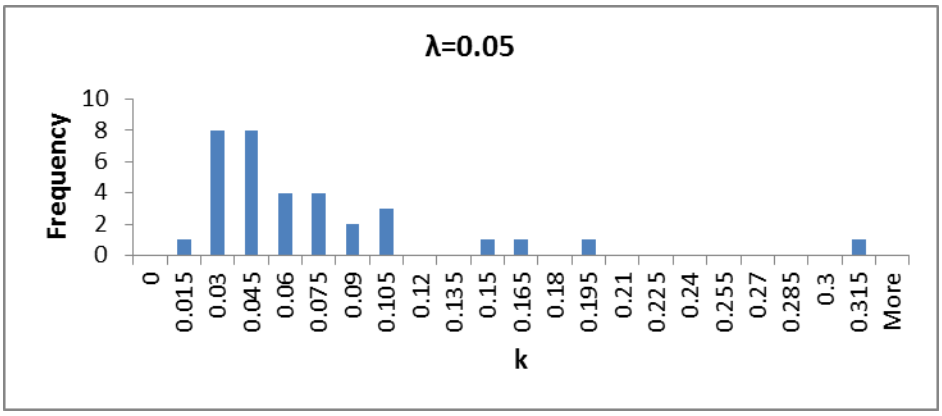

Figure C.4 Histogram of the fitting parameter k in the case of λ=0.05 for the watersheds of study with standard CN pattern. Range and standard deviation of the k values have increased in comparison to the original case of λ=0.2.

Similar to the original case of λ in chapter 5, runoff depth (Q) in an ungauged watershed with a standard CN pattern was calculated in terms of EIA fraction (f_{EIA}) for 4 rainfall depths of 12.5, 25, 50 and 75 mm (i.e. 0.5, 1, 2, and 3 in). Table C.3 shows the results in the case of λ=0.05. Actual CN (CN_{∞}) in the second column of this tables is calculated in terms of f_{EIA} based on Eq. (5.30). CN values for each rainfall depth (P) are calculated based on Eq. (5.8). The *k* parameter in is considered as 0.05. The storage index S is then calculated from Eq. (5.6). Finally the runoff depth (Q) for each rainfall depth (P) is calculated from Eq. (C.1) and (C.2). Since the actual f_{EIA} values in our study sites based on the proposed SWLS method were all less than 0.5, plot of runoff depth (Q) against EIA fraction (f_{EIA}) for different rainfall depths is presented for f_{EIA} between zero and 0.5. This plot which is shown in Figures C.5 can be utilized to show the sensitivity of runoff

depth to EIA fraction for different rainfall depths in ungauged watersheds with standard CN pattern.

Table C.3 Runoff depth in terms of EIA fraction in ungauged urban watersheds with a standard CN pattern in the cases of λ=0.05

f_{EIA}	CN_{∞}	CN				S (mm)				Q (mm)			
		P= 12.5 mm	P= 25 mm	P= 50 mm	P= 75 mm	P= 12.5 mm	P= 25 mm	P= 50 mm	P= 75 mm	P= 12.5 mm	P= 25 mm	P= 50 mm	P= 75 mm
0	40	72.32	57.41	45.05	41.46	97.23	188.46	309.82	358.57	0.56	1.19	3.46	7.84
0.05	42.9	73.64	59.44	47.67	44.26	90.93	173.33	278.81	319.91	0.64	1.41	4.13	9.19
0.1	45.7	74.96	61.47	50.29	47.05	84.85	159.21	251.04	285.85	0.73	1.65	4.86	10.63
0.15	48.6	76.28	63.50	52.91	49.84	78.99	145.98	226.02	255.60	0.84	1.91	5.66	12.18
0.157	49	76.47	63.80	53.29	50.25	78.16	144.15	222.62	251.52	0.85	1.95	5.78	12.41
0.16	52.8	78.24	66.51	56.80	53.98	70.66	127.87	193.18	216.53	1.01	2.36	6.97	14.67
0.17	62.8	82.85	73.61	65.95	63.73	52.58	91.06	131.12	144.54	1.56	3.75	10.81	21.63
0.2	77.3	89.51	83.87	79.19	77.83	29.75	48.86	66.77	72.36	2.97	7.12	19.20	35.45
0.25	86.2	93.64	90.21	87.37	86.54	17.26	27.57	36.73	39.49	4.69	10.90	27.33	47.39
0.3	90.1	95.43	92.97	90.93	90.34	12.16	19.20	25.33	27.16	5.88	13.36	32.07	53.80
0.35	92.3	96.44	94.52	92.93	92.47	9.38	14.73	19.33	20.69	6.76	15.10	35.17	57.80
0.4	93.7	97.08	95.51	94.20	93.83	7.64	11.95	15.63	16.72	7.43	16.38	37.36	60.52
0.45	94.6	97.53	96.19	95.09	94.77	6.44	10.05	13.12	14.02	7.96	17.37	38.98	62.50
0.5	95.3	97.85	96.70	95.74	95.46	5.57	8.67	11.30	12.07	8.40	18.16	40.24	64.01
0.55	95.9	98.11	97.08	96.24	95.99	4.91	7.63	9.93	10.60	8.75	18.80	41.24	65.19
0.6	96.3	98.30	97.39	96.63	96.41	4.38	6.81	8.85	9.45	9.05	19.33	42.05	66.14
0.65	96.7	98.46	97.64	96.95	96.75	3.96	6.15	7.98	8.52	9.31	19.77	42.72	66.93
0.7	97.0	98.60	97.84	97.22	97.03	3.61	5.60	7.27	7.76	9.53	20.15	43.29	67.58
0.75	97.2	98.71	98.01	97.44	97.27	3.32	5.15	6.68	7.13	9.72	20.48	43.78	68.14
0.8	97.4	98.80	98.16	97.63	97.47	3.07	4.76	6.17	6.59	9.89	20.77	44.20	68.62

f_{EIA}	CN_∞	CN				S (mm)				Q (mm)			
		P= 12.5 mm	P= 25 mm	P= 50 mm	P= 75 mm	P= 12.5 mm	P= 25 mm	P= 50 mm	P= 75 mm	P= 12.5 mm	P= 25 mm	P= 50 mm	P= 75 mm
0.85	97.6	98.89	98.29	97.79	97.65	2.86	4.43	5.74	6.12	10.04	21.02	44.57	69.04

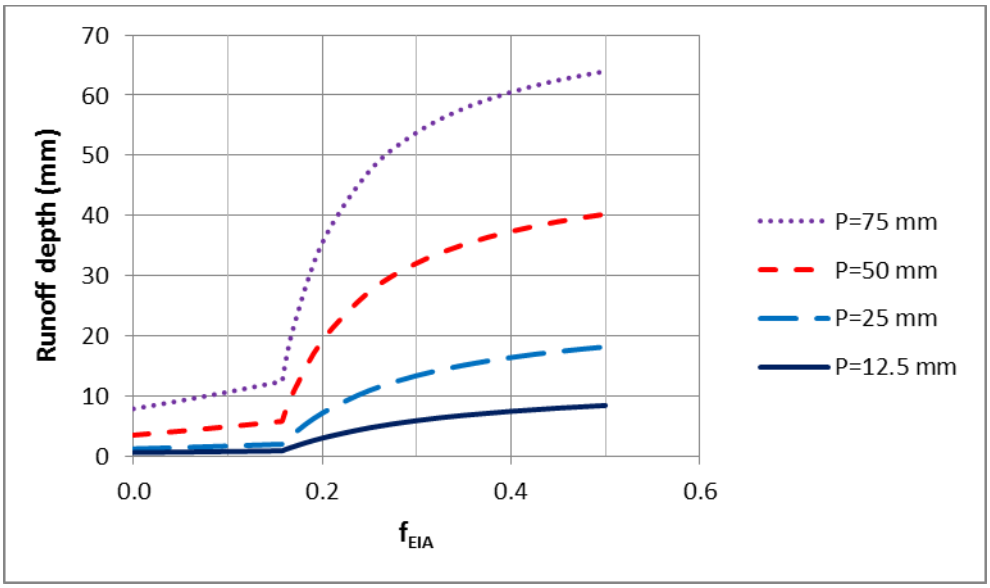

Figure C.5 Runoff depth (Q) against EIA fraction (f_{EIA}) for different rainfall depths in the case λ=0.05.

Comparing the presented curves of Q vs. f_{EIA} in Figure C.5 with the observed values was performed in a similar way as Figure 5.15. Runoff depths were calculated using the actual f_{EIA} , CN_∞ , and k values of study sites with standard CN pattern for the same rainfall depths in Figure C.5. The results are presented in Table C.4. For each watershed in Tables C.4, f_{EIA} is obtained from the proposed SWLS method (Table 5.2). CN_∞ and k values can be found from Table C.2. Also, CN for each rainfall depth is calculated based on Eq. 5.8 using actual CN_∞ and k values of the watershed. Other steps for the runoff

calculation are the same as Table C.3. The obtained pairs of (f_{EIA} , Q) from Table C.3 were added to the plot of Q vs. f_{EIA} to compare the developed curves for ungauged watersheds to the actual data. The result is presented in Figure C.6. The results show no substantial difference between two cases of λ=0.2 and 0.05. Also, more scatter of actual data around the curves is seen in higher rainfalls which can be explained similar as for Figure 5.15.

Table C.4 Actual runoff depth (Q) in the study sites with standard CN pattern for different rainfall depths using the actual f_{EIA} , CN_{∞} , and k values in the case of λ=0.05

Site Name	CN				S (mm)				Q (mm)			
	P= 12.5 mm	P= 25 mm	P= 50 mm	P= 75 mm	P= 12.5 mm	P= 25 mm	P= 50 mm	P= 75 mm	P= 12.5 mm	P= 25 mm	P= 50 mm	P= 75 mm
AHUG	85.1	74.8	62.7	56.9	44.48	85.65	151.11	192.32	1.93	4.04	9.31	16.59
GCP	92.0	85.9	77.5	72.5	21.98	41.71	73.70	96.22	3.89	8.12	17.87	29.60
Como 3	81.9	69.3	54.4	47.2	56.12	112.52	212.83	284.27	1.43	2.85	6.14	10.71
TBEB	88.6	80.9	72.1	68.0	32.69	60.11	98.48	119.47	2.71	5.89	14.15	25.28
EK	95.1	91.1	85.5	81.9	13.17	24.72	43.16	56.25	5.61	11.65	25.15	40.57
PC	92.1	86.3	79.0	75.1	21.77	40.21	67.42	84.16	3.93	8.36	19.06	32.34
SAP	89.7	82.7	74.8	71.3	29.27	53.13	85.40	102.42	3.02	6.61	15.95	28.34
TBO	92.6	87.2	80.7	77.3	20.40	37.17	60.83	74.55	4.13	8.88	20.46	34.84
MG1	83.5	78.7	76.9	76.8	50.35	68.82	76.27	76.90	1.65	5.14	17.42	34.20
MG2	86.1	78.0	70.7	68.3	41.09	71.49	105.20	118.05	2.12	4.94	13.35	25.51
P1	83.0	72.9	63.2	59.8	52.08	94.62	147.62	170.49	1.58	3.58	9.55	18.65
P2	80.4	69.7	60.8	58.1	61.87	110.17	163.93	183.07	1.24	2.93	8.49	17.42
P3	80.9	74.8	72.2	72.0	60.12	85.70	97.70	98.96	1.29	4.03	14.25	29.03
Tapestry	83.3	72.3	60.1	54.8	50.77	97.33	168.54	209.88	1.63	3.45	8.23	15.16
Smith Pond	74.6	67.7	65.3	65.2	86.56	121.15	134.72	135.76	0.70	2.56	10.52	22.81
BW1	88.4	81.2	74.0	71.2	33.33	58.77	89.27	102.62	2.66	6.02	15.38	28.30
EBA	80.3	67.3	53.0	46.7	62.30	123.51	225.40	289.52	1.23	2.49	5.68	10.47
EHA	93.7	88.6	81.2	76.4	17.18	32.79	58.92	78.53	4.70	9.72	20.89	33.77

Site Name	CN				S (mm)				Q (mm)			
	P= 12.5 mm	P= 25 mm	P= 50 mm	P= 75 mm	P= 12.5 mm	P= 25 mm	P= 50 mm	P= 75 mm	P= 12.5 mm	P= 25 mm	P= 50 mm	P= 75 mm
ERA	88.8	85.2	83.6	83.4	31.95	44.22	49.87	50.49	2.77	7.75	23.18	42.72
HI	92.2	90.7	90.4	90.4	21.59	25.97	26.95	26.98	3.95	11.31	31.31	53.90
HPA	94.4	89.5	81.9	76.4	15.20	29.67	55.98	78.38	5.12	10.40	21.59	33.81
LCA	76.0	66.2	60.8	59.9	80.43	129.42	164.10	170.35	0.81	2.32	8.48	18.66
LOA	91.3	87.2	84.4	83.7	24.16	37.23	47.05	49.33	3.60	8.87	23.97	43.17
LUA	96.5	95.1	94.5	94.4	9.32	12.99	14.92	15.19	6.78	15.88	37.80	61.63
MBA	90.3	90.1	90.1	90.1	27.18	27.78	27.79	27.79	3.24	10.85	30.93	53.43
OFA	95.1	94.4	94.3	94.3	13.11	14.94	15.21	15.22	5.62	15.01	37.62	61.61
PP1	90.8	86.1	82.6	81.6	25.84	41.01	53.68	57.09	3.39	8.23	22.17	40.27
PP2	91.8	86.6	81.2	79.1	22.70	39.28	58.63	67.12	3.79	8.52	20.96	36.99
PP3	87.7	78.7	67.2	61.1	35.57	68.73	123.75	161.91	2.48	5.15	11.46	19.56
RRI	88.6	83.5	80.1	79.4	32.59	50.25	63.08	65.84	2.72	6.95	19.96	37.38
SCA	87.6	81.0	75.5	73.9	35.85	59.60	82.32	89.49	2.46	5.94	16.42	31.08
TBA	83.9	75.7	69.4	67.7	48.81	81.67	112.22	121.08	1.72	4.26	12.58	25.02
TCA	78.8	76.9	76.7	76.7	68.42	76.23	77.00	77.01	1.06	4.61	17.29	34.17
TPA	83.2	76.3	72.4	71.7	51.25	78.76	97.04	100.31	1.61	4.44	14.33	28.76

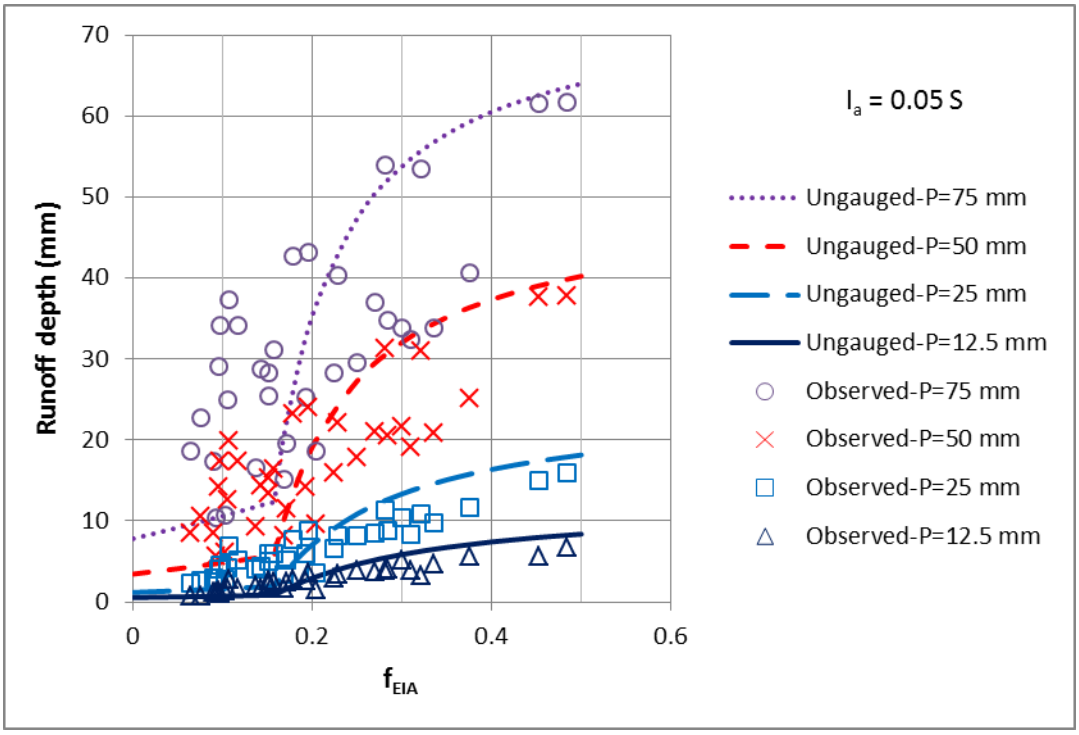

Figure C.6 Comparison of the developed Runoff depth vs. EIA fraction curves for ungauged watersheds with the actual data in the case λ=0.05.

To examine the effect of infiltration capacity of the soil on the amount of runoff depth in higher rainfall depths, weighted average hydrologic soil group (HSG) in the watersheds of study (as discussed in section 5.5.2 and Table 5.4) were used. As an example, Figure C.7 displays different HSGs corresponding to the actual (f_{EIA},Q) data and compares them with the developed Q vs. f_{EIA} curve for ungauged watersheds at P=75 mm in the case of λ=0.05. As expected, Figure C.7 depicts that the points including HSGs with higher infiltration capacity and lower runoff potential (e.g. HSGs A and B) are generally lower than the higher runoff potential HSGs in the plot. However, there are points (especially in lower f_{EIA} values which correspond to more pervious watersheds) that do not follow this pattern. The interpretation of this Figure would be the same as Figure 5.16.

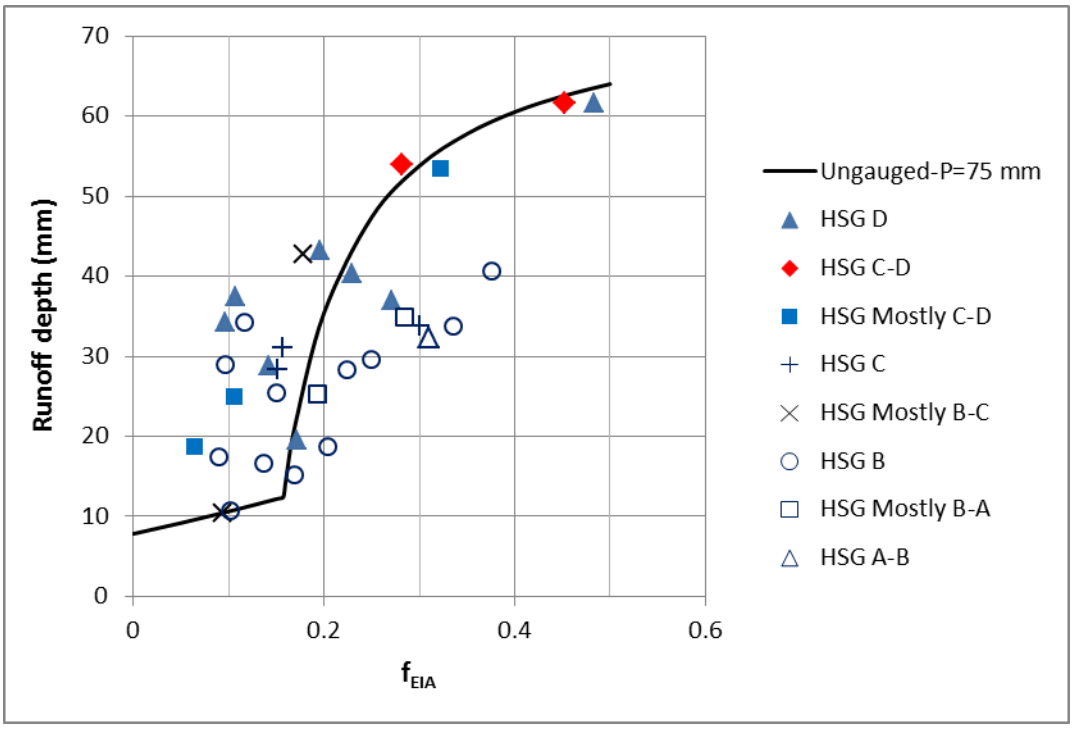

Figure C.7 Using hydrologic soil group (HSG) to partially explain the scatter of the actual data in comparison to the developed Runoff depth vs. EIA fraction curve for ungauged watersheds with P=75 mm in the case λ=0.05.